



# **Fish Ageing by Otolith Shape Analysis**

**Institute of Freshwater Research, Drottningholm, Sweden**

**Istituto di Ricerche sulla Pesca Marittima, Ancona, Italy**

**Image Science Software GmbH, Berlin, Germany**

**Imperial College of Science, Technology and Medicine, London, England**

**FAIR CT97 3402**



**Final Report, March 2002**

# Fish Ageing by Otolith Shape Analysis



**Final Report to the European Commission**

**EC contract no. FAIR CT97 3402**

**Coordinator:** Stellan F. Hamrin (1998-2000), Peer Doering-Arjes (2001)

**Manager:** Peer Doering-Arjes

**Contract duration:** 1 January 1998 – 31 December 2001

## **Participants:**

**Institute of Freshwater Research, National Board of Fisheries  
SE – 178 93 Drottningholm (Coordinator and Contractor)**

Scientific team: Peer Doering-Arjes, Stellan F. Hamrin, Håkan Wickström, Patrik Clevestam, Niklas Bergström, Massimiliano Cardinale

Tel. + 46-8-620 04 00, Fax + 46-8-759 03 38

Email [peer.doering-arjes@web.de](mailto:peer.doering-arjes@web.de)



**Istituto di Ricerche sulla Pesca Marittima – Consiglio Nazionale  
delle Ricerche**

**Largo Fiera della Pesca, I-60100 Ancona (Contractor)**

Scientific team: Enrico Arneri, Gianfranco Giannetti, Fortunata Donato

Tel. + 39-071-207 88 49, Fax + 39-071-553 13

Email [arneri@irpem.an.cnr.it](mailto:arneri@irpem.an.cnr.it)



**Image Science Software GmbH**

**Heilbronner Straße 10, D – 10711 Berlin (Contractor)**

Scientific team: Michael Schatz, Manfred Kastowsky, Ralf Schmidt

Tel. +49-30-89 09 53 26, Fax +49-39-89 09 53 21

Email [michael@ImageScience.de](mailto:michael@ImageScience.de)



**Imperial College of Science, Technology and Medicine,  
Biochemistry Dept./ Mechanical Engineering Dept.  
Biochemistry Building, South Kensington Campus, GB-London  
SW7 2AY (Contractor)**

Scientific team: Marin van Heel, Manfred Kastowsky, Ardan  
Patwardhan, Richard Hall, Richard Sayles  
Tel. + 44-20 75 94 53 16, Fax + 44-20 75 94 53 17  
Email m.vanheel@ic.ac.uk



**Danish Institute for Fisheries Research, Dept. of Fish Biology  
P.O.B. 101, DK – 9850 Hirtshals (Sub-contractor)**

Scientific team: Helge Paulsen  
Tel. + 45 33 96 32 11, Fax + 45 33 96 32 60  
Email hep@dfu.min.dk



**Danish Institute for Fisheries Research, Dept. of Marine Fisheries  
Charlottenlund Castle, DK – 2920 Charlottenlund (Sub-  
contractor)**

Scientific team: Henrik Mosegaard  
Tel. + 45 33 96 34 61, Fax + 45 33 96 33 33  
Email hm@dfu.min.dk



**The Fisheries Laboratory of the Faroe Islands  
Noatun, PO Box 3051, FR-110 Torshavn (Sub-contractor)**

Scientific team: Hjalti i Jakupsstovu, Eyðfinn Magnussen, Rogvi  
Mouritsen  
Tel. + 29-8-31 50 92, Fax + 29-8-182 64  
Email hjaltij@frs.fo



**Elektronenmicroscopie voor Materiaalkunde / Visielab,  
Universiteit Antwerpen, RUCA  
Groenenborgerlaan 171, B-2020 Antwerpen (Sub-contractor)**

Scientific team: Nora de Clerck, Erik Claes, Dirk van Dyck  
Tel. + 32-3- 218 02 89, Fax + 32-2-218 03 29  
Email nodecle@ruca.ua.ac.be



**SkyScan  
Vluchtenburgstraat 3, B-2630 Aartselaar (Sub-contractor)**

Scientific team: Alexander Sasov  
Tel. +32-3-877 57 05, Fax + 32-3-877 57 69  
Email sasov@skyscan.be



## CONTENT

Final Report to the European Commission.....	2
1. ABSTRACT .....	5
2. EXECUTIVE SUMMARY .....	8
2.1. Introduction .....	8
2.2. Results .....	9
2.3. Discussion - Conclusion .....	12
3. INTRODUCTION.....	14
4. MATERIALS AND METHODS .....	18
4.1. Sampling of otoliths.....	18
4.2. 2D Methodology.....	25
4.3. 3D Methodology.....	25
5. RESULTS.....	26
5.1. Sampled otoliths .....	26
5.2. 2D Methodology and 2D Shape Analysis of Otoliths .....	30
5.2.1. Databases .....	32
5.2.2. 2D Shape Analysis.....	39
5.2.2.1. Eel.....	43
5.2.2.2. Turbot .....	57
5.2.2.3. Anchovy.....	88
5.2.2.4. Cod.....	124
5.3. 3D Methodology and 3D Shape Analysis of Otoliths .....	157
6. DISCUSSION.....	179
6.1 General background.....	179
6.2 Methodology for 2D otolith shape analysis.....	180
6.3 Age determination based on 2D shape .....	185
6.4 Methodology for 3D otolith shape analysis.....	189
6.5 2D / 3D considerations .....	192
7. CONCLUSIONS .....	195
8. REFERENCES .....	197
9. DISSEMINATION LIST.....	203

## 1. ABSTRACT

Depletion of our fish stocks due to overfishing is undoubtedly the single most important problem facing the fishery industry world-wide. Knowledge of the age profile of a fish population is of primary importance for stock assessment and thus for stock management. The purpose of this study was to develop and evaluate objective and robust fish ageing methods based on two-dimensional images and on three-dimensional shape and density distributions of otoliths. In the course of the project a large database of otolith shapes was established for a number of important species. The database has been used to test newly developed methods and algorithms in the context of this project and it will continue to serve that purpose for new methods to be developed in the future.

Otoliths grow continuously throughout the life span of the fish and their species-specific shape develop from a simple rounded one in juveniles to, later in life, acquire often highly intricate patterns of lobes. Many otoliths show – when sectioned – a pattern of growth rings reminiscent of the growth rings of trees. In traditional fish ageing, age is usually derived from the analysis of such incremental changes in the body hard parts such as otoliths and scales. However, age determination by the interpretation of growth patterns is, difficult, excessively time consuming, and still not very reproducible. Thus, in spite of the importance of age determination for a reliable stock assessment, large variations in traditional ageing by annual zone counting are often found in results from different laboratories and even from within a single laboratory. Indeed, for validation of our new ageing methodologies we thus could not resort to a database of traditionally aged fish but rather had to collect database consisting largely of otoliths of fish with a precisely known age.

The main purpose of our project was to arrive at a simple and fast ageing technique avoiding any extensive handling or manipulation of the otoliths. The best candidate for such an economic ageing technique is to simply analyse the outer shape of an otolith lying flat on a support surface. The size and the complexity of the outer shape of otoliths change throughout the life span of the fish. This two-dimensional outer shape (“contour”) of the otolith is only one aspect of the three-dimensional growth pattern of an individual otolith. To determine the three-dimensional shape and growth pattern of otoliths is a complicated and expensive undertaking that, however, provides the necessary validation of the simple two-dimensional contour analysis technique.

We have been the first to investigate the true three-dimensional (3D) growth pattern of otoliths by the new technique of X-ray microtomography, a technique applied previously to, for example, detect internal crystal faults in diamonds. A substantial number of otoliths of different species (anchovy, cod, turbot and eel) and of different ages have been measured in three dimensions by this new technique and one of the visible results are a series of three-dimensional large plastic models of otoliths which can now be used for demonstration/education purposes. We had hoped to even see the internal growth rings by this new technology which would have allowed us to – in three dimensions – picture the full growth history of a *single* otolith. The (internal) annual rings of the otoliths, however, yielded no contrast in the three-dimensional X-ray density distributions and thus the three-dimensional growth information that has been visualised stem from different individual otoliths. We thus augmented the three-dimensional data by measuring a three-dimensional stack of otolith sections imaged with a light microscope. The annual growth rings are clearly visible in these optical measurements. From all three-dimensional data collected, two-dimensional (2D) contour data could be generated similar to the contour data obtained directly

from digitising otolith images. The 3D data collected have all been entered into a 3D shape database, which is now available for distribution to the scientific community.

An extensive set of software tools and methodologies has been developed for 2D contour analysis of otoliths. In contrast to most such analyses, our techniques retain the phases of the complex Fourier descriptors and not just their amplitudes. The analysis thus implicitly includes the relative alignment of the otoliths with respect to each other allowing for the positions of contour details to enter into the computational analysis and not just their mere presence. Our unbiased automatic classification of contours represents a robust method for the 2D otolith shape analysis, which exploits virtually all information present in the contours. A total of 68 complex, normalised Fourier descriptors proved to be sufficient for the shape classifications.

In order to maintain reproducibility in recording 2D images of otoliths in all collaborating laboratories, we first designed and assembled an "otolith workstation" capable of handling the wide range of sample sizes at hand. The otolith workstation hardware and software components were used successfully for collecting the images that form the first input for the shape databases. Otolith shape databases were created from anchovy, cod, eel and turbot otoliths, and they contain a total of about 7000 otolith images. The images have all been converted to contour information using the newly developed algorithms and these contours plus other extra information have been incorporated into each entry in the databases, which have now been made available to the scientific community.

For cod, the otolith shape analysis was found to yield reliable additional age information. There are indeed very characteristic otolith shapes for young and old cod. When shape information was included, our automatic classification schemes yield about 95% correct classifications on individual fish. In this case, however, the simplest age prediction scheme based on otolith weight alone, already gives scores of up to 87 % correct classifications on individual fish.

For eel, the variability in otolith shapes among individuals of the same age is very high and this usually is a limiting factor, which largely obliterates the possible shape variations as function of fish age. From otolith shape alone (i.e. without including otolith size or weight) age could be predicted correctly for only less than about 1/3 of all individual eel samples; whereas when using otolith size alone, the predictive power is already much better. Eigenimage decomposition showed that the shapes of eel otolith are indeed highly variable and that these variations are not age-related.

From the analysis of a limited turbot data set (only including ages 400 days to 800 days old juveniles) we can conclude that in this age range the age-shape relation is rather weak and that shape analysis is not directly suited for ageing. This conclusion cannot be extended to turbot of all ages where the predictive power of the analysis could be much better (but no data was available for testing). Traditional ageing of juvenile turbot based on otolith annuli readings will probably provide the better results.

For anchovy the main result is that a shape-age relation is clearly visible but it cannot be used for reliable ageing of individual fish. The many shape analysis tools developed unambiguously reveal small trends in the development of shape as function of age, but they fail to provide a practical ageing strategy.

For all four targeted species we found that the size factor (like the physical length or the surface area of the otolith) was a more powerful predictor of age than the pure shape of the otoliths. The significance of otolith contour shape, for age prediction, increased from eel, over anchovy, to cod. In conclusion, the assumption that pure otolith shape information, disregarding other easily accessible information such as otolith length or weight, is sufficient for age measurement of an *individual* fish is not correct. This situation can change completely when otolith shape can be used in connection with information on fish body size and otolith size, to estimate the age. Moreover, one is often not necessarily interested in the age of each individual fish (to a precision of +/- 0.5 years), but rather only interested in the distribution of the ages in a population in the context of stock assessment. Otolith shape analysis could still make a significant contribution on that larger scale.

## 2. EXECUTIVE SUMMARY

### 2.1. Introduction

#### Task 1 Otolith data of fish of known age

In order to investigate the hypothesis that age in fish is expressed in the two-dimensional (2D) and three-dimensional (3D) shape of the otolith, a large number of otoliths was required. The objective of this task was to collect and scan known and unknown age individuals of cod, eel, turbot, salmon and sea-trout in order to investigate the relation of age and possible effects of origin, sex, size and environment on otolith shape. The images achieved were together with relevant background data delivered to tasks 2 and 3 and constituted the basis for a database on otolith contours.

Otolith weight was introduced as another variable, since the results indicated that otolith shape as such was not sufficient to reliably describe the development of otoliths in relation to age.

#### Task 2 Two-dimensional methodology development

The basic working hypothesis underlying the project was that fish age information is coded in the 3D otolith shape and internal density distribution. Although the 2D shape of an otolith lying flat on a support table is inferior to the 3D density distribution it was expected that the much easier accessible 2D shape contains enough information which could be used for reliable age determination using multivariate statistical analysis and pattern recognition.

All software development of this project was done within the context of the image processing system IMAGIC-5 which is background of Image Science.

#### Task 3 Three-dimensional methodology development

The full growth history of otoliths is reflected in their three-dimensional growth increments. Thus the 3D aspects of otoliths were measured to be able to validate the 2D techniques and to cross check the implicit assumptions made in the 2D analyses. 3D software development was performed in close collaboration with the work done in task 2.

To get the three-dimensional densities of otoliths X-ray micro tomography as well as light microscopy of successive sections of the otoliths were used.

#### Task 4 Application to another economically important species

Known age reference data were not be available for all species concerned. It was thus crucially important to design a strategy of age determination for economically important fish without resorting to known-age fish for a calibration of the procedures. The idea in the project proposal was to exploit the experience gained with species for which a known-age reference data set was available for ageing Adriatic anchovy (*Engraulis encrasicolus*). For calibration of age, in the absence of a known-age reference data base, conventional annulus-counting techniques were performed. The

accuracy of the annulus-counting age determination was increased by additional validation studies which included daily increments counts.

## 2.2. Results

### Task 1 Otolith data of fish of known age

Otoliths of known and unknown age were collected from cod, eel, turbot, salmon and sea-trout. A total of 9,390 otoliths was acquired. From the cod, eel and turbot materials three databases including silhouette images and corresponding background data on individual fish (age, length, weight, etc.) were stored on CDs which will be made available to interested researchers.

During the course of the project we experienced that due to time and financial constraints salmon and sea-trout of known age had to be given lower priorities. They were difficult and very expensive to achieve in appropriate numbers. Thus most work was devoted to cod and eel otoliths. For similar reasons the remaining otolith materials collected from salmon and sea-trout could not be utilised further within the project. That material is now stored at IFRD.

In order to compare our method of ageing with the traditional methods a subsample of 260 cod otoliths were sent around to different laboratories for traditional ageing. Also eel otoliths from one of the lakes were sorted into the three possible age classes by traditional ageing before being used for the database.

#### *Deliverables*

Selected cod otoliths and background information were acquired, scanned and delivered to task 2 and 3.

Selected eel otoliths and background information were acquired, scanned and delivered to task 2 and 3.

Selected salmon, sea-trout and turbot otoliths and background information were acquired, scanned and delivered to tasks 2 and 3.

### Task 2 Two-dimensional methodology development

The first task was to design and assemble an "otolith workstation" which could be used for imaging otoliths, for subsequent image analysis and the development of the fish ageing methodology. Every otolith workstation consisted of a PCs with a stereo-microscope equipped with a digital camera. The otoliths were placed on a glass plate and silhouette pictures of the otoliths were taken using transmitted light. The otolith workstations worked excellent and were used by partners 1-3 during the whole project.

For subsequent image processing we used the IMAGIC-5 image analysis system and developed additional algorithms specific for the tasks of the project. The otolith images were binarised and subjected to filters (a combination of morphological operators) yielding a black-and-white binary image containing one single object. Automatic object finding and contour detecting algorithms

were applied to finally get normalised discrete Fourier descriptors (NFDs) of closed contour lines around the otoliths.

Classification was done on both, the NFDs and the binarised images using multivariate statistical classification techniques implemented in IMAGIC-5. The analyses were performed using various data-sets of cod, eel, turbot and anchovy otoliths. Reproducibility test showed that the experimental errors in imaging and image processing were extremely small.

Although the 2D shape analysis indicated some trends, the results which we obtained during the project unfortunately did not suggest that age is strongly correlated to the overall 2D shape of the fish otoliths. Neither single NFDs or eigenimages nor the overall 2D shape of otoliths could be used to reliably age single fish as was expected by the original project hypothesis. This is obviously due to the erroneous biological hypothesis and not because of methodological problems.

Tools to support traditionally annulus counting were implemented into IMAGIC-5 but since the project hypothesis, that the overall 2D shape of otoliths and fish age are closely related, could not be verified this validation task did not become so much important as it was expected in the proposal.

The otolith contour images as well as additional information were stored on the CDs containing the “2D” databases.

### *Deliverables*

Month 3	Image Science software package IMAGIC-5 implemented on the target computer.
Month 5	Start of otolith data-bases.
Month 5	Modification of existing IMAGIC-5 programs to be suitable for 1-D images (Fourier descriptors) started.
Month 6	Preliminary workstation assembled.
Month 12	Preliminary algorithms for automatic 2-D contour detection implemented into IMAGIC-5.
Month 12	First algorithms for supporting annulus counting implemented into the MORFO command of IMAGIC-5.
Month 18	First data-base of 2-D contours.
Month 18	First version of 2-D contour-analysis software implemented into IMAGIC-5.
Month 18	First classification results.
Month 18	First version of classification software.
Month 24	Importance of the size factor tested.
Month 24	Different weighting schemes for size versus shape descriptors tested.
Month 24	Refined data-base of 2-D contours.
Month 24	Refined algorithms for automatic 2-D contour detection.
Month 24	Refined classification.
Month 24	Validation of 2-D contour classification results with results of traditional ageing methods for turbot, eel, cod and anchovy.
Month 24	First version of the annulus counting software.
Month 24	First improvement of the otolith workstation.
Month 30	Refined versions of the contour-analysis software distributed for all species.

Month 30	Refined versions of the classification software distributed for all species.
Month 30	Refined versions of the software distributed for all species.
Month 36	Updated IMAGIC-5 contour-analysis software including updated digitisation tools on CD. Updates distributed to all partners.
Month 36	Refined data-bases for cod and eel (together with Partner 1).
Month 36	Updated IMAGIC-5 classification software on CD. Updates distributed to all partners.
Month 36	Eigenimage analyses of 2-D otolith contours for cod.
Month 36	Updated IMAGIC-5 software on CD. Updates distributed to all partners.
Month 36	Second improvement of the otolith workstation and its software.
Month 42	Final algorithms for automatic 2-D contour detection.
Month 42	Final classifications of 2-D shapes.
Month 47	Final user feed-back for all software developed within the project.
Month 47	Final data-bases of 2D contours.
Month 48	Distribution of the final version of the otolith workstation software and the final database.

### Task 3 Three-dimensional methodology development

3D image processing and methodology developments included 3D analyses for cod, eel, turbot and anchovy, the creation of otolith models, 2D/3D cross validation and the creation of 3D databases on CDs, which will be made available to the public.

One of the main tasks was to obtain the 3D density distribution of the otolith growth pattern. Although the X-ray micro-tomography technique has proven to be a valuable tool in visualising the outer 3D surface of the otolith, attempts to visualise the internal structure using this technique have been unsuccessful due to the lack of X-ray contrast in the annuli structure.

However, using light microscopy images of 2D slices of a cod otolith which was also imaged with X-ray tomography we were able to link 3D shapes and 2D cross sections of otoliths and to thus map the growth rings in three dimensions. A number of critical tests showed that we have good reproducibility for both the imaging procedures and the subsequent 3D image reconstruction and 3D shape analysis.

#### *Deliverables*

Month 12	First 3D-reconstructions available
Month 18	First rapid prototyping models based on 3D-reconstructions
Month 24	First version of 3D software for evaluation of 3D annuli structure from light microscopy sections
Month 24	First 3D density distribution of the internal structure of an otolith
Month 30	Cross validation of 2D and 3D technologies for known age fish
Month 36	First extended 3D database of all scanned otoliths on CD ROM for internal use
Month 42	3D density distributions of otoliths
Month 46	3D rapid prototyping models of all species delivered
Month 48	Cross validation of 2D and 3D technologies for all fish

#### Task 4 Application to another economically important species

Ageing of anchovy from the Adriatic fishery by “traditional” annulus counting has been performed on about 3000 otoliths. The validation of the annulus ageing by means of daily ring counting encountered some difficulties applying the methodology for juvenile otolith to adult fish. It proved to be not feasible to obtain reliable daily increment definition in samples of anchovy larger than 60-70 mm which are still juveniles.

New images of anchovy otoliths were cross checked and added to the final database, in order to have a better balance in the age classes. A final CD of the anchovy data base was created.

Images of anchovy otoliths were used during the whole project to develop the 2D analyses algorithms and to test the project hypothesis with all methods of task 2. We investigated the possibility to age individual anchovy by 2D shape analysis as well as the possibility to distinguish different landing sites by 2D shape differences. Results were not positive in either cases. The individual variability seems to be too high and the general shape variation (round to elongated) is not sufficient to properly determine age classes. Failure in detecting different “putative” stocks could be due to lack of geographic variability in otolith shape of Adriatic anchovy.

#### *Deliverables*

Month 6	Existing otoliths delivered for scanning
Month 12	Complementary otoliths acquired through fishing, scanning of otolith collection initiated, refined annulus counting initiated
Month 24	Scanning of most otoliths finished
Month 24	3D scanning of selected otoliths
Month 30	Test of ageing-software on “known-age“ otoliths initiated, refined annulus counting finished
Month 36	Test of ageing-software on “known-age“ otoliths finished

### **2.3. Discussion - Conclusion**

#### Task 1 Otolith data of fish of known age

The work on the collection of known age otoliths was planned only for the first three years. However, it was worthwhile to extend this work into the last year and to complete the collections.

Eel of known and unknown age were collected by fishing with fyke nets in four lakes. Otoliths from recaptured and pen caged cod were available in the Faroes and also from recaptures in the commercial fishery. Turbot was sampled in the Kattegat.

Work on the salmonids and to a certain degree also on turbot was given lower priorities in order to put most efforts into cod and eel otoliths. Also the eel otoliths of unknown age were left outside due to time and financial constraints.

## Task 2 Two-dimensional methodology development

From a methodological perspective, we have developed shape analysis tools which can be directly applied for various tasks in fish biology. Our unbiased automatic classification of contours represents a robust method for the 2D otolith shape analysis which exploits virtually all information present in the contours. Whereas we found that the correlation between age of a fish and its otolith shape may not - for all species - be used for directly ageing each individual, the approach may in combination with otolith size frequency analysis employed for precisely estimating the age structure of a fish population determined from large samples of otoliths. Our methodology for 2D otolith shape analysis may also be applicable for other tasks in fish biology (stock discrimination analysis, phylogenetic studies, indices of fluctuating right and left asymmetry for detection of environmental stress etc.).

Even if a fully automated ageing workstation is currently out of our reach we can at least offer one of the most efficient shape analysis tools available on the market.

## Task 3 Three-dimensional methodology development

One of the main tasks was to obtain the 3D density distribution of the otolith growth pattern. Although the X-ray micro-tomography technique has proven to be a valuable tool in visualising the outer 3D surface of the otolith, attempts to visualise the internal structure using this technique have been unsuccessful due to the lack of X-ray contrast in the annuli structure. However, using the combination of X-ray micro-tomography and light microscopy of sections of the same otolith, we have been able to link 3D shapes and 2D cross-sections of otoliths and to thus map the growth rings in three dimensions.

## Task 4 Application to another economically important species

As far as age is concerned otolith shape analysis on anchovy showed that the only signal detected is a general change from round to elongated shape from young to old individuals and a modulation in the region of the gap between rostra from less to more indented. Individual variability appears to be very large. Thus the possibility to use this shape changes to accurately age individual anchovy seems remote. Also the investigation on the possibility of distinguishing anchovy from different areas in the Adriatic, based on otolith shape, has been unsuccessful. A large variability in shape was found but no classification, even considering only one specific age class, was able to discriminate in a reliable way between the two different landing ports (i.e. fishing grounds).

### 3. INTRODUCTION

Age determination of fish is a basic activity of major importance for calculation of mortality rates in fisheries stock assessment as well as estimating vital statistics in fish biology and ecology.

It has been estimated that more than one million fish are individually aged annually (Campana and Thorrold, 2001). High fishing mortalities and thus low expectancy of life time duration in many fish stocks world wide makes a precise and accurate determination of age compositions vital for the estimation of the state of the stocks and thus for a sustainable exploitation. Errors are usually considered in two categories 1) accuracy i.e. bias in relation to true age and 2) precision i.e. reproducibility in relation to repeated measurements.

Since errors in age determination from both categories in different ways influence parameters used in stock assessment like spawning stock biomass, fishing mortality, and recruitment (Reeves, 2001), the development of objective and robust ageing methods has been the goal of a number of studies (see: (Campana, 2001)).

#### **Otolith growth mechanisms and relation to age of fish**

Some of the most widely used structures for age determination in fishes are the otoliths (ear stones). The otoliths are solid calcareous bodies situated in otic sacs in the inner ear labyrinth in both sides of the brain cavity. These structures function both in the auditory system that detects sound waves and in the vestibular system which enables the organisms to detect tilting and acceleration and thus to maintain balance. Traditionally, seasonally varying optical density of accreted otolith material has been employed to count the annual number of growth zones and thereby to give an estimate of the individual age in years. In the literature, the term "otolith" is often used to describe any one of the three pairs, sagitta, asteriscus, and lapillus, but in most species the *sagitta* is the largest otolith and has most often been used in age estimation, however it is important to define this in any study. Besides for age information otolith morphology has also been studied in connection with identification of species (Hecht and Hecht, 1979) and the geographical variations in fish populations (Messieh et al, 1989; Castonguay et al, 1991; Campana and Casselman, 1993; Friedland and Reddin, 1994).

Otolith calcium carbonate is in the form of twinned aragonite, although abnormal crystalline otoliths are composed of calcite (Morales-Nin, 1985) or vaterite (Gauldie, 1986). Calcium reaches the endolymph primarily from the blood plasma (Kalish, 1989; 1990; 1991; Wright et al., 1992). Otolith calcification is rate-limited by the number of nucleation sites provided by the insoluble matrix (Crenshaw, 1982; Mann et al., 1983) as well as by physico-chemical conditions at the otolith surface. The rate of insoluble matrix production will therefore be the ultimate determinant of the rate of otolith calcification (Saitoh and Yamada, 1989; Wright et al., 1990). This matrix is also a significant factor controlling the shape of the otolith (Degens et al., 1969; Dunkelberger et al., 1980; Mugiya, 1987; Gauldie, 1991; Zhang and Runham, 1992; Gauldie, 1993; Payan et al., 1999). As in mollusc shell, otoliths possess a soluble proteinaceous matrix that is capable of regulating the rate of mineral deposition (Wright et al., 1991). Variations in the rate of production of this protein may therefore regulate the rate of mineralisation. The less soluble otolith matrix is composed of a collagen-type protein (Degens et al., 1969). The matrix is more dense in the early development phase and its amino acid composition changes with age (Morales-Nin, 1986a; 1986b).

For most fish species, otoliths have been the most reliable indicators of age by counting their annual and, for younger fish, daily patterns which form a permanent record of life history events (Campana 1999). However, consistent age readings requires, depending on the species, a highly experienced reader and the criteria for determining age needs two or more age-readers to verify the age assigned to an individual fish. As a matter of fact, this makes the otolith age reading method highly subjective. Consequently, agreement among readers (i.e. precision) rarely exceeds 90% and is usually much lower (e.g. Kimura and Lyons, 1991). Moreover, the methods are expensive and time-consuming. The increased complexity in the otolith preparation for precise age estimation (see: (Bedford, 1983)) may make the traditional ageing techniques economically infeasible when a large number of individuals have to be aged (Cardinale et al., 2000).

Several authors have investigated if alternative methods can overcome the problems linked with the subjectivity and high costs of otolith reading technique. In particular, the use of otolith weight as a proxy of age has been advocated (e.g. (Boehlert, 1985; Pawson, 1990; Radtke et al., 1990; Fletcher, 1991; 1995; Wilson et al., 1991; Worthington et al., 1995; Fletcher and Blight, 1996; Cardinale et al., 2000; Cardinale and Arrhenius, 2002)). These studies found that otolith weight explained between 70 and 90 % of variability in fish age (cited from Araya et al., 2001).

It is also known that the external structures like shape and other morphometric features of the otolith reflect the actual growth stage being mainly influenced by sex, age, year-class, stock and environment (Casselmann et al., 1981; Castonguay et al., 1991; Lombarte and Lleonart, 1993; Begg and Brown, 2000). Castonguay et al. (1991) stated that differences in otolith shape are due to the age effect rather than to stock differences.

The idea of the FAbOSA project was to use this assumption that age in fish is expressed in the two-dimensional (2D) and three-dimensional (3D) shape and density distribution of the otolith. The project hypothesis even expected that the much easier accessible 2D shape contains enough information to be used for reliable age determination using multivariate statistical analysis and pattern recognition. This method should subsequently be developed to become a fast (hence more economic) and reliable method for ageing of fish than traditional annuli counting. In order to distinguish among ages and to eliminate any bias due to age reading procedures the FAbOSA project was mostly working with otoliths of known aged fish.

## **The project approach**

Traditional counting of annual growth structures relies on the fluctuating contrast in internal optical density of the seasonal accretions. A dynamic manipulation of the illumination is often needed for the identification of annual structures that may change or even shift in phase with increasing age. The development of objective, reproducible and precise methods for age determination demanded the construction of a set-up that was optimally independent of the operator.

Otoliths were scanned using a standard protocol for acquiring the pictures with the "Otolith Workstations" designed for the project. The Otolith Workstations consist of a PC with a stereomicroscope equipped with a digital camera. The otoliths were placed on a glass plate and a silhouette picture of the otolith was taken using transmitted light. The images were binarised and subjected to a combination of morphological operators yielding a final black-and-white binary image containing one single object. An edge-finding algorithm was applied to obtain the closed contour line (Kastowsky et al., 2002a). The resulting closed-contour was interpolated and transformed into the corresponding Normalised Fourier Descriptors (NFDs) (Wallace and Wintz,

1980). Although it is possible to analyse contours by various methods like Artificial Neural Networking, direct pattern recognition etc. the FAbOSA project was working with Fourier descriptors because they provide a standardised reproducible method with a high degree of transparency of the results (Kastowsky et al., 2002b).

In the following part we give some information on the species which were used in the FAbOSA project.

## **Cod**

Atlantic cod is a fast growing benthic fish species of great importance to most fisheries in the North Atlantic. Although cod are often comparatively easy to age by traditional methods, counting annuli in the otoliths, the amounts of otoliths required to be aged every year in e.g. assessment work makes alternative methods attractive. Shape analysis of cod otoliths might be a fast and objective ageing method. However, shape is influenced by sex, age, year-class, stock and environment (Casselmann et al., 1981; Castonguay et al., 1991; Lombarte and Leonart, 1993; Begg and Brown, 2000). By using a material of cod from two stocks from the Faroes (Faroe Plateau and Faroe Bank), both divided in a reared and a released portion, we aimed at distinguishing the importance of the different influences mentioned above.

## **Eel**

Eels are difficult to age, becoming very old after a long, but slow growth. Their otoliths are also relatively small compared to other species and thus the yearly growth increments are small and densely packed (Berg, 1990; Panfili and Ximenes, 1994; Poole and Reynolds, 1996). Different methods are used when ageing eels. In recent time only the otoliths (*sagittae*) are used. Most often eel otoliths are aged by counting annuli after grinding and polishing in a sagittal or transverse plane. There is also a “burn and crack” method, where the whole otolith is burned in a flame and then divided along the transverse plane before counting the annuli (Moriarty, 1973; Hu and Todd, 1981; Graynoth, 1999).

All these methods are laborious and quite time consuming. After the preparation of readable otolith samples the interpretation of the different structures is still a difficult task as true annuli are difficult to distinguish from false checks. This requires time and much experience (Panfili et al., 1994; Svedäng et al., 1998). An experienced eel otolith reader gave an estimate of eight eels aged per day (40/week) (Reizenstein, personal communication.). This estimate includes the total amount of time spent on age determination, from preparing the sample for storage, cleaning the otoliths and recording data in electronic format. A more objective and fast method for ageing of eels should be of great importance, making age and growth studies more easy to perform. With more and better knowledge on this highly variable species, the management of the European eel as well as indirectly of other eel species (e.g. the American and the Japanese eels) could be considerably improved.

The main ideas behind the FAbOSA project actually originate from a study on eel otoliths of known age by Doering and Ludwig (1990) and Doering et al. (1992). Growth rates, sex ratios and recapture rates were some of the parameters studied. Several stocking studies of that kind were commenced in Sweden in 1979 and during the early 1980's (Wickström 1984; Wickström et al., 1996). The FAbOSA project took advantage of already existing otolith material from such lakes and additional materials were collected within the project by test fishing. Eels otoliths were also

collected from two bays in the huge Lake Mälaren where young eels had been stocked in more open environments.

### **Turbot and anchovy**

In order to cover as wide as possible an array of taxonomical and ecological differences in fish, two additional species were chosen to investigate the age-shape relationship. Turbot (*Scophthalmus maximus*) of the North Sea and the Baltic Sea and anchovy (*Engraulis encrasicolus*) of the Adriatic Sea could be considered a kind of ecological opposite for many aspects. First of all the Baltic and the Adriatic, although they share some common features such as low salinity, shallow depth, land-enclosed seas, pollution problems due to high antropisation of the surrounding land, are conversely quite diverse in latitude and therefore in climatic characteristics. Moreover turbot is a slow growing, long lived, benthic fish. An ichthyophagous predator, with no schooling behaviour, and with a very well determined and relatively short spawning season, it has left-right asymmetrical opaque otoliths thus with a high protein content. Anchovy is a fast growing, short-lived pelagic fish, with a definite schooling behaviour, feeding on planktonic crustaceans. Anchovy has a long spawning season (more than 6 months) in the Adriatic, its otoliths are symmetrical and transparent (protein poor).

Otoliths samples of turbot and anchovy were processed in a similar way but with different final aims. Turbot otoliths from reared individuals were used to compare the predictive value of otolith size and shape in ageing of this species. So turbot was used to investigate on the methodological side while anchovy otoliths were used to test the applicability of the methodology to large-scale samples in a routine stock assessment perspective.

### **Salmon and sea-trout**

Otoliths from salmon and sea trout of known age were collected within the FAbOSA project. However, due to unforeseen conditions it was very difficult and expensive to achieve the required and balanced number of samples from the wild adult salmonids. Therefore the work on salmonids was stopped after the otoliths were prepared. In that way more time and efforts could be devoted to the other species. The salmonid otoliths of known age are now stored at the Institute of Freshwater Research, Drottningholm.

## 4. MATERIALS AND METHODS

The project Fish Ageing by Otolith Shape Analysis is founded on well selected otolith collections for a number of species. The description of these input materials therefore constitutes the 'Materials' subpart of this chapter. The basic methods applied will be summarised. We kept these descriptions as short as possible because we would prefer to give deeper introductions into the specific methods whenever referred to in the 'Results' part of this report. We like to note that part of the information on the otolith samples will again be presented in the respective 'Results' section for the shape databases, however, in slightly different context.

### 4.1. Sampling of otoliths

#### 4.1.1. Sampling of cod otoliths

The Fishery Laboratory of the Faroes and the Aquaculture Research Station initiated an enhancement programme for Atlantic cod in 1991 because the fishery collapsed in 1990 due to a substantial stock decline (Jakupsstovu and Reinert, 1994; Fjallstein and Jakupsstovu, 1999). Pre-spawning cod individuals were caught using bottom trawls when the fish were assumed to be in or near their spawning grounds (Fig. 4.1.) on the Faroe Bank (1991-1993) and the Faroe Plateau (1992, 1994) representing two discrete spawning (Jakupsstovu and Reinert, 1994).

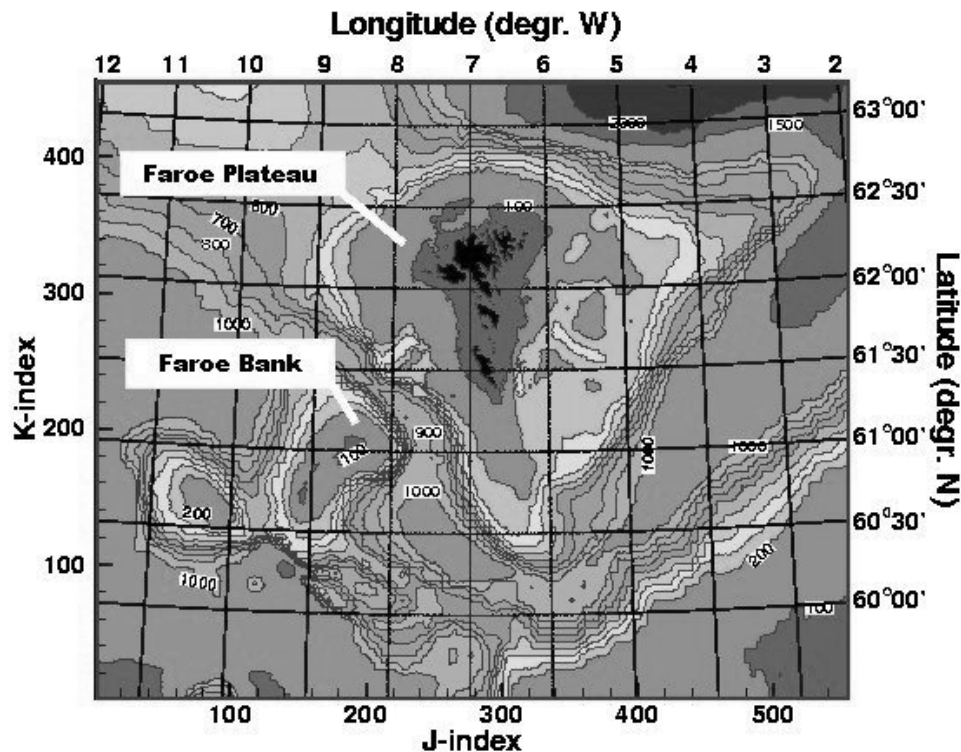


Figure 4.1. Faroe Bank and Faroe Plateau

Cod individuals from the two stocks were reared in pen cages and fed three times a week with chopped herring (*Clupea harengus*) and sprat (*Sprattus sprattus*). Binding flour was added, but no colour. They were tagged and kept near the sea surface in three separate cages, which consisted of floating rings mounted with common nets with a depth of approximately four and a diameter of eight meters. Cod individuals from the Bank and the Plateau were mixed in all 3 cages, approximately half Bank and half Plateau in each cage. Each year, sub-samples were taken between January and April. 49,992 of age 1 individuals were released from Faroe Bank in 1994 and 1995 (Tab. 4.1.) and 8,408 from Faroe Plateau in 1995 (Tab. 4.2.) while initially 3,500 from the Bank and 3,000 from the Plateau were kept in pen cages until spring 2000. Individuals from Faroe Bank pen cage (FBP) and from Faroe Plateau pen cage (FPP) constituted two separated stocks reared at the same growing conditions (temperature and food intake) while recaptured individuals from Faroe Plateau (FPR) were the wild counterpart. For each fish, sex and maturity were evaluated by macroscopic examination of the gonads, total fish length and wet weight were recorded to the nearest 1-mm and to the nearest 1-gram respectively. Area of sampling (Bank or Plateau) was recorded for each fish collected (Fig. 4.1.). Otoliths (sagittae) (both left and right) were removed from each individual sampled and stored in dry envelopes for shape analysis. For FPR individuals, length was not always available since for tagged fish captured by professional fishermen often the otolith only was delivered.

Hatching period	Apr. 93	Apr. 93	Apr. 94	Apr. 94	
Average length at release (cm)	19.4	23.1	18.9	24.6	
Average weight at release (g)	79	130.7	76.3	175	
Release date	3 Feb. 1994	9 June 1994	9. Feb. 1995	7. July 1995	Sum
Released cod	9,991	11,939	14,970	13,092	49,992
	Recaptured cod				
1994	0	13	0	0	13
1995	2	6	0	3	11
1996	0	8	2	13	23
1997	2	19	9	56	86
1998	2	36	8	52	98
1999	3	5	3	11	22
2000	0	2	0	5	7
2001	0	0	0	1	1
Sum	9	89	22	141	261
Unknown year recaptured	1	10	1	9	21
SumAll	10	99	23	150	282

**Table 4.1. Faroe Bank cod release and recapture**

Hatching period	Apr. 94	Apr. 94	
Average length at release (cm)	24.2	31.2	
Average weight at release (g)	145.9	392	
Release date	29. June 1995	19. July 1995	Sum
Released cod	2,698	5,710	8,408
Year	Recaptured cod		
1994			0
1995	73	110	183
1996	117	454	571
1997	63	147	210
1998	15	49	64
1999	3	4	7
2000	1	3	4
2001	0	1	1
Sum	272	768	1.040
Unknown year recaptured	2	14	16
SumAll	274	782	1.056

**Table 4.2. Faroe Plateau cod release and recapture**

#### 4.1.2. Sampling of eel otoliths

In addition to an already available collection of known age otoliths, eels were collected by test fishing from Lakes Frisksjön and Ommen among other lakes and sites. Both lakes are medium-sized (c. 300 ha), mesotrophic and situated close to the Baltic Coast in Southeast Sweden. The lakes were essentially free from eels when stocked with young eels of homogenous size and age (glass eels, elvers). Most eels caught during the years after stocking were considered to be from the stocked batch and thus of known age. Test fishing for eel was done during early summer according to an informal standard procedure using paired fyke nets (summer fykes) which are normally set perpendicular to the shoreline in chains of eight pairs (Moriarty, 1972; Wickström et al., 1996). This fishing gear was emptied about twice a week and the catch of unit effort was expressed as numbers and weight per fyke net cod end fished for one night. The eels caught were deep-frozen as close in time to the catch as possible and kept there until transport to the institute. After thawing length and weight were measured before the otoliths were prepared from the inner ears of the eels. The *sagittae* were cleaned manually and with ethanol before stored in paper envelopes or plastic tubes. During the course of FAbOSA it was decided also to weigh the otoliths. This was done on an electronic 4-digit balance (Sartorius Basic BA110 S). Both weighing and the scanning for images required very clean otoliths and therefore ultrasonic cleaning was introduced as a standard procedure.

## Selection of eel otoliths for scanning

### Lake Frisksjön

For the purpose of age analysis, otoliths taken from known age eels caught in Lake Frisksjön were selected for 2D-shape analysis. Older materials as well as eels caught for the purposes of the FAbOSA project were selected for digital scanning. Five (5) year classes (i.e. eels caught in 5 different years) were included in the analysis. The aim was to get a wide range of ages from young to old. Both left and right otolith were scanned except for eels caught in 1984 and 1985, where only one side (left or right) was available. Only yellow females were selected. Vaterite otoliths were excluded from the data set intended for further analysis.

With the exception of eels caught in 1992, all available otoliths were used from each year class. The otoliths from the catch in 1992 were selected at random from a larger material.

Lake	Stocking	Catch	Age	N	N individuals	Usable for analysis
Frisksjön	1979	1984	5+	8	8	6
	1979	1985	6+	18	18	18
	1979	1990	11+	148	74	140
	1979	1992	13+	188	94	186
	1979	1998	19+	180	90	164
Ommen	1979, 1984, 1989	1996	7+ or 12+ or 17+	284	142	282

**Table 4.3. Eel from Lake Frisksjön and Lake Ommen**

### Lake Ommen

Otoliths from Lake Ommen eels were selected for scanning to compare similarly aged eels from different lakes. (2D-shape analysis of same age otoliths with respect to environmental conditions (lakes)). Eels caught in 1996 were used. The thought being that we could obtain suitable numbers of the respective cohorts (age classes) from this material, 7+, 12+ and 17+ for comparison with lake Frisksjön eels of 5/6+, 11/13+ and 19+ respectively. A sample of 142 eels was selected at random from a larger sample. Like in Lake Frisksjön, only yellow females were selected and all vaterite otoliths were excluded. Both left and right otoliths were scanned for all eels/individuals.

### Traditional ageing of selected eels

To verify expected ages, eels were traditionally aged. For eels/otoliths originating from Lake Frisksjön, random samples of approximately 15% per age class of selected/scanned individuals were selected for the first round of age validation/determination. This was done after scanning for 2D contours. All eels smaller than 470 mm were also included from 1998, because it was suspected that eels of different origin and age might be in the lake. After findings of unknown origin eels in the 1998 material, a second set of eels were aged to minimise the risk of contamination. All eels < 550 mm were now aged. Eels of ages deviating from the expected age were excluded from further analysis.

Lake	Stocked	Catch	N aged	Exp age	# deviates	N scanned	N individuals
Frisksjön	1979	1984	2	5+	1 (8591)	8 (5L, 3R)	8. All diff
Frisksjön	1979	1985	2 (11.1%)	6+	0	18 (10L,8R)	18. All diff
Frisksjön	1979	1990	13 (18%)	11+	0	148	74 (pairs)
Frisksjön	1979	1992	16 (17%)	13+	0	188	94 (pairs)
Frisksjön	1979	1998	17 (19%)	19+	5	180	90 (pairs)
Frisksjön	1979	1998	8 (9%)	19+	3		

**Table 4.4. Traditionally aged eel from Lake Frisksjön**

For eels from Lake Ommen all otoliths intended for shape analysis were aged traditionally in order to classify them with respect to one of three stocking occasions. Classification was done using expected ages of the three age classes  $\pm 2$  years as grouping boundaries (Tab. 4.5.). At random 142 eels from the 1996 test fishing were selected for scanning and subsequent ageing.

There was no way of anticipating exact sample sizes of the different age classes/stockings. However, based on previous experiences, we expected a majority to be from 1979 and 1984 stockings in roughly equal sizes and a smaller portion to be from the stocking made in 1989.

Lake	Stocked	Year of catch	Expected age	N after ageing	Grouping interval
Ommen	1979	1996	7+	9	Estimated age $\leq 9+$
Ommen	1984	1996	12+	117	Estimated age 10+ - 14+
Ommen	1989	1996	17+	16	Estimated age $\geq 15+$

**Table 4.5. Age grouping of eel for Lake Ommen**

### Procedure of traditional ageing

Left side sagittal otolith was placed on a microscope slide with sulcus side (proximate side) facing up. The otolith was embedded in polyester (Crystalbond mounting wax, Buehler, USA) and ground in the sagittal plane with a series of wet grinding paper (600-800-1200 grade) with a constant supply of water (Svedäng et al., 1998). Grinding was stopped when otolith primordium was reached. A stereo microscope (Panfili and Ximenes, 1992) was used for this. Finally the otolith was etched in a 1-% solution of Hydrochloric Acid (HCl) for 20-50 seconds and rinsed in water.

Age was determined from ocular otolith readings (Holmgren and Wickström, 1988). An otolith consists of slow growing hyaline zones (winter) and fast growing opaque zones (summer), forming annuli. Several transects from centre to edge were examined in order to observe the winter zones on several parts of the otolith cut and to exclude supernumerary zones. The age was

obtained by counting the number of annuli. Problems and uncertainties were noted. Otolith cuts were read using transmitted light microscope (Leitz Dialux 20) magnifications 10-40x. All otoliths were read at two or more times by one reader. In uncertain cases, the right side otolith was also used.

#### **4.1.3. Sampling of turbot otoliths**

Otoliths for comparison of variability in body length and otolith length were obtained from a set of otoliths sampled from the commercial fishery in the Baltic in 1988. The fish were aged using traditional counting of annuli. For the present study the first 100 otoliths (when available) of each age group (2-7 years) were used, which fulfilled the criteria of same ageing result by two experienced, independent readers, and both otoliths being available and intact. For each fish total length was measured to nearest semi-cm below. Length of the otoliths was measured to nearest 0.01mm using a microscope ruler. Age effect on fish of same length but different age was compared for the length groups 30, 31, 32, 33, 34, 35 and 36 cm where at least 20 individuals were available.

Turbot of known age were obtained from a rearing experiment. The turbot were reared from hatching until a size of approx. 5 cm at a commercial Danish hatchery (Maximus). The eggs originated from the North Sea stock used by Stolt Sea Farms, Øye, Norway for production of turbot larvae for aquaculture. To make them comparable all fish originated from one female and one male, which were reared together for the whole period. Fertilisation and egg incubation took place in Øye. Hatching date was 7 July 1992. The juveniles were transferred at age 3 days to on-growing at the Danish Institute for Fisheries Research, Hirtshals, Denmark. Rearing was conducted in 34□ seawater at ambient temperature in mesocosm on natural plankton for one month indoors. Then the fish were fed commercial turbot food pellets once a day. Age at first sampling was 371 days. From age 400 days to age 800 days samples of 25 fish were taken every second week. Samples were not taken at random, but individuals were selected between 10 and 20 cm to obtain individuals of same size but different age during the whole experimental period.

Total length was measured to the nearest mm-below. Both sagitta otoliths were removed and measured. The mean of the two values was used in calculations. Otolith length was measured to nearest 0.01mm using a microscope ocular ruler. Otolith area was measured in mm<sup>2</sup> with a planimeter and a microscope drawing board. Otolith length was registered with a precision of 0.01mm using a Cahn® microbalance. Otolith size (length, area and weight) was calculated as mean of the left and the right otoliths. For individuals where only one otolith was available, measured size was adjusted for mean difference between left and right otoliths. Only the length groups 13, 14, 15, 16, 17, 18, 19 and 20 cm, which contained at least 20 individuals, were included in the analyses.

Otolith images were produced with the aid of a video camera mounted on a dissection Wild M5 microscope at 12x magnification fitted with a Kappa BW PAL system video camera. Maximum contrast between otolith and air was obtained using transmitted light. Pictures contain information on sampling date, specimen no., dorsal/ventral, Total body length and wet weight. Wet weight measured on a Mettler electronic balance to nearest 0.01g. Otolith contours were obtained using the IMAGIC-5 picture analysis programme. Otoliths contours were classified in

groups, and the group classification related to age of the fish, according to the methods described in Kastowski et al., 2002b.

<i>Sampling dates:</i>	Dorsal	Ventral	Total
<i>13 July 1993 (age 371 days)</i>	18	18	36
<i>26 July 1993</i>	19	21	40
<i>09 August 1993</i>	18	19	37
<i>23 August 1993</i>	23	20	43
<i>06 September 1993</i>	20	23	43
<i>20 September 1993</i>	15	22	37
<i>04 October 1993</i>	17	22	39
<i>18 October 1993</i>	21	22	43
<i>01 November 1993</i>	12	22	34
<i>15 November 1993</i>	15	24	39
<i>29 November 1993</i>	18	23	41
<i>13 December 1993</i>	21	24	45
<i>27 December 1993</i>	17	24	41
<i>10 January 1994</i>	21	23	44
<i>24 January 1994</i>	14	21	35
<i>11 February 1994</i>	16	25	41
<i>28 February 1994</i>	21	24	45
<i>30 March 1994</i>	12	23	35
<i>18 April 1994</i>	17	21	38
<i>05 May 1994</i>	22	26	48
<i>23 May 1994</i>	16	22	38
<i>15 June 1994</i>	20	23	43
<i>26 June 1994</i>	14	24	38
<b>Total</b>	<b>407</b>	<b>516</b>	<b>923</b>

**Table 4.6. Sampling information for turbot**

#### **4.1.4. Sampling of anchovy otoliths**

Anchovy otoliths (sagitta) were routinely extracted from samples in the framework of an ongoing programme on stock assessment of small pelagic fish in the Adriatic. A monthly sample from each major landing port is taken, from this sample anchovy otoliths were extracted from a stratified sample of 5 fish for each 0.5 cm length class. Otoliths were cleaned and dry stored, the age was determined by standard techniques (Giannetti, 1985) using a dissecting microscope under reflected light and immersing the otolith in ethanol on a petri dish with a dark background. Around 70 to 80% of the otolith examined are currently successfully aged. From this set of aged otoliths, a sub sample of 1640 otoliths from Ancona (central Adriatic) and 1120 otoliths from Chioggia (northern Adriatic) and 120 otoliths from San Benedetto (central Adriatic) were chosen for the shape analysis study. They were divided into 5 age classes, from 0 to 5, and being couples of left and right otoliths they represent 820 and 560 and 60 fish respectively. Most of the otoliths

were collected in 1995 and, where it has been necessary to integrate with other years, years close to 1995 were chosen. All the otoliths were weighed by means of an analytical balance with accuracy of 0.1 mg.

## **4.2. 2D Methodology**

Otoliths were scanned using a standard protocol for acquiring the pictures with the "Otolith Workstations" designed for the FAbOSA project. The Otolith Workstations consist of Microsoft NT based PCs with an Olympus SZ9 stereomicroscope equipped with a Leica DC100 digital camera (1/2" chip). A 0.5 NA objective was used with a magnification of 6.3 x or 8 x. The otoliths were placed on a glass plate and a silhouette picture of the otolith was taken using transmitted light. These silhouette images were subsequently stored in a TIFF image file. Additional information about otoliths and fish was stored in ASCII text files with a specific FAbOSA format.

Each image was binarised and subjected to filters (a combination of morphological operators) yielding a black-and-white binary image containing one single object. An edge-finding algorithm is applied to obtain the closed contour line. The resulting closed-contour is interpolated and finally subjected to discrete Fast Fourier transform from which the associated Normalised Fourier Descriptors (NFDs) are obtained (Wallace and Wintz, 1980). About 2000 closed-contour sample points are extracted typically from each otolith image and these contours are interpolated to yield 4096 contour sample points compatible with the (Fast) Fourier Transform algorithm. The resulting complex Fourier coefficients are subjected to normalisation. The first most significant 128 complex Fourier coefficients were stored in the IMAGIC-5 header of the otolith image. Classification was done on both the NFDs and the binarised images using multivariate statistical classification techniques implemented in the IMAGIC-5 system (Van Heel, 1984; 1989).

All 2-D methodology was performed within the IMAGIC-5 image analysis system (Van Heel et al., 1996), which is distributed by Image Science (Partner 3). The object and contour finding algorithms as well as the classification methods used are described in detail in the results chapter.

## **4.3. 3D Methodology**

To obtain the outer shape as well as a precise image of the inner structure (3D density) a standard desktop X-ray microtomograph (Sasov and van Dyck, 1998) was used. A filtered back-projection algorithm was applied to calculate the 3-D densities from the X-ray projection images. Subsequent 3D image processing was performed with IMAGIC-5 (Van Heel et al., 1996). Large scale models of otoliths were created using standard rapid prototyping techniques. Details are reported in the results chapter.

## 5. RESULTS

### 5.1. Sampled otoliths

#### 5.1.1. Sampled cod otoliths

1,421 otoliths from known age and 805 from wild cod were weighed and scanned.

Species, category, stock	Number of otoliths
Cod, tagged and recaptured, Faroe Plateau	486
Cod, tagged and recaptured, Faroe Bank	51
Cod, pencaged, Faroe Plateau	478
Cod, pencaged, Faroe Bank	406
Cod, unknown age (traditionally aged)	805
<b>Total</b>	<b>2,226</b>

Table 5.1. Sampled cod otoliths

#### 5.1.2. Sampled eel otoliths

In total about 3,700 otoliths of known age were collected. From Lake Ellenösjön 225 eels (i.e. 450 otoliths) of unknown age were sampled (Tab. 2).

Due to time constraints and lack of personnel, only the otoliths from Lake Frisksjön and Ommen eels were considered for further analyses. These two eel populations were regarded to give the best opportunities to analyse and compare eel otoliths with the same background (geographical and genetical) but grown in two different environments.

From Lake Frisksjön some small individuals were suspected to be too young to come from the stocked batch. A subsequent check by traditional ageing did show they were of obscure origin and therefore they were omitted from the FAbOSA database. By analysing some of these divergent otoliths for their content of strontium and calcium it was confirmed they did not belong to the stocked batch of eels (Tzeng et al., 1997). As Lake Ommen was stocked three times (in 1979, 1984 and 1989) with young eels, traditional ageing was required to allocate the otoliths into the possible year classes.

Eventually, after several checks for mistakes and inconsistencies, images with adherent data from 514 otoliths from Lake Frisksjön eels and 282 otoliths from Lake Ommen eels were entered into the final Eel Database on CD. The distribution over different ages is given in Table 3.

<b>Species, category</b>	<b>Number of otoliths</b>
Eel, known age	2,700
Eel, known age, but mixed with fraction of unknown	1,000
Eel, unknown age	450
<b>Total</b>	<b>4,150</b>

Table 5.2. Sampled eel otoliths

<b>Lake</b>	<b>Age</b>	<b>Number of otoliths</b>
Frisksjön	5	6
	6	18
	11	140
	13	186
	19	164
Ommen	7	18
	12	232
	17	32

Table 5.3. Eel otoliths and age of fish

### 5.1.3. Sampled turbot otoliths

A total of 923 otoliths from cultured turbot were sampled and scanned.

<b>Sampling dates:</b>	<b>Dorsal</b>	<b>Ventral</b>	<b>Total</b>
13 July 1993 (age 371 days)	18	18	36
26 July 1993	19	21	40
09 August 1993	18	19	37
23 August 1993	23	20	43
06 September 1993	20	23	43
20 September 1993	15	22	37
04 October 1993	17	22	39
18 October 1993	21	22	43
01 November 1993	12	22	34
15 November 1993	15	24	39
29 November 1993	18	23	41
13 December 1993	21	24	45
27 December 1993	17	24	41
10 January 1994	21	23	44

24 January 1994	14	21	35
11 February 1994	16	25	41
28 February 1994	21	24	45
30 March 1994	12	23	35
18 April 1994	17	21	38
05 May 1994	22	26	48
23 May 1994	16	22	38
15 June 1994	20	23	43
26 June 1994	14	24	38
Total	407	516	923

Table 5.4. Sampled turbot otoliths

#### 5.1.4. Sampled anchovy otoliths

Anchovy otoliths came from samples from commercial landings, collected in the framework of an ongoing programme on stock assessment of small pelagic fish in the Adriatic (Cingolani et al., 1998). At first there is a monthly random sampling of the catch of the fleet in the various ports. Then from this sample, for ageing purposes, 5 anchovy by 0.5 cm length class were chosen, otoliths (sagitta) extracted, and age determined by standard techniques (Giannetti, 1985). Successfully aged otoliths formed the basis of the database used by this project. From this group of otoliths a sub-sample, described in the tables below was scanned according to the already described protocol and weighed by means of an analytical balance (0.1 mg).

Otolith specimens were collected from three different landing sites in the Adriatic: Chioggia in northern Adriatic, Ancona and San Benedetto in central Adriatic. All 2880 aged anchovy otolith samples were weighted. In all cases both sagitta were collected from each specimen. Summary of scanned samples by port is given in the following table.

Landing site	Number of samples
Ancona	1640
Chioggia	1120
S. Benedetto	120
Total	2880

Table 5.5. Sampled anchovy otoliths

In the table 5.6 the number of left and right otoliths that were aged and scanned is given:

<b>Landing site</b>	<b>Age 0*</b>	<b>Age 1*</b>	<b>Age 2*</b>	<b>Age 3*</b>	<b>Age 4*</b>	<b>Total*</b>
Ancona	100/100	250/250	200/200	200/200	70/70	1640
Chioggia	100/100	100/100	130/130	130/130	100/100	1120
S. Benedetto	-	-	30/30	30/30	-	120
Total	400	700	720	720	340	2880
* (First numbers are for left, second for right body side otoliths)						

Table 5.6. Anchovy otoliths and age of fish

All the images referring to the anchovy samples were thus organised in a database and saved on CD.

## 5.2. 2D Methodology and 2D Shape Analysis of Otoliths

This task-complex was one of the most challenging of the project parts. Not only had the software and hardware for the otolith workstation to be developed, but these developments had to be made very quickly because other partners needed it to begin the imaging of otoliths to establish the databases required for other project tasks.

The very first action was to decide on the hardware features of the otolith workstation. The following list summarises the result:

- Olympus zooming stereo-microscope SZX9
- Two optics for normal and large working distance combined in a revolver
- Additional aperture for increased depth-of-field
- Integrated light-base for optimal illumination (silhouette images)
- Additional light-sources for reflected light imaging
- Leica DC100 digital camera allowing real-time focusing
- Workstation computer featuring a high-performance graphics terminal
- Calibration standards
- Software (for details see below)

The workstations were delivered to partners, which were instructed how to perform calibrations to achieve the maximal precision in absolute size measurements. After partners became familiar with the use of the otolith workstations, we defined the imaging protocols for the species and thereafter, the main database imaging began.

The workstation software was intended for otolith imaging and also for the retrieval of related sample data. Fortunately, there was a special image acquisition module for the Leica DC100 digital camera. This application was integrated into the Sample Data Input Form (SDI Form) so that the user can take an image and subsequently enter the sample data (Kastowsky et al., 2002a). The files created by the SDI Form are written in a well defined text-format so that the user has no difficulty with format specifics. For every single image we have one extra sample data file holding information such as fish length, fish weight, and more. A special IMAGIC-5 (van Heel et al., 1996) command was programmed so that the image files plus these sample data can be combined into a single multi-purpose IMAGIC-5 file, which constitutes a database for further evaluations. Additional software components were created so that the user can easily generate special purpose IMAGIC-5 databases, e.g. databases with special focus on features like, sex or sample origin. Moreover, provisions were made to allow the creation of output from IMAGIC-5 files that can easily be read into standard MS Windows programs like EXCEL. In order to be able to visualise and convert image formats, we also provided the Paint Shop Pro third-party software with the otolith workstation. Therefore we can summarise the workstation software as follows:

- Leica DC 100 image acquisition software
- Sample Data Input Form for imaging and sample information
- Utility for database construction ("ListMaker")
- Utility for database searches within the sample text files ("TagSearch")
- Utility for construction of database tables ("TableMaker")

- Utility to transpose a shape descriptor table ("Transpose")
- Utility to facilitate comparison especially of image files ("Compare")
- Paint Shop Pro for image format conversions
- IMAGIC-5 graphical user interface version
- IMAGIC-5 launcher for the console based application
- FABOSA Help with instructions concerning the different applications

Although these developments were extensive, the workstations were provided to partners on time. During the project, several updates of the above-mentioned software were distributed to partners. The final user feedback acknowledged the overall functionality of software components and was basically very positive.

Soon after the otolith workstations were delivered to the project partners, the otolith shape imaging began for cod, eel and anchovy. Turbot otolith images were produced with an existing camera system. In the following text/paragraphs, we will describe the established 2D and 3D databases in more detail, since they constitute the input from which all results are derived.

The establishment of databases in the context of this project means that we created otolith shape databases in the form of 2D and 3D data collections. In the case of 2D, the shape information is initially captured as an otolith silhouette image. The reason why we specialised on the silhouette images instead of using reflected-light images is for sake of the highest measurement precision. While in reflected-light images many factors may disguise the 2D shape, in the silhouette images we have well defined edges between object and background with a high contrast so that the most precise 2D shape information can be obtained. The 3D rawdata consists of successive tomographic cross-sections, basically based on the contrast between air and the otolith registered with x-ray radiation. One of the world-wide few sets of x-ray micro-tomographic equipment suitable for the probing of relatively small samples such as our otoliths was employed. The 3D rawdata databases contain the cross-sections for several scanned otoliths of all investigated species. For some specimens, we provided not only the cross-section data but also sets of light-microscopic images. Thus, for 3D we have not only the outer shape but we have also a fair representation of the otolith inner structure.

The otolith collections from which the specimen for our databases were obtained mostly included additional information such as fish weight and several other attributes. In addition to that, we have weighed all otoliths, since this is not a standard procedure. All these individual attributes were collected together with the silhouette images. After application of automated image analysis procedures, a number of further shape descriptors are obtained. Moreover, selected geometrical otolith shape features are calculated during image processing. Details on that are given elsewhere in this report. Here it suffices to note that all these different bits of information establish what we call a 2D database. The parts are:

1. Silhouette image for each individual otolith, mostly one from each body side.
2. Sample information accompanying each otolith image.
3. Shape descriptors for each otolith.
4. Selected geometrical otolith shape features such as e.g. area.

Except for the raw images, most data can be stored in separate spreadsheet tables and therefore such database tables summarize the contents of whole set of otoliths. These tables contain:

1. Original sample information.
2. Additional geometrical features.
3. Full set of 256 Normalised Fourier Descriptors (NFD) for shape.
4. Selected set of 68 Normalised Fourier Descriptors for shape and the Size Factor.
5. IMAGIC-5 files of type 1-D NFD from which shapes can be reconstructed.
6. ID tables for cross-referencing.

Whereas the original shape and sample information is contained in a large number of individual files, the latter files contain the relevant information in compact form. However, we do make both kinds of information available to users of the databases.

Finally, it should be mentioned that there are further materials collected for each species to supplement the databases. These materials include:

1. Ageing protocol - document explaining the ageing procedures.
2. Imaging protocol - document describing the imaging procedures.
3. Glossary - image with annotations on the otolith nomenclature.
4. Controls - repeated measurements.
5. Pictures - CD cover, participating staff of institutes and other.

### 5.2.1. Databases

#### *2D databases*

We have created four such individual 2D shape databases for cod, turbot, eel and anchovy and made them available on CD (Kastowsky et al., 2002a). We have compiled a manuscript for publication, which describes the databases in detail. Here we like to shorten the presentation to brief overview about the database contents.

The cod database actually consists of two parts. In the first part, there are known-age and in the second part there are traditionally-aged cod both from the Faroe Islands.

<b>Directory</b>	<b>Selected (left+right)</b>	<b>Odd (left+right)</b>
Faroe Bank Pencage	388	18
Faroe Bank Recapture	48	3
Faroe Plateau Pencage	440	38
Faroe Plateau Recapture	550	4
<b>Total</b>	<b>1426</b>	<b>63</b>

Table 5.7: Known age cod in the 2D database (part 1)

<b>Origin</b>	<b>Age 1*</b>	<b>Age 2*</b>	<b>Age 3*</b>	<b>Age 4*</b>	<b>Age 5*</b>	<b>Age 6*</b>	<b>Total*</b>
Faroe Bank Pencage	-	37/41	37/39	37/38	45/48	33/33	189/199
Faroe Bank Recapture	-	-	2/3	12/14	7/10	-	21/27
Faroe Plateau Pencage	-	41/39	44/37	51/49	48/45	43/43	227/213
Faroe Plateau Recapture	41/41	142/145	67/73	20/21	-	-	270/280
<b>Total</b>	<b>82</b>	<b>445</b>	<b>302</b>	<b>242</b>	<b>203</b>	<b>152</b>	<b>1426</b>

\* (First numbers are for left, second for right body side otoliths)

Table 5.8: Age of known age cod in part 1 of the 2D database

Origin	Selected (left)	Selected (right)	Total
Faroe Plateau Spring Surveys	756	49	805

Table 5.9: Traditionally-aged cod in the 2D database (part 2)

Faroe Plateau Spring Surveys							
Age 2	Age 3	Age 4	Age 5	Age 6	Age 7	Age 8	Total
99/1	133/45	181/3	98/0	190/0	48/0	7/0	756/49

\* (First numbers are for left, second for right body side otoliths)

Table 5.10: Age of traditionally-aged cod in part 2 of the database

The eel database consists of two parts, each formed by samples from one of two Swedish lakes, namely Lakes Frisksjön and Lake Ommen. Samples from these two origins are considered as known-age fish.

<b>Origin</b>	<b>Age</b>	<b>Selected (*)</b>	<b>Total</b>	<b>Odd</b>
Frisksjön (caught in 1984)	5	4/2	6	2
Frisksjön (caught in 1985)	6	10/8	18	-
Frisksjön (caught in 1990)	11	70/70	140	26
Frisksjön (caught in 1992)	13	93/93	186	6
Frisksjön (caught in 1998)	19	82/82	164	20
<b>Total</b>			<b>514</b>	<b>54</b>

\* First numbers are for left, second for right body side otoliths

Table 5.11: Known-Aged Eel from Lake Frisksjön stocked in 1979 (part 1 of the database)

<b>Origin</b>	<b>Age</b>	<b>Selected (*)</b>	<b>Total</b>
Ommen (stocked in 1989)	7	9/9	18
Ommen (stocked in 1984)	12	116/116	232
Ommen (stocked in 1979)	17	16/16	32
<b>Total</b>			<b>282</b>

\* First numbers are for left, second for right body side otoliths

Table 5.12: Known-Aged Eel from Lake Ommen caught in 1996 (part 2 of the database)

The database of conventionally-aged anchovy otoliths consists of three parts, which are distinguished by the harbor where the catches were landed and which essentially stand for different geographic origins and thus environment.

<b>Origin</b>	<b>Number of samples</b>
Ancona	1640
Chioggia	1120
S. Benedetto	120
<b>Total</b>	<b>2880</b>

Table 5.13: Anchovy in 2D database

<b>Origin</b>	<b>Age 0*</b>	<b>Age 1*</b>	<b>Age 2*</b>	<b>Age 3*</b>	<b>Age 4*</b>	<b>Total*</b>
Ancona	100/100	250/250	200/200	200/200	70/70	1640
Chioggia	100/100	100/100	130/130	130/130	100/100	1120
S. Benedetto	-	-	30/30	30/30	-	120
<b>Total</b>	<b>400</b>	<b>700</b>	<b>720</b>	<b>720</b>	<b>340</b>	<b>2880</b>

\* First numbers are for left, second for right body side otoliths

Table 5.14: Anchovy in 2D database

The turbot dataset is based on harvests made during a fish hatching experiment. The sample catches were made bi-weekly. Because turbot is a flatfish, dorsal and ventral otoliths are distinguished rather than the body side. Since the initial age of the hatched fish is known, the age at a given catch date can be evaluated and thus the dataset is of known-age fish.

<b>Sampling dates</b>	<b>Dorsal</b>	<b>Ventral</b>	<b>Total</b>
13 July 1993 (age 371 days)	18	18	36
26 July 1993	19	21	40
09 August 1993	18	19	37
23 August 1993	23	20	43
06 September 1993	20	23	43
20 September 1993	15	22	37
04 October 1993	17	22	39
18 October 1993	21	22	43
01 November 1993	12	22	34
15 November 1993	15	24	39
29 November 1993	18	23	41
13 December 1993	21	24	45
27 December 1993	17	24	41
10 January 1994	21	23	44
24 January 1994	14	21	35
11 February 1994	16	25	41
28 February 1994	21	24	45
30 March 1994	12	23	35
18 April 1994	17	21	38
05 May 1994	22	26	48
23 May 1994	16	22	38
15 June 1994	20	23	43
26 June 1994	14	24	38
<b>Total</b>	<b>407</b>	<b>516</b>	<b>923</b>

Table 5.14: Turbot in 2D database

All these and much more detailed information can be retrieved from the database CDs, which will be made available to the public on request. The CD covers of the established databases are shown.

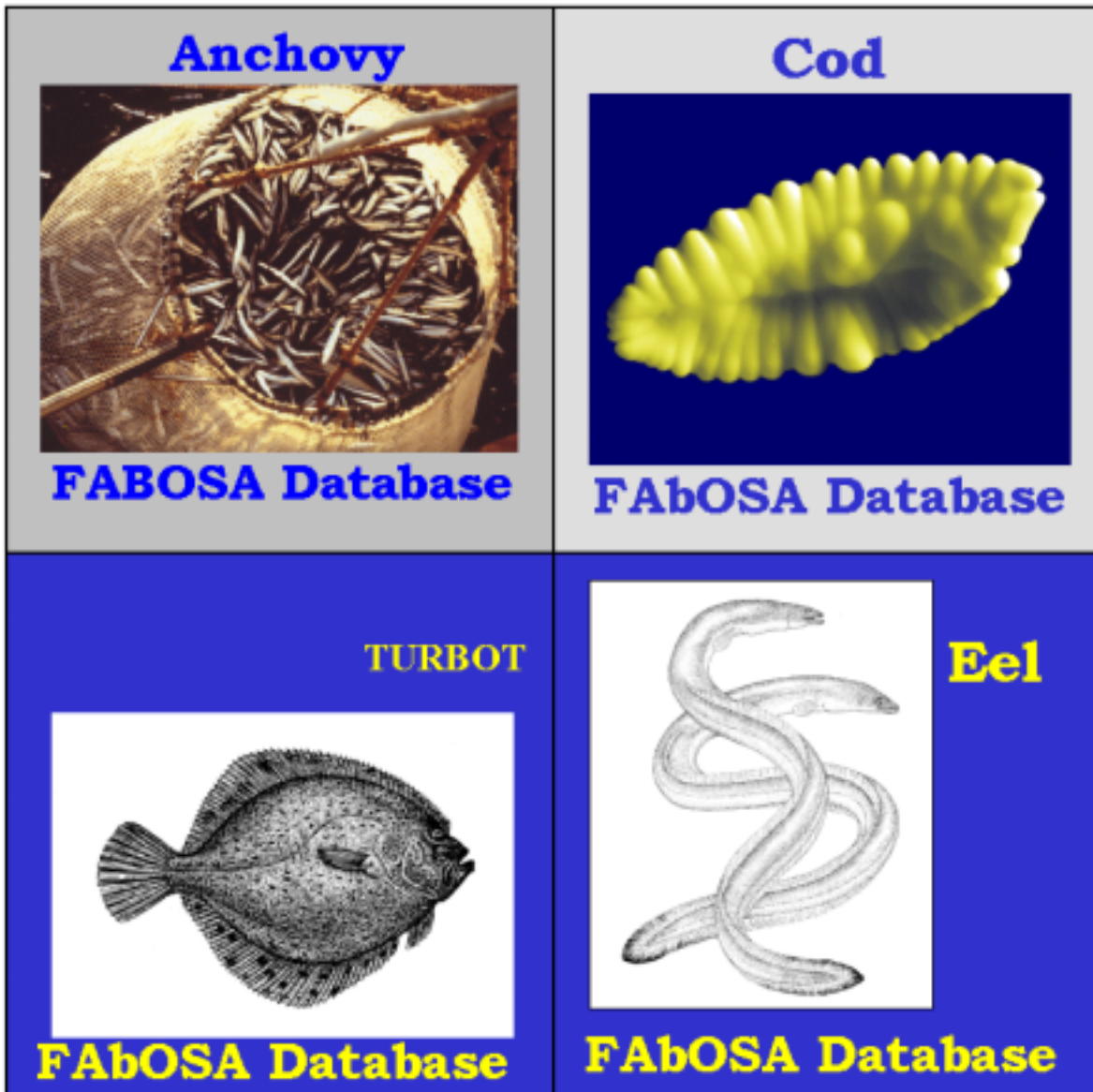


Figure 5.1: CD covers of 2D databases for anchovy, cod, turbot and eel.

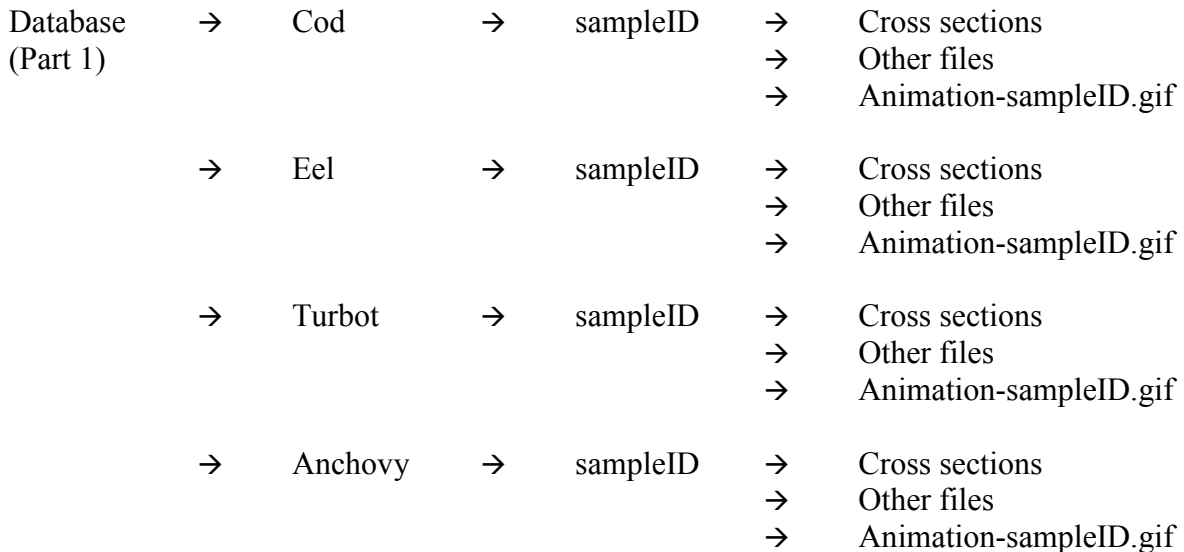
### 5.2.1.2. 3D Databases

The 3D database contains several entries covering all four targeted species (Kastowsky et al., 2002d). Since there are relatively few individual entries, the 3D database was not subdivided into separate parts for each species. The organization of the 3D database follows very practical considerations:

- Rawdata such as cross-section images, forms part 1 of the database.
- Workfiles used in image processings form part 2 of the database.
- Large scale model building data constitutes part 3 of the database.
- Inner structure data is combined into part 4 of the database.

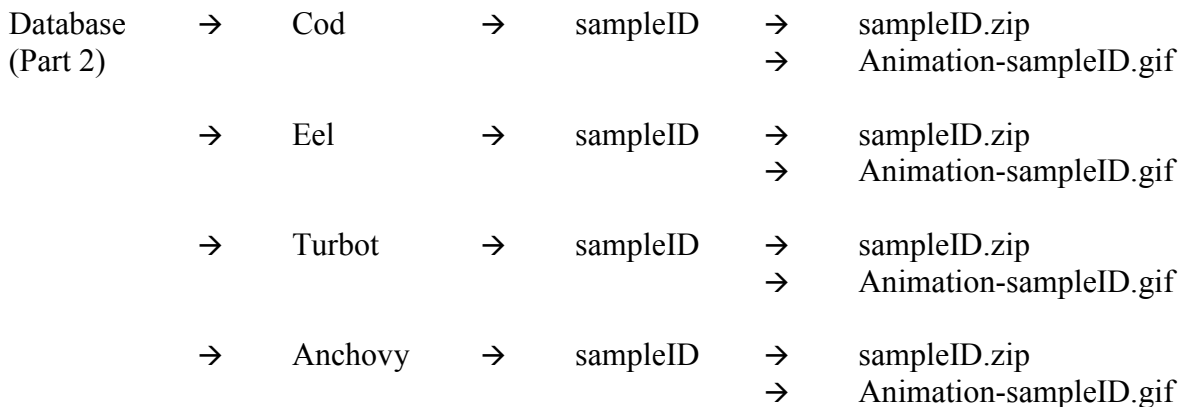
All these materials will be made available on CDs on request. Here we like to very briefly describe the available 3D information.

The rawdata is basically organised as obvious from the following scheme:



Each individual entry is stored under the respective species subfolder. The reference name is derived from the original sample identification. For each sample, the original cross-section files are stored in the 'Cross sections' folder. 'Other files' contains any additional information available including sample descriptions and real world object size. The animated GIF files are provided for convenience. These should be viewable in most standard internet browsers and enable quick identification of the sample.

The second part of the database is constituted of a number of workfiles that can be used with the IMAGIC-5 program package. Since 3D files are generally very huge, they can lead to disk storage problems. For example, some temporary files created had file sizes close to 1.5Gbyte. Therefore, all workfiles are stored in a compressed form along with an animated GIF file for ease of identification.



For some selected otoliths, large scale models were produced. The data needed for that purpose was decided to be stored on a separate CD forming 3D database part 3.

Database (Part 3)	→	Cod	→	sampleID	→	Cross sections
					→	Other files
					→	Work files
					→	Animation-sampleID.gif
	→	Eel	→	sampleID	→	Cross sections
					→	Other files
					→	Work files
					→	Animation-sampleID.gif
	→	Turbot	→	sampleID	→	Cross sections
					→	Other files
					→	Work files
					→	Animation-sampleID.gif
	→	Anchovy	→	sampleID	→	Cross sections
					→	Other files
					→	Work files
					→	Animation-sampleID.gif

The organisation of this part is similar to that of part 1. However, here we stored additional information needed for the preparation of large-scale rapid prototyping plastic models.

The final database part 4 contains input raw data as well as resulting files for the combination of otolith 3D volume information and otolith inner structure.

Inner Structure	→	Alignment and Masking etc.
	→	FABOSA 3D Database (x-ray scans) etc.
	→	FABOSA 3D Workfiles (x-ray scans) etc.
	→	STL files (x-ray scans)...
	→	Inner Structures (light-microscopic images) etc.
	→	Model Densities etc.
	→	3D Inner Structure

Fig 5.2 shows the cover layout chosen for the 3D database CD.

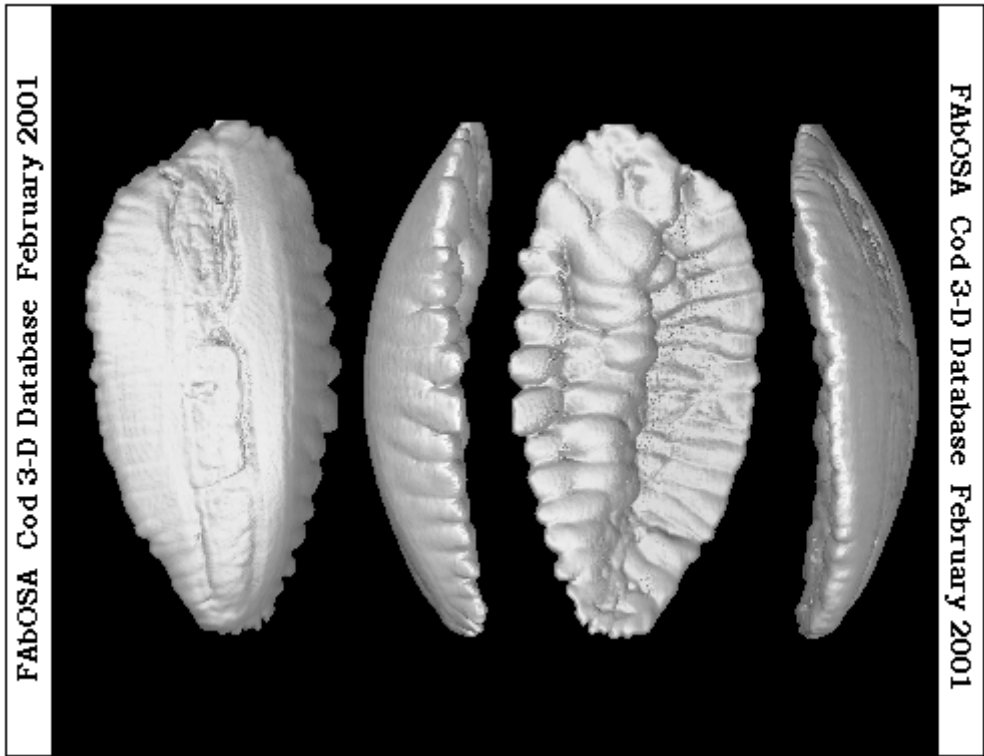


Figure 5.2: CD backside cover for the 3D database

In conclusion we can say that comprehensive materials were collected and combined into databases for 2D otolith shape as well as for 3D otolith outer form and inner structure. The databases are primarily meant to be applied within this project, however, the layout has been chosen in such a way that this work can be used by external users as well.

### 5.2.2. 2D Shape Analysis

The next steps towards our goal of ageing fish by analysing the otolith shape concerned the implementation of all required methods to extract the 2D shape data from the original silhouette input image. This also included the development of a special output file format compatible with the IMAGIC-5 standards.

The first step in every shape analysis method concerns the detection of the 2D object within the image frame. Then one can determine the outer contour and standardise the contour information to obtain the so-called Normalised Fourier Descriptors (NFDs). For object finding, we used procedures already available in IMAGIC-5. Unfortunately, while the basic procedure for calculation of NFDs is described in the literature (Wallace and Wintz, 1980), we found out that this procedure may be responsible for some unwanted noise in the NFDs. Therefore we had to devote some effort to establish an improved version of the NFD calculations. After successful conclusion of this part, we finalised the basic software for the initial 2D shape abstraction. At that

time we focused on 68 selected most significant shape descriptors plus one size-related parameter. Several inquiries from partners requested a higher precision in the contour resolution. Therefore, in the final IMAGIC-5 version, the level of detail in the contours can be chosen as 68 or 256. It should be noted here that we could demonstrate that the initially used level of detail was sufficient for NFD-based shape classifications. The reason for this finding is the fact that the variability in otolith shapes is usually the limiting factor and not the level of detail in shape description. However, we supplied the upgrades as demanded.

The initial 2D image databases are usually termed e.g. "Cod2D". In contrast to this, database files containing the shape information in form of NFDs have names like "Cod1D". It should be stressed here that NFD files contain the shape information in a much denser form as 2D files. This data reduction made it possible to store several special purpose database compositions into the final database CDs.

Some drawback on NFD or 1D files is the fact that they contain the shape information in an abstract, non-graphical form. We had therefore early on decided to provide users with a specialised tool for reconstruction of the graphical information. This tool has developed into one of the most powerful concepts within the set of 2D shape analysis instruments. We will come back to that when discussing applications of these tools in connection with shape classifications.

Before turning attention to the multivariate statistical analyses, one aspect of the otolith workstation development should be considered in more detail. It concerns the requirement that the workstation is applicable for all species, at least all species relevant in this project. The hardware was therefore designed to be exact for the size range of 2 millimetres as well as for the size range of 20 millimetres. We could achieve that requirement by implementing two optics settings combined in a single revolver. On the software side we had to account for annotations in the images supplied by one subcontractor. We solved this problem using object size sensitive filtering techniques available in the IMAGIC-5 morphology libraries. Also, the definition of species specific imaging protocols prompted us to implement specific software features such that e.g. the automatic mirroring of right body-side otoliths can be performed.

The IMAGIC-5 program package has several tools for multivariate statistical analysis and classification. However, the special situation with 2D shapes required substantial modifications of the standard routines (Kastowsky et al., 2002b; 2002c). For example, the overall size factor is believed to be an important descriptor. However, shape and size cannot usually be studied in a mixed analysis. The literature is full of contributions to this topic. So we had to have provisions that allow for proper treatment of shape versus size descriptors.

The underlying principles of shape descriptors may be highlighted here before addressing their specific application in shape classification concepts.

The set of points in the outer contour line around an object defines a shape. If all shapes to be considered have the same number of points along the contour line and one knows which point of the one contour relates to the other, a comparison of shapes would easily be done by pair wise superimposition of the two sets of points in the sense of a best fit and then evaluating the remaining sum of pair wise distances. Such approaches are well-known and have exact mathematical solutions.

However, the contours of different objects in digital images almost never have the same number of points. Also it is not known which points on the one contour relate to a given point in the other contour. Therefore the original shape information must be transformed into more suitable shape descriptors. Such shape descriptors can be defined in quite different ways. We have selected an approach based on the Fourier-coefficients obtained from the time series of contour points (Wallace and Wintz, 1980). For further details we must refer to the original literature. Here we briefly summarise the main features of the approach.

The Fourier shape descriptors can easily be normalised. In practice, this means that the normalised sets of shape descriptors for any shapes can directly be compared to each other by calculating the Euclidean distance between the shape descriptor sets. In our case we have either 68 selected Normalised Fourier Descriptors  $S(n)$  or the full set of 256 descriptors  $A(n)$  so that we can write:

$$D_{68}(i, k) = \sqrt{\sum_{n=1}^{68} (S_i(n) - S_k(n))^2}, \text{ and}$$

$$D_{256}(i, k) = \sqrt{\sum_{n=1}^{256} (A_i(n) - A_k(n))^2}, \text{ where}$$

$i, k$  denote shapes  $i$  and  $k$ ,

$D_{68}(i, k)$  denotes a shape distance for sets of 68 selected Normalised Fourier Descriptors,

$D_{256}(i, k)$  denotes a shape distance for sets of 256 selected Normalised Fourier Descriptors,

$S_i(n)$  denotes the  $n$ -th component of 68-dimensional NFD vector for shape  $i$ , and

$A_i(n)$  denotes the  $n$ -th component of 256-dimensional NFD vector for shape  $i$ .

Of course, set  $S$  is a subset of  $A$ .

These equations may look more complicated than they should. In fact, everybody knows how to calculate the Euclidean distance in 3D space. The extension to higher-dimensional spaces is then quite natural.

The most important features of shape distances  $D(i,k)$  are the following:

- If and only if  $D(i,k) = 0$ , then shape  $i$  and  $k$  are the same.
- For any two different shapes  $i, k$  we have:  $D(i,k) > 0$

In practice, one employs an important feature of distance measures: If two shapes are similar, the distance between them is relatively small, whereas the shape distance between quite dissimilar shapes is quite large. In other words, shape distances are a suitable means of establishing the

relatedness among shapes. Before we part from the mathematics and focus on the use of shape distances in classifications, the use of weights in distance calculations shall be explained.

The individual components of an N-dimensional vector may be considered with specific weights. If all weights are positive, the new distances basically have the same features as before, however, stressing different features in N-space:

$$D_N(i, k) = \sqrt{\sum_{n=1}^N w(n) \times (C_i(n) - C_k(n))^2}, \text{ where}$$

$D_N(i, k)$  denotes the distance between objects  $i$  and  $k$  in N-space

$C_i(n)$  denotes the n-th component of a N-dimensional feature vector for object  $i$

$w(n)$  denotes a non-negative weight of the n-th component

When shape distances are calculated, the weights are all same. However, when the distance between objects is to be calculated from feature vectors composed of shape descriptors plus a size factor, the weights can be used to properly balance the importance of the individual components for the total distance measure.

In summary, we have explained the concepts of Normalised Shape Descriptors and shape distances based on Euclidean distances. Also, the application of individual weights has been outlined.

Now we will address to shape classifications based on Normalised Fourier Descriptors for shape.

One of the most powerful statistical tools in IMAGIC-5 is the hierarchical classification using the Ward criterion (Ward, 1982). It's prominent feature is that it can be applied to large datasets with more than 100,000 entries. In our case, the calculations are based either on pure shape distances with or without individual weights, or they are based on mixed feature vectors comprised of shape descriptors plus one size factor, again with or without individual weighting schemes. The first step in each classification is the calculation of the initial distance matrix, i.e. the set of all pairwise internal distances for a given set. This distance matrix can be used for statistical evaluations over the set as will be demonstrated later. In the hierarchical classification the initial distance matrix is used to establish nearest-neighbour relations which subsequently greatly enhance the performance of the algorithm (van Heel et al., 2000).

The result of a hierarchical classification is a partitioning of the initial set into K classes such that each class is most compact, i.e. has the smallest internal variance, while the inter-class variances become maximal, i.e. classes themselves are separated as far as possible from each other. This approach is termed after Ward and has been successfully applied in microscopical image analysis for many decades. We found it also suitable for the shape classifications tasks.

It is important to understand the results of a shape classification, therefore we present a simple example. Consider the following set of different objects: five apples, three beans, and four bananas. Assume that we classify according to the 2D silhouette shape of objects lying on a table ignoring differences in size. When we classify into three classes, we will probably find the apples in one class, the beans in another, and yet the bananas in the third class. When we classify into six classes the result is not very predictable but we might find that the five apples are further divided into subgroups, as might be found for the other objects. When we classify the initial collection into only two classes, we might find apples and beans in one huge class, and bananas in a separate one.

This example is simple, since we have clearly recognizable objects. But what is the situation for a huge number of unknown otolith shapes? In principle, there is no theoretical approach to determine the most appropriate number of classes into which a set should be divided. However, we have demonstrated for a set of eel otolith shapes that in practice, we can reasonably well determine a good choice for the number of classes looking at outliers.

#### **5.2.2.1. Eel**

In the eel otolith dataset we found two samples that showed heavy vaterite crystal formation. When we classified all eel otolith shapes in an unbiased shape classification run, modifying the number of classes, we obtained a situation where the vaterite objects were separated out from the rest to form their own classes of 'strange shapes'. This situation is demonstrated in the Fig. 5.3.

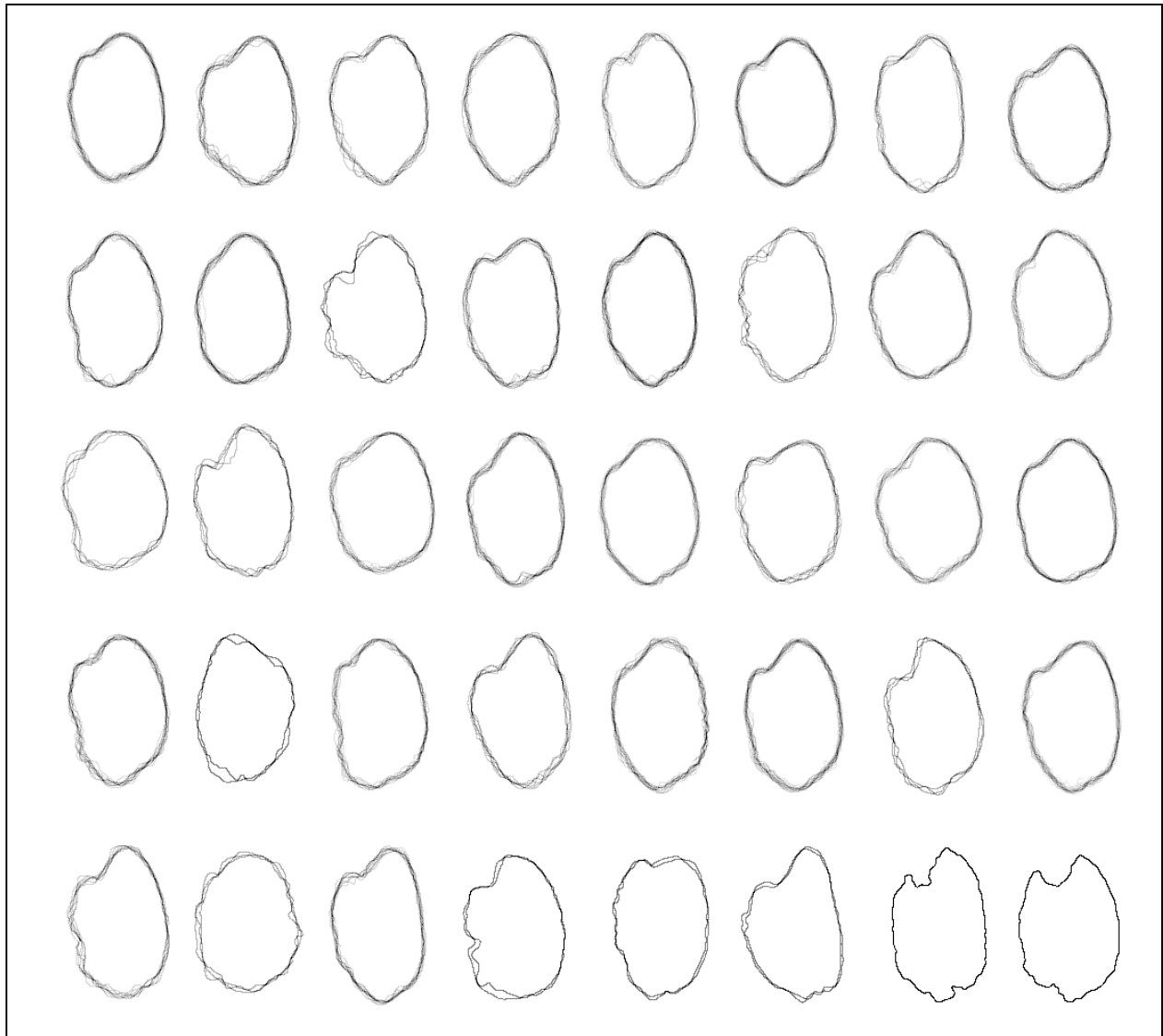


Figure 5.3: Representation of the 40 shape classes into which the whole eel otolith dataset was divided. Note the two last "strange" shapes. The maximum number of individuals in a single shape class is 23; the average is 10. The total number of shapes is 378.

This example illustrates one basic shape analysis concept, namely unbiased shape classification. We have explained how we defined the distance measured between shapes. The shape classification result for the first time gives us an understanding how useful the shape distance is for our purposes. Without going into too much of argumentation, we feel very satisfied with the shape classification results as judged by visual inspection of Fig. 5.3. Of course, there are many cases where shape classes differ significantly, however, there are also some cases, where the differences are subtle. But in each case we could convince ourselves that the suggested shape classes are meaningful.

There is no standard procedure how to use otolith shape classification results for our intention to determine the age of a fish. We will therefore proceed with the above example and demonstrate one tested method of detection of shape-age relations.

From the standpoint of the classification algorithm, the above mentioned 40 shape classes are well defined. When we asked the fish biologists if they could recognise any familiar shape patterns within these shape classes, they stated that they could not. The only vague assumption was that otoliths from young eel usually have a pretty round shape whereas older may be more deformed.

As one can see in Fig. 5.3, many shape classes have a lot of very similarly shaped members. It means that this shape feature is found in a lot of different samples, suggesting that this could be an important feature. It is therefore an interesting hypothesis to check if such classes show a specific age composition.

We counted the number of otoliths from young and old fish per shape class and calculated the reliability of a simple age prediction for some classes. Results are shown in Table 16.

<b>Class</b>	<b>Young</b>	<b>Old</b>	<b>Reliability %</b>
1	8	13	
2	7	3	70
3	4	3	
4	13	0	100
5	6	4	
6	11	12	
7	2	6	
8	5	10	
9	1	8	89
10	8	7	
11	1	2	
12	3	6	
13	8	8	
14	1	3	
15	7	6	
16	9	3	75
17	3	2	
18	0	4	100
19	11	1	92
20	5	6	
21	16	5	76
22	3	4	
23	9	4	
24	8	3	
25	4	7	
26	1	1	

27	7	3	70
28	3	3	
29	7	4	
30	3	13	81
31	0	3	
32	9	11	
33	2	5	
34	2	1	
35	0	9	100
36	0	2	
37	2	0	
38	0	2	
39	0	1	
40	0	1	

Table 5.16: Reliability of a simple age prediction for some classes. In columns Old and Young the number of class members is given. A reliability for the majority vote is given for cases where there is some clearly recognizable shape-age relation.

Table 5.16 shows that 116 out of 378 otoliths can be assigned with high predictive power to characteristic age-classes. In general, however, the trends are relatively poor, so that on average, the fraction of predictable cases is only 1/3. This is clearly not an encouraging result.

Fig. 5.4 shows in grey the classes for which some shape-age relation may exist.

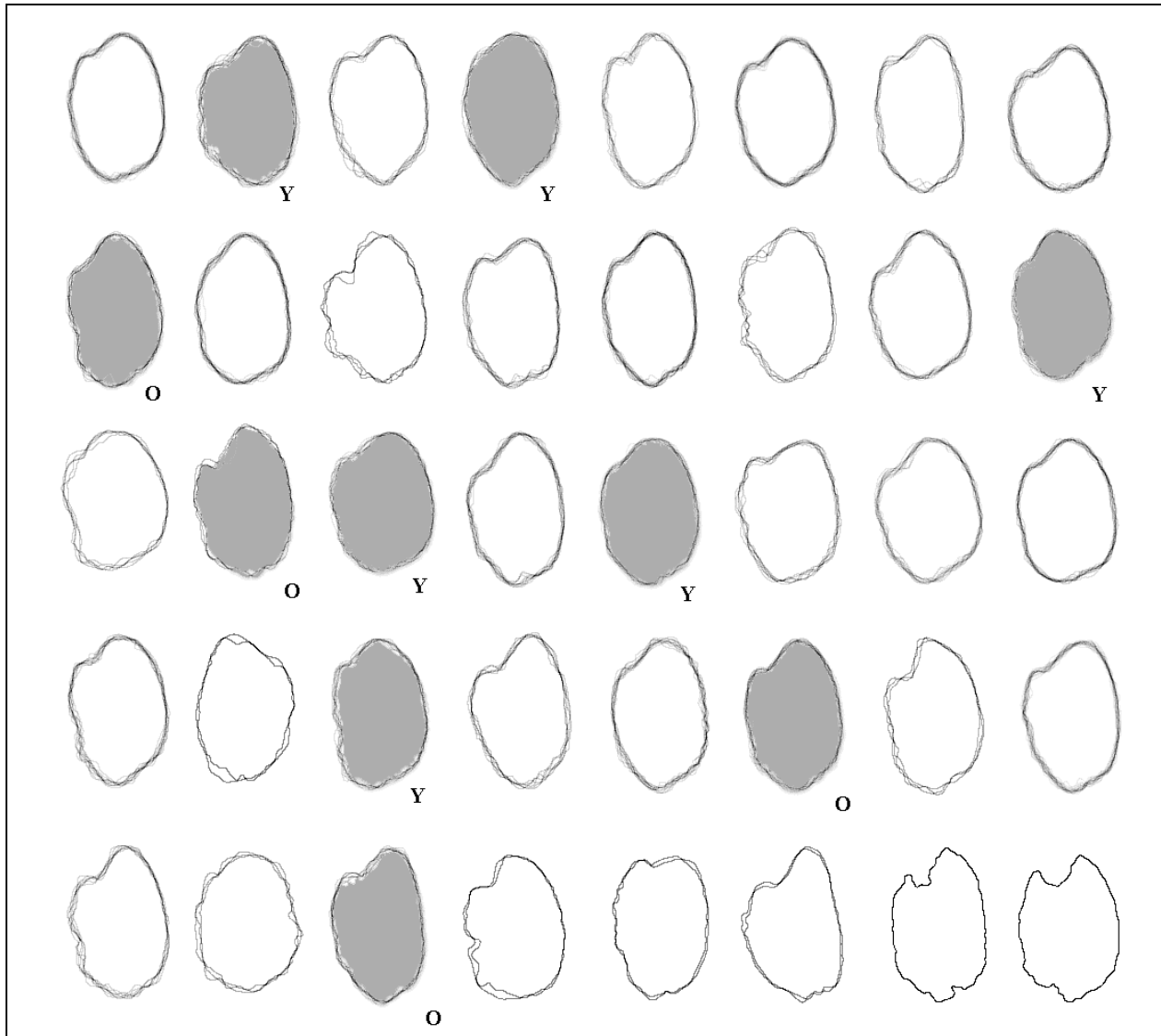


Figure 5.4: Representation of the same 40 shape classes as in Fig. 5.3, however, shape classes that might show a significant shape-age relation are greyed. Y and O denote the categories young and old.

We are presenting results for eel here in order to exemplify how shape classifications can be used to elucidate possible shape-age relations. More details will be reported in the species-specific result parts. However, at this point we like to demonstrate that the otolith overall size has an acceptably well defined relation to age. In other words, from otolith shape alone we could predict age only for less than 1/3 of all samples, whereas using the otolith size demonstrated to be a more accurate tool for prediction.



**Figure 5.5:** Samples in the eel dataset were arranged such that location numbers 1-192 stand for young and 193-378 stand for old fish. The differences in the overall otolith size are obvious. It is clear that an age prediction based on size alone gives correct predictions for much more than 1/3 of all samples.

The relatively negative results obtained using only otolith shape information for age prediction as compared to the high predictive power of the overall otolith size prompted us to look at mixed classifications using shape and size. It was clear that a mixed analysis requires the selection of proper weights for shape versus size. We solved this question by setting up a numerical optimisation process. First, we shall explain the target function subjected to optimisation.

The target function is the classification score, which is obtained as follows:

1. Classify the dataset into two classes.
2. Calculate the percentage of young and old in each class.
3. The class with the highest percentage is defined to be the predicted young or old.
4. The remaining other class is defined to predict the opposite age feature.
5. Now we can calculate the classification score as the percentage of correct predictions.

A classification score of 100% means perfect prediction. The lower the percentage, the lower the reliability of the ageing model. Fig. 5.6 shows the increase in the classification score when the importance of the otolith size versus shape is increased.

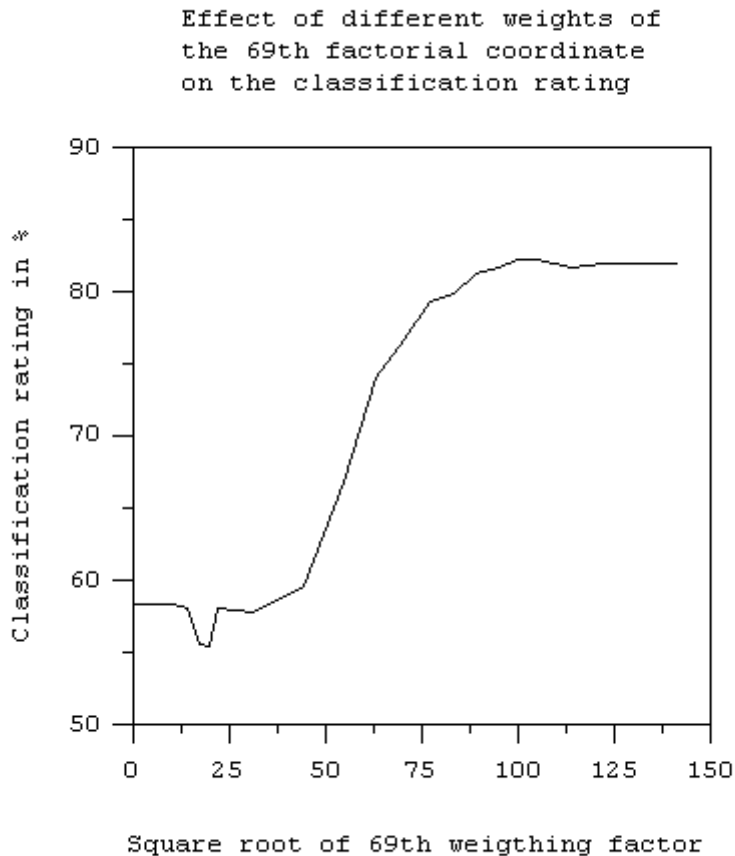


**Figure 5.6:** Classification ratio is used synonymously for classification score. Mixed shape-size distances were based on 68 NFDs and one size factor (factor 69). One can see that increased weight of the otolith size information improves the classification ratio. The maximum goes up to 83% classification score. Using size information alone gives a classification score of only 82%.

This result suggests that there is in fact a small amount of ageing-relevant information in the shape of an eel otolith, however, the overall size clearly is the dominating effect.

It should be noted that there were extensive discussions between the methodology oriented and the fish biology partners about the question of the use of biased shape analysis. Our basic shape analysis concepts are unbiased and are based on the following logic for implications:

- For same shapes, we infer same features.
- For similar shapes, we infer similar features.
- For different shapes, we cannot infer same features but we cannot exclude them as well.

This is the standard way of logical implications and it means with respect to age predictions based on shape:

- If two otoliths have the same shape, we predict the same age.
- If two otoliths have similar shapes, we predict similar age.
- If two otoliths have different shapes, we cannot strictly predict same or different age.

These concepts may be extended to incorporate other features in addition to shape, as was demonstrated above with the size effect. However, implication logic remains the same.

Concepts where this logic is overridden by a set of rules, were not considered. However, this appears not to be a real problem, since no project partner could provide us with any clues on the existence of such rules for ageing.

We have therefore addressed our attention to otolith shape understanding, which means that we wanted to elucidate typical shapes and shape differences within datasets and try to interpret these as effects of ageing.

Initially we investigated the silhouette otolith shapes, i.e. the filled contours. While the results were instructive, there were some practical limitations so that we decided to test if image analysis based on the contour line representations would give additional information. This was in fact true as will be demonstrated in the following paragraphs. For brevity, we will therefore leave out the results obtained for filled silhouette otolith shapes.

From the Normalised Fourier Descriptors, 2D contour line representations can be produced. These contours are then fed into 2D eigenimage analysis, which is one of the most valuable and reliable workhorses of the IMAGIC-5 program system.

The basic concept of the multivariate statistical analysis, which aims at the calculation of suitable eigenimages may briefly be described here. A digital image of size  $N \times M$  may be considered as a vector of length  $N \times M$ . Assume that we have  $K$  images which are all mutually linear independent. This condition is basically true in practical settings. Then, there is a  $K$ -dimensional subspace of the  $N \times M$  space for which a basis set can be determined. A basis set consists of  $K$  vectors forming an orthonormal coordinate axis system. We can apply arbitrary unitary transformations to any basis set leaving orthonormality intact. Of all these possible systems, the eigenimage analysis yields the one with the following special features:

- Eigenimages form an orthonormal, right-handed set.
- Eigenimages are sorted according to their eigenvalues (variance contributions).
- The first eigenimage reflects the average over the set of images.
- The second eigenimage has the highest discriminating power with respect to image variance.
- Higher eigenimages have lower discriminating power than previous ones.

What are the merits from eigenimages? Since eigenimages are ranked according to their importance to the total image information, one can simply leave out high-indexed eigenimages and thereby apply a considerable data reduction. Such kinds of techniques are e.g. used with

highly sophisticated streaming video formats. For our purpose of image understanding, this aspect of eigenimages is not really of interest. The main gain of eigenimages for us comes from the inspection of the first two to three eigenimages, especially of the second, which contains the information on the most striking features in the images. It should be noted that there is a lot of resemblance of the eigenimage approach with the principal components analysis of NFDs. However, we do favour the eigenimages because the results are in image space rather than in the quite abstract NFD space.

First, some examples of the input contours are shown in Fig. 5.7.

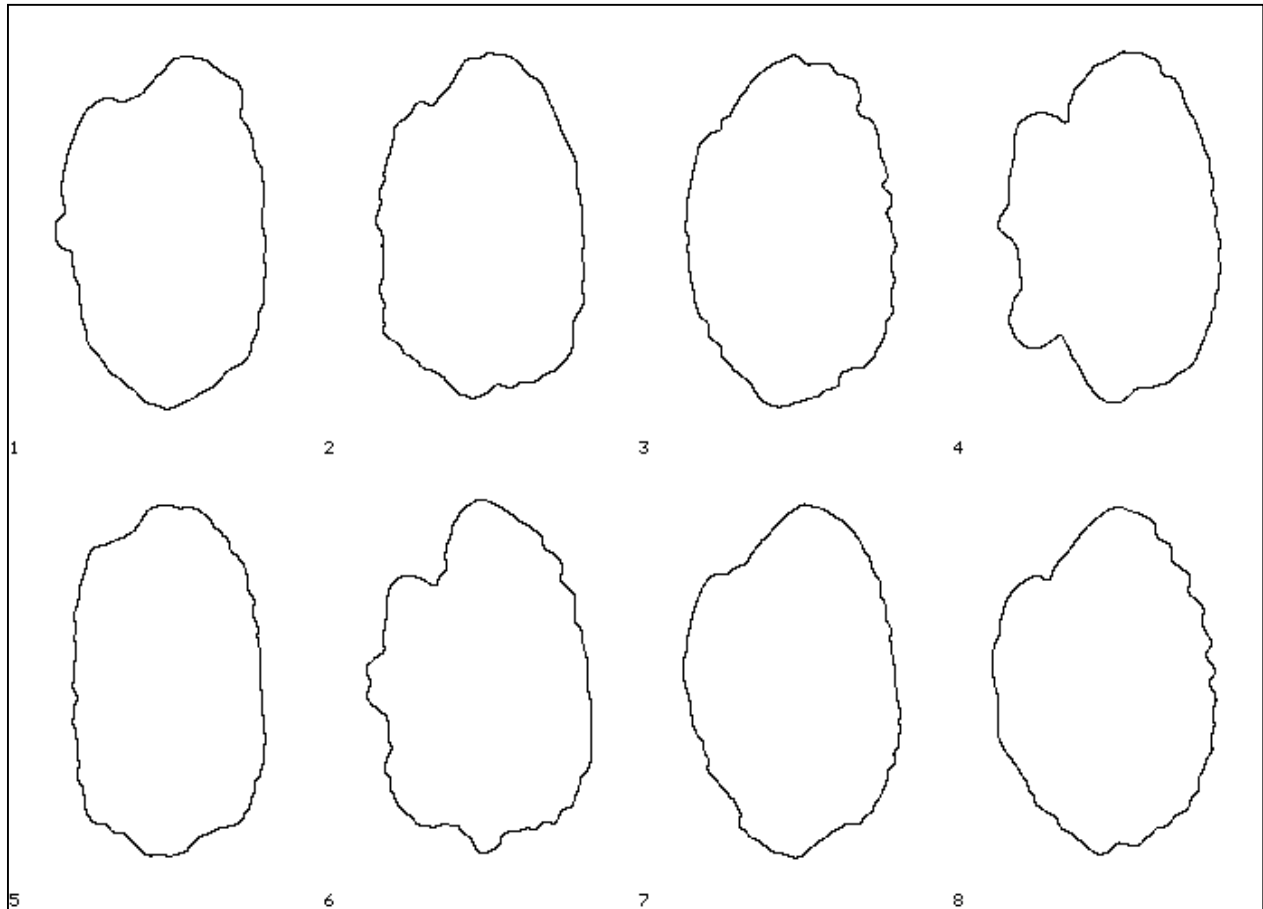


**Figure 5.7:** Arbitrarily selected contours of eight eel otoliths from Lake Frisksjon. Note that contours are sufficiently detailed with respect to the easily recognisable variability between shapes. Contour lines are 1 pixel thick.

The Lake Frisksjon dataset contains a total of 514 entries. This set was subjected to eigenimage analysis, which is a relatively computer-time consuming process, frequently run as an overnight job. In Fig. 5.8 the first eight resulting eigenimages are shown.

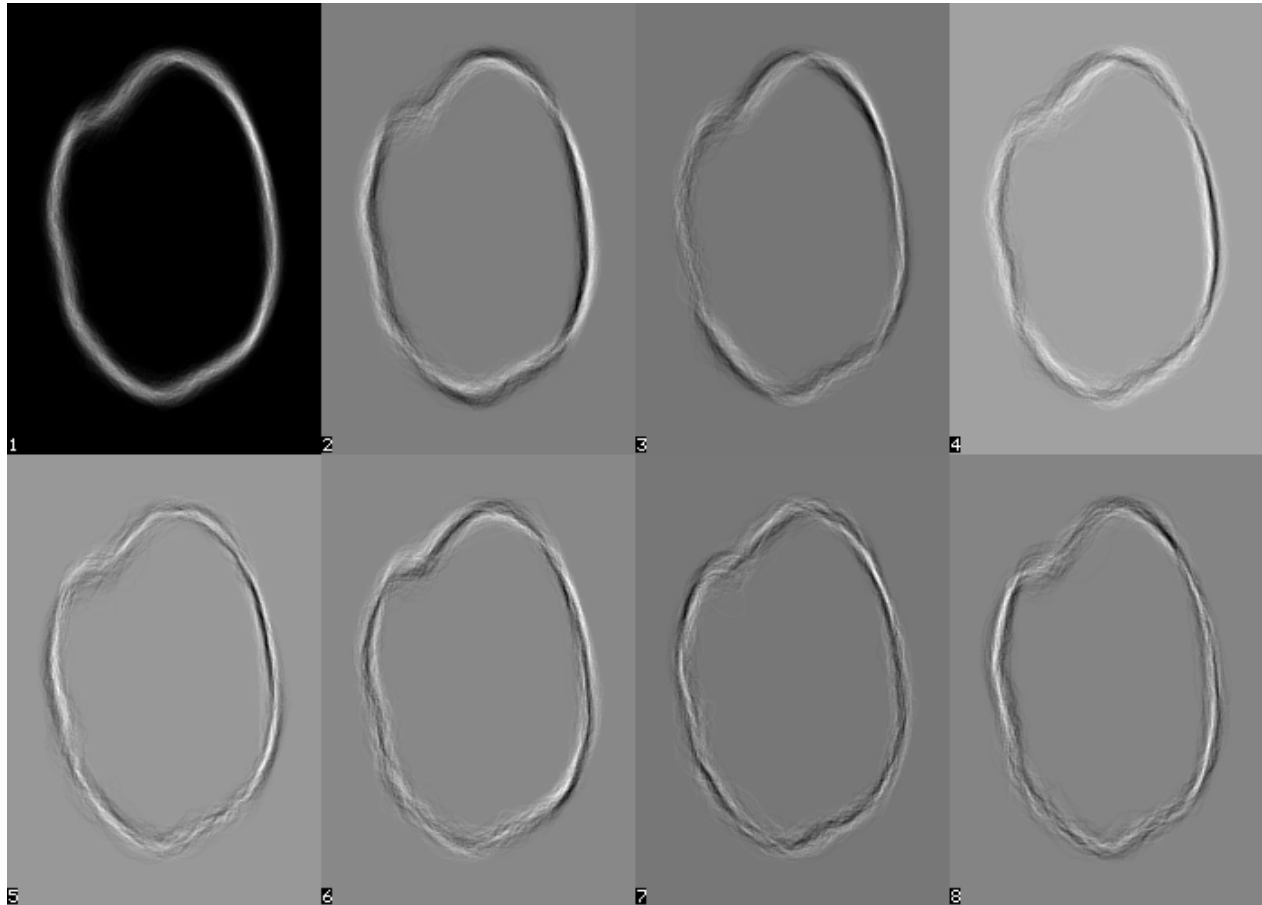


**Figure 5.8:** The first eight eigenimages for the Lake Frisksjon dataset containing 514 individual shapes. Eigenimage 1 represents the set average. Eigenimage 2 is the most discriminating eigenimage indicating the main shape transition within the dataset. Other eigenimages show image features of less importance. In practice, higher eigenimages describe complex shape transitions, which are difficult to interpret for humans.

We were interested to detect and understand possible shape changes related to age. The eigenimages reflect pure shape features for the complete set. Therefore we must extract the shape features from eigenimages and then determine if there is an understandable relation to age.

For the moment we leave the first eigenimage and have a closer at the second. One can easily recognise in Fig. 5.8 that there are a dark and a bright contour system. Let us consider them as a linear combination of two extreme shapes. Then eigenimage 2 suggests that the main shape transition contained in the complete dataset is the transition from shape A to B, or vice versa. This can be described by a simple mathematical formula for a line:

$$X = \lambda * (B - A) + A, \text{ where } \lambda \in [0,1]$$

It is therefore easy to understand the meaning of eigenimage 2, especially after the two extreme shapes A and B have been isolated using standard image processing. We call this process eigenimage decomposition. The result of the eigenimage decomposition is shown in Fig 5.9.

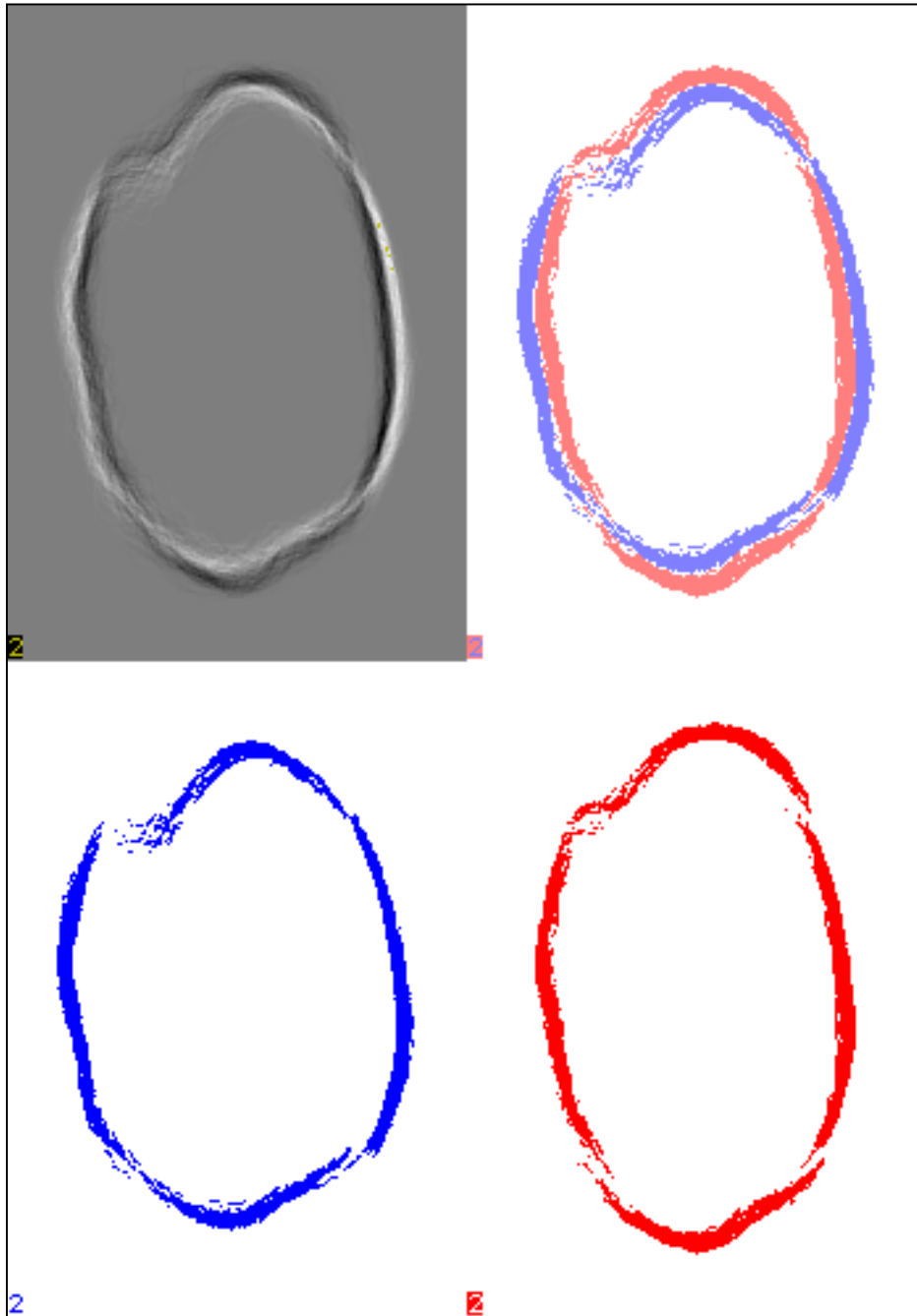


**Figure 5.9:** Eigenimage 2 for the Lake Frisksjon dataset (top left) is decomposed into its two constituents depicted in blue and red (bottom). The components in the reconstruction image (top right) are now clearly visible. The suggested main feature is a round-to-elongated shape transition.

Since we did not use any age information in this analysis, we do not know the meaning of round and elongated shapes. However, by calculating shape averages over young and old eel otoliths, one can expect to find an appropriate assignment for the eigenimage components. However, the obtained results shown in the Fig. 5.10 do not suggest that the main shape transition is age related

at all! This is consistent with the poor outcome of simple shape classifications reported earlier. In Fig. 5.10 otolith shapes for young and old eel are compared against the extreme shapes extracted from the second eigenimage.

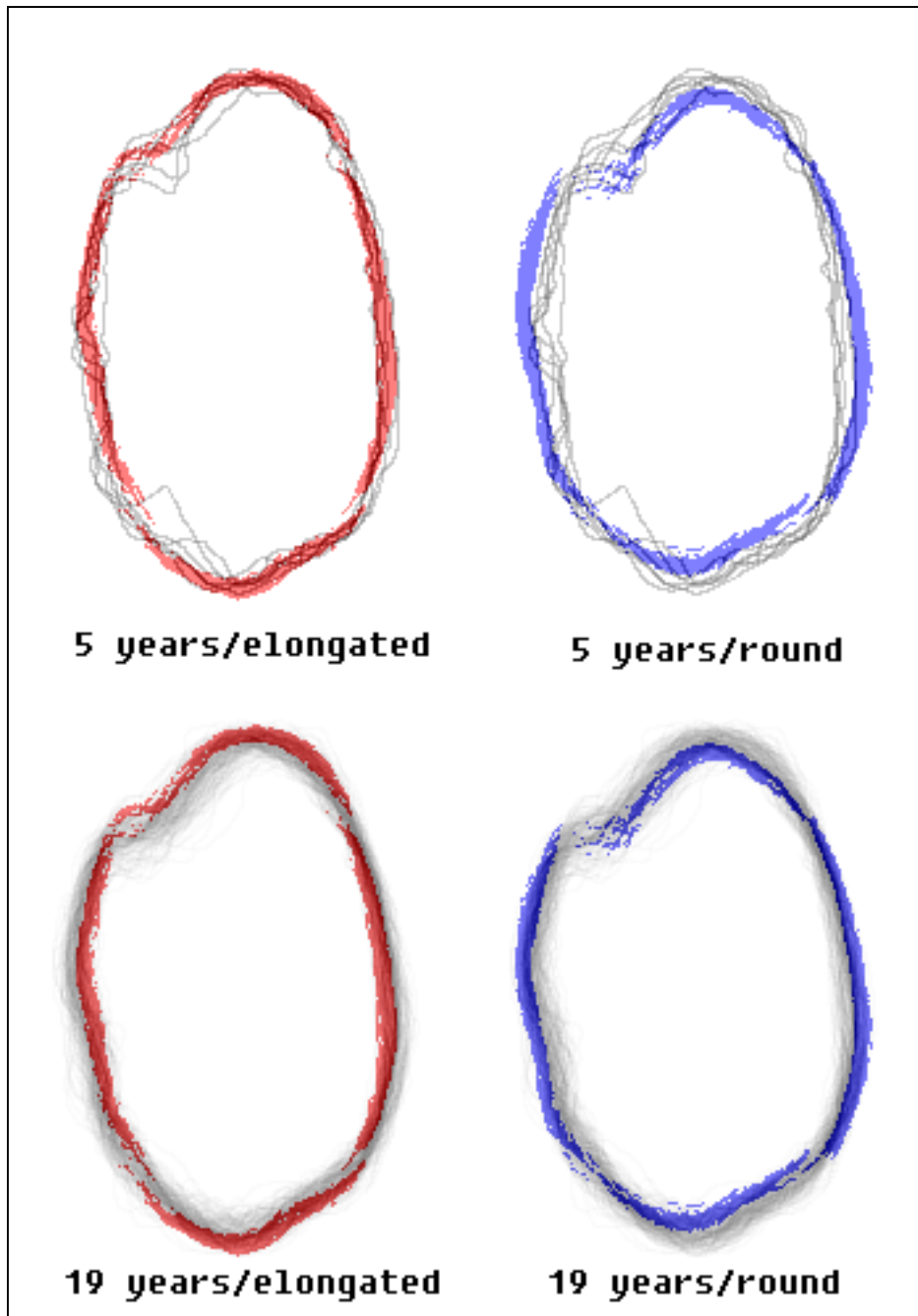


**Figure 5.10:** Decomposition shapes from eigenimage 2 are blue and red. Summed images over age classes appear as grey tones. The sum calculated for 5 years old eel is over few individuals, however, the vague indications seen here were also found for six year old fish. Age group 5 seems to consist of elongated shapes. Age group 19, however, seems to be right in the middle between the elongated and round decomposition shape. This and other indications suggest that the elongated-round shape extremes are not related to age.

The conclusion drawn from the comparison of age-group shape-averages with the extreme shapes from the eigenimage 2 decomposition was that shape features are not age related. This might have not been convincing enough from Fig. 5.10 but it is absolutely clear from a plot of factorial coordinate F2. As we mentioned before, for every single eigenimage there is one associated coordinate value for a shape. This coordinate value is called factorial coordinate. We expect factorial coordinate number 2 to be correlated with age, if the main shape effect seen in the complete dataset is indeed age-related. Fig. 5.11 gives the answer.

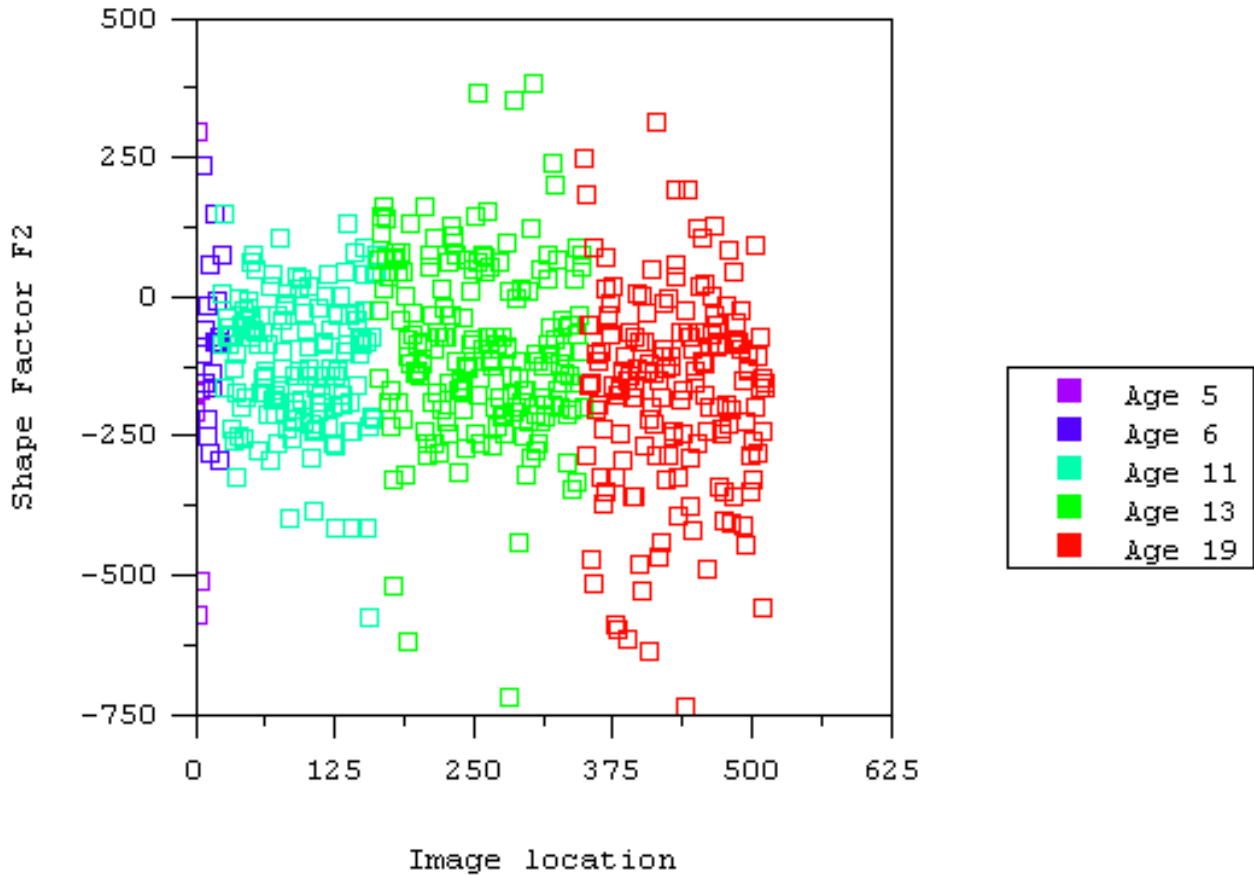


**Figure 5.11:** Diagram of factorial coordinate F2 over image location for the eel dataset Lake Frisksjon. Age groups are indicated by colours. There is no clear-cut relation of F2 with age.

There is no indication of a relationship between age and shape coordinate F2. This result is negative but it confirms the much easier understandable finding obtained from the shape classifications. We can even go further and infer that the shapes of eel otolith are highly variable as suggested by the eigenimage decomposition. However, this broad range of variations is not age-related. It remains a challenge to find out what the shape variations within the eel dataset stand for. It could well be that there are strong environmental effects, or even genetically predetermined growth factors.

It should be mentioned that the factorial shape coordinates for higher eigenimages did not reveal any shape-age relations. Therefore the findings described in detail for shape factor F2 are of general relevance.

Since we found that the shape of eel otoliths is not related to the fish age, one could argue that there is something wrong with the samples. We use other sample descriptors to check the internal database consistency. One possible plausibility check is the plot of fish length versus fish weight. While there might be several factors influencing the growth of an individual eel, the statistic over a sufficiently large database must reveal the usual growth pattern, i.e. older fish are longer and the longer a specimen is, the heavier it should be. We could in fact obtain very significant length-weight relations as can be seen in Fig. 5.12.

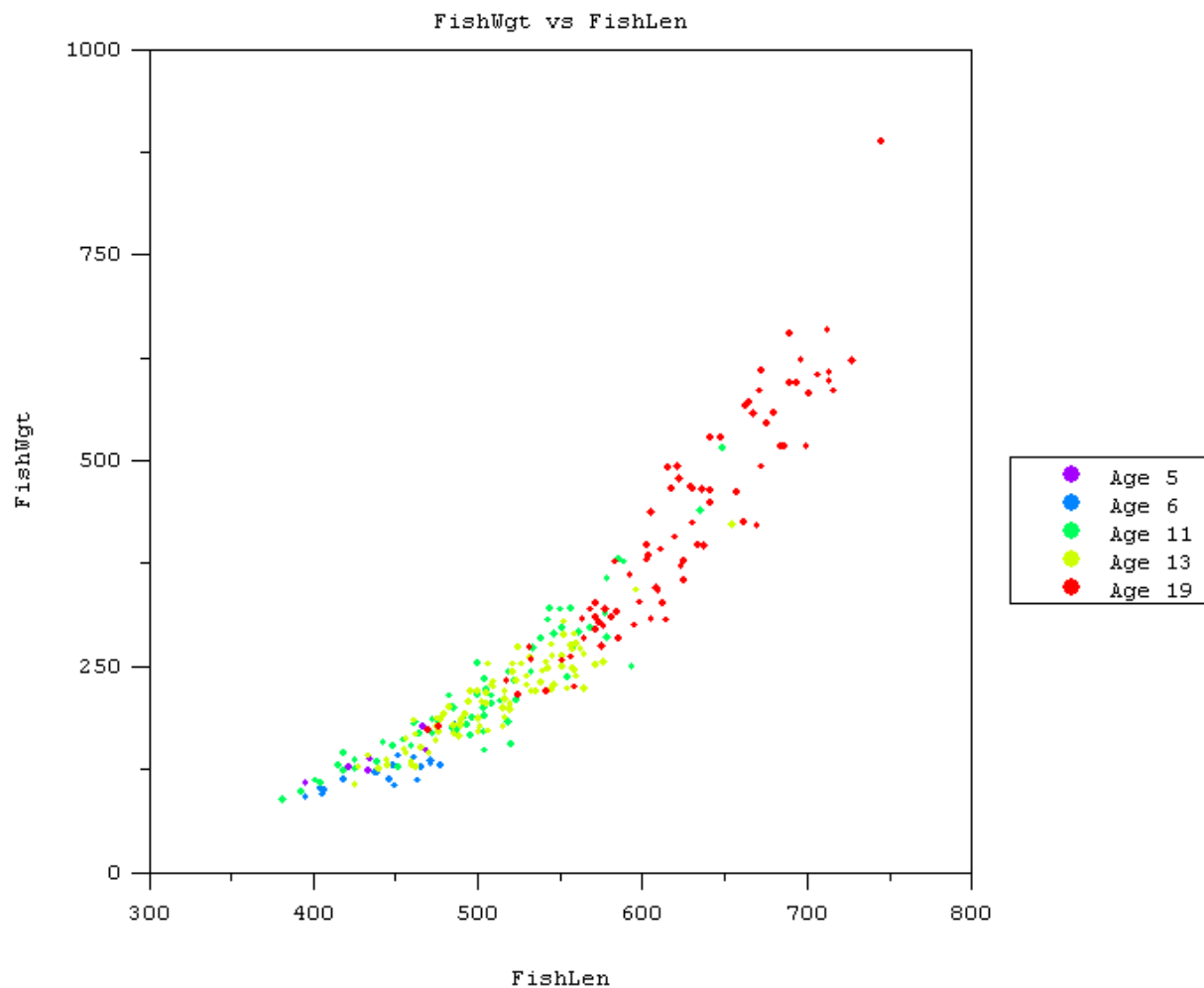


**Figure 5.12:** Fish weight in grams over fish length in millimetres for the dataset of 514 eel from Lake Frisksjon. Note that the point clouds for different ages overlap. However, the course of the length-weight curve suggests a quite normal growth behaviour.

As a summary for eel we can therefore say that

- the 2D shape databases and other sample data are available and allow a variety of analyses
- the established shape analysis methods perform as intuitively expected
- the age composition of pure shape classes does not suggest any exploitable shape-age relation
- otolith size alone is almost as good a predictor for age as a combination of otolith shape size
- the most significant shape change within the Lake Frisksjon dataset is not age-related
- the dataset itself seems to be consistent as inferred from the fish length versus fish weight relation.

Although from a more theoretical point of view, it is impossible to draw any conclusions from a negative result, we are convinced that there is in fact no generally exploitable shape-age relation for eel otoliths. It could well be that the age information is not totally missing but heavily disguised within the 2D shape, which we focused on. In fact, eel otoliths seem to have a complex curvature into the 3rd dimension, which might not appropriately be accounted for in the 2D silhouette images. Moreover, since for imaging the otolith is placed on a glass plate, we select one very specific silhouette out of a set of related ones, which we would obtain, if the positioning of the otolith were slightly different. Such effects were studied in more detail for cod and are reported elsewhere in this report.

In the following we will present results for other species, i.e. for turbot, anchovy and cod. The sequence of species eel, turbot, anchovy, cod indicates the increasing importance of the otolith shape for ageing. For eel we have already shown the failure to obtain a significant shape-age relation. In contrast to this, we will demonstrate that for cod there are shape-age relations that can be used for ageing.

#### **5.2.2.2. Turbot**

Before going into details on turbot, the initial situation concerning image and sample info inputs may be described. The situation differs from that for other species, since the turbot inputs were not obtained with our standardised hardware and software. Instead of this, there was a huge number of annotated images of known-age turbot otoliths available. So we took these and started our usual input procedures. Next, the internal consistency of the images was checked. For this purpose, we analysed a set of images showing one sample in different arrangement (2D rotation). Unexpectedly, we obtained different shapes for the different images of the same specimen. The nature of the problem was identified to be a non-quadratic pixel size of the camera used for imaging. Since we expected a quadratic pixel format, the apparent effect was that the rotated samples seem to be deformed with respect to each other depending on how they were positioned for imaging. We accurately determined the pixel deformation and corrected the error. In the following we will therefore refer to the corrected images only. Another difference as compared to the inputs for other species concerns the sample data. Since there were no sample data in our standard form available, we derived some description from the sample name. After having managed these extra preparations, the turbot data could be used in the usual way.

The big turbot dataset consists of 925 otolith images. There are mostly images for both dorsal and ventral otoliths. One should point out here that turbot is a flatfish. The asymmetry of the body is also present in the shape of dorsal and ventral otoliths. Therefore, dorsal and ventral otoliths must be treated separately.

There were no sample information files but the file names contain some of the required sample data. Otoliths are from reared fish and were obtained from biweekly sampling catches. There are 408 dorsal and 517 ventral otoliths according to the original description in the dataset. Few errors were detected and corrected (confusion of names for dorsal and ventral, samples rotated by 180° with respect to the usual placement). After these corrections, 405 dorsal otoliths remained in the selected dataset. Most of the results given below are based on this dataset of 405 dorsal turbot otolith shapes. The similarly prepared ventral otolith dataset consists of 520 entries.

As already mentioned, the turbot rearing tanks were sampled biweekly. The number of otolith samples per catch is roughly the same for all sampling dates. Therefore, the distribution of fish-age over the dataset-index is almost linear.

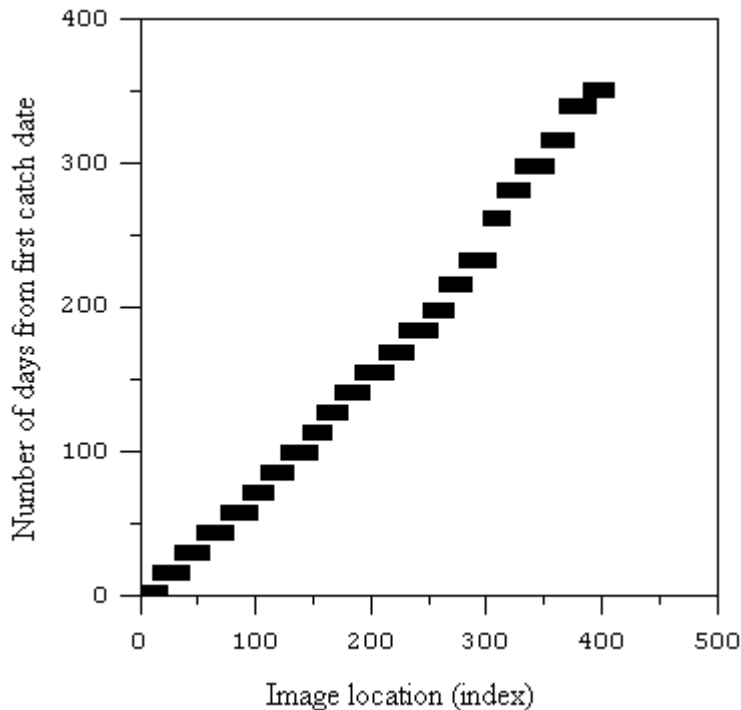


**Figure 5.13:** Number of days from the first catch date. Note that the age of fish increases with the image location. The image location is simply the database index under which the entry is referred to by the IMAGIC-5 software. Since the database is sorted in this appropriate way, one can easily evaluate age features from simple diagrams.

The processing of the otolith silhouette images into Normalised Fourier Descriptors was performed as mentioned before for eel. As usual, contour images were then reconstructed and visually inspected. No errors were detected.

The first round of classifications was carried out on the complete dataset. Unexpectedly, it was extremely difficult to identify any age-related otolith shape classes. An explanation for this lies in

the special dataset composition. The differences between samples from two successive harvests are so small that any statistical evaluation of gross changes within the dataset gets disguised by a lot of unwanted interference. This can easily be understood from the following example. For ease of understanding, assume we have one sample per catch date and a total of  $N_c$  catches. In the dataset we have just one entry for the first catch date and also just one for the final catch date. Therefore we have one 'measurement' for that specific age difference. In contrast to this, there are  $N_c$  measurements for the smallest age difference. In other words, the dataset composition is in no way suited for the determination of any global changes, i.e. for larger age differences. But since there is no other resource for known-age turbot, we decided to use special subsets of the full dataset. Therefore only some results for the full dataset are given here.

We have already mentioned that our way of reasoning is such that for same shapes we infer same features, e.g. age. Also, similar shapes should stand for similar features. Using standard shape classification as implemented in IMAGIC-5, we can easily determine the most similar pairs of otolith shapes. This can be done using the so-called nearest neighbour list or by analysing the shape classes for the critical case. The latter approach means that we start to partition the full set of 405 shapes into initially  $N=405$  classes. This is trivial, since each shape forms a class. When we create 404 classes, one pair of the most-similar shapes within the dataset must aggregate into a class with two members, while all other classes remain as before. This aggregation process goes on, until the first shape class with three members appears. The partitioning with lowest  $N$ , where there are never more than two members in a shape class is called the critical case. In our case we have  $N=373$  and there are 341 single-member classes and 32 classes with two members. We might look at these 32 otolith pairs as being the most-similar shapes within the dataset. In principle, we could have applied a shape distance threshold for selecting larger or smaller subsets of similar pairs of otolith shapes but the described procedure can be performed without need for any additional data processing and programming.

The location numbers and the age difference for the 32 pairs most similar shape pairs are listed in Tab. 5.17.

<b>Location</b>	<b>Location</b>	<b>Age Difference</b>
121	148	14
222	90	112
239	362	133
294	158	119
45	253	168
95	57	14
270	93	158
300	201	77
113	309	177
279	112	130
181	131	42
252	276	32
382	330	58
31	211	140
195	215	14

47	54	0
332	152	168
257	368	119
293	289	0
302	34	217
341	173	171
170	383	212
249	359	133
51	245	154
130	223	70
329	235	98
220	167	42
272	129	116
146	212	56
397	147	251
311	219	93
405	404	0

**Table 5.17:** Location refers to the image position or index within the complete dataset. The age difference is the number of days between catch dates. Since we listed the 32 pairs of very similar shapes, one expects both members to stand for the same age, i.e. to have zero age distance. This is clearly not generally the case!

The actually occurring age differences range from 0 to 251 days. Average and standard deviation are  $103 \pm 70$ . This result may be interpreted as either complete lack of any shape-age relation or as a shape-age relation overshadowed by much stronger but unknown effects.

Some other evaluations were tried for the complete dataset without getting any significant shape-age relations. Therefore, it was finally tested whether the shape analysis can be enhanced by selecting appropriate subsets of the complete dataset.

How the triage was defined can be seen in Fig. 5.14. In the new set, the numbering is 1...128 for young and 129...218 for old specimen. The young and old subsets roughly span the same catch date range. The number of samples is slightly different with 120 young and 90 old. This dataset will be referred to as the 218-dataset in the following.

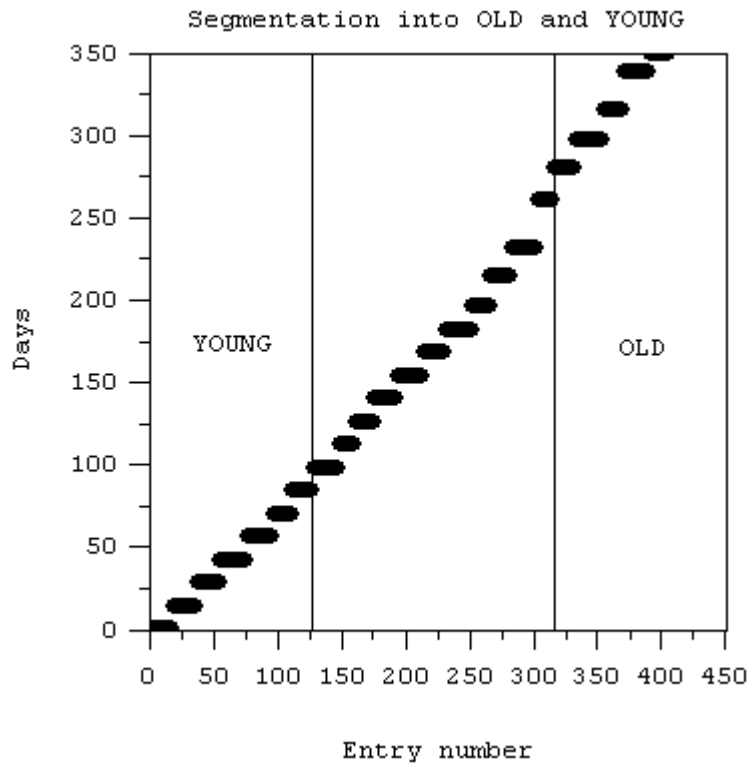


**Figure 5.14:** Division into three portions of the original turbot dataset. Smaller subsets for young and old specimen were defined and a considerable middle-portion was left out to avoid any overlap.

Since the 218-dataset was constructed for the purpose to distinguish between turbot otolith shapes of old and young specimens, it is only natural to try a shape classification into just two groups.

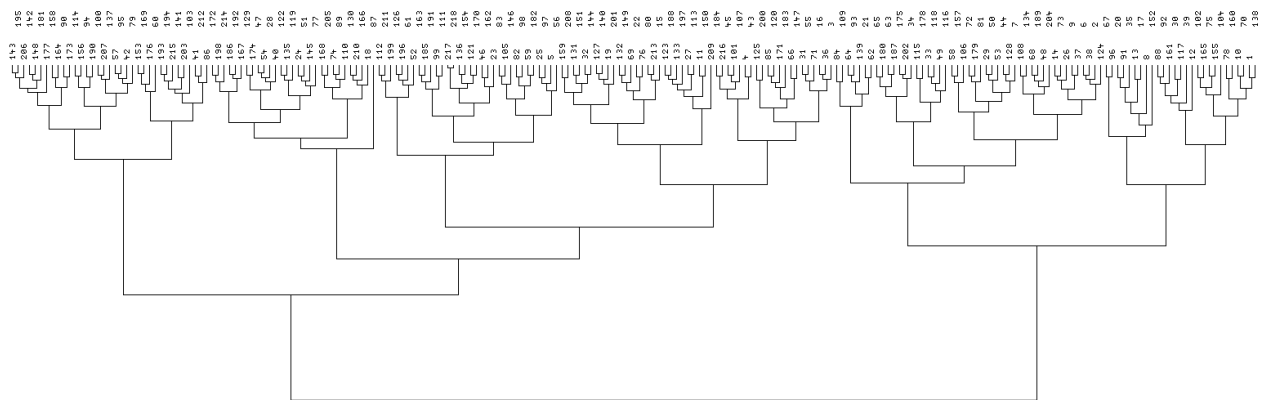


**Figure 5.15:** Hierarchical classification tree for the turbot 218-dataset. The most-significant branching at the baseline produces one large class (left branch) and one smaller class (right branch). The location numbers (two top rows become legible using a higher magnification) can be used to determine the number of young and old specimen in a class.

After counting the number of young and old specimen in some principal classes, one finds that there are indeed at least two larger subgroups that are dominated by old and young members, respectively. It means that these groups could be used to study the shape features in more detail and then try to learn from them.

However, it has to be mentioned that a large portion of the dataset cannot be attributed to old or young since the container classes are too heterogeneous in composition. As will be detailed later, about 1/3 of all objects can be assigned "young" or "old", while 2/3 have to remain "unknown".

A summary and preliminary conclusion may be appropriate at this point. We initially tried to identify age-related shape classes in the complete dataset. Then we streamlined the dataset so as to enhance any inherent age-effects. However, even this dataset is composed of otolith shapes without clear-cut relation to age. Only one third of the dataset shows indications for a positive shape-age relation.

A classification into 13 shape classes was suggested because of the behaviour of some surprising shapes in the dataset. This approach is similar to the procedure described for eel. Leaving out the strange shape, the remaining 12 turbot otolith shape classes were analysed in more detail as shown in the Tab. 5.18.

Class	Members	Young	Old	Prediction	Reliability %	Fraction %
1	8	7	1	Young	88	3.7
2	26	12	14			
3	31	19	12			
4	7	5	2			
5	14	3	11			
6	26	16	10			
7	21	18	3	Young	86	9.6
8	19	4	15	Old	79	8.7
9	15	13	2	Young	87	6.9
10	27	15	12			
11	9	7	2	Young	78	4.1
12	14	8	6			

**Table 5.18:** The determination of age-related shape classes and their evaluation with respect to age-prediction is shown for 12 turbot otolith shape classes. If the numbers of old and young members of a class indicate a significant age-relation, we can calculate the reliability as the quotient of number of correct predictions over the total number. Fraction are calculated as quotient of all class members over the total number of dataset entries. Note that only about 1/3 of all otolith shapes belong to classes with some age-prediction power. The number of correctly aged samples is even smaller than that!

Previously, we couldn't detect any shape-age relations in the complete dataset. Now we have some vague hints but the results are not really encouraging. We therefore need to look at the few

otolith shape classes for which some trend was recognisable and try to understand the underlying shape features.

The otolith shape classes can be visualised in several ways. The average over 2D shapes is helpful in some instances, in other cases one needs the graphical representation of the average NFDs. Both are shown in Fig 5.16.

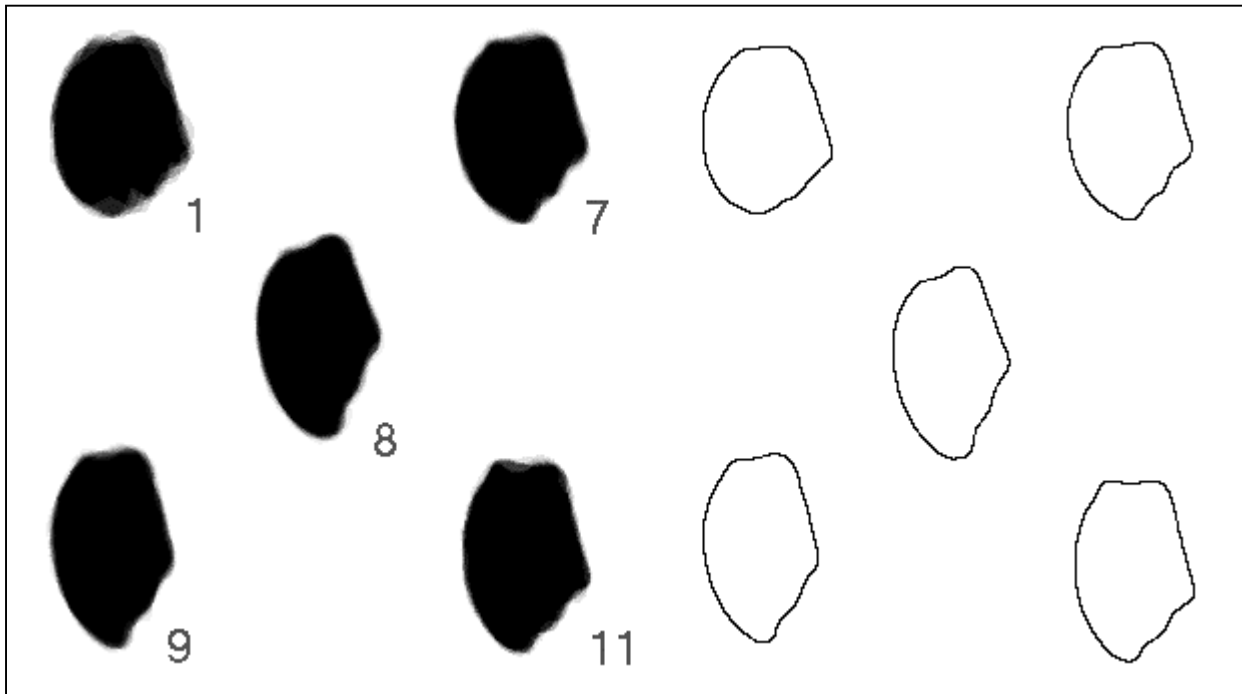


**Figure 5.16:** To the left are filled-contour averages, to the right are NFD averages. The object in the centre represents class 8. Class 8 is the one that stands for 'old' otoliths, while all others have predicate 'young'. Class numbers correspond to classes as defined in the text.

The fainter grey tones in the left images indicate variable otolith portions. However, these variations are small as compared to the clearly recognisable shape differences between the different shape classes.

Shape class 8 specifically contains old otoliths. The class average stands for an overall object shape that is elongated in the one direction and thin in the other. This overall shape is quite dissimilar from class 1, which obviously consists of round shaped otoliths.

The same kind of round overall-shape is somehow visible for shape class averages 7 and 11. The shape class 9 average is somehow in-between the two extremes 1 and 8. It looks pretty close to 8, so one should expect class 9 to be an 'old' class - but it is not!

This example demonstrates that some features may become apparent from the class averages. It is, however, very error-prone to only follow intuitive-visual analysis based on just looking at the

graphical representations. The better way is to rely on objective parameters such as the ones obtained from an eigenimage analysis over the dataset.

Therefore, so far we can only give very tentative conclusions for turbot:

- The observed age-related shape properties of otolith from 'old' versus 'young' specimen can be rationalised in terms of elongation or roundness of contours.
- It appears that round shaped otolith correspond to young fish while more elongated ones correspond to old.
- The differences are very subtle and could only be revealed after the middle-aged portion of the complete dataset was removed.
- There is a large proportion in the original dataset for which age-related features do not exist or are not statistically relevant.

To conclude this part of the report, an image showing all 13 shape classes for the turbot dataset is shown Fig. 5.17. It might become clear from this figure how difficult the task of ageing by otolith shape analysis is:

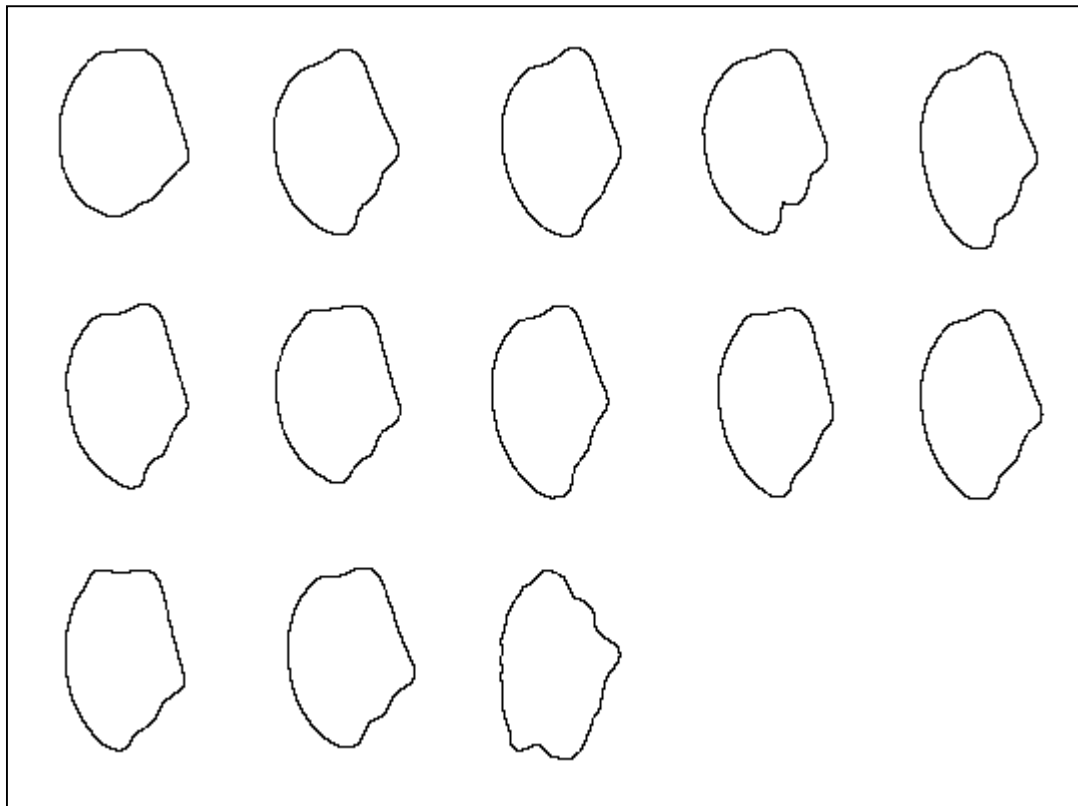


**Figure 5.17:** All 13 shape classes for the turbot 218-dataset. The numbering is from left to right and starts with 1 at the top left. Note that the last class consists of the 'stranger' only! The classes have the following number of members: 8, 26, 31, 7, 14, 26, 21, 19, 15, 27, 9, 14, 1.

There were some more results from investigations for turbot, which can however be left out here, since they just confirm the findings described so far. Therefore only the results from the analysis of ventral otoliths will be given in the following.

Out of the total of 925 turbot otolith samples, 520 are ventral otoliths. Similarly as for the dorsal otoliths, the dataset was split to obtain subsets for 'young', 'middle-aged' and 'old'.

Index in the 925 dataset	Index in the ventral dataset	Days from first catch date	Type	Ventral dataset
2	1	1	young	total of 147
275	147	84	young	
277	148	98	middle	total of 256
718	403	261	middle	
720	404	280	old	total of 117
925	520	349	old	

**Table 5.19:** Division of the 520 dorsal turbot otolith dataset into young, middle-aged and old samples.

The 520 ventral dataset was subjected to classification in the same way as for the dorsal 405 dataset. Especially, in this case 19 classes were demanded. This is in analogy to the 405 dataset. It might be argued, however, that one should classify the whole dataset into  $19 \cdot 520 / 405$ , which is about 25. This would take into account that there are significantly more entries in the ventral dataset than in the dorsal. We will come back to this topic later.

The classification was analysed. Tab. 5.20 summarises the results.

Class No	# young	# middle	# old	Tentative Meaning	Reliability
1	16	16	5	young	76%
2	9	12	5		
3	3	16	10	old	77%
4	8	11	7		
5	14	21	5	young	74%
6	8	15	4		
7	5	8	1		
8	3	12	6		
9	4	11	1		
10	3	19	12	old	80%
11	8	10	11		
12	17	16	8		
13	4	18	9		
14	3	22	8		
15	7	8	6		
16	13	7	2	young	87%
17	10	8	5		
18	1	14	3		
19	10	13	9		

**Table 5.20:** Determination of age-specific classes and their reliability for age prediction.

The notes in the table columns "Tentative Meaning" and "Reliability" are for the most obvious cases. There are smaller classes that might show age-shape correlation. However, here the main point is that there are five classes within the complete dataset for which some kind of pretty reliable prediction can be made. It should be noted that calculations for the leftmost two columns in the above table leave out all 'middle' aged objects. On average, the middle-aged group consists of as many objects as 'young' and 'old' together.

For the above five age-specific classes, shape averages were calculated and are shown in Fig. 5.18.

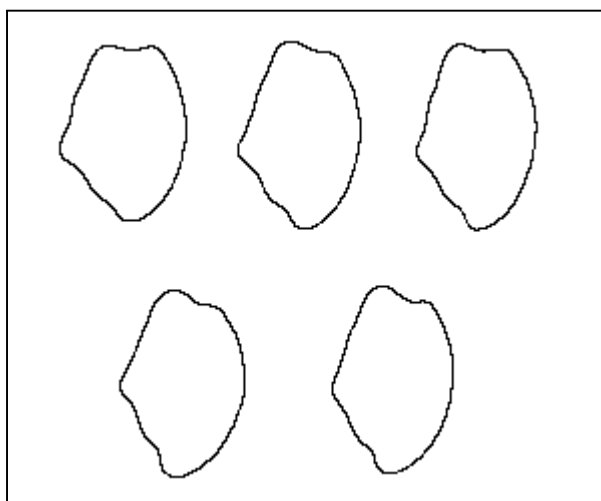


**Figure 5.18:** Classes in the upper row are 1, 5, and 16. The other classes are 3 and 10. For more details refer to the above table.

This time, there is no evident feature like "thin" and "thick" or "round" and "elongated". There is no good explanation for the different behaviour as compared to dorsal otoliths. However, our turbot specialist in the project stated that ventral otoliths may generally be more variable in shape and if he was to decide which type of otolith to use, he used the dorsal.

The formation of 25 classes out of the 520 ventral otolith images should produce an average class size of  $520/25 = 20.8$ . There is however one class containing only one member so that we get instead  $519/24 = 21.67$ . We find classes of size between 8 and 37, and the one outsider class.

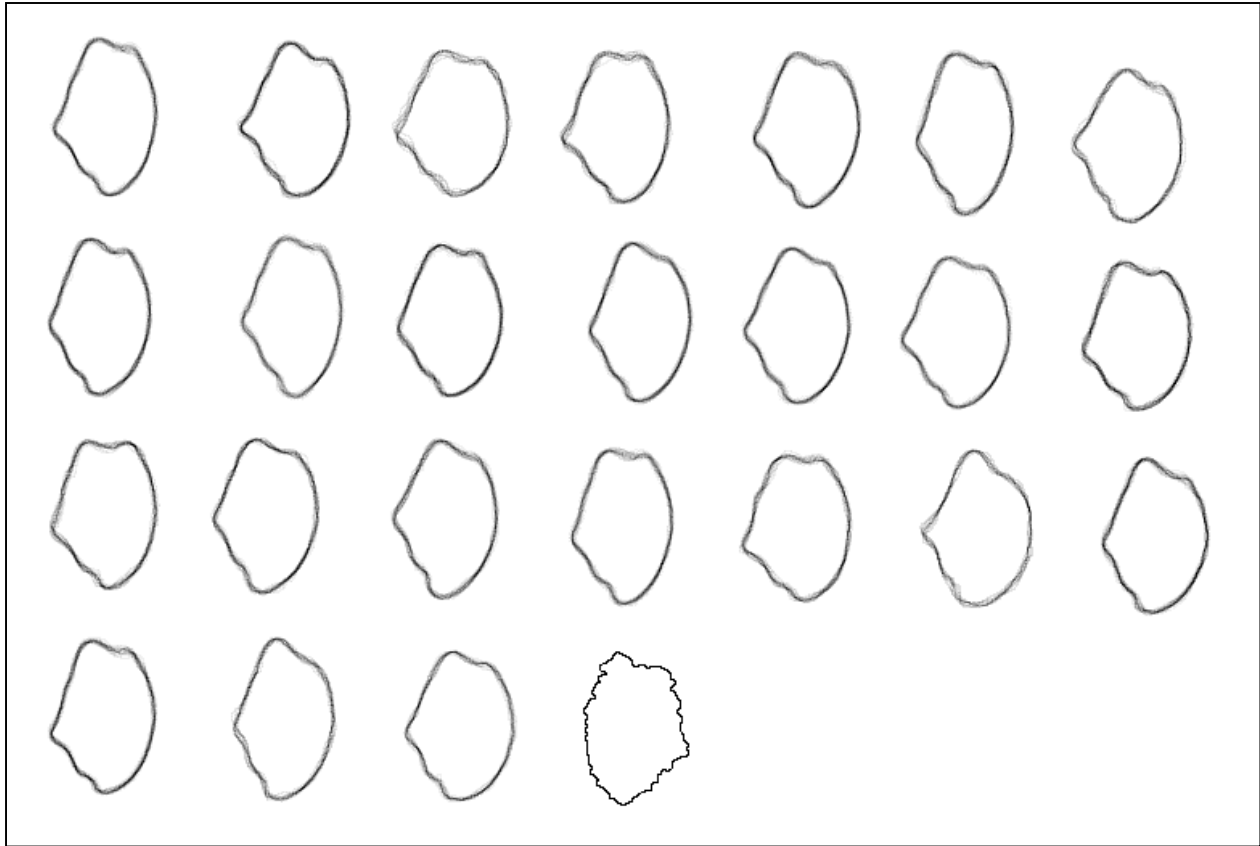


**Figure 5.19:** Class averages for 25 classes for the 520 ventral turbot otoliths. Note that the last class contains an outlier!

Some classes seem to consist of a narrow range of variations only. There is only few fading around the contour line indicating highly conserved geometry. Other classes, e.g. class 3, show spurious contours indicating high internal variance within the class. Please remember that the dorsal group was consistent when classified into 19 classes. We might therefore say that the ventral group has  $100 \cdot (24/19)\% = 126\%$  of the variance of the dorsal group.

The 25 shape classes were analysed as already shown several times. Therefore we can skip details here and look at the very final results and conclusions.

The main result from this analysis can be summarised in three shape class averages, two for young samples and one for old. The shapes are extremely similar so that a rational understanding of the shape features becomes very tricky. We must therefore acknowledge that the ventral otolith are either even less related to age than the dorsal ones, or that there is no shape-age relation at all.

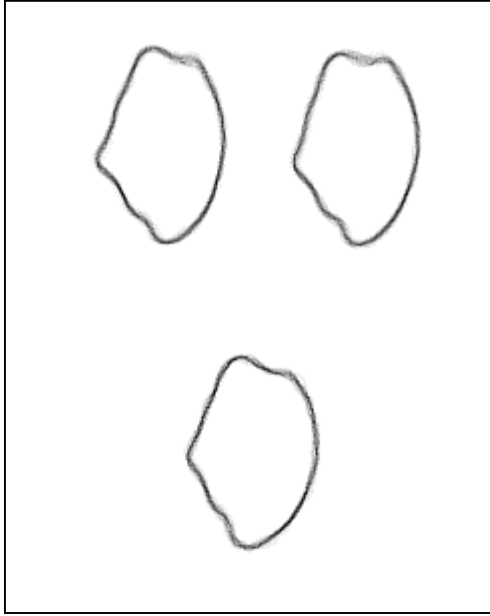


**Figure 5.20:** The upper two averages are for young otolith, the lower is for old. Note that shape differences are very subtle.

We can summarise all results for turbot:

1. It was found that the more or less continuous age-structure of the turbot dataset makes it hard to unambiguously define correlations of age with shape.
2. One way to circumvent the above problem is to split the dataset in three portions (ca. 1/4 young, 2/4 middle, 1/4 old) and disregard the middle portion.
3. Close examination of the dorsal and ventral datasets yielded some insight into the question of how many classes should optimally be distinguished within each of the datasets.
4. Appropriate numbers of different classes to be considered are 19 and 25, for the dorsal and ventral groups, respectively.
5. In both the dorsal and ventral groups there is unfortunately only a small fraction of all objects that can be classified with good reliability of mostly more than 80%.
6. The portions of the total dataset that are somehow age-specific are 33% and 15%, for the dorsal and ventral datasets, respectively.
7. The classes that specifically contain young or old otoliths do not obviously follow a visual pattern. Such a pattern was believed to be identified for dorsal otoliths but couldn't be verified for the ventral otoliths.
8. Most of the shapes in the datasets, however, aggregate into classes having heterogeneous age-structure.

9. In conclusion it appears that there is no reliable shape-age prediction for the majority of samples in the turbot dataset.

When these results were discussed with the project partners, some felt their initial assumption confirmed that otolith shape cannot be used for ageing turbot. Still there was an open question as to what degree the otolith size can be employed for that purpose. In the following we will therefore present important results on that topic before again addressing shape analysis on turbot otoliths including eigenshape determination and interpretation.

We wanted to establish the predictive value of otolith size and other similar measures for ageing of turbot. Having an idea of how reliable such models are, we expect to get an idea of how good the shape analysis results are in comparison.

The simplest way to obtain information on the age of a fish is measuring body length, and relate it to an age/body-length key. Fish growth rate, and thereby the age/body-length relation is, however, subject to a high degree of variation being dependent on temperature, food availability, salinity genetic factors etc. This limits the use of body length alone to estimate age, and age-body length keys have to be revised frequently. Age is usually obtained from analysis of increment formations in body hard parts such as otoliths and scales. Such age determinations are both difficult and time consuming. They also involve a subjective element. Continued training of otolith readers and intercalibration exercises are therefore necessary. However even experienced readers face situations, where it is impossible to identify any increments in the body hard parts. Because of these difficulties, there is a considerable interest in alternative methods for ageing of fish. Many studies have demonstrated that otolith growth is more conservative, i.e. steady, than body growth, with the effect of slow growing fish having larger otoliths than faster growing fish of the same size.

Therefore, if otolith size is less affected by growth rate than body length, then otolith size could be a better estimator of age, than body length measurements. Combining measurements of body length with age related information from the otoliths could be a method to age fish in cases where increment readings cannot be used. In the present study, it is investigated whether otolith length has a better relation to age than body length measurements, and whether otolith size, or similarly otolith length, otolith area, otolith weight and shape contain additional information which can be used in combination with body length measurements to estimate age. Variability in otolith size is compared to variability in body size in a group of field-caught and traditionally aged turbot. A more detailed study of age effects on otolith size and shape is performed on a group of reared turbot of the same size and background, having age and thereby growth rate as the only variable.

### Description of samples and procedures

Otoliths for comparison of variability in body length and otolith length were obtained from a set of turbot (*Scophthalmus maximus*) otoliths sampled from the commercial fishery in the Baltic in 1988. The fish were aged using traditional counting of annuli. For the present study the first 100 otoliths, if available, of each age group (2-7 years) were used, which fulfilled the criteria of same ageing result by two experienced, independent readers, and both otoliths being available and

intact. For each fish total length was measured to nearest semi-cm below. Length of the otoliths were measured to nearest 0.01mm using a microscope ruler. Age effect on fish of same length but different age was compared for the length groups 30, 31, 32, 33, 34, 35 and 36 cm where at least 20 individuals were available

Turbot of known age were obtained from a rearing experiment. The turbot were reared from hatching until a size of approximately 5cm at a commercial Danish hatchery (Maximus). The eggs originated from the North Sea stock. The juveniles were transferred to on-growing at the Danish Institute for Fisheries Research, Hirtshals, Denmark. Rearing was conducted in 34□ seawater at ambient temperature. The fish were fed commercial turbot food pellets. From age 400 days to age 800 days samples of 25 fish were taken every second week. Samples were not taken at random, but individuals were selected to cover the size range 10-20cm during the whole experimental period. Total length was measured to nearest mm-below. Both sagitta otoliths were removed and measured. The mean of the two values was used in calculations. Otolith length was measured to nearest 0.01mm using a microscope ocular ruler. Otolith area was measured in mm<sup>2</sup> with a planimeter and a microscope drawing board. Otolith length was registered with a precision of 0.01mm using a Cahn microbalance. Otolith size (length, area and weight) was calculated as mean of the left and the right otoliths. For individuals where only one otolith was available, measured size was adjusted for mean difference between left and right otoliths. Only the length groups 13, 14, 15, 16, 17, 18, 19 and 20cm which contained at least 20 individuals were included in the analyses. Otolith shape was analysed by comparison of contour images. Otolith images were produced with the aid of a video camera mounted on a dissection microscope with 12x magnification. Maximum contrast between otolith and air was obtained using transmitted light. All image processings, as explained in previous report sections, were performed with the IMAGIC-5 program suite. Otolith contours were classified into shape groups and the age composition within these groups was then determined by counting the number of shapes from young and old specimen.

### Body total length – otolith length

For the age groups 2-7, the body length and the maximal otolith diameter show a consistent relation. The individual variations are considerable but one might accept an overall linear relation as shown in the below Fig. 5.21.

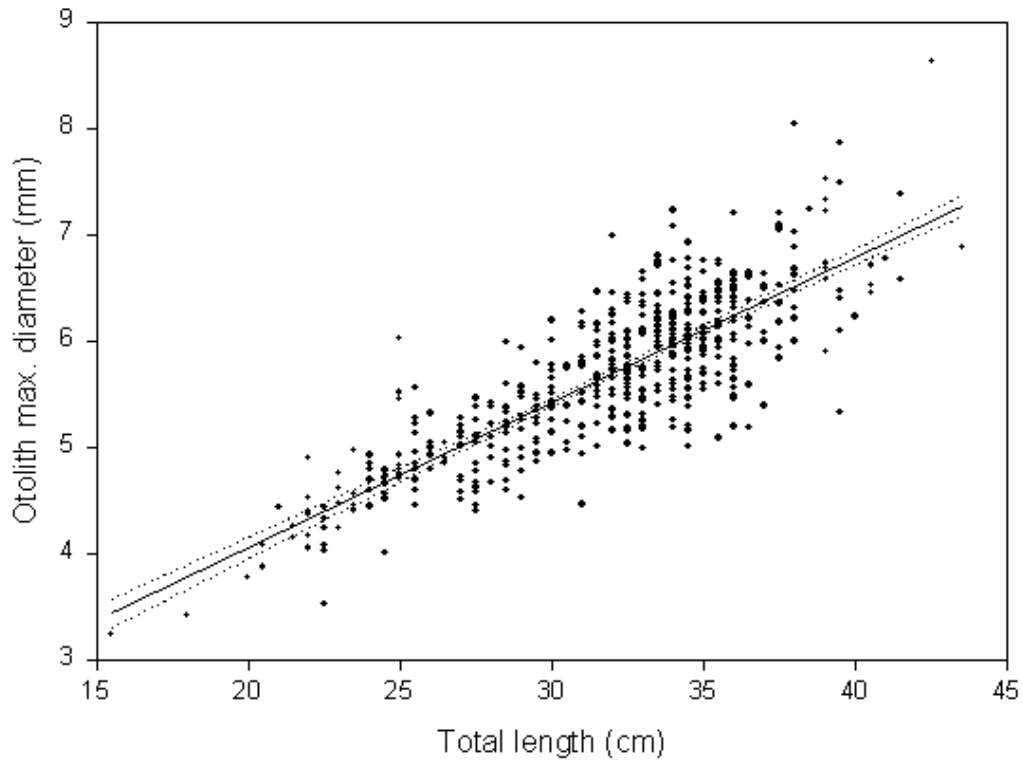


**Figure 5.21:** A plot of otolith length against total body length for 528 turbot in the age groups 2-7 years shows that otolith length increases linearly with body length.

Variability of otolith length and body length at age was compared by calculating standard deviations for body length at age and for otolith length at age for each age group. There was no significant difference between standard deviations of body length and otolith length as can be seen in Fig. 5.22.

### Body and otolith size (Mean and STD) of 2-7 years turbot

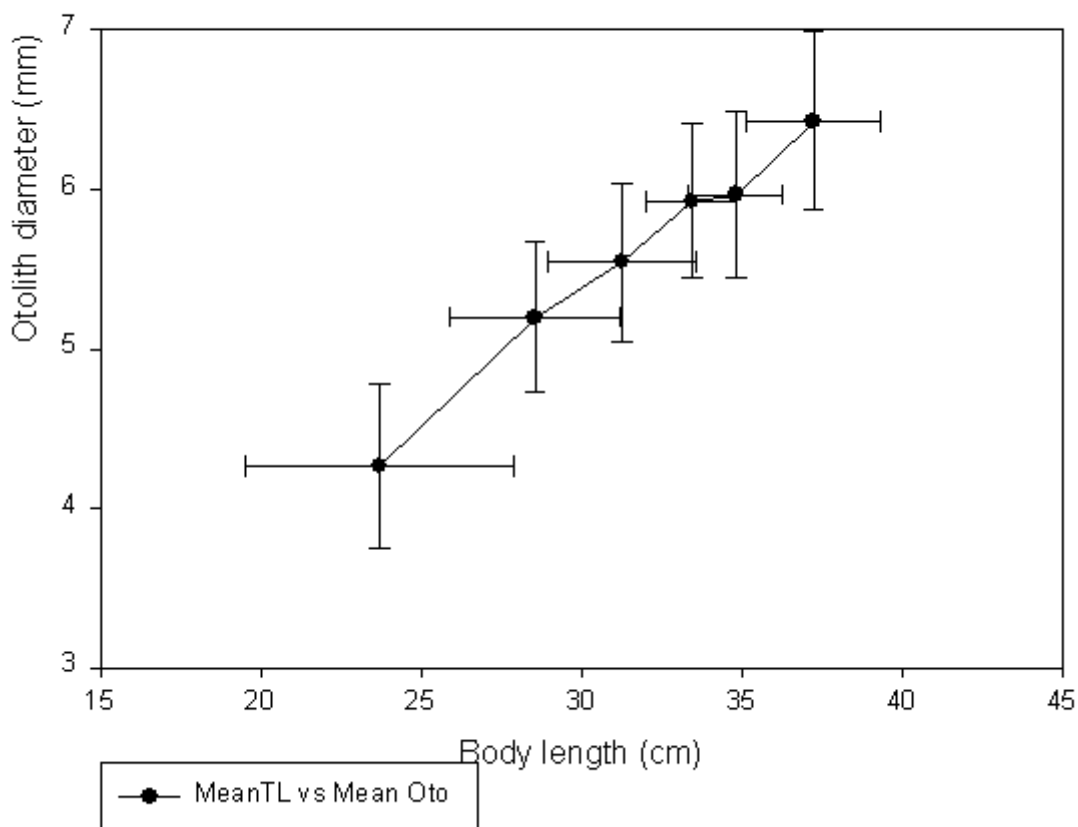


**Figure 5.22:** The average body size and otolith size for the individual age groups are plotted. The error bars indicate the respective standard deviations.

Otolith length was plotted against age for each cm length group in the range 30 cm to 36 cm. Regression lines were calculated for each length group. As shown in the below figure, the slopes range between  $0.0107\text{year}^{-1}$  and  $0.110\text{year}^{-1}$  equal to an increase in otolith length per year of 0.17% to 1.97% with a mean of 0.92% for the 7 length groups. The increase is significant, but the correlation coefficient so low (mean  $r^2 = 0.025$ ) that only 2.5% of the variation in otolith length is explained by the age effect.

Baltic wild turbot  
age 2-7 years

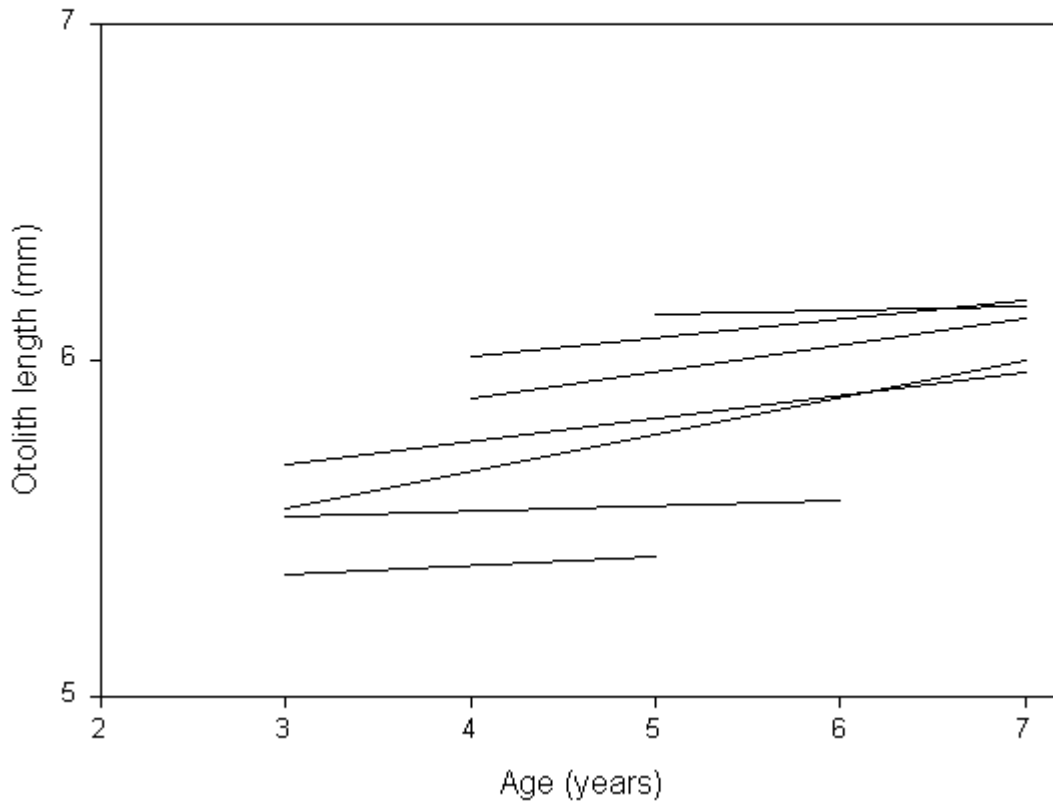


**Figure 5.23:** Regression lines for the individual body length groups.

The variability in otolith length at same body length is exemplified in the following plot for the 59 individuals in the 34cm length group.

### Otolith size 34 cm Baltic turbot of different age

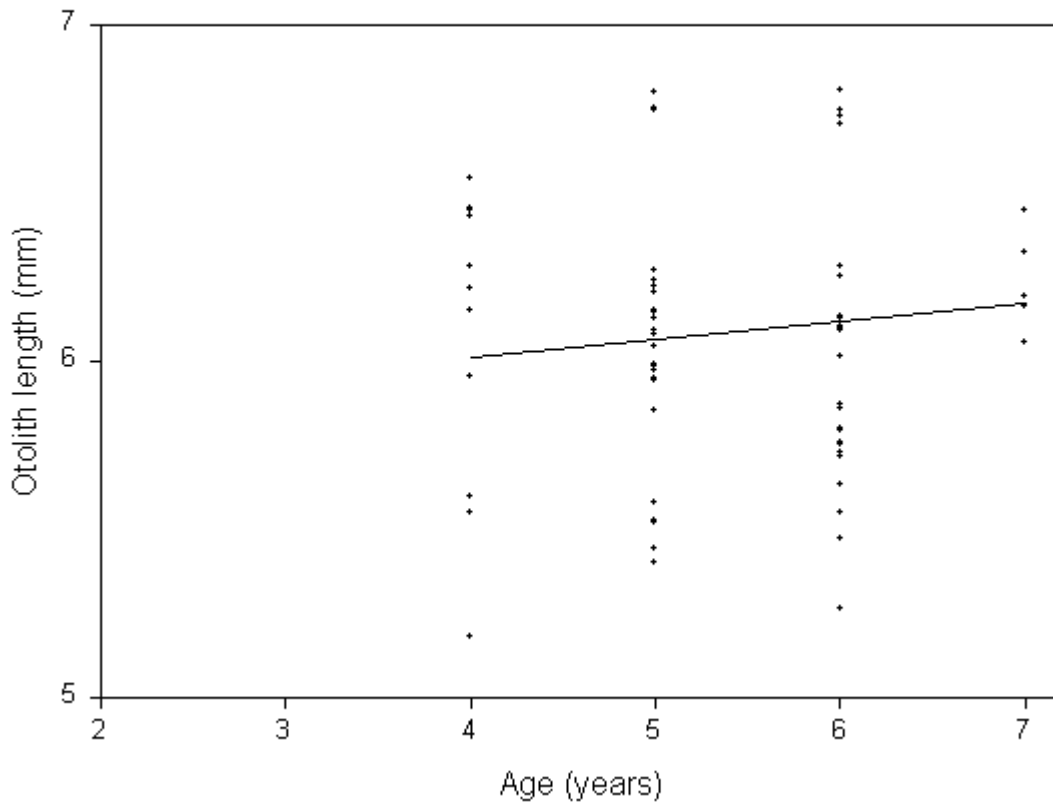


**Figure 5.23:** The 34cm length group was chosen as a typical example. Although one sees the high variability in otolith length, a trend is clearly recognizable.

#### Otolith size and area

A similar analysis of variability in otolith length at age was performed for the reared turbot. The results are shown in the next three figures.

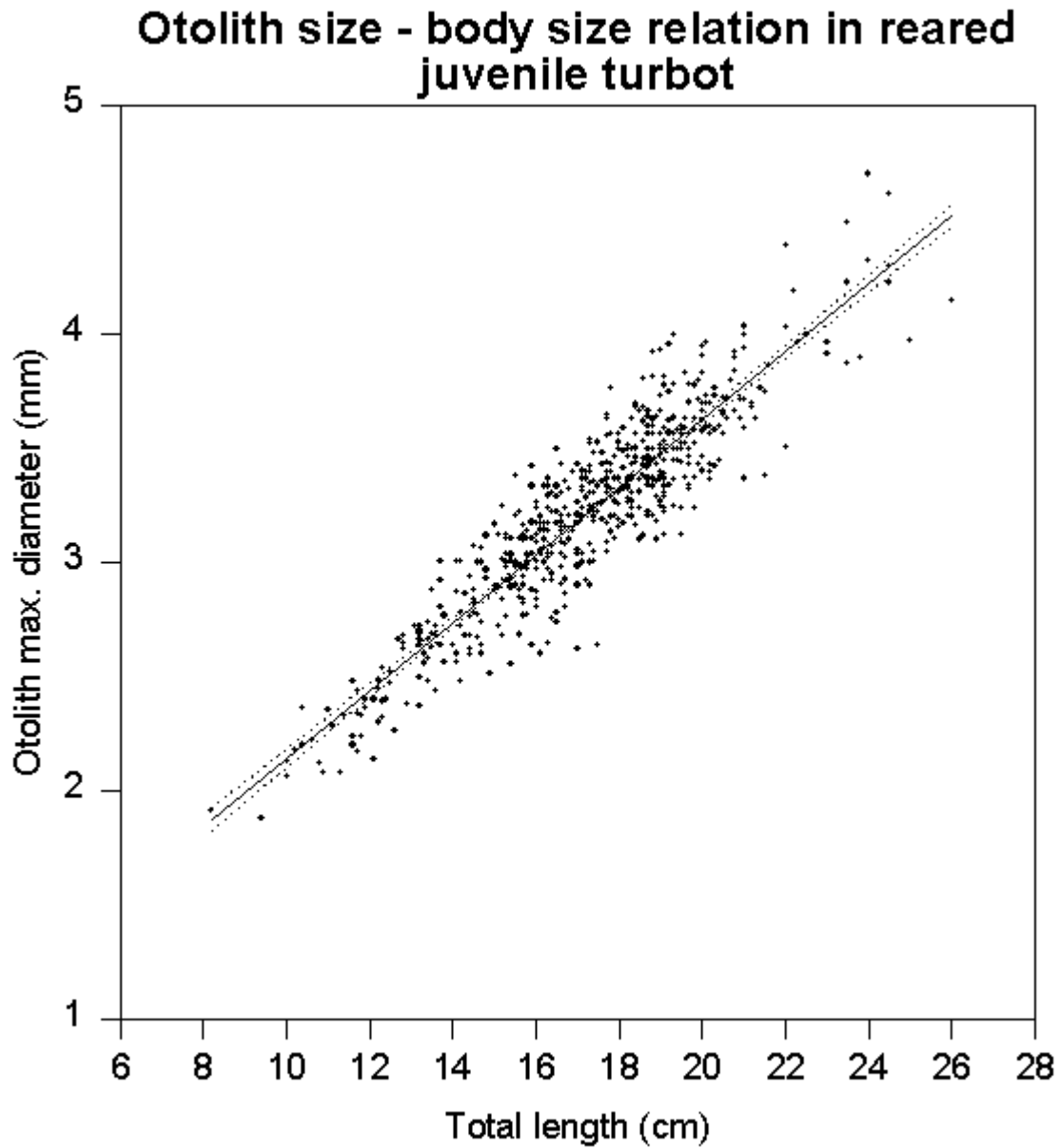


**Figure 5.25:** A clearly visible linear relation between the body length and the otolith length is suggested from the plot of data for reared juvenile turbot.

#### D. otolith diameter - age relation for all length groups

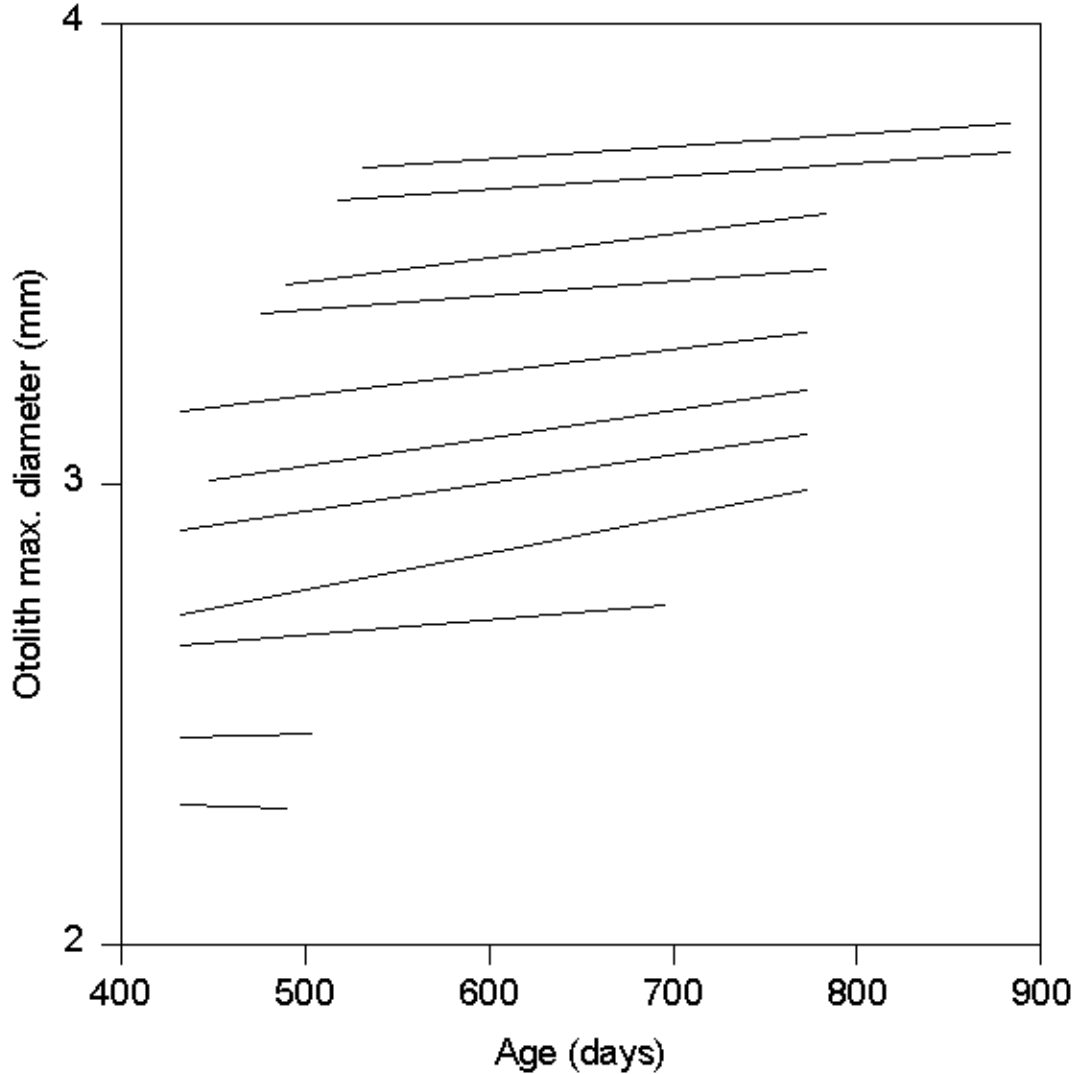


**Figure 5.26:** The regression slopes for the reared juvenile turbot. Note that even for the relatively short duration of the rearing experiment a general tendency can unambiguously be established.

The slopes of the otolith length-age regressions range from  $0.105 \cdot \text{year}^{-1}$  to  $0.289 \cdot \text{year}^{-1}$  with a mean of  $0.182 \cdot \text{year}^{-1}$ , equal to an increase in otolith length per year of 2.9% to 10.6% with a mean of 6.0% for the 13cm to 20cm length groups. The correlation coefficients range from 0.020 to 0.122 with a mean of 0.068. Age is therefore explaining 6.8% of the variability in otolith length for fish of same length.

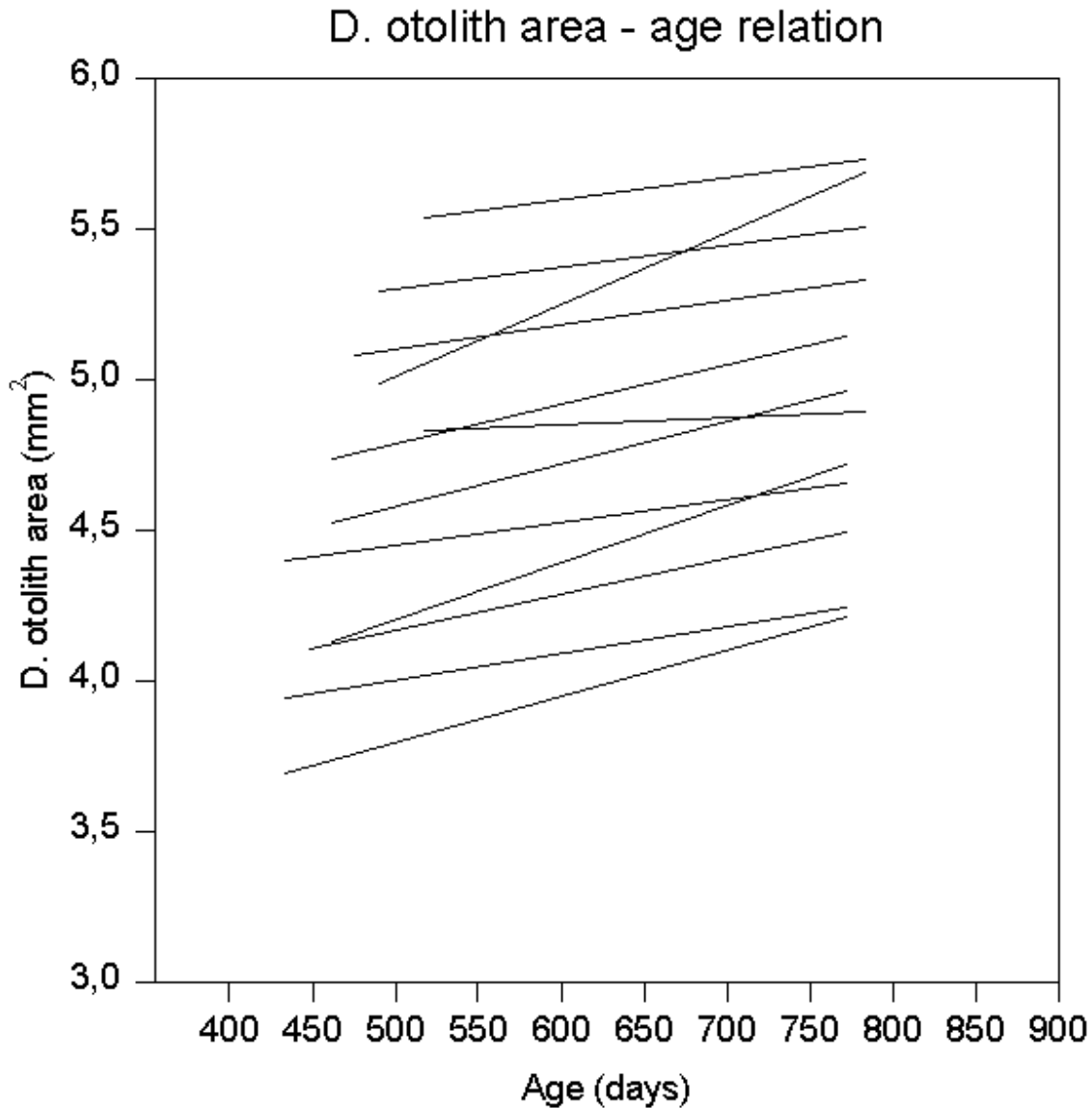


**Figure 5.27:** The regression slopes for the reared juvenile turbot. For this analysis, the otolith area has been used.

In the following we address to the otolith area, which might be a little bit more reliable than the maximal otolith diameter, since the area does not depends on the specific profile of the countour line at a selected position. In other words, the measurements of the maximal diameter might be more error prone due to random variations.

The slopes of the otolith area-age regression were ranging from  $0.071 \cdot \text{year}^{-1}$  to  $0.566 \cdot \text{year}^{-1}$  with a mean of  $0.382 \cdot \text{year}^{-1}$ , equal to an increase in otolith area per year of 2.4% to 14.4% with a mean of 9.0% for the 8 length groups. The correlation coefficients range from 0.002 to 0.168 with a mean of 0.100. Age is therefore explaining 10.0% of the variability in otolith area, for fish of same length. The slopes of the otolith weight-age regressions range from  $0.474 \cdot \text{year}^{-1}$  to

1.041\*year<sup>-1</sup> with a mean of 0.779\*year<sup>-1</sup>, equal to an increase in otolith weight per year of 10.0% to 37.5% with a mean of 20.9% for the 8 length groups. The correlation coefficients range from 0.063 to 0.302 with a mean of 0.229. Age is therefore explaining 22.9% of the variability in otolith weight, for fish of same length.

As for the wild turbot, for reared fish there is approximately the same clearcut growth-related tendencies. Therefore we restrict ourselves just to showing the results for reared fish as summarised in the Tab. 5.21.

Length group (cm)	N	Otolith length		Otolith area		Otolith weight	
		Age effect %*Year <sup>-1</sup>	Correlation coefficient	Age effect %*Year <sup>-1</sup>	Correlation coefficient	Age effect %*Year <sup>-1</sup>	Correlation coefficient
13	23	4.7	0.020	2.4	0.002	37.5	0.302
14	32	10.6	0.122	10.0	0.158	21.5	0.249
15	49	7.7	0.115	14.4	0.168	23.6	0.287
16	87	7.4	0.091	8.4	0.061	15.8	0.142
17	78	5.7	0.059	13.0	0.165	21.6	0.273
18	88	3.5	0.032	3.1	0.010	10.0	0.063
19	97	5.6	0.062	10.0	0.103	17.8	0.222
20	58	2.9	0.043	10.4	0.136	19.1	0.293
Average value		6.0	0.068	9.0	0.100	20.9	0.229

**Table 5.21:** Effect of age on otolith length, area and weight for reared turbot age 400 to 800 days. Regressions of otolith size versus age. Age effect calculated from size at day 400.

The increased age effect using weight instead of length follows the general changes in proportions which can be expected when moving from a one dimensional system (length) to a three dimensional system (weight – a function of volume). As an example, an increase in length of 6% would generate an increase in area of  $1.06 \times 1.06 = 11.2\%$  and an increase in weight of  $1.06 \times 1.06 \times 1.06 = 19.1\%$ . This is close to the mean age effect observed, and shows that the mean size of the otoliths follows the proportional model.

If the variation in individual otolith length were reflected in the variation in otolith weight, then correlation coefficients of the length and of the weight regressions would be almost similar, despite the higher slopes of the weight regressions. It was found that the correlation coefficients for the weight parameter were much higher (mean 0.229) than the coefficients for length (mean 0.068) and area (mean 0.100). Otolith weight is therefore less variable than could be expected from the variation in otolith length, and is therefore a better predictor of age in individual fish.

### Otolith shape

Some aspects of the following presentation have also been covered in a previous paragraph. However, for consistency, we decided to present the otolith shape results here again in full detail because they are used in a different context and exploited in a different way than before.

Otolith shape was investigated from a total of 925 otolith images of which 408 were left otoliths and 517 were right otoliths. Of the 408 otoliths, 405 could be used for description of shapes in the form of Fourier descriptors. The initial analysis of the Fourier descriptors showed that shape did not change in a progressive way that could be identified in the present dataset, which was sampled at bi-weekly intervals over a period of 400 days. It was therefore decided to concentrate on comparing otolith shapes in the 128 youngest and the 90 oldest fish. In order to obtain a reasonable number of fish in each Fourier descriptor class the 218 otoliths were classified in 12 classes.

The results shown Tab. 5.22 demonstrate that 7 of the classes are heterogeneous and contains young and old individuals in comparable numbers, while 5 classes are dominated by young or old fish. Of these five classes, four are characteristics for young fish.

Class	Otoliths in class	Otoliths from young	Otoliths from old	Group reliability %	Fraction of total data %
1	8	7	1	young 88%	3.7%
2	26	12	14		
3	31	19	12		
4	7	5	2		
5	14	3	11		
6	26	16	10		
7	21	18	3	young 86%	9.6%
8	19	4	15	old 79%	8.7%
9	15	13	2	young 87%	6.9%
10	27	15	12		
11	9	7	2	young 78%	4.1%
12	14	8	6		
Total	218	128	90		<b>33%</b>

**Table 5.22:** Evaluation of the composition of 12 shape classes based on Fourier descriptors for shape. The number of young and old class members was determined. There were 128 "young" and 90 "old" turbot in the dataset.

The Fourier descriptor class averages for the five classes, which are either dominated by young or by old fish, are shown in Fig. 5.28.

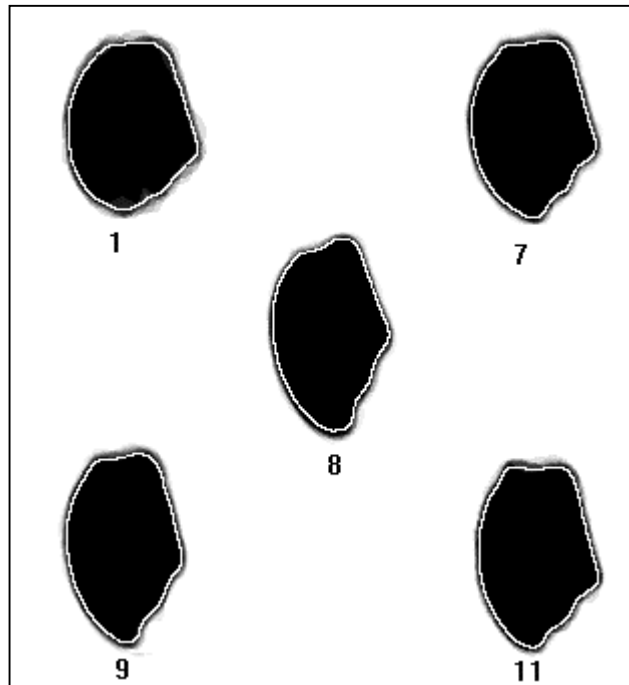


**Figure 5.28:** The five shape classes with either predominantly young or old specimen. The shape class in the center stands for "old" fish, while others are for "young".

Class no. 8 is dominated by old fish otoliths. This class average stands for an overall objects shape that is elongated in one direction and thin in the other. This overall shape is dissimilar from class no. 1, which contains round shaped otoliths. The same kind of round overall shape is somehow visible for class averages no. 7 and 11. Class no. 9 appears to look very much like class no. 8, but represents young individuals. This example demonstrates that some features may become apparent from the Fourier descriptor class averages, which are not apparent for the human eye.

It has been demonstrated repeatedly, that although there is general proportionality between otolith size and body size, otolith growth is affected by somatic growth rates with slow growing individuals having relatively larger otoliths than faster growing individuals. It has even been demonstrated that otolith growth can continue when there is no somatic growth, e.g. during starvation. The slow growing individuals in a cohort will therefore have a smaller body size and otolith size, than the faster growing individuals, but the otoliths will not be as small as could be expected in a situation of a proportional growth. A possible effect of this could be that otoliths size would be less variable than body size.

This was investigated by comparing variability of otolith length and body length in relation to age in a sample of Baltic turbot from the commercial fishery. The results showed no indication of a difference between standard deviations of the two parameters. Otolith length measurements are therefore equal in precision to body length measurements for estimation of age. The explanation

for this is probably the high variability in the shape of the otoliths, which gives a high variability in length.

A comparison of otolith lengths in individuals of same body length but different age shows that otolith length increases slightly with increasing age, confirming previous observations of relatively large otoliths in slow growing individuals. The growth rate effect on otolith length was calculated for both the wild and the reared turbot. The effect was most pronounced in the reared turbot where the otoliths were on average 6% larger in individuals of age 400days + 1 year compared to individuals of same length being 400 days old. In the wild fish, the mean increase was 0.9% for individuals of 4 years compare to individuals of same length but 3 years old. It should be noted that an age increase of one year is relatively higher in the reared (400 days old fish) than in the wild (3 years old fish), the two groups are therefore not directly comparable.

A calculation of the age effect on otolith size shows that mean otolith size is affected by age in proportion to measuring size in one dimension (length), two dimensions (area) or three dimensions (weight). Looking at individual otoliths it is observed that the variability in otolith length is not reflected to the same degree in area and particularly in weights. A comparison of age effects on otolith length, -area and -weight shows much higher correlation coefficients for the otolith weight-age regressions, than for the length and area regressions. Otolith weight is therefore reflecting age better than otolith length or area. Based on these results it can be concluded that age determinations based on body length measurements can be improved by adding age informations from otolith weight -age regressions. The predictive power of including otolith weight is estimated to be 22.9%.

At this point we should note that it is still an open question, if we can quantify our findings for appropriate use in practise? Let's say we have a 50 cm fish which should be 4years old based on length measurement and an age-length key. The otolith weight - age regression for this length group indicates that the fish should be 6 years. ( $R^2 = 0,229$ ). What is our final estimate of age for this fish?  $4 \text{ years} + 2 \times 0.229 = 4,45 \text{ years}$  ?

The results of the Fourier descriptor shape analysis demonstrate that only 33% of the otoliths could be correctly classified as young or old. The average ability to distinguish between "young" and "old" fish was approx. 84%. The predictive power of the shape analysis is therefore 84% of the 33% equal to 28%. As the age difference between "young" and "old" fish is about one year, it can be concluded that the predictive power of otolith shape is nearly similar to otolith weight. Otolith weights are easy to obtain, but the variations in weights can probably not be explained further, and it's therefore unlikely that the predictive power of using otolith weights can be improved. The use of otolith shape analysis, on the other hand, is dependent on a sophisticated Fourier analysis classification tool, as the IMAGIC-5 software. However, shape classifications could possibly be improved with access to more otoliths, and this would increase the predictive power.

The value of using otoliths weight or shape for age estimation of fish with different origin is dependent on the extent of natural variations. If otolith shape is affected by e.g. sex, stock or environment it will be reducing the predictive ability of a classification based on fish with a different origin. The turbot otoliths used here are from fish reared during the whole lifespan. Visually these otoliths appear to be more rounded than otoliths from fish caught in a natural

environment. Shape classifications should therefore be established for fish representative for the fish population later to be aged by otolith shape analysis.

In the light of these findings it becomes clear that the task of fish ageing by otolith shape - when taken serious - is even tougher than basing an ageing model on body length or otolith weight. We do have a pretty conserved general shape but the shape variations for same age samples are high and the shape change trends between young and old fish are small. Therefore, we face the same, if not even more severe, problems in employing otolith shape than the problems we face for other more standard descriptors.

So even if we could not come up with any readily applicable ageing model so far, we like to understand how the turbot otolith shape develops in the growing fish. As we have seen for eel, the best method is the eigenimage analysis in combination with the decomposition of the most significant and most discriminating eigenimage.

Eel and turbot are somewhat similar in so far as only few shape classes based on NFDs could be identified which may be specific for age. When we applied eigenimage analysis to the eel dataset, it became clear that there are well recognisable shape differences, however, these are not age-related. So finally we have to check this out for turbot.

For the eigenimage analysis, the 405-turbot dataset was used. 768x768 contour reconstruction images were generated and the inner region of 350x300 pixels was cut out. Some examples are shown in Fig. 5.29 and the resulting eigenimages are shown in Fig.5.30.

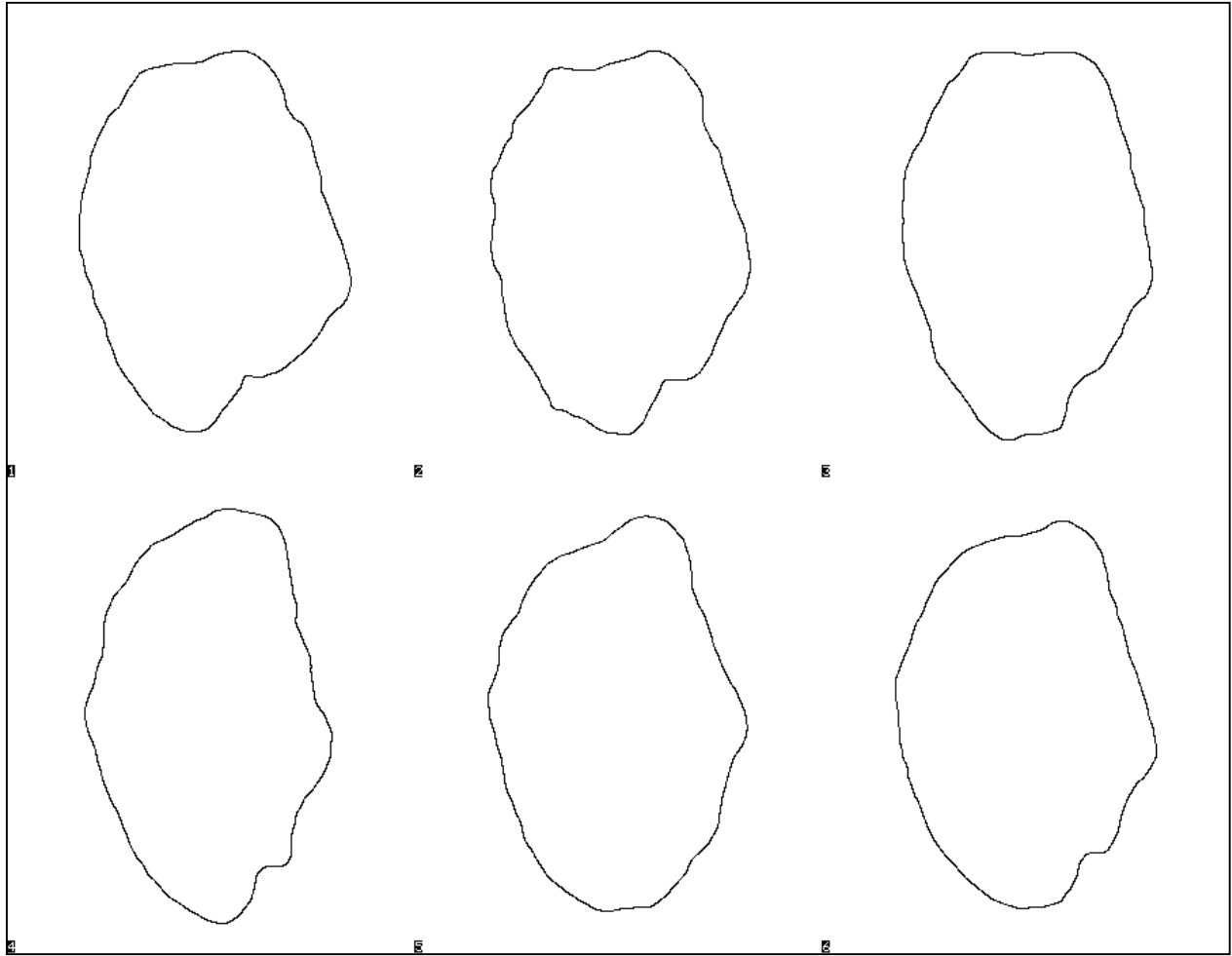


**Figure 5.29:** Contour reconstructions for the first six otolith shapes in the 405-turbot dataset.

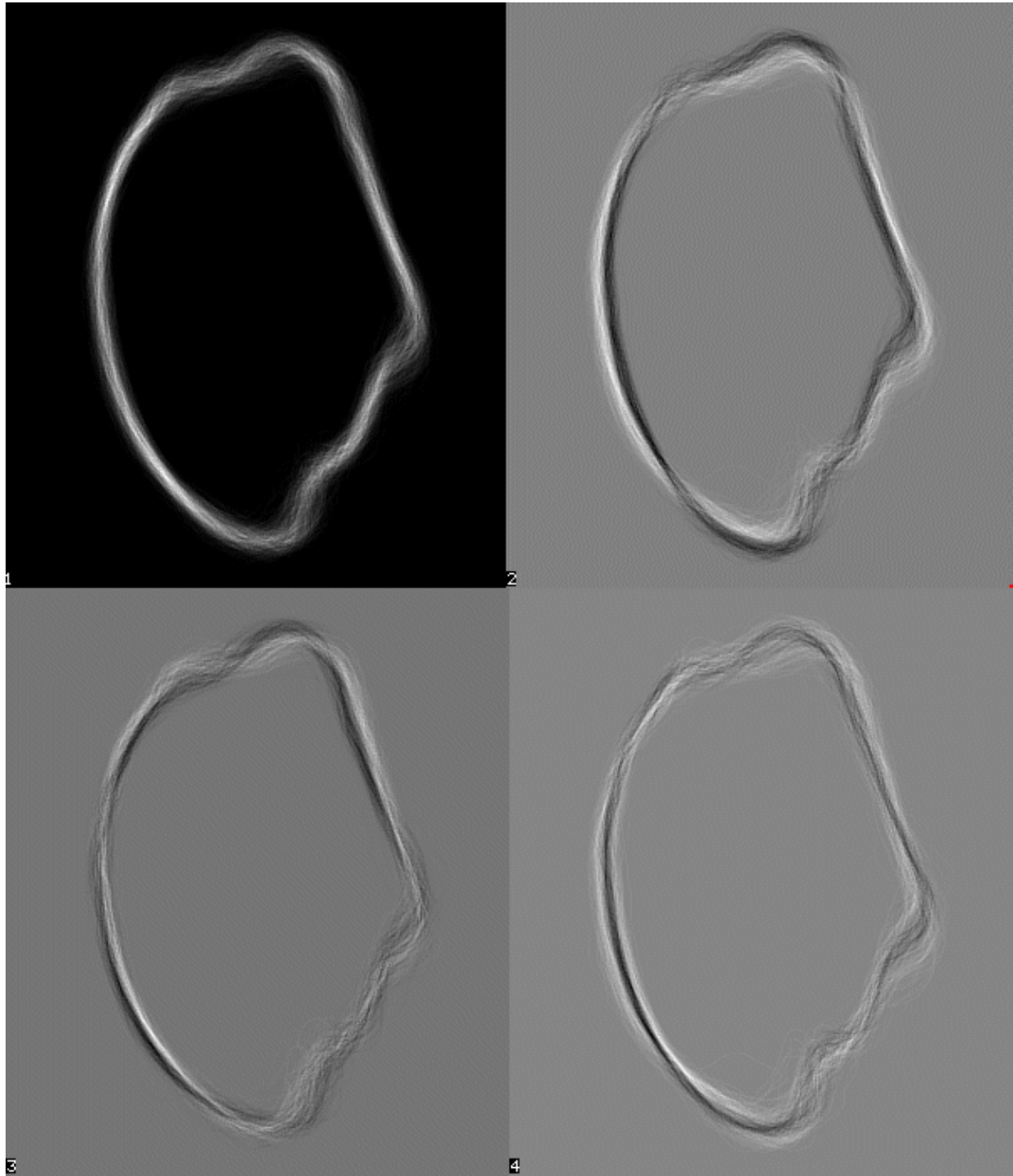


**Figure 5.30:** The first four most important eigenimages for the 405-turbot otolith dataset. Note that the first eigenimage represents the shape average, while the second is the most discriminating eigenimage.

As for eel, the second eigenimage is very well defined and can be decomposed into two contour systems. The other eigenimages were not used. The decomposition of the second eigenimage is shown in Fig. 5.31.

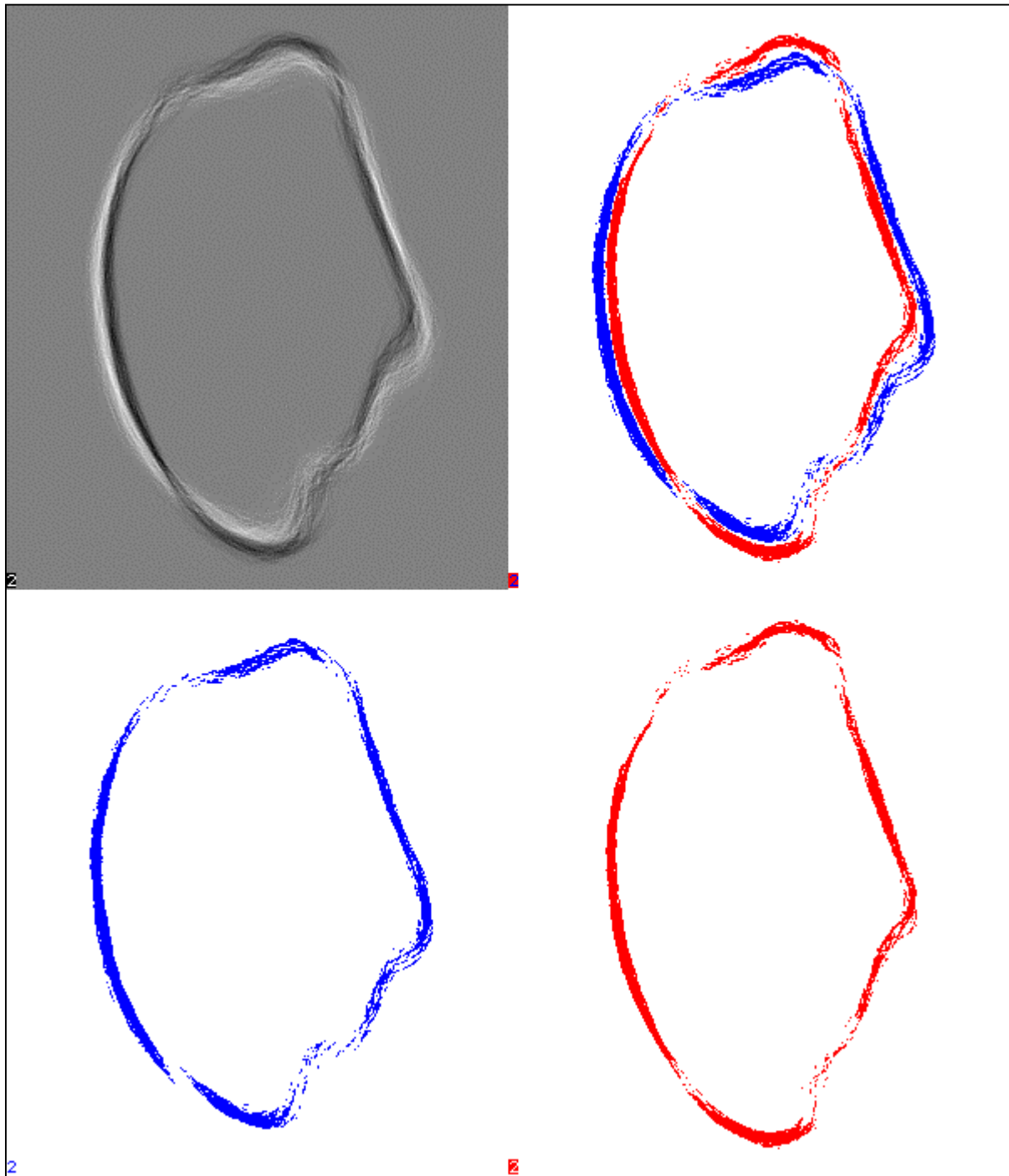


**Figure 5.31:** Decomposition of eigenimage 2 for the 405-turbot otolith dataset.

First of all it is interesting to mention that the left (blue) contour system looks similar to the shape type previously recognised to stand for "old". Similarly, the right (red) contour system resembles the shapes for "young" otolith specimen. The question therefore is, if the associated factorial shape factor 2 (F2) is correlated to age.

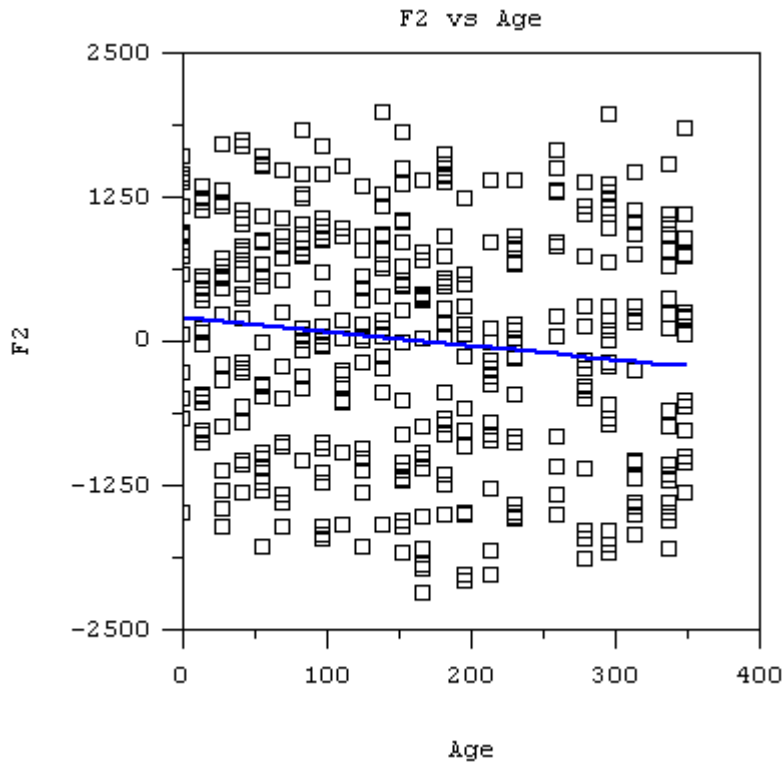


**Figure 5.32:** Plot of the factorial shape factor (F2) associated with eigenimage 2 over age for the 405-turbot otolith dataset. The regression line is shown in blue. Age is given in days from first harvest.

In fact, a subtle tendency can be found in the plot of F2 over age. However, the shape-age relation is very weak as suggested by the huge variations. This finding is consistent with our previous results indicating that only a small fraction of the total dataset can be assigned to age-specific shape classes.

Since the trend is so insignificant, one would like to ask if it is a 'real' feature or just a random coincidence. This can however not be decided by means of any statistical evaluation but only by plausibility. Since we see an unconvincing or no trend, we have to show that other features do indeed discriminate more than our poor shape descriptors. If this is the case, we might decide to call our weak trend a lack of a positive shape-age relation. One reasonable feature is the overall otolith size as available from the Fourier shape descriptor normalisation. A plot of the size factor over age is given in Fig. 5.33.

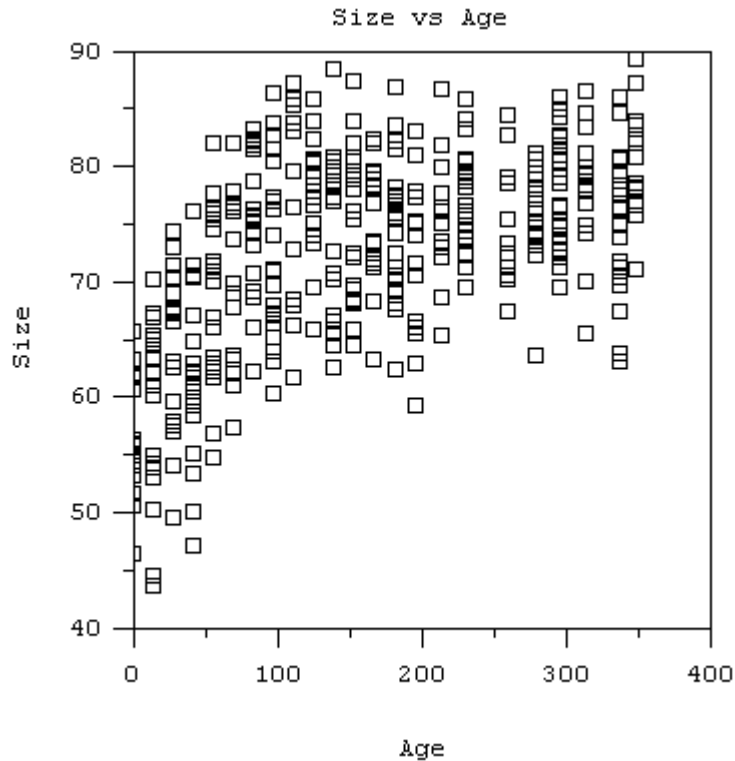


**Figure 5.33:** Plot of the overall otolith size over age for the 405-turbot otolith dataset. Size values are relative figures. Age is in days from first harvest.

This is a pretty conclusive and plausible diagram, although one would expect that the otolith size is continuously increasing with age and not stagnating. Our way of reasoning is now as follows. If we take otolith overall size as a predictor for age, we clearly get a reasonable result. However, in reality this result would not satisfy. But predictions based on shape alone are obviously magnitudes of order worse than that. In other words we might say that, practically, we do not have any useful shape-age relation.

In summary we can say:

- In several approaches we could establish few basic shape classes, which somehow allowed to be assigned to the young and old otolith groups. We used a dataset where we removed the medium-age samples. Even then a characteristic assignment was only possible for 33% of all otoliths. This already indicated that the age-shape relation is not very strong.
- Using eigenimage analysis for the complete dorsal dataset, the shape factor F2, which very clearly captures some kind of important shape change within the collection of samples, is unable to significantly correlate to age and otolith size alone would probably give a much better age prediction.

Our conclusion must therefore be that we cannot find a positive age-shape relation in the given dataset. That is at least true when we consider any practically useful approach. One possible explanation for our findings might be that the shape changes are too small to become evident for the sampled life time of turbot fish of only about one year.

### 5.2.2.3. Anchovy

The contour images were prepared as usual. It was checked that important shape features are well within the resolution of our methods. A typical example is shown in Fig. 5.34.

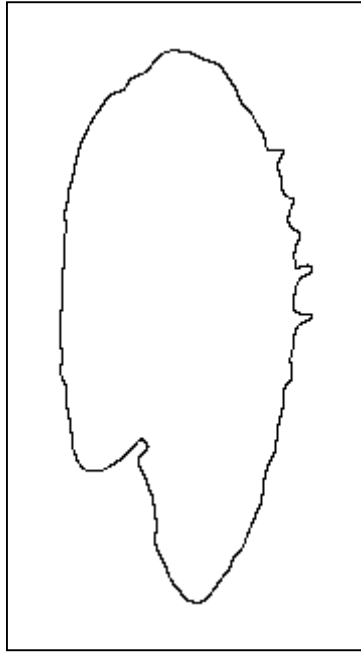


**Figure 5.34:** The contour representation of a typical anchovy otolith. Note the so-called spikes to the right.

Calculation of eigenimages was performed using standard settings and Euclidean metric. After 23 iterations, the program reported that convergence is achieved soon. The total processing time was more than 26 hours. The time per iteration was a bit more than 70 minutes on average. The three highest ranking eigenimages are shown in Fig. 5.35.

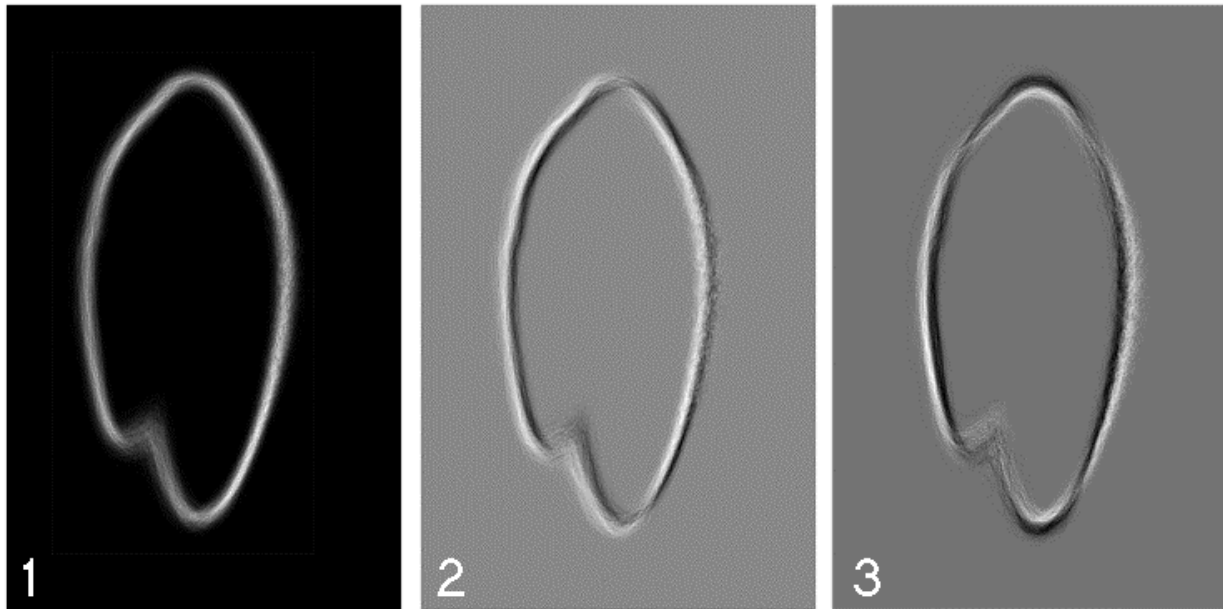


**Figure 5.35:** The first three eigenimages obtained for the anchovy dataset consisting of 900 contour shapes.

One can see in the leftmost average image that in the notch region, where a gap between rostrum and antirostrum is located, a high variability is indicated by a pretty dark contour stretch. Other regions appear far brighter, even where there are frequently spikes along the otolith contours. Please note that we look at size-normalised shapes of anchovy of very different ages from 0 to 4! The most significant eigenimage besides the average is shown as image number 2. One can see dark and bright contour systems similar as for eel and turbot. It seems as if the dark contour is shifted with respect to the bright one. It will be shown later that this is in fact true. Again, in eigenimage 2, one can recognise the highly variable notch region.

The second most significant discriminating eigenimage is shown as image number 3. Again we have two contour systems. In this case, the contour systems are not just shifted with respect to each other but the white contour is broader at half-height than the dark one. We know such slim-to-thick shape variations from previous results. Further eigenimages were visually inspected but they seem to reflect more complicated shape relations. We therefore skip them at the moment.

The second eigenimage was decomposed into the two contour systems. These were then coloured and overlaid. Fig. 5.36 shows the results.

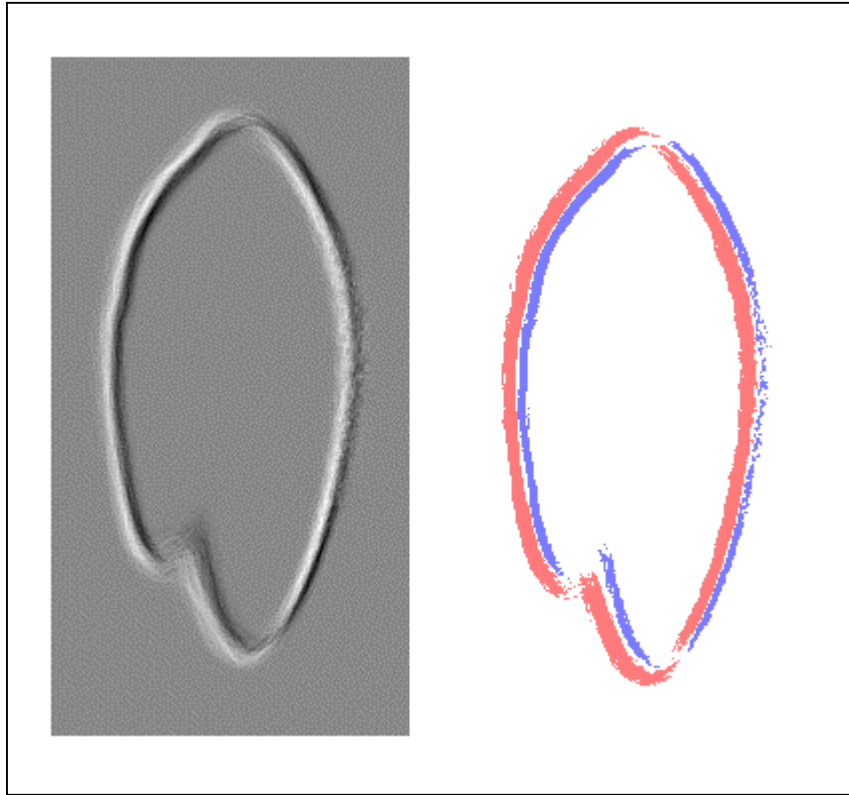


**Figure 5.36:** Comparison of the two contour systems from the decomposition of the second eigenimage for the 900 anchovy otolith shapes dataset.

A more detailed understanding can be achieved if the separated contour systems are fitted onto each other as demonstrated in the next series of Fig. 5.37.

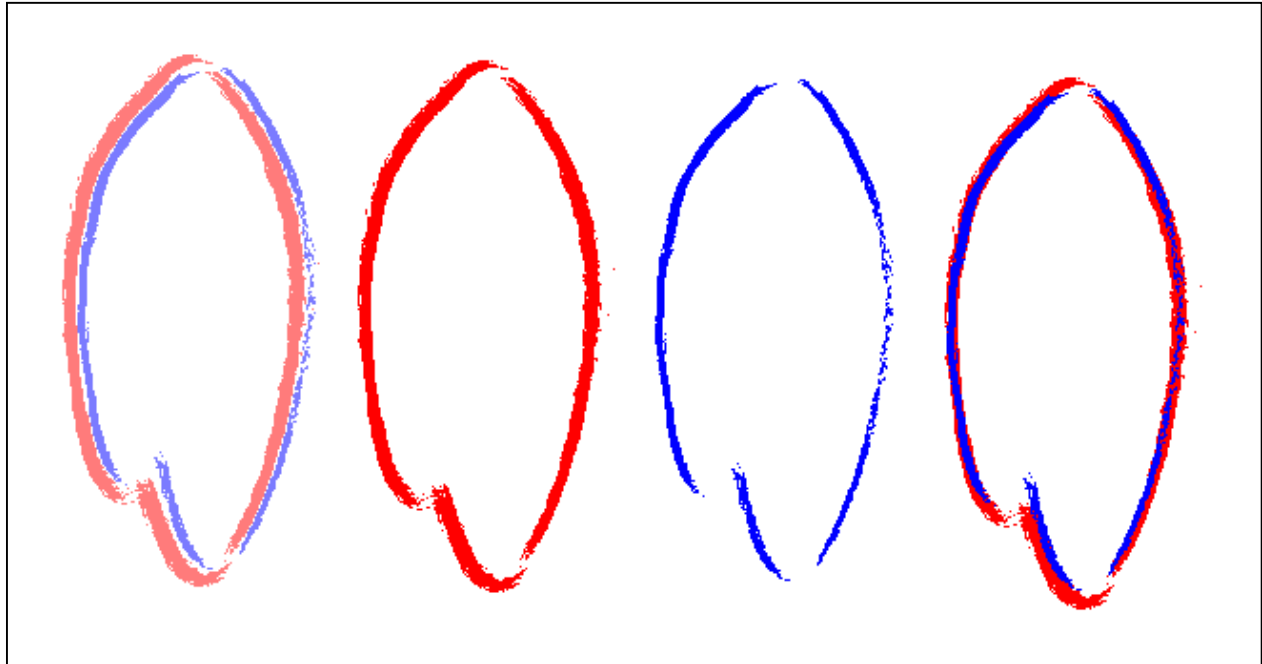


**Figure 5.37:** The two contour systems fitted nicely onto each other. Note that the fit is mostly optimal except for the bottom region including rostrum and antirostrum.

In the original eigenimage, the blue contour system is shifted to the right of the red one. When systems are overlaid free-hand, it can easily be seen that the two basic shapes are not so dissimilar as may be inferred from the original figure. The main shape differences occur at the rostrum and antirostrum and especially at the notch region between them. So far we can say that we have the same width at half-height but a significant length difference. The notch region is obviously a 'hot spot', i.e. a variable region within the whole shape.

In the Fig. 5.38, the length differences are marked and the differences in the notch region are highlighted. So far we do not know what effects are seen here.

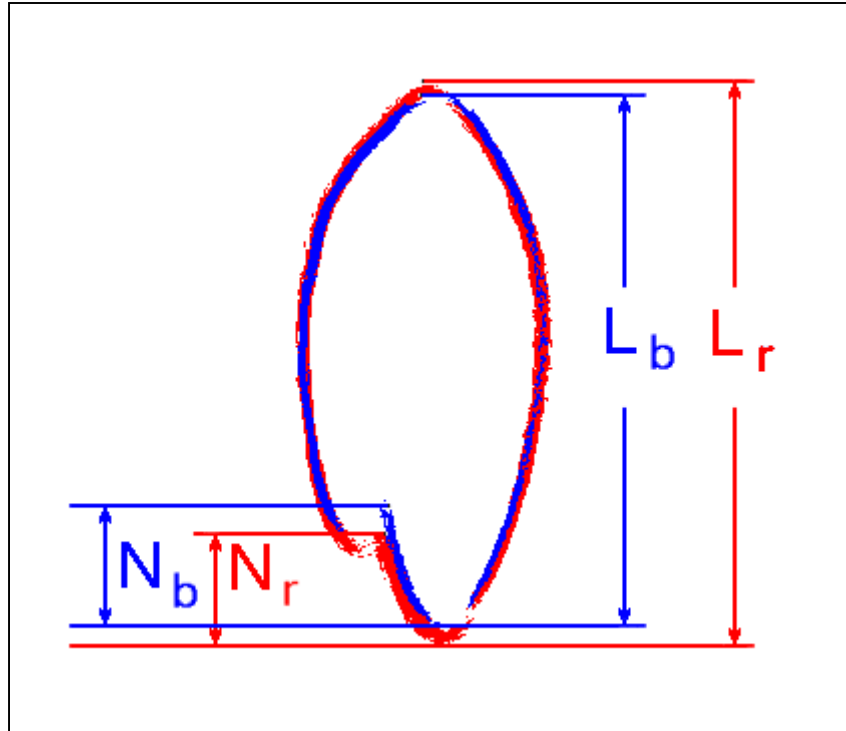


**Figure 5.38:** The two contour systems are arranged such that some length measurements can be made. Indices b and r stand for blue and red, respectively.

Let us say the red shape is the reference shape, then the blue one differs from the reference by having shorter rostris. As a consequence, the centre of the contour is slightly shifted to the side of the more massive rostrum. Thus, the eigenimage catches mainly this shift, while the meaning is that both rostris are shorter. Note that in the above image we tried to establish well defined shape features, however, the exact location of the gap between the two rostri is hard to determine. However, we find  $L_r = 282$  is significantly greater than  $L_b = 265$ . Since  $N_r = 56$  and  $N_b = 60$  we can estimate that the antirostri must differ by the same amount as the two rostri. The length difference amounts to about 6%.

Before we discuss the meaning of the above established shape variations, we might address to the third eigenimage, which suggests a very clear shape change. The decomposition into two contour systems is readily done but in some regions the variability in the contours is so high that one has to make a good guess at where the contour would lie. The added contour segments are specially marked in the Fig. 5.39. They are only meant to guide the eye and give a better impression of the hole contour.

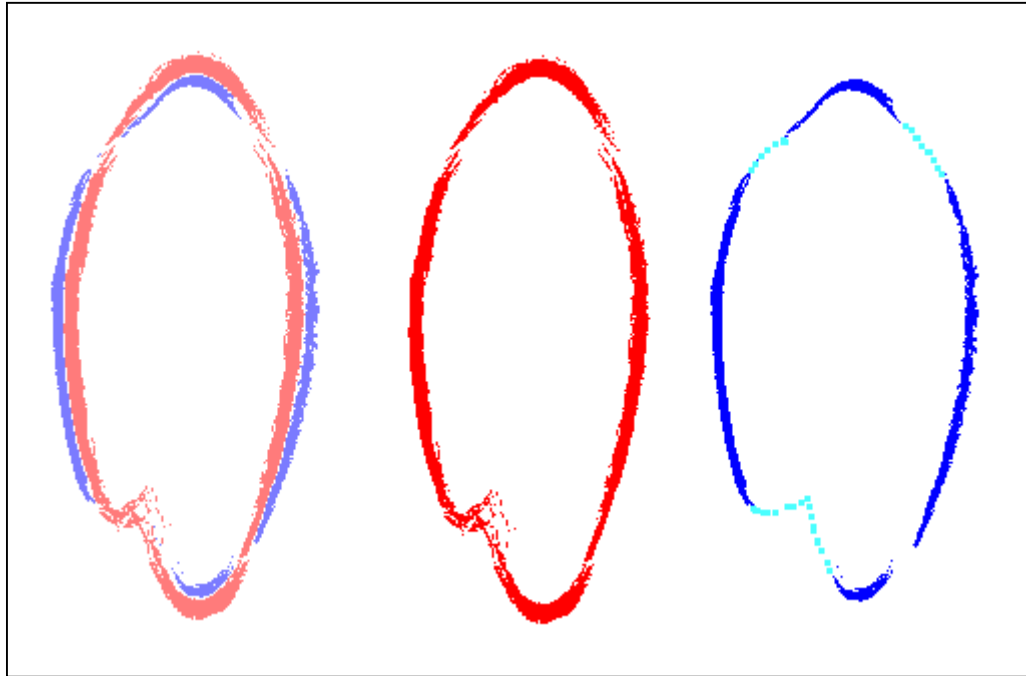


**Figure 5.39:** Decomposition of the third eigenimage for the 900 anchovy otolith shape dataset. Assumed contour stretches are shown in light-blue.

Besides the elongated versus round shape discrimination, there is one more detail to be mentioned. When looking at the top portion of the blue contour system above, one can see that there is a kind of nose or buckle at the top of the otolith. The red shape does not show such a buckle. So the full story about the third eigenimage is that it combines the elongated and round forms and the absence or existence of a buckle at the otolith tip opposite to the rostrum. At this point, we cannot say what this means with respect to age.

The most straightforward way to test for shape age relations is the analysis of the factorial coordinates associated with the eigenimages. The concept of eigenimages was mentioned before. For sake of brevity, we cannot give extensive background on these concepts here but must refer the reader to standard mathematics textbooks on Linear Algebra as well as to specialised publications (see: (van Heel et al., 2000)). Also refer to the respective passages in previous text paragraphs.

Factorial coordinates give the amount of contribution of an eigenimage to the total image. Since the first eigenimage is the average image, there is not much of a shape discrimination in connection with the first factorial coordinate.

The second and higher factorial coordinates are however very specific for a given type of shape. In the following, diagrams for the first three factorial coordinates over the image location (storage index within the dataset) are shown. Note that the dataset is composed such that age increases with image location. The red lines indicate the end of a year group. The youngest fish age is zero years, the oldest four years.

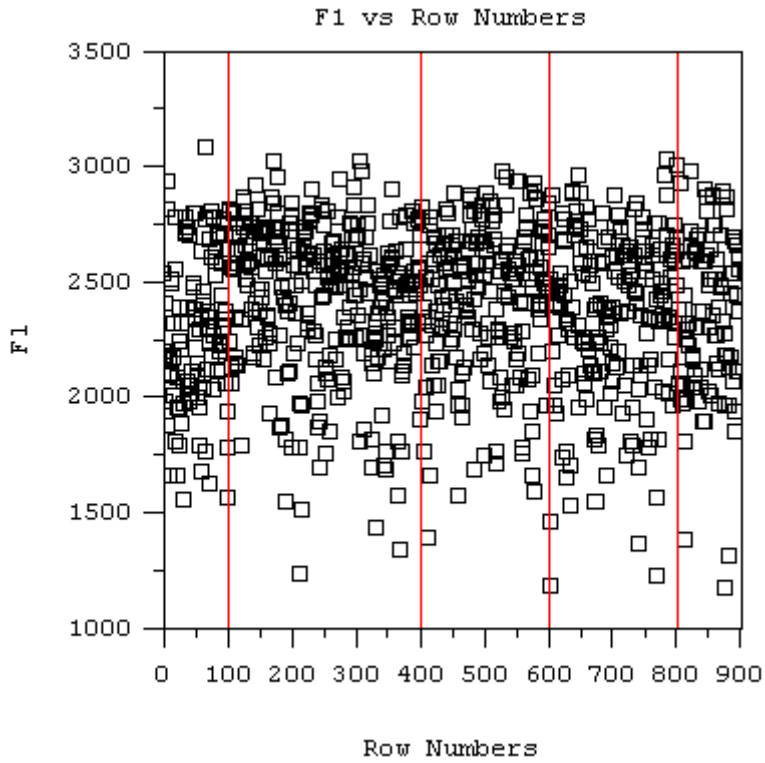


**Figure 5.40:** Factorial coordinates (F1) to eigenimage 1 for the 900 anchovy otoliths dataset.

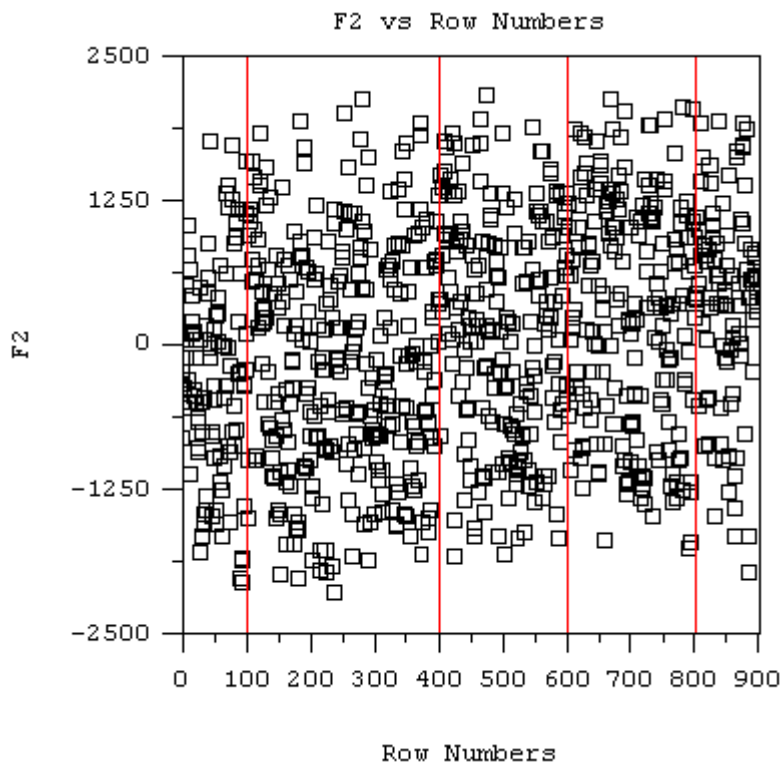


**Figure 5.41:** Factorial coordinates (F2) to eigenimage 2 for the 900 anchovy otoliths dataset.

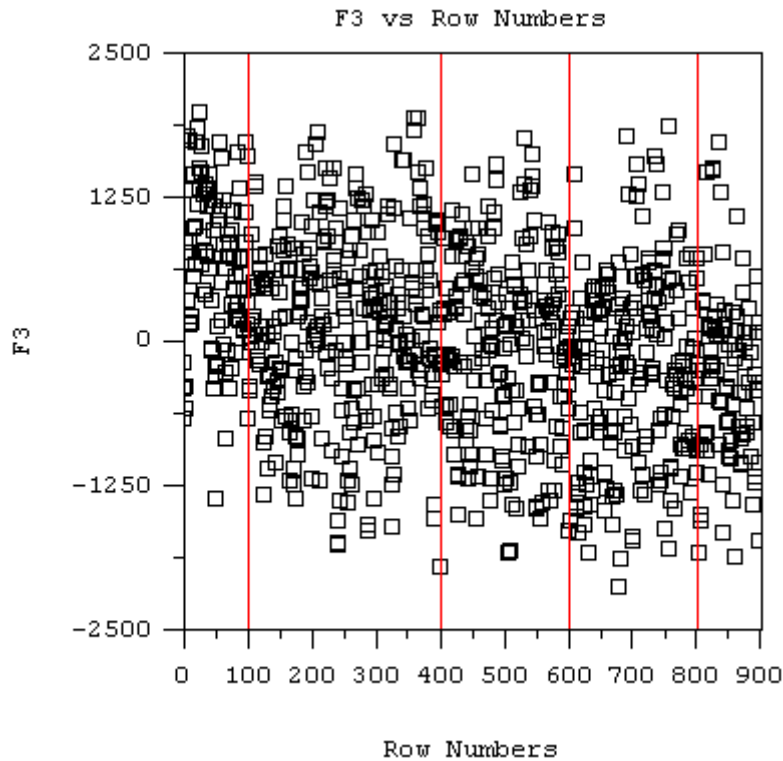


**Figure 5.42:** Factorial coordinates (F3) to eigenimage 3 for the 900 anchovy otoliths dataset.

There is no striking correlation of shape factors with age! Only slight trends may be seen in F2 and F3 but these trends are rather weak and the corresponding distributions of factorial coordinates are heavily overlapping. There is no other conclusion as to say that

- there is a clearly recognizable shape-age trend
- the statistical noise is very high
- age groups predicted on the basis of factorial coordinate F3 are heavily overlapping.

So the main point here is that we do have a shape-age relation but it cannot practically be used for reliable ageing. That this is true can be demonstrated with the usual plots of one factorial coordinate versus another. If separable clusters or clouds of points are found in the dataset, they appear as separable clouds in such a plot. This can nicely be seen in the Fig. 5.43 showing a scatter plot of F3 versus F2 for selected anchovy otolith samples of age groups 0 and 4.

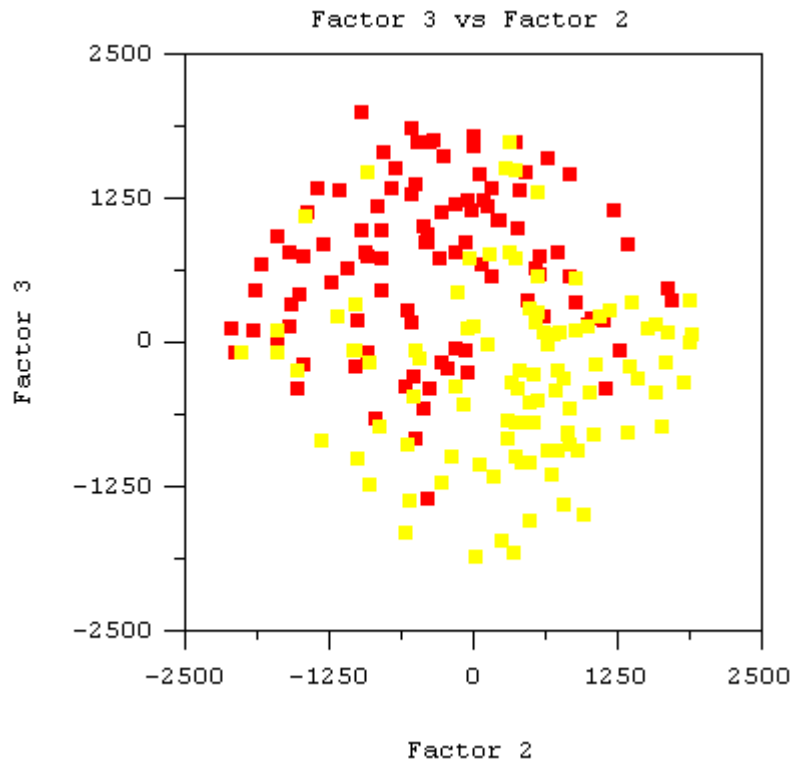


**Figure 5.43:** Coloured factor-factor plot for selected anchovy otoliths. Red boxes stand for age 0, yellow boxes are for age 4. One recognises that factor 3 gives a much better age-discrimination as compared to factor 2.

The plot suggests that the two extreme anchovy age-groups can somehow be separated on the basis of two factors only! However, even for these extremes there is some overlap. Unfortunately, the overlap is unacceptable for smaller age differences, as can be seen in Fig. 5.44.

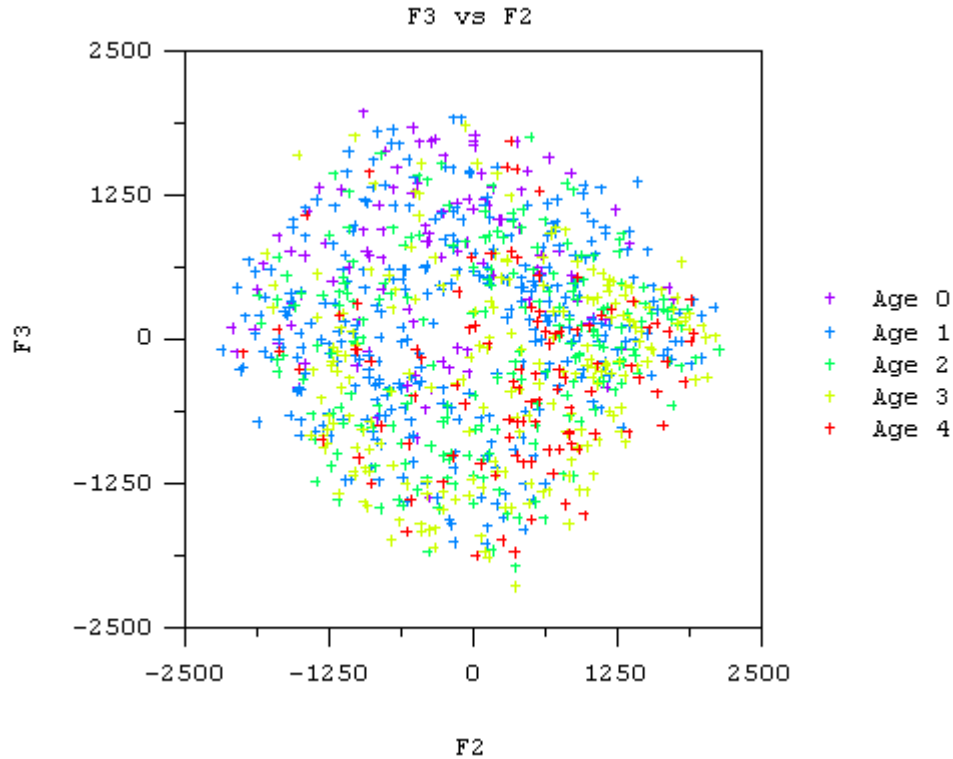


**Figure 5.44:** Coloured factor-factor plot for all anchovy otoliths. Age groups do not form distinct clusters or can at least not be separated from each other.

An anchovy otolith frequently shows several spikes at one side. Due to the presence or absence of such spikes, the normalised contour line has longer stretches on the right or left side. The calculation of Normalised Fourier Descriptors is sensitive to such variations. It was therefore of interest to investigate, if the effects seen in the previously shown eigenimages are real or just artefacts produced in the NFD calculation. This question was addressed as follows. Slightly smoothed contours showing somewhat diminished spikes were generated. An example is shown in Fig.5.45.

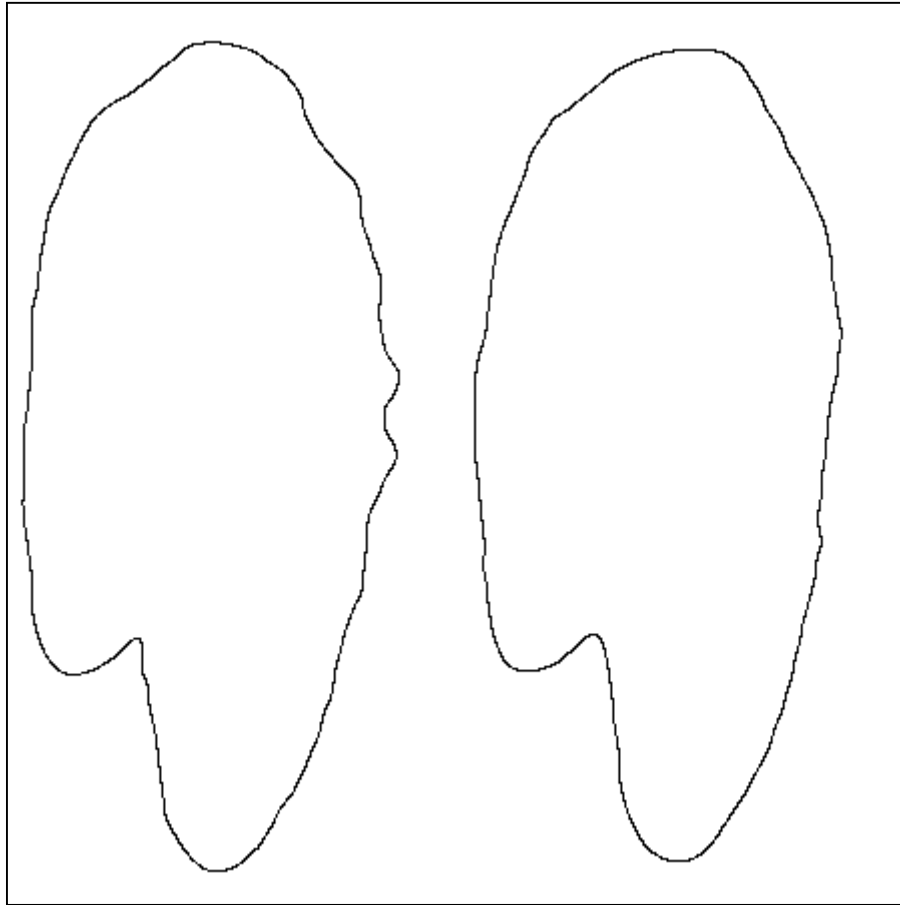


**Figure 5.45:** Original (left) and smoothed (right) anchovy otolith contours.

It was hoped that the smoother contours contain relevant shape information, while the detrimental effects from the spikes are largely reduced. Smoothed contours were then subjected to the multivariate statistical analysis yielding a new set of "smoother" eigenimages.

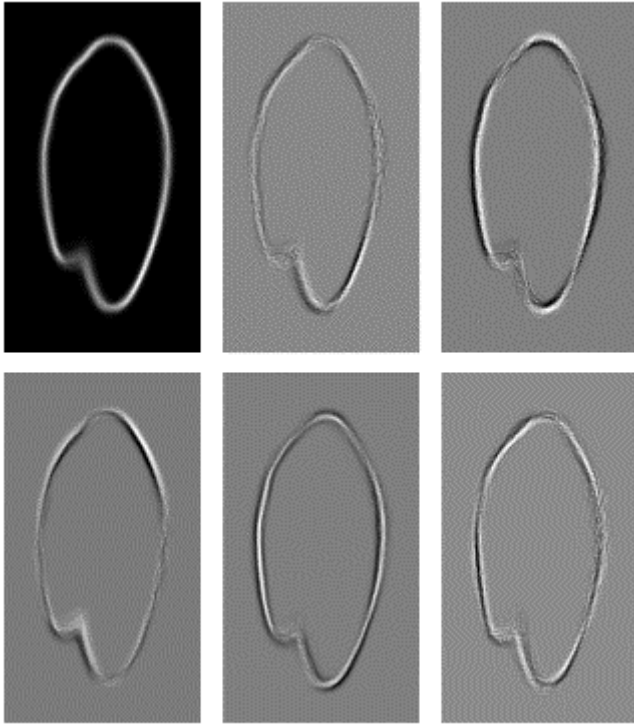


**Figure 5.46:** The first six eigenimages derived from the smoothed anchovy otolith contours.

For brevity we like to leave out the very details and just state the conclusions:

- The first eigenimage is as expected.
- There are some differences in the second eigenimage as compared to previous results.
- The differences indicate that spikes in fact influence the alignment of contours.
- The shape features derived from eigenimage decomposition are virtually the same as in the first round of calculations.
- The third eigenimage very closely corresponds to previous results.
- The conclusions drawn from the high-detail contours are valid for the low-detail contours.

Since the main result for anchovy suggests that the age-discriminative power of otolith shape is not sufficient for practical use, we considered if by looking at smaller subparts of the contour we could eventually improve the importance of shape. We have shown that the main shape feature in the second eigenimage has to do with the gap region between rostrales. The question was therefore if we could gain something by just looking at that region. An image of the region-of-interest within the full image is shown in Fig. 5.47.

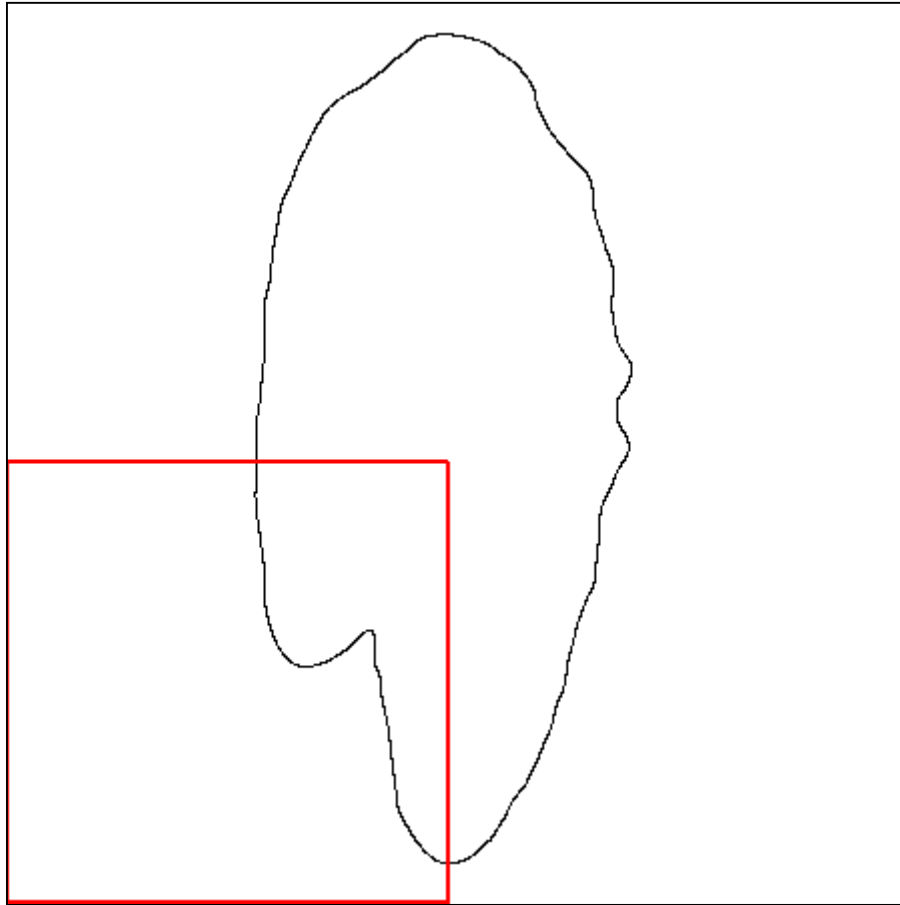


**Figure 5.47:** The gap between rostrum, i.e. the region-of-interest (ROI), is marked by a red square.

This ROI was cut out from each full contour image and was analysed in the usual way. The resulting most discriminative eigenimage is shown in Fig. 5.48.

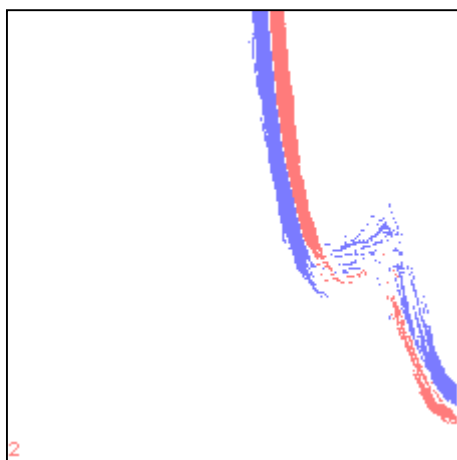


**Figure 5.48:** Eigenimage 2 for the gap between rostrum. The colors indicate the decomposed line systems.

The analysis of the factorial coordinates revealed no clues. Without going into more details, it can be concluded that

- the ROI analysis as such performed as expected
- the interpretation is not very straightforward
- this partial contour segment does not give better results concerning an age prediction.

The above presented results mostly concern eigenimages and factorial shape coordinates. However, we could also use the Normalised Fourier Descriptors as was done for eel and turbot. We wanted at least to test, if there is any more information available from the calculation of average shapes.

All 900 anchovy otolith shapes were used to calculate NFD averages over age groups:

- Locs 1...100 belong to class 1 (age 0)
- Locs 101...400 belong to class 2 (age 1)
- Locs 401...600 belong to class 3 (age 2)
- Locs 601...800 belong to class 4 (age 3)
- Locs 801...900 belong to class 5 (age 4)

Graphical representations are shown in Fig. 5.49.

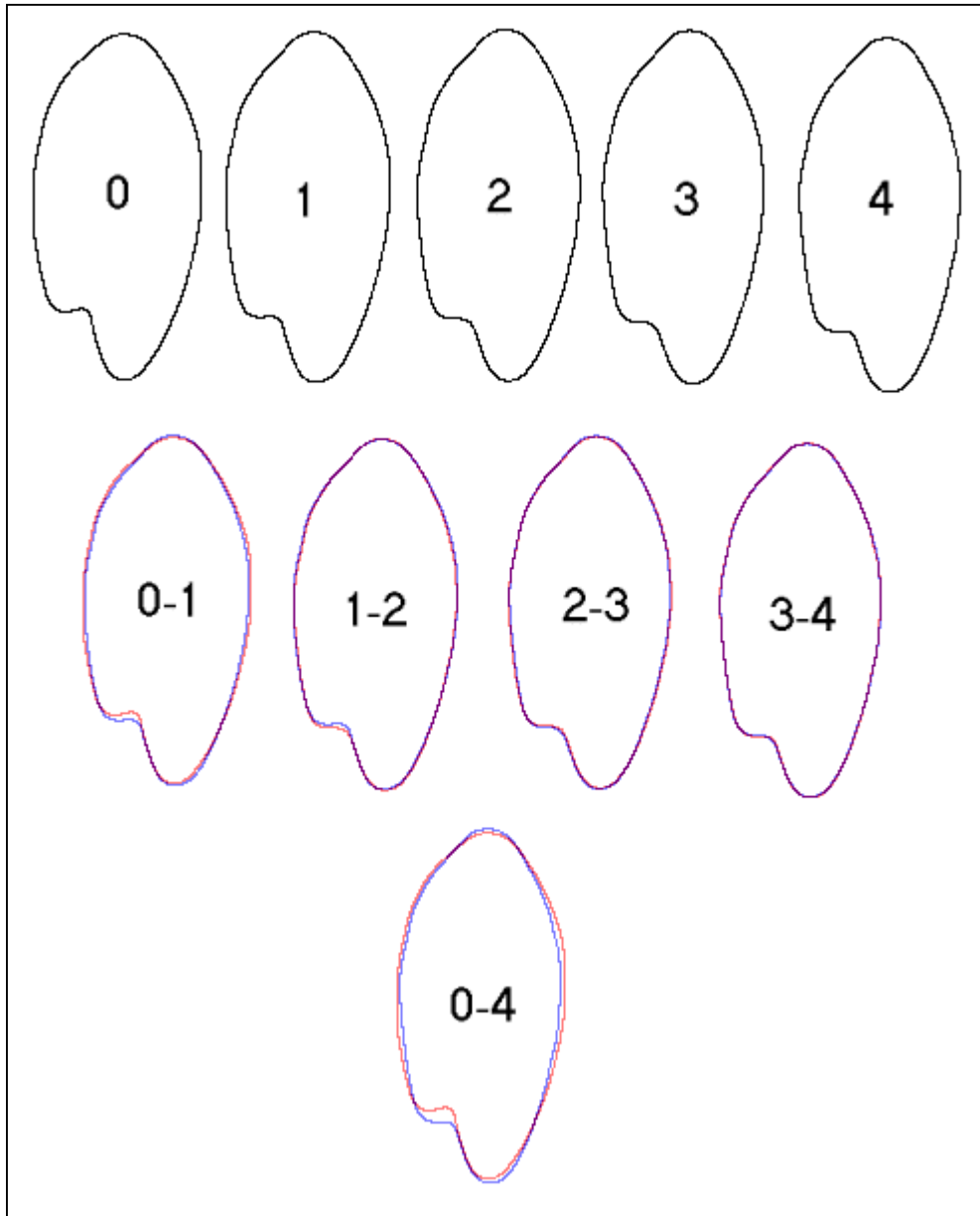


**Figure 5.49:** The top row shows age group NFD averages. The middle row shows contours of neighbouring age groups and at the bottom a comparison of the extreme year group averages is given. Note that an NFD average gives one precise contour.

The dominating first impression is that there are only small shape variations. Only the overlay of the age 0 and age 4 averages makes clear that there are indeed shape changes concerning a very subtle elongated-to-round transition and a more pronounced gap-shape modulation. The gap-shape seems to develop from highly indented (age 0) over less indented (age 1) to its final form (age 2,3,4). The ellipticity changes from wider or more round (age 0) to thinner or longer (age 4). However, note that the terms elongated and round are rather exaggerating the real situation! Indeed, isometric otolith growth is a good first approximation for anchovy. One aspect should, however, not be overseen here. It concerns the nature of the shape variations within an age group. If the variations are very high, the average may not reflect a 'real' otolith shape. In other words,

we do not have NFD averages in the sense of a median. But in our case we can assume that the shapes span a huge spectrum of possibilities, therefore the averages may be treated with care! However, note that the elongated-round shape transition was not ruled out by the previously mentioned eigenimage analysis! In so far, the obtained general trend may be real.

We can test the elongated-round shape correspondence with age by using some of the additional geometrical features that are automatically calculated during original image workup. Thus, the maximal internal distance within an otolith contour is established and then the maximum distance in a perpendicular direction is determined. These two features might tell us how useful the round-to-elongated shape transition is for ageing. The following diagrams show the actual feature distributions.

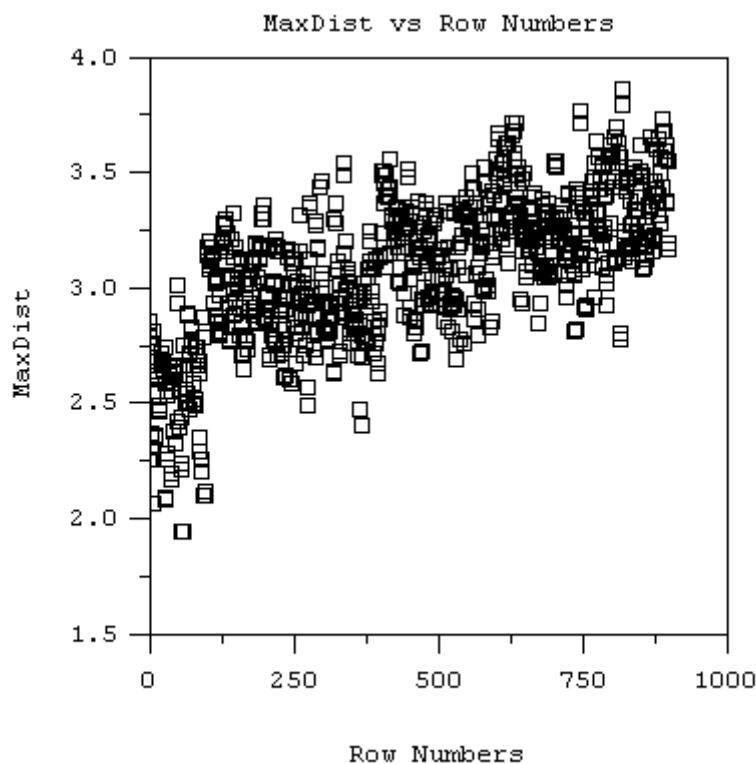


**Figure 5.50:** Maximal internal distance within contours from all 900 anchovy otoliths.

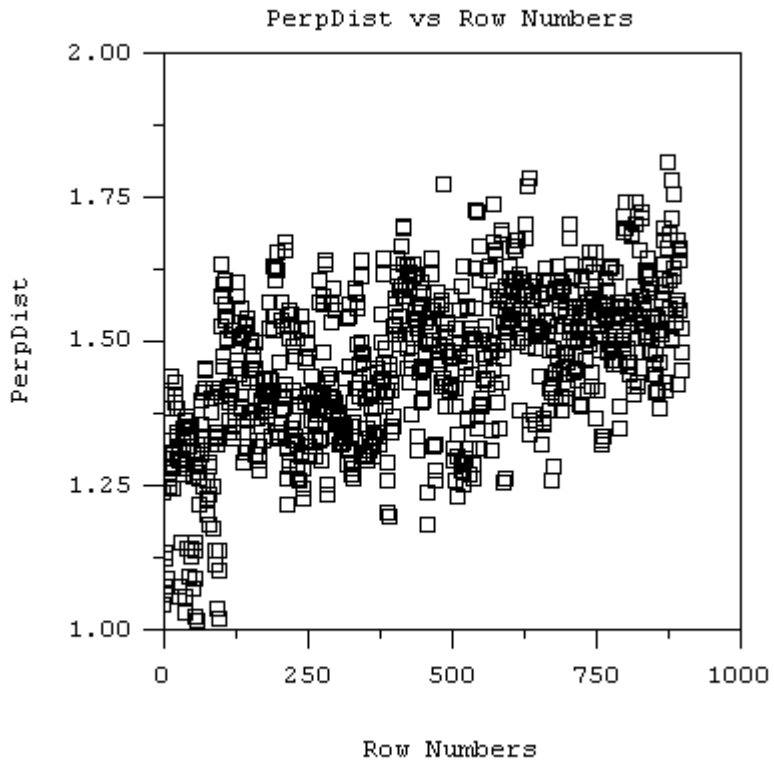


**Figure 5.51:** Maximal perpendicular distance within contours from all 900 anchovy otoliths.

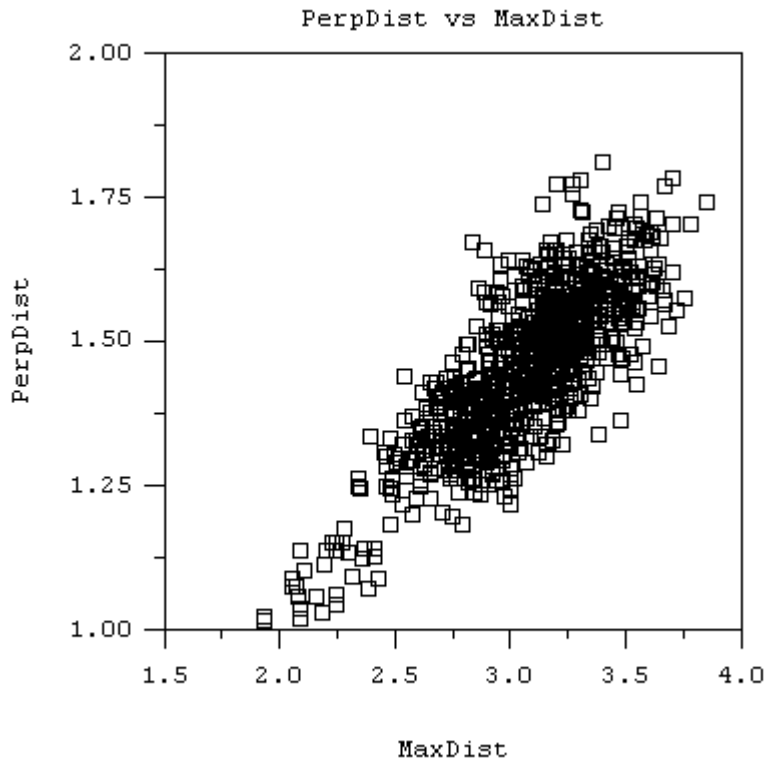


**Figure 5.52:** Maximal internal distance over perpendicular distance within contours from all 900 anchovy otoliths.

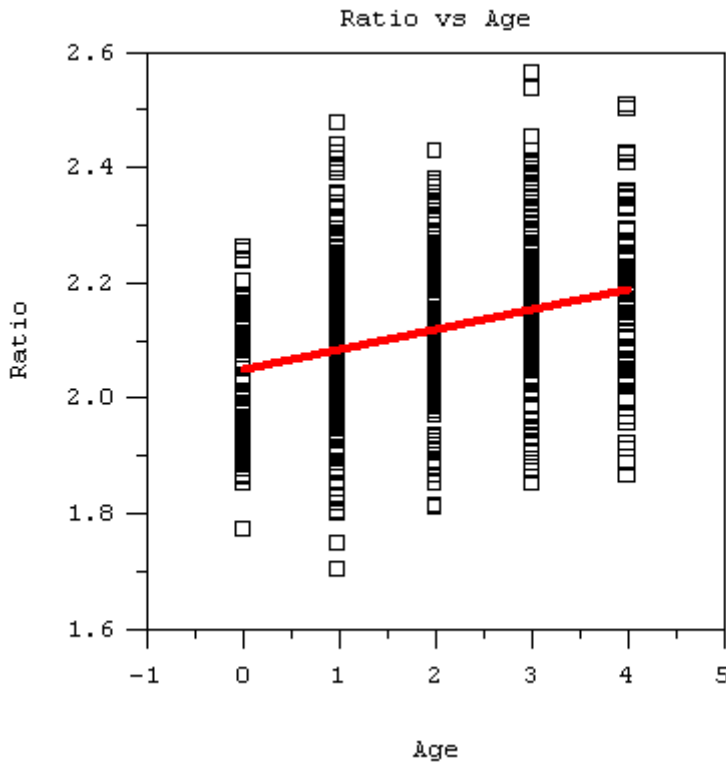


**Figure 5.53:** Ratio of maximal internal distance over perpendicular distance within contours from all 900 anchovy otoliths. The linear regression shown in red roughly suggests that there is a variation in the length-to-width ratio for anchovy otoliths.

The last diagram makes clear that indeed there is a simple round-to-elongated transition since the ratio (MaxDist/PerpDist) increases significantly with age. The correlation for this linear regression is about 0.10. Thus, the variations in the ratio are very high but the trend can unambiguously be identified.

One should stress at this point that we are still looking for otolith shape features for the goal of predicting the age of the fish from which the sample is. The above mentioned finding shows that our methods are extremely sensitive and can unveil very subtle shape features. However, we must not forget that we would like to obtain shape features that are discriminative and reliable. The reliability for e.g. the above mentioned ration of length-to-width measures does not at all suffice the requirements for an acceptable ageing procedure. In other words, since e.g. the maximum contour internal distance, which is an absolute measure (in real-world millimetres), predicts age much better than the shape-related (unit-free) length-to-width ratio, we learn that the overall size of an otolith is more powerful for ageing than this simple otolith shape feature.

Before we conclude the anchovy otolith shape analysis, we like to present some results from shape classifications and evaluating the age-composition of shape classes.

Using the NFDs from the smoothed contours, a classification into 25 classes was performed. Shape class averages were calculated using NFDs. Graphical representations are shown in Fig. 5.54.

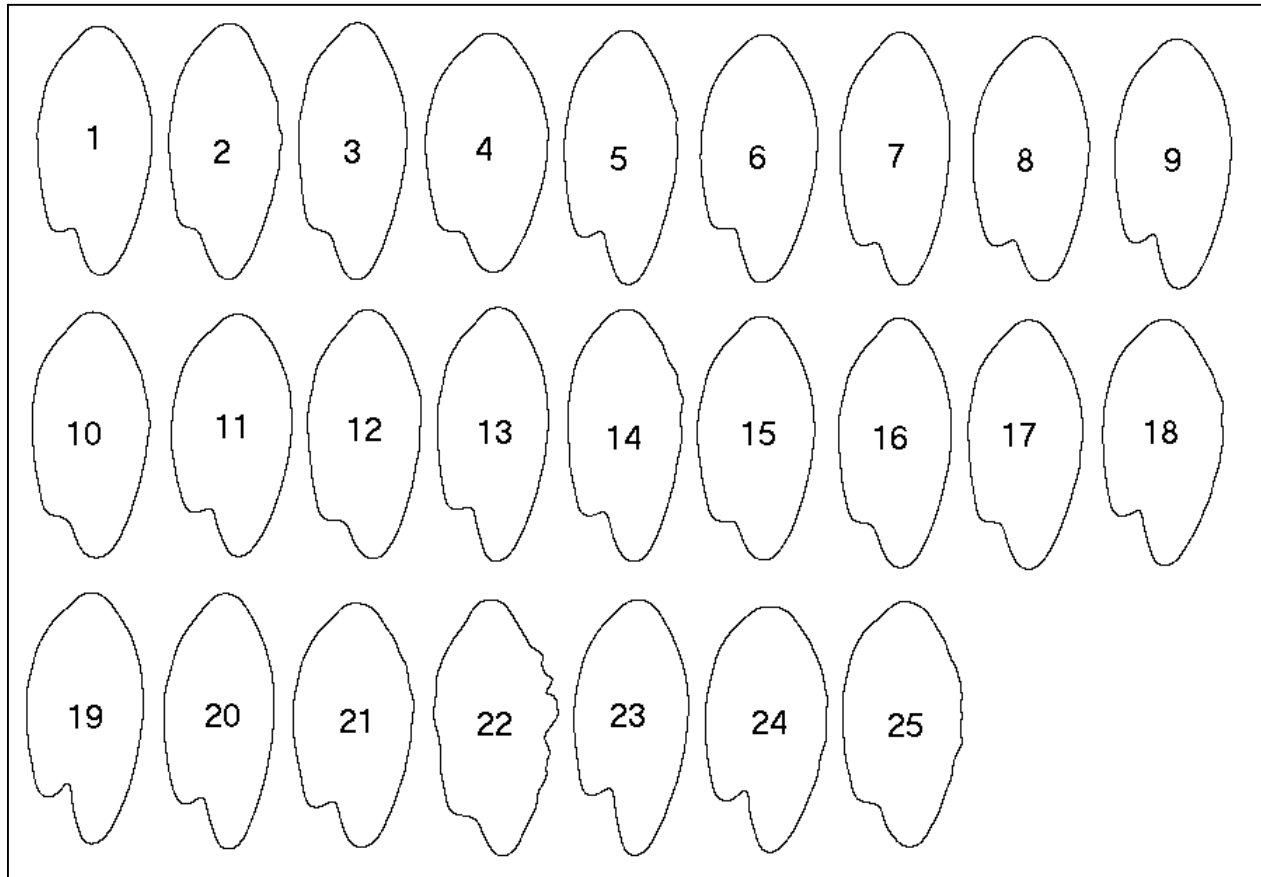


**Figure 5.54:** Class-averages for 25 classes for the dataset of 900 otolith shapes from anchovy. Note that class 22 consists of three outliers, while the expected average number of class members is about 38. This suggests that the number of classes is not far from the optimum.

These classes were analysed for their age composition. One has to remember that the five age groups consist of different number of samples, namely 100, 300, 200, 200, 100 for ages 0, 1, 2, 3 and 4, respectively. Therefore the counts were adjusted with proper weighting factors of 6, 2, 3, 3, 6. The results are shown in Tab. 5.23.

Class	Age 0 (factor 6)	Age 1 (factor 2)	Age 2 (factor 3)	Age 3 (factor 3)	Age 4 (factor 6)	Predicted Age
1	30	60	48	42	48	
2	0	8	15	45	24	3
3	0	22	27	54	60	<b>3-4</b>
4	42	38	21	12	24	1-2

5	0	26	24	18	48	<b>4</b>
6	48	42	33	15	6	0-3
7	0	12	30	48	54	<b>2-4</b>
8	12	18	33	36	36	2-4
9	18	44	15	21	18	1
10	6	22	30	27	48	4
11	102	34	3	9	6	<b>0</b>
12	0	18	36	42	36	2-4
13	18	24	33	27	24	
14	6	10	9	9	6	
15	24	44	54	24	18	1-2
16	0	24	69	45	66	2-4
17	18	42	33	57	18	1-3
18	66	22	0	3	0	<b>0</b>
19	42	26	21	6	6	0
20	0	22	18	24	24	
21	30	20	27	18	6	
22	0	0	0	6	6	
23	24	14	12	6	0	
24	90	4	0	0	0	0
25	24	4	9	6	0	0

**Table 5.23:** Composition of 25 shape classes for the 900 anchovy otoliths dataset. Weighting factors by which original data have been multiplied are stated in the column headings. Classes with an obvious age preference are marked by bold entries for "Predicted Age".

The essence that can be abstracted from this table is that very young and very old anchovy otoliths may be distinguished within the dataset. However, the vast majority of otolith from 'middle-aged' fish falls in the grey-zone and cannot be assigned consistently. Instead of this, we see broad variations in the shape class age-composition. For example shape class 17 has members from all age groups. A definitive prediction can obviously not be made!

These results are very consistent with the findings from the eigenimage analysis, where the dataset was easily separable into age 0 and age 4 samples, however, all age groups together are heavily overlapping with respect to shape features.

Taking all results so far into consideration, one gets the notion that the shape analysis for anchovy is considerably more promising than for turbot. However, we do not need to apply highly sophisticated shape analysis tools but can simply derive a fish-weight/fish-length key that has a higher predictive ageing power than otolith shape. Therefore, the only question remaining is, if a combination of otolith shape with other factors is promising.

Some geometrical and non-geometrical sample features were analysed and compared with respect to their age-predictive power. Tab. 5.24 lists the results.

Feature	versus Age	versus FishLen
ContLen	0.51037	-
ContArea	0.54497	-
MaxDist	0.587846	0.734168
PerpDist	0.393497	-
Apex 1	0.504334	-
Apex 2	0.566171	-
Ratio	0.1205154	-
SizeFactor	0.565154	0.711413
FishLen	0.813962	-
FishWgt	0.794033	-
OtoWgt	0.464937	0.517464

**Table 5.24:** Table of correlation values for geometrical and non-geometrical sample features versus age and fish length. Note that some features correlate better with fish length than with age. This could indicate that we might have a problem with erroneous age readings. For anchovy, there are no known-age otolith databases available. Therefore age determinations based on annulus counting were performed. All correlation coefficient are for quadratic fits.

One should add one more set of correlation coefficients, namely fish length versus fish weight give a correlation coefficient for a cubic fit of 0.944265 and for a second order fit of fish weight against fish length we obtain 0.926157. These two figures indicate a high and therefore consistent cross-correlation between fish weight and fish length. One can therefore set up a combined statistical model for age that gives even slightly better correlations than a single factor.

Looking at the previously introduced ratio of width-to-length, we see a poor correlation coefficient with age of only about 0.12. Other shape related features such as factorial coordinates could be tested also but it is absolutely clear that they are much poorer than most of the features considered in the above table.

One final presentation for anchovy is shown in Fig. 5.55. The size factor is related to the overall size of an otolith and is therefore usually correlated to age, since the otolith size steadily increases due to constant accretion. However, if we take the 'estimated age' we eventually introduce errors. Therefore we tried to estimate the age from the relatively consistent fish length/fish weight descriptors. We leave out details here and just show the result.

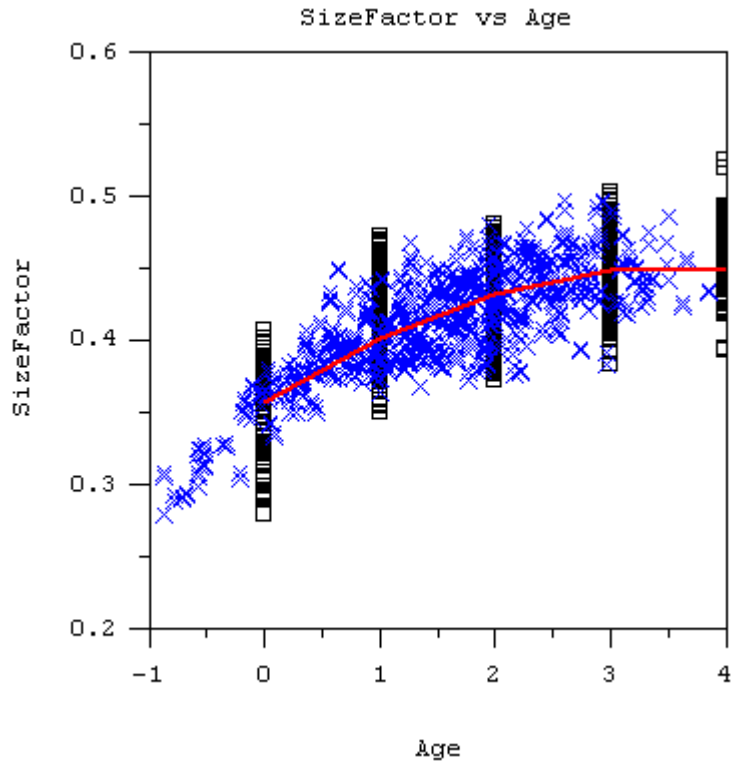


**Figure 5.55:** The size factor describes the overall size of an otolith. Here we see the size factor plotted against an age model derived from the fish length/fish weight key. Note that some otolith in the age 0 group are so small that they can formally be regarded as -1 year old! Black boxes are size factor at estimated age (annulus counting) and blue crosses are 'estimated age' from a fish length/fish weight model. The red line is a number of stepwise linear regressions between neighbouring age groups.

While there is some prospect in such statistical models, our primary goal was to establish shape-age models for ageing. For anchovy, we have to acknowledge that many shape analysis tools yield consistent insight into the otolith shape features unambiguously revealing small trends but failing to provide a practically useful strategy to use otolith shape for ageing.

For anchovy, the task of ageing an individual fish by classifying the shape of its otolith may have been too challenging because we need to differentiate between several different age groups from age 0 to age 4. Therefore it remains an interesting question if there are any detectable shape differences between the shape of otoliths landed in different harbours. Fish landed in different harbours comes from geographically distinguishable regions of the Adriatic Sea. Therefore, the question behind such an analysis is about the identification of different putative stocks and effects of environment.

The most straightforward approach is for just two harbours. Therefore we established otolith datasets of samples from two different landing sites in the Adriatic, namely, Chioggia in the northern part, and Ancona in the central part. The shape analysis methods were explained earlier. We used eigenimage analysis and NFD-based shape classification, as well as classifications based on factorial eigenimage coordinates. The pooled dataset is composed of 1640 samples from Ancona and 1120 from Chioggia belonging to five different age groups. Otolith from both body

sides were available so that we have a total of 2760 images. Two strategies were tried: classification of the complete dataset into 2 groups by eigenimage analysis and classification into 50 groups by means of NFD-based shape classification, followed by counting the harbour site composition of shape classes.

In previous paragraphs we have shown that smoothed contours are to be preferred for anchovy because they give better shape alignment while not losing any significant shape information. In order to prepare smoothed contours, a two-step approach was employed. In the first step the normalised contours were generated as smooth contour images (512\*512 pixels). To obtain the smoothing, only 68 out of all 256 NFDs were used in the contour reconstructions. Filled otolith reconstructions were then generated and taken as input for the usual contour finding and NFD calculations. From these final NFDs hollow contours were constructed that should now have an improved mutual alignment. We have addressed this topic in previous paragraphs in more detail. The whole approach finally gives contour images with slightly smoothed contours and high-precision alignment. The final images mentioned above were 250\*150 subsections of 256\*256 pixels as shown in the images of Fig. 5.56 and Fig. 5.57.

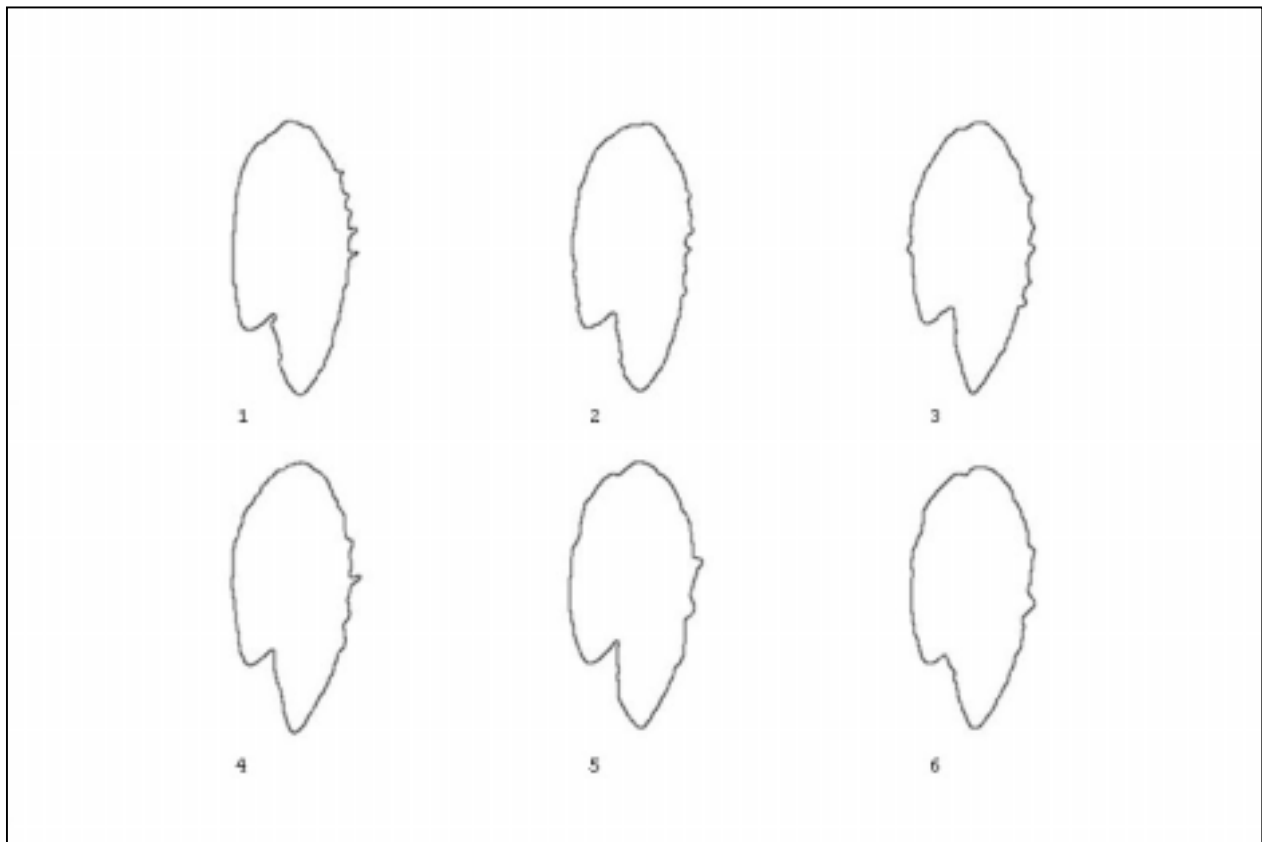


**Figure 5.56:** Typical anchovy otoliths contours re-constructed using all 256 Normalised Fourier Descriptors (NFDs). Note the several spikes in the first image.

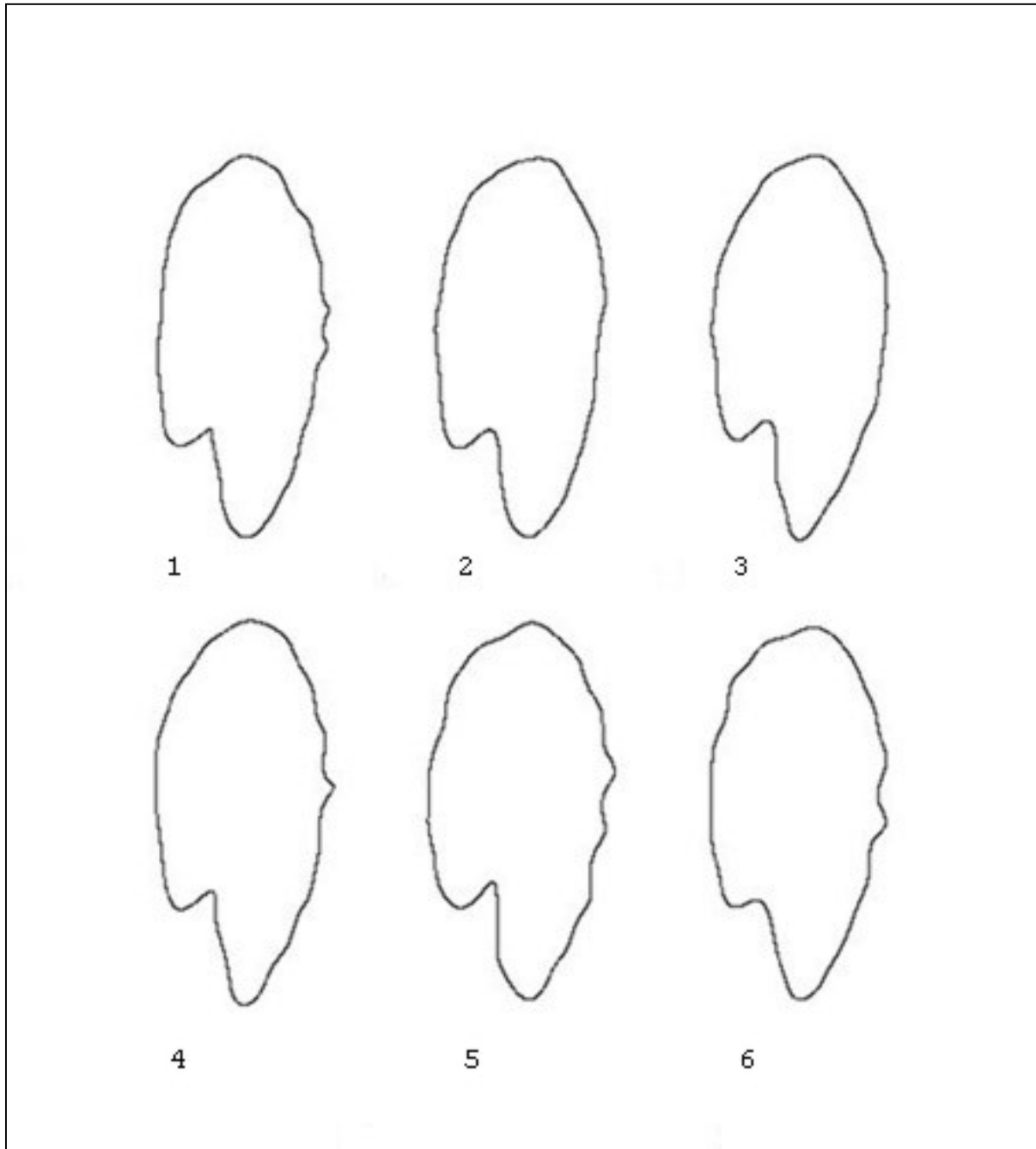


**Figure 5.57:** Smoother contours constructed from only 68 NFDs. Note that the spikes in the first contour are minimised as compared to the previous figure. Other shape features are greatly conserved. As an effect of the smoother contours, the mutual alignment of shapes reconstructed from NFDs is significantly improved as compared to reconstructions from 256 NFDs.

Eigenimage analysis was performed separately on the Ancona and Chioggia sets, as well as on the combined dataset. Sets of the first ten eigenimages for Ancona, Chioggia and the combined data set are shown in the following figures.

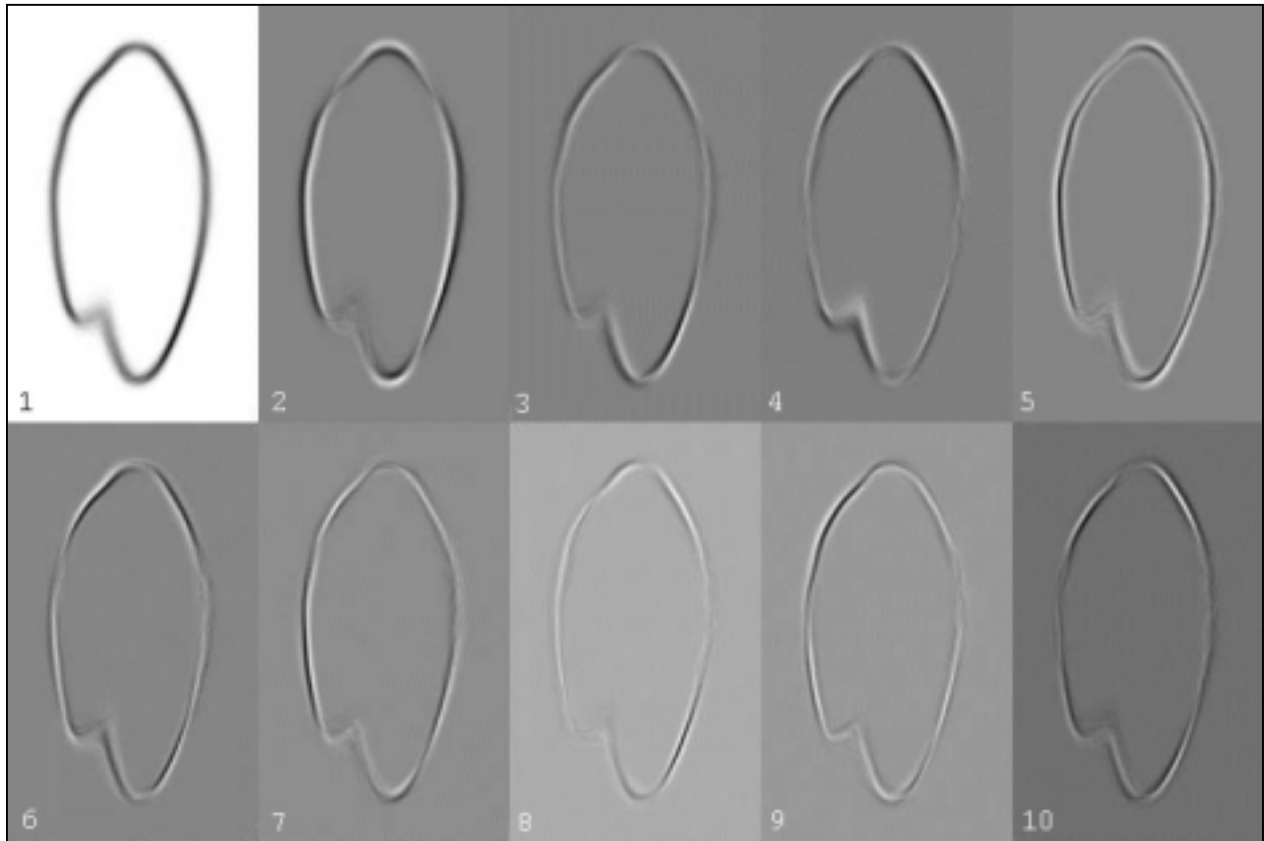


**Figure 5.58:** Eigenimages for the Ancona dataset. The second eigenimage clearly captures an allometric shape change. Higher eigenimages are extremely well defined, however, as usual difficult to interpret.

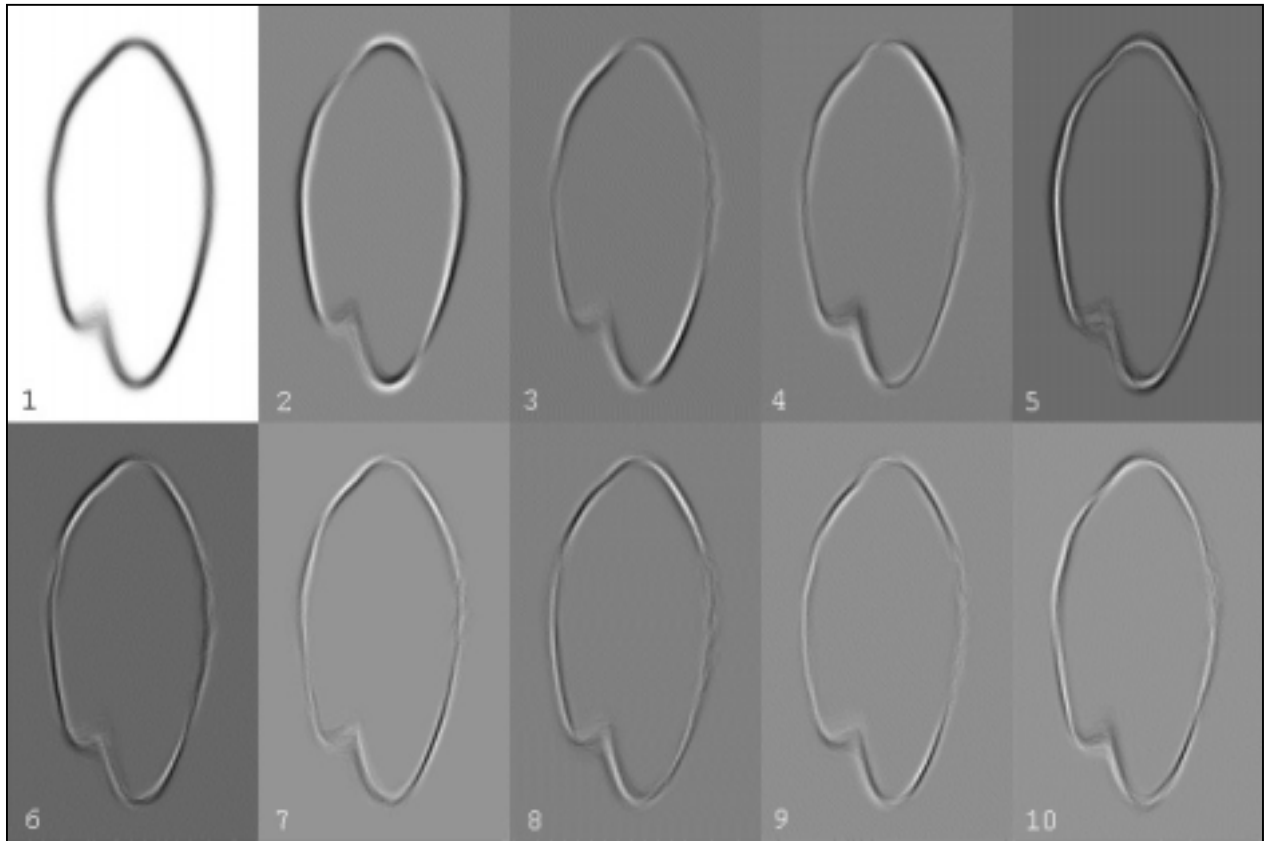


**Figure 5.59:** Eigenimages for the Chioggia dataset.

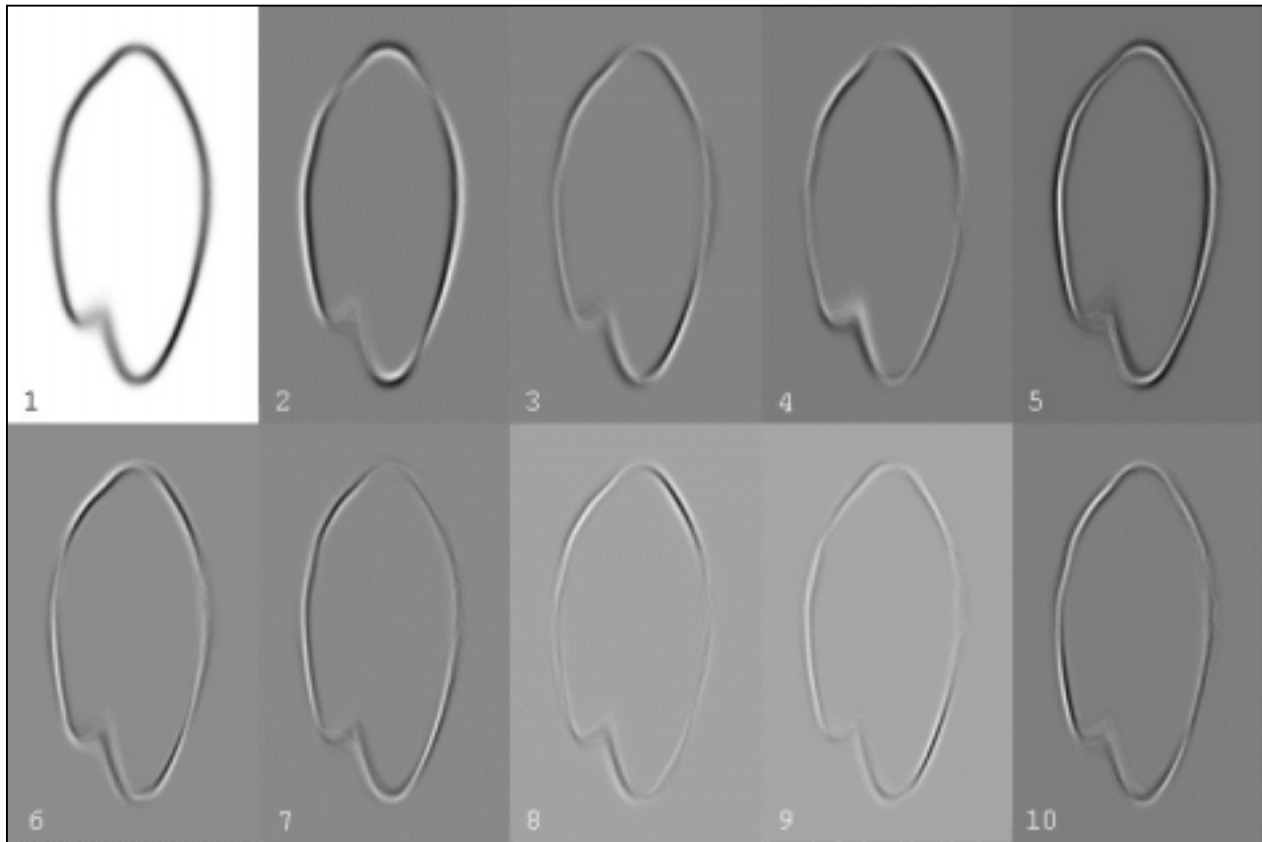


**Figure 5.60:** Eigenimages for the combined dataset. Highly defined contour systems can easily be distinguished in the second and higher eigenimages. The improvement of the quality of eigenimages is merely a welcomed effect of the larger number of samples in the combined dataset. Note that dark and bright zones are somehow arbitrarily defined to satisfy the condition of a right-handed eigenimage system. For comparison of eigenimages the meaning of dark and bright is completely interchangeable, i.e. the second eigenimage is simply the dark-bright inverse of the previous Ancona and Chioggia eigenimages.

The first eigenimage has average (median) characteristics, while the second shows the most discriminating feature in the dataset. They correspond very well to previously obtained eigenimages from unsmoothed contour reconstructions suggesting a round-to-slim shape change as the most important feature. This has been described in earlier paragraphs.

In general the main variation in shape is the same when only the Ancona or Chioggia datasets were used, and when the combined dataset was analysed. However, the eigenimage analysis on the combined dataset resulted in a slightly clearer set of characteristic shapes probably due to the higher number of samples fed into the statistical evaluations.

All 69 factorial coordinates were now used to classify the combined dataset into two groups. For a perfect discrimination into landing sites, we expect two classes: 1640 for Ancona and 1120 for Chioggia. In practice we will have mixtures.

The classification into two shape classes revealed that from the 1640 samples landed in Ancona 866 members were found in class 1 and 774 in class 2. For Chioggia there were 492 in class 1 and 626 in class 2. There is, therefore a small preference for samples from Ancona to be classified into class 1 and samples from Chioggia to be classified into class 2. Anyway, each class composition is close to the theoretically expected composition if there is no landing site differentiation.

Harbour	Number of Samples		Shape Class 1		Shape Class 2	
	Count	Percentage	Count	Percentage	Count	Percentage
Ancona	1640	59%	866	64%	774	55%
Chioggia	1120	41%	492	36%	626	45%

**Table 5.25:** Results for the classification of the combined anchovy dataset into two shape classes. Class composition differences do not suggest any landing site specificity in shape.

From the separate eigenimage analyses of the Ancona and Chioggia datasets it may become clear that factorial coordinate 2, i.e. factor 2 or F2, is somehow able to distinguish the shape of otoliths from very young fish from the otolith shape of older fish. Age group zero for Ancona has mostly negative F2 values, while in older fish F2 can have any value. Small F2 values are specific for Chioggia fish of age 0 and 1. Whereas in Ancona small F2 values are more specific only for age 0. Anyway, the spread in the F2 distributions is heavy as can be seen in the below figure. All the other age classes of both catch sites show a wide range of F2 values overlapping with those of age 0, so that at least the age-predictive discriminating power is low.

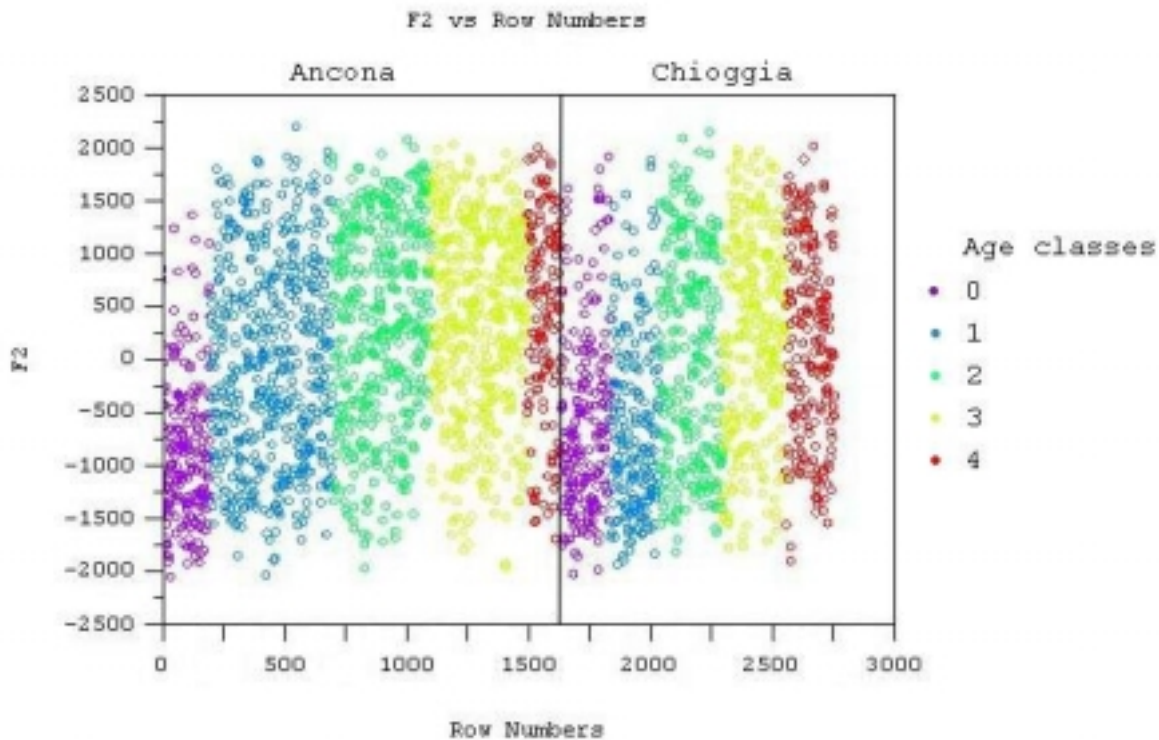


**Figure 5.61:** The factorial coordinates F2 for the separately evaluated datasets of otoliths from Ancona and Chioggia are shown. Values from age groups are indicated by individual colors. Note that F2 for both Ancona and Chioggia datasets for age group 0 is relatively small as compared to older samples.

While these results show that we were able to find differences in shape, these differences could not be linked with the landing sites of catches. For the purpose of discriminating the two landing sites we have split the combined dataset into two big classes. However, what might come out if we allow for more consistent shape classes and then look at their individual composition? We have performed such an alternative classification using NFDs.

The complete dataset, including Ancona and Chioggia samples was classified into 50 shape classes and it was visually verified that the shape classes were meaningful. As a first, preliminary, step the composition of classes was inspected to see if there was any age specific feature, i.e. if there was some class specific for certain age groups. This had already been done for the Ancona dataset alone (see previous paragraphs) using 25 shape classes, here it was repeated adding the Chioggia dataset.

For illustration, in Fig. 5.62 and Fig. 5.63 selected shape classes for “old anchovy” and for “young anchovy” are shown.

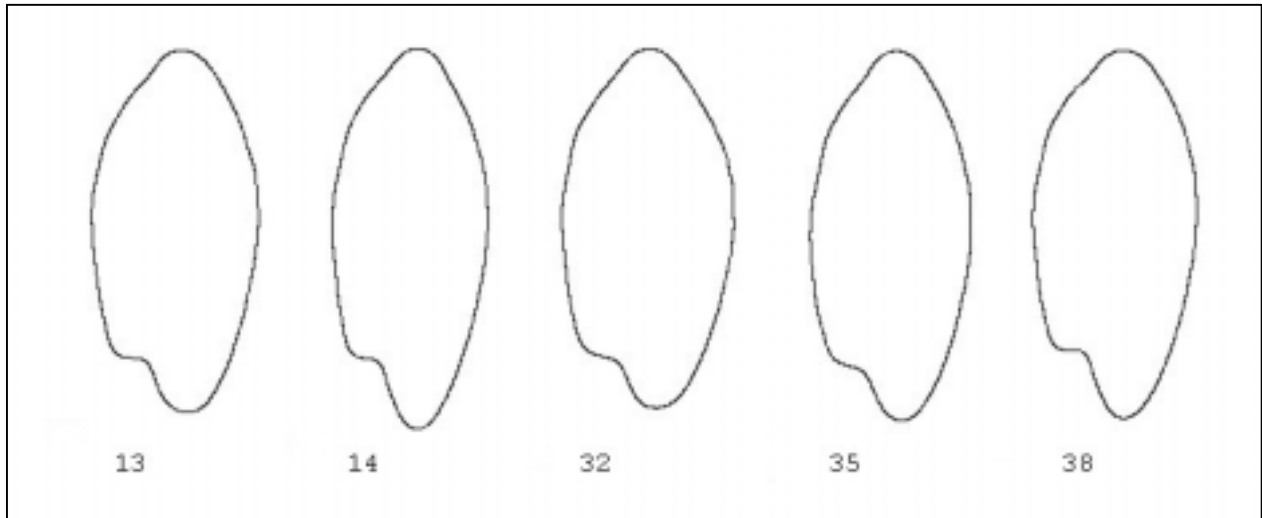


**Figure 5.63:** Typical shape class representations for young anchovy otolith samples.

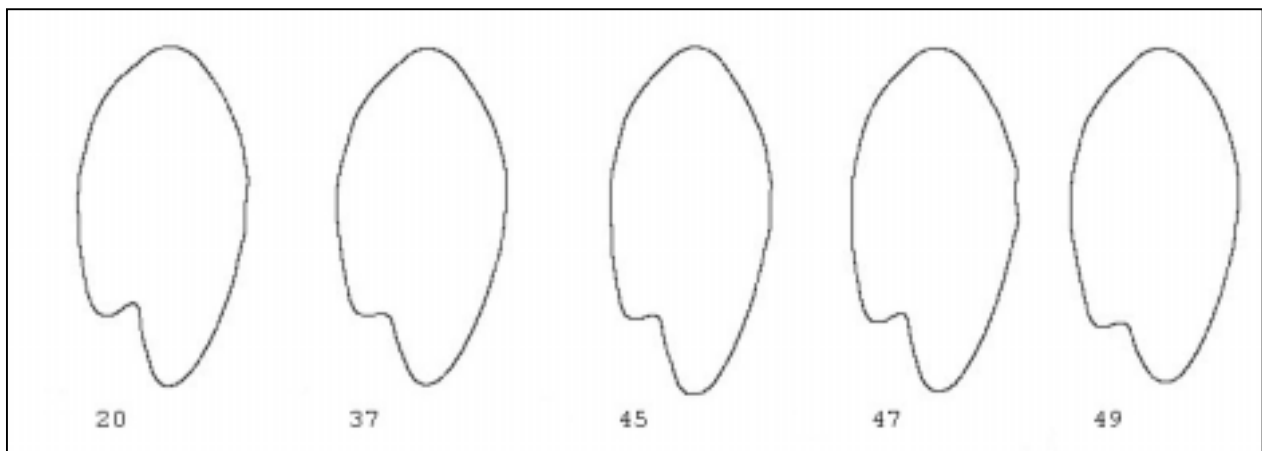


**Figure 5.63:** Typical shape class representations for old anchovy otolith samples.

The corresponding composition of the 50 classes in terms of age is shown in Tab. 5.26.

Class	Members	% Age 0	% Age 1	% Age 2	% Age 3	% Age 4
1	68	5.9	13.2	33.8	33.8	13.2
2	38	36.8	42.1	7.9	10.5	2.6
3	50	6	14	26	40	14
4	98	12.2	25.5	34.7	16.3	11.2
5	53	13.2	18.9	17	28.3	22.6
6	64	6.3	14.1	43.8	25	10.9
7	35	31.4	40	20	5.7	2.9
8	69	14.5	30.4	29	17.4	8.7

9	67	14.9	35.8	16.4	17.9	14.9
10	74	32.4	28.4	16.2	16.2	6.8
11	38	0	18.4	28.9	44.7	7.9
12	19	15.8	15.8	42.1	21.1	5.3
13	77	1.3	11.7	28.6	37.7	20.8
14	74	0	9.5	21.6	47.3	21.6
15	78	7.7	35.9	17.9	25.6	12.8
16	67	1.5	11.9	37.3	38.8	10.4
17	38	2.6	13.2	42.1	26.3	15.8
18	85	31.8	41.2	17.6	7.1	2.4
19	58	37.9	24.1	19	13.8	5.2
20	43	79.1	11.6	2.3	4.7	2.3
21	10	0	10	30	50	10
22	36	19.4	36.1	13.9	19.4	11.1
23	27	44.4	25.9	3.7	14.8	11.1
24	71	26.8	32.4	22.5	15.5	2.8
25	69	2.6	10.3	28.2	35.9	23.1
26	31	4.8	2.4	26.2	28.6	38.1
27	69	9.3	25.6	25.6	23.3	16.3
28	79	0	16.4	31.3	31.3	20.9
29	25	0	3.8	34.6	25	36.5
30	90	22.7	36.4	25	6.8	9.1
31	39	2.6	10.3	28.2	35.9	23.1
32	42	4.8	2.4	26.2	28.6	38.1
33	43	9.3	25.6	25.6	23.3	16.3
34	67	0	16.4	31.3	31.3	20.9
35	52	0	3.8	34.6	25	36.5
36	44	22.7	36.4	25	6.8	9.1
37	48	37.5	37.5	12.5	12.5	0
38	95	3.2	15.8	37.9	21.1	22.1
39	60	5	28.3	21.7	28.3	16.7
40	91	15.4	31.9	26.4	19.8	6.6
41	59	1.7	23.7	22	30.5	22
42	51	15.7	23.5	21.6	23.5	15.7
43	116	7.8	29.3	19.8	31.9	11.2
44	26	7.7	30.8	15.4	42.3	3.8
45	45	33.3	35.6	13.3	11.1	6.7
46	27	0	18.5	14.8	51.9	14.8
47	44	45.5	36.4	11.4	2.3	4.5
48	23	39.1	17.4	17.4	26.1	0
49	45	24.4	37.8	17.8	11.1	8.9
50	43	16.3	53.5	14	11.6	4.7

**Table 5.26:** The age composition of shape classes for the combined dataset of otoliths from Ancona and Chioggia.

As previously found for the Ancona dataset, only the well known round to elongated deformation in shape is evident, while correlation with age is poor. In general the age composition of each of the 50 classes extends over all the five age groups. If there is shape related information better than age, it must clearly reveal itself in the form of feature-characteristic shape-classes. So it was tried to find such specific shape classes for the two catch sites.

Two different approaches were tried, one using the combined dataset including all age groups and a second analysis was performed separately on the four specific age groups. This second procedure was performed on partial datasets of same size, where possible. The individual age group datasets are composed as follows:

- Age 0: 200 Ancona + 200 Chioggia = 400
- Age 1: 200 Ancona + 200 Chioggia = 400
- Age 2: 200 Ancona + 200 Chioggia = 400
- Age 3: 200 Ancona + 200 Chioggia = 400
- Age 4: 140 Ancona + 140 Chioggia = 280

The “combined” dataset contains all the above samples from age 0 to age 4, pooled together. There are thus 1880 samples in both cases. Two classifications were performed on the “combined” data set. In one case again 50 classes were constructed and analysed. In another case only 10 broader classes were made. The number 50 and 10 were chosen arbitrarily to test two different classifications, one with many narrow and the other with few broader shape classes. Results are shown in the following tables for the classification into 50 classes and into 10 classes. In very few classes there was a significant ( $P > 0.05$ , Kolmogorov-Smirnov test) deviation from the 50% hypothesis for 'no site specificity for the shape class'.

50 classes				
Shape classes	Ancona	Chioggia	N	K-S test
1	9	9	18	no
2	19	28	47	no
3	18	28	46	no
4	39	31	70	no
5	8	21	29	no
6	30	10	40	*
7	25	20	45	no
8	16	18	34	no
9	13	13	26	no
10	13	15	28	no
11	23	17	40	no
12	31	23	54	no
13	25	12	37	no
14	4	1	5	no

15	19	12	31	no
16	9	16	25	no
17	32	29	61	no
18	20	16	36	no
19	23	34	57	no
20	24	17	41	no
21	15	2	17	no
22	18	13	31	no
23	19	23	42	no
24	16	20	36	no
25	27	18	45	no
26	25	20	45	no
27	9	8	17	no
28	14	14	28	no
29	14	10	24	no
30	34	36	70	no
31	12	34	46	no
32	12	31	43	no
33	24	21	45	no
34	18	19	37	no
35	14	10	24	no
36	25	21	46	no
37	24	9	33	no
38	4	9	13	no
39	23	37	60	no
40	16	17	33	no
41	26	13	39	no
42	18	12	30	no
43	25	29	54	no
44	22	22	44	no
45	21	23	44	no
46	20	26	46	no
47	14	17	31	no
48	16	37	53	no
49	11	5	16	no
50	4	14	18	no

**Table 5.27:** Significance tests for the 50 shape classes for the combined anchovy dataset. According to the Kolmogorov-Smirnov test, only one shape class has a significant preference for one of the landing sites.

10 classes			
Ancona	Chioggia	N	K-S test
38	80	118	*
110	81	191	no

158	80	238	*
74	90	164	no
158	172	330	no
94	98	192	no
54	50	104	no
61	60	121	no
98	123	221	no
103	106	209	no

**Table 5.28:** Significance tests for the 10 shape classes for the combined anchovy dataset. According to Kolmogorov-Smirnov tests, only two shape classes have a significant preference for one of the landing sites.

The analysis by age group was performed processing together the 400 samples of each age group, to be classified into 10 (a number arbitrarily chosen) shape classes. In one case (Age 4) it was 280 sample into 10 classes. Results are shown in Tab. 5.29. Again the occurrence of deviation from the 50% hypothesis is not frequent so the catch site specificity of shapes inside a given age group is very low.

<b>Age 0</b>				
<b>Shape class</b>	<b>Ancona</b>	<b>Chioggia</b>	<b>Sum</b>	<b>signif.</b>
1	22	9	31	no
2	21	23	44	no
3	13	15	28	no
4	24	20	44	no
5	9	24	33	no
6	18	26	44	no
7	27	24	51	no
8	27	20	47	no
9	13	5	18	no
10	26	34	60	no

<b>Age 1</b>				
<b>Shape class</b>	<b>Ancona</b>	<b>Chioggia</b>	<b>Sum</b>	<b>signif.</b>
1	27	25	52	no
2	10	17	27	no
3	16	36	52	no
4	33	15	48	no
5	18	12	30	no
6	24	19	43	no

7	13	32	45	no
8	17	22	39	no
9	11	1	12	*
10	31	21	52	no

<b>Age 2</b>				
<b>Shape class</b>	<b>Ancona</b>	<b>Chioggia</b>	<b>Sum</b>	<b>signif.</b>
1	30	32	62	no
2	33	48	81	no
3	8	5	13	no
4	22	28	50	no
5	39	15	54	no
6	23	23	46	no
7	25	12	37	no
8	6	2	8	no
9	0	17	17	*
10	14	18	32	no

<b>Age 3</b>				
<b>Shape class</b>	<b>Ancona</b>	<b>Chioggia</b>	<b>Sum</b>	<b>signif.</b>
1	35	34	69	no
2	21	17	38	no
3	27	30	57	no
4	19	10	29	no
5	17	15	32	no
6	22	8	30	no
7	27	10	37	*
8	23	52	75	*
9	7	23	30	*
10	2	1	3	no

<b>Age 4</b>				
<b>Shape class</b>	<b>Ancona</b>	<b>Chioggia</b>	<b>Sum</b>	<b>signif.</b>
1	13	8	21	no
2	15	15	30	no
3	19	14	33	no
4	21	31	52	no
5	6	14	20	no

6	13	6	19	no
7	16	16	32	no
8	28	21	49	no
9	8	14	22	no
10	1	1	2	no

**Table 5.29:** Significance tests for the 10 shape classes for the combined anchovy dataset. According to Kolmogorov-Smirnov tests, only few shape classes have a significant preference for one of the landing sites. Note that evaluations were carried out separately for age groups, i.e. unwanted cross-correlations are avoided.

Assuming as specific those classes where around 70% of the objects were classified to one of the two groups, there are three specific classes out of ten for Age 0. The major component in these classes makes up on average about 72% of all cases. The three classes contain a total of 82 cases out of 400 (20.5%). Therefore the overall score for prediction of the catch site is  $0.72 \times 0.205 \times 100 = 15\%$ . A similar evaluation can be made for the other age groups and is summarised in the next table.

Age	% in specific classes	% cases	% overall score
0	72	20.5	15
1	75	39.3	30
2	86	17.8	15
3	73	43.0	31
4	-	-	-

**Table 8+6.** Summary on the calculated predictive power for landing site specificity for all age groups in the combined anchovy dataset.

In age group 4 there are no unambiguous specific classes and in the other age groups the scores are from 15% to 31%. Because of the pretty shaky behaviour of these scores, one might again get the impression of a lack of a real shape relation to catch site. The possibility that in such a case the numbers would merely reflect a random coincidence (as detected by the Kolmogorov Smirnov test) is high. Even considering them as non-random events, the prediction score is low and cannot probably be used at the level of assigning individuals reliably to one of the two catch sites.

#### 5.2.2.4. Cod

However, we should now focus on cod for which the situation is much better. We will see that the shape of cod otoliths is almost as powerful in age prediction than conservative measures such as otolith weight.

One important aspect concerning the shape analysis of cod otoliths should be considered first. It is the level of detail, which is required to properly represent an otolith shape. Cod otoliths have a number of lobes between which narrow indentations occur. In early stages of the project we took

a limited subset of all available Normalised Fourier Descriptors into account. While this means some smoothing of the contours, we believed that the relevant shape information is sufficiently described. Other project partners, however, required to increase the level of detail so that for example all lobes are well resolved. In the final IMAGIC-5 software version the level of detail can be determined by the user. The highest level of detail corresponds to 256 NFDs, while the lower level works on 68 NFDs. In a temporary software test version even 512 NFDs were considered.



**Figure 5.64:** The influence of the number of NFDs on the level of detail in reconstructed cod otolith shapes. From left to right one can see contours evaluated from 68, 256, and 512 NFDs. The two right shapes are virtually identical, while clear smoothing is visible in the left shape.

In the smoothed shapes, individual lobes are not well resolved. However, what we apprehend as big differences, are only small variations with respect to NFDs.

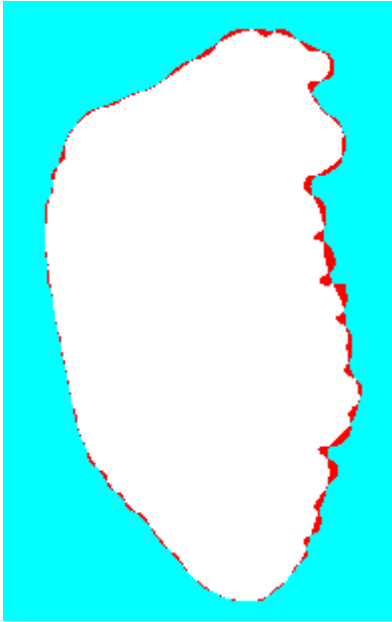


**Figure 5.65:** The differences between low and high resolution contours are shown in red.

The smoothing effect with a low number of NFDs can easily be seen. Note that the differences are not local but global.

We used cod otolith contour reproductions at the different detail levels and fed these images into the usual eigenimage calculations. These investigations were done early in the project. At that time, we used filled shapes rather than contour lines in the multivariate statistical analysis. The effect is a different kind of eigenimage. However, for the conclusions we like to make, this is of no concern.

It should be mentioned that the dataset consisted of 353 cod otolith shapes from age groups as indicated in tab. 5.30.

<b>Image Locations</b>	<b>Number of samples</b>	<b>Age</b>
1...100	100	4
101...193	93	5
194...272	79	2
273...353	81	3

**Table 5.30:** Organisation of the 353 cod (Faroe Plateau Pencage) otolith dataset.

The following series of Fig. 5.66 to Fig. 5.68 show the first four eigenimages obtained for the differently detailed shapes.

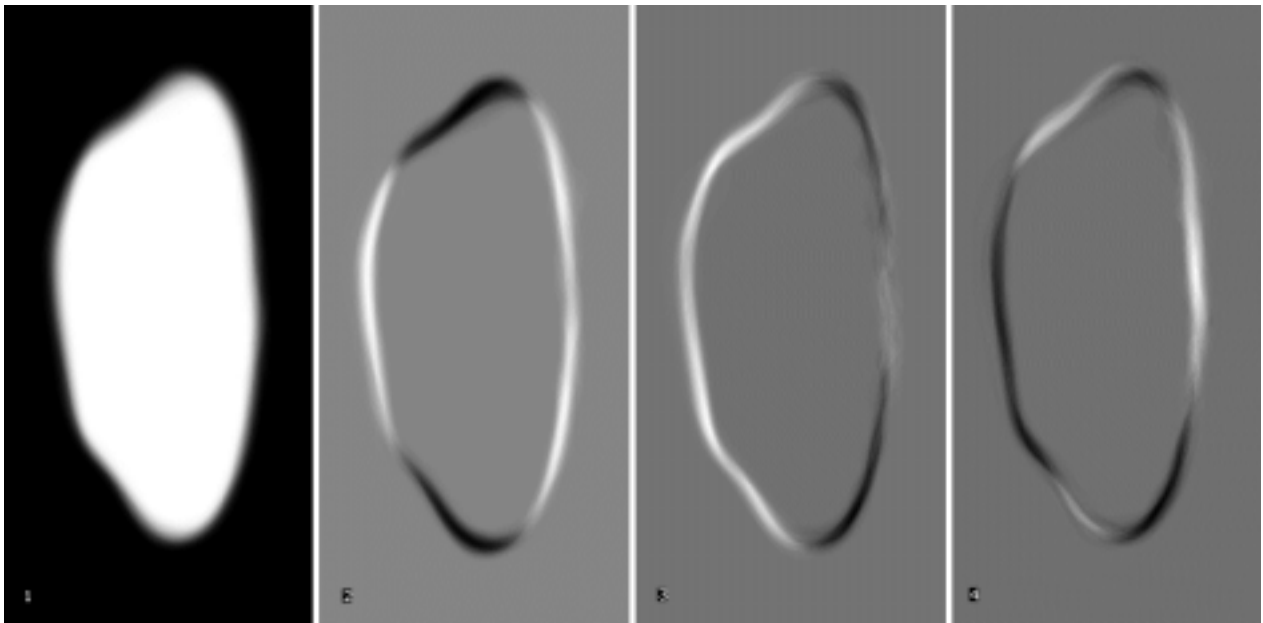


**Figure 5.66:** Eigenimage for reconstructed contours from 68 NFDs.

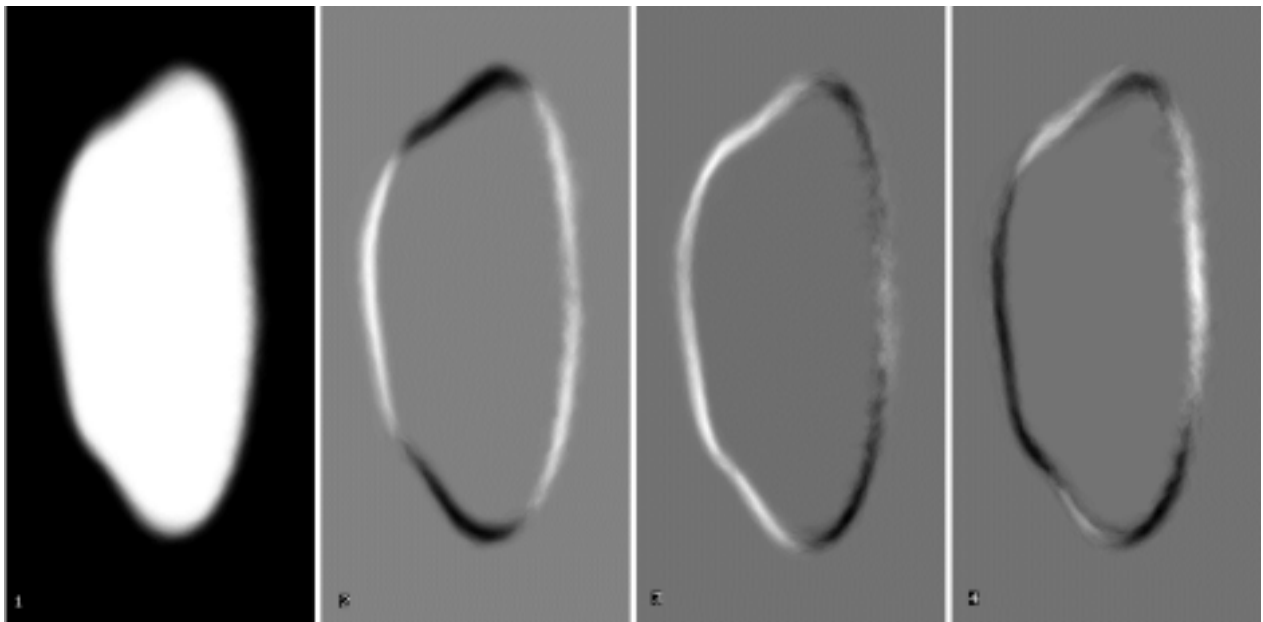


**Figure 5.67:** Eigenimage for reconstructed contours from 256 NFDs.

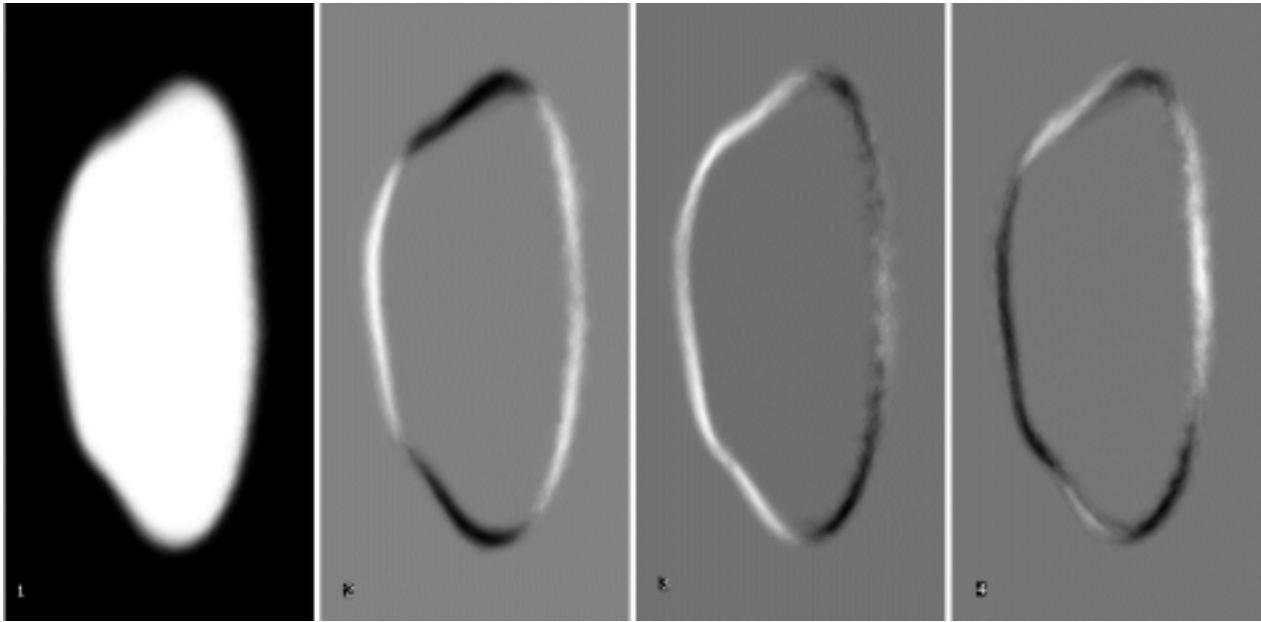


**Figure 5.68:** Eigenimage for reconstructed contours from 512 NFDs.

The essential features in all eigenimages are the dark and bright regions, where there are significant and consistent shape variations in the otolith shape. For example, eigenimage 2 has two bright vertical zones and darker zones at the top and bottom. Since bright and dark mean more and less, we can rephrase the shape change trend captured in eigenimage 2 as

- otoliths get broader at mid-height and shorter in vertical direction.

These features are visualised in the next Fig. 5.69.

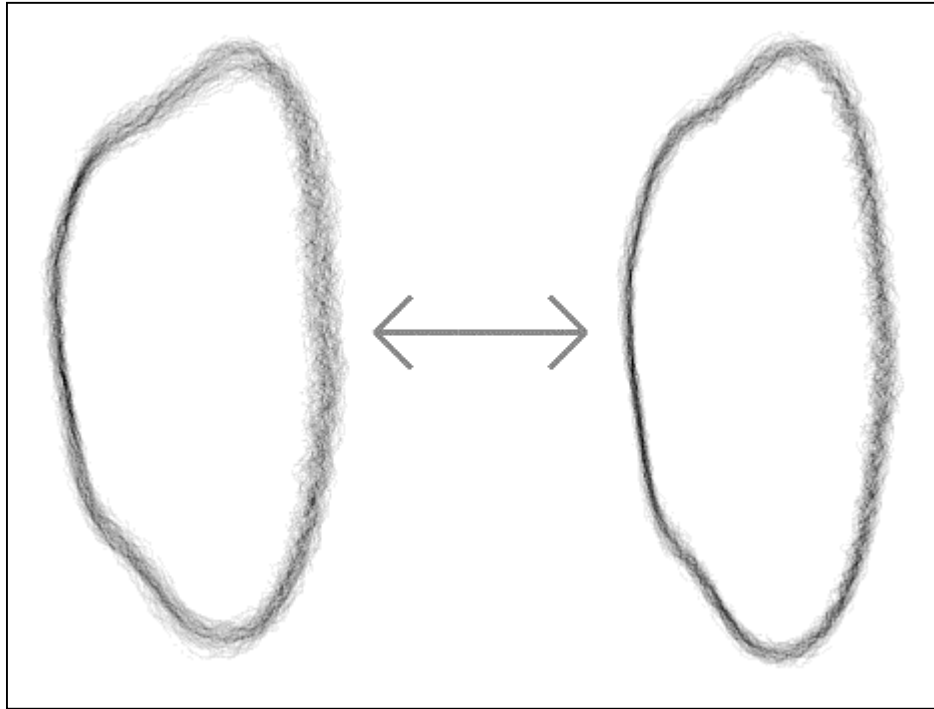


**Figure 5.69:** The most significant shape change suggested by eigenimage 2 for the dataset of 353 pencaged cod from the Faroe Plateau region. The left shape is an average old, the right an average young otolith shape.

Note that lobes are not visible in the eigenimages even for the 512 NFDs level of detail. This means that even though we treated the lobes at a very high level of detail, the essential, i.e. consistent shape features do not include the lobes. Or in again other words, the lobes, especially the position where lobes occur along the otolith contour, are no consistent feature. Effects from inconsistent features, however, cancel out each other similar to a destructive interference.

If one looks very closely at eigenimage 3, one can see that to the right there are grey-tone variations for the 256 and 512 NFD detail level but no or fewer for the 68 NFD level. It means that the higher level of detail does in fact give small contributions but at a much lower level of importance than the very basic shape features.

So we might say that when a shape with great detail is fed into the eigenimage analysis, this does not mean that the results necessarily require such a high input precision! In our case, the 256 NFD level of detail is significantly higher than what we really need! But we can also argue that there were no negative effects from having more details initially. It seems in fact that the eigenimage analysis performs in an extremely stable fashion. It reduces the overflow in details to the required by simply wiping out inconsistent information.

We have performed shape classifications based on the eigenimages at the different levels of detail. Findings suggested that the resulting shape classes are very similar. Since it is very hard to compare whole classifications against each other we skip these results and just give our final conclusions:

- Reproductions using 68 NFDs are smoothed as compared to the 256 NFD versions.
- Reproductions at levels 256 and 512 are virtually identical.
- Eigenimages derived from differently detailed reproductions are basically the same.
- Classifications based on eigenimages give similar data partitions.
- Introducing more than required otolith contours details into the eigenimage analysis does not give any problems. Therefore, we decided to give the user a chance to decide for either 68 or 256 NFDs, with the suggested default being 256.
- There are characteristic otolith shapes for young and old cod.

The above dataset was used for the special purpose of determining the required level of detail in the contours. The Cod Faroe Plateau Pencege dataset was however also found to be suited for elucidation of the reliability of ageing based on shape and size because

- there are about equal number of samples per year group
- the total number of samples is reasonable as compared to other available database subsets
- all samples have been processed in Drottningholm, i.e. we can avoid any mixed-mode Drottningholm / Berlin samples.

The dataset has the following structure.

Location	Number of samples	Names	Age	Description
1...45	45	dc947...dc1183	2	left
46...86	41	dc948...dc1184	2	mirrored right
87...132	46	dc1185...dc1303	3	left
133...174	42	dc1186...dc1304	3	mirrored right
175...226	51	dc725...dc825	4	left
227...275	49	dc726...dc826	4	mirrored right
275...325	51	dc827...dc927	5	left
326...374	49	dc828...dc928	5	mirrored right
total	374			

**Table 5.31: Organisation of the 374 cod Faroe Plateau Pencege otolith dataset.**

The absolute otolith size (parameter 69) is obtained during the initial image processing yielding the NFDs. Before we show classification results based on shape alone, size alone and combinations of both, we like to demonstrate the high predictive power of otolith size in the next figure.

Parameter 69 versus Location Numbers

Cod FaPLPen of age 2, 3, 4, and 5

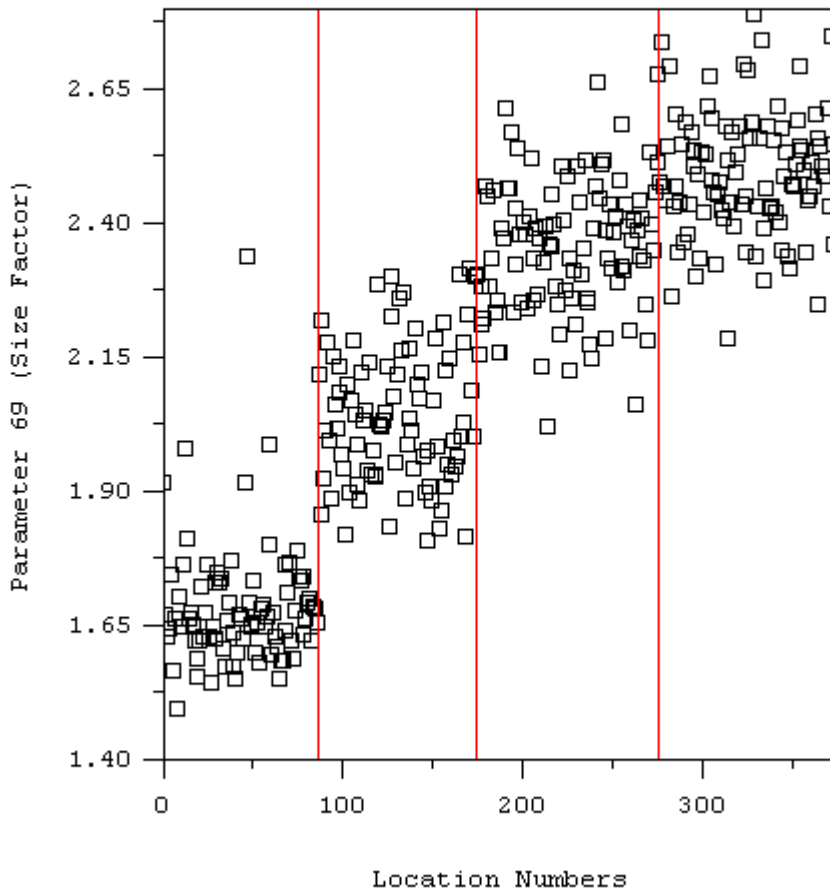


**Figure 5.70:** The otolith size factor increases with increasing age. The red lines are separators between the age groups. Note that age groups are fully separable. For other age groups the separation is acceptable.

Tab. 5.32 lists average values and standard deviations and the same information is given in graphical form in Fig. 5.71.

No. samples	Average size	Std. deviation	Upper limit	Lower Limit
86	1.6799	0.1139	1.7938	1.5660
88	2.0377	0.1298	2.1675	1.9079
100	2.3472	0.1346	2.4818	2.2126
100	2.4902	0.1164	2.6066	2.3738

**Table 5.32:** Otolith size factor averages over age groups.

Mean value and standard deviation  
of the size parameter for Cod FaPLPen  
of age 2,3,4, and 5 years

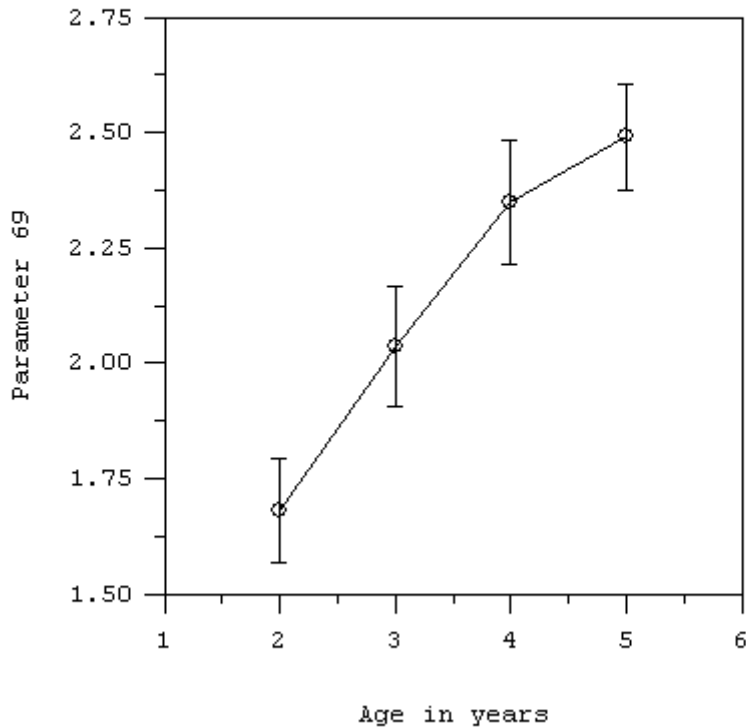


**Figure 5.71:** Average otolith size factor (parameter 69) over age. Standard deviations are indicated by vertical error bars.

What one can learn from these results is that the otolith size is a pretty good predictor for the age of the fish. From Fig. 5.71 it is clear that fish of age 2, 3 and 4 can be aged with considerable reliability. For older fish, the size factor variations get smaller and therefore the discrimination between age groups 4 and 5 is much lower than for the other age groups. Results for classifications based on size alone are given in Tab. 5.33.

Class	Age 2	Age 3	Age 4	Age 5	Correct predictions
1	81	5			94.2%
2	4	65	2		91.5%
3		21	85	19	68.0%
4			33	79	70.6%

**Table 5.33:** Age prediction based on the size factor (parameter 69) for the cod Faroe Plateau Pencege dataset. If samples from 5 year old fish are left out, the percentage correct predictions for age group 4 is 80.1%.

Keeping these findings in mind, we will now see how far we can come by using the otolith shape information alone. Previously we have shown that there are pronounced otolith shape changes with increasing age of the fish. Now we present ageing reliabilities for pure shape classes.

Class	Age 2	Age 3	Age 4	Age 5	Correct predictions
1	71	27	8	2	63%
2	8	36	21	17	44%
3	5	23	44	33	42%
4	2	3	27	43	57%

**Table 5.34:** Age prediction solely based on the otolith shape for the cod Faroe Plateau Pencege dataset. If samples from 5 year old fish are left out, the percentage correct predictions for age group 4 is 80.1%.

Tab. 5.35 suggests that the reliability for ageing of otolith shape is inferior to the otolith size factor.

Note that we have previously mentioned that the otolith weight and the otolith size factor are closely related. Assuming a constant material density within the otolith, the otolith weight and volume are related by the equation:  $\text{weight} = \text{volume} \times \text{density}$ . Moreover, in a first approximation, the volume is related to the cubed size factor:  $\text{volume} \sim \text{size factor}^3$ . In other words, we can combine these two equations into:  $\text{weight} \sim \text{size factor}^3$ . It is now clear that both, the otolith size factor and the otolith weight are similarly well suited for age prediction.

One interesting question is, if a combination of the size factor plus shape descriptors gives better results than the different descriptors alone. A series of classifications with weighted parameters was conducted to find the optimum weighting scheme.

W(2)	W(6)	W(10)	W(62)	W(63)	W(67)	W(68)	W(69)
0.1515213	9.88098	13.17	0.62133	1.248285	6.885185	3.5	10623.05

**Table 5.35:** Optimum weighting scheme for 68 NFDs (parameters 1...68) and the size factor (parameter 69). All parameters not listed have zero weight.

Tab 5.36 suggests that the size factor has overwhelming importance, however, a small influence of some shape descriptors might be allowed to improve the results of age prediction.

Class	Age 2	Age 3	Age 4	Age 5	Correct predictions
1	81	5			94.2%
2	4	73	5		89.0%
3	1	10	76	22	69.7%
4			20	77	79.4%

**Table 5.36.** Age prediction based on an optimised weighting scheme for a combination of shape descriptors and the size factor for the cod Faroe Plateau Pencege dataset. If samples from 5 year old fish are left out, the percentage correct predictions for age group 4 is 87.3%.

As compared to the classifications based on the size factor alone, basically the separation between age 4 and age 5 has been improved. In other words, for age groups 4 and 5, where the age prediction is difficult because the otolith size and weight doesn't differ that much, the appreciation of the otolith shape improved results. In so far we can say that cod is one species for which the otolith shape analysis gives some additional information that makes an age prediction more reliable.

When all the results for the species became available to the project partners, they suggested to try to combine all available sample information, of course except age, into a single age prediction model. It is clear that a vast statistical survey was never intended and is therefore not connected to any software development tasks with respect to IMAGIC-5.

We used the S-Plus statistical software package (S-PLUS 2000, 1999) to develop suitable models initially including all available sample data. The targeted species is cod, since we have established that the otolith shape has the highest chance of all investigated species to be an important factor for ageing. Tab 5.37 lists the available sample data.

Short Name	Full Name	Units
F1	Shape Factor F1	None
F2	Shape Factor F2	None
F3	Shape Factor F3	None
F4	Shape Factor F4	None
F5	Shape Factor F5	None
Age	Known Age	Years
Size	Size Factor	Millimeters per Pixel
Weight	Otolith Weight	Milligrams
FishWeight	Fish Weight	Grams
FishLen	Fish Length	Millimeters
ContLen	Contour Length	Millimeters
Area	Contour Area	Squared Millimeters
MaxDist	Maximal Distance	Millimeters

PerpDist	Perpendicular Distance	Millimeters
Apex1	Major Apex Distance	Millimeters
Apex2	Minor Apex Distance	Millimeters
Angle	Angle between Apices	Degrees

**Table 5.37:** Names and units of all available sample data. The last seven entries are geometrical features calculated and stored during image processing.

Please note that the otolith shape factors F1 to F5 are the factorial coordinates derived from the contour-line-only MSA image analysis. We have limited ourselves to the first five most important shape factors, while a total of 69 is available. The maximum internal distance is between any two contour points, as is the maximum perpendicular distance. The distances called Apex 1 and Apex 2 are explained in Fig. 5.72ff.

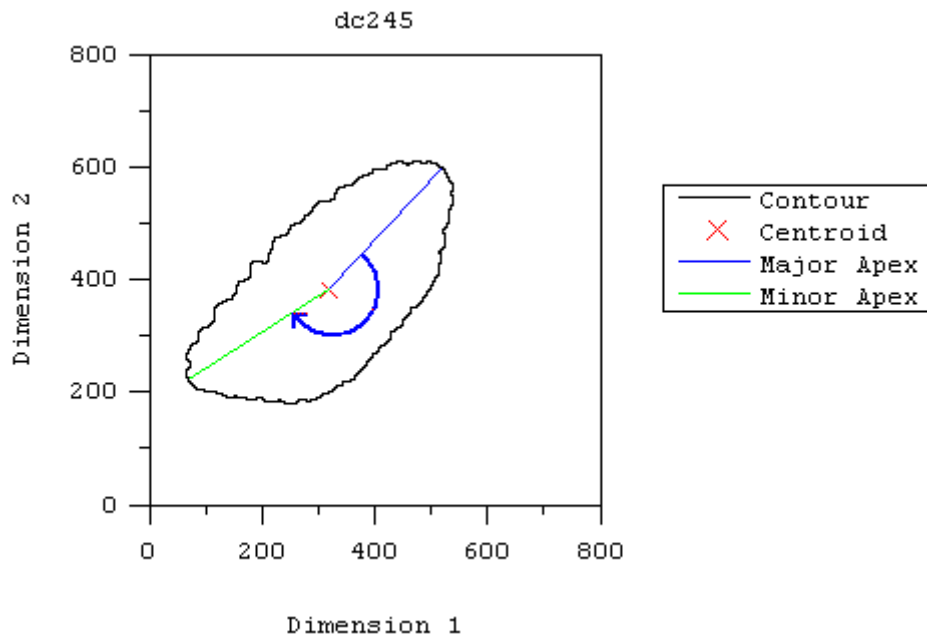


**Figure 5.72:** Definition of the Major Apex (Apex 1) and Minor Apex (Apex 2) and the Angle enclosed between. Both apices originate from the contour centroid and extend to farthest upper and lower contour points. The contour of a left body side otolith is shown.

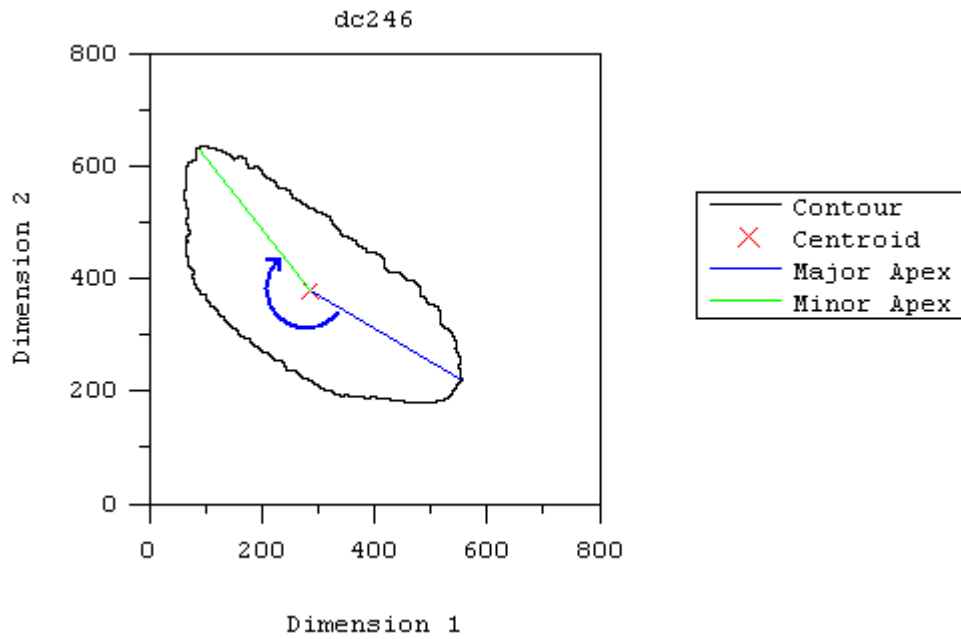


**Figure 5.73:** Definition of the Major Apex (Apex 1) and Minor Apex (Apex 2) and the Angle enclosed between. Both apices originate from the contour centroid and extend to farthest upper and lower contour points. The mirrored contour of a right body side otolith is shown.

Note that the angle between the apex vectors captures an important otolith size feature as explained below.

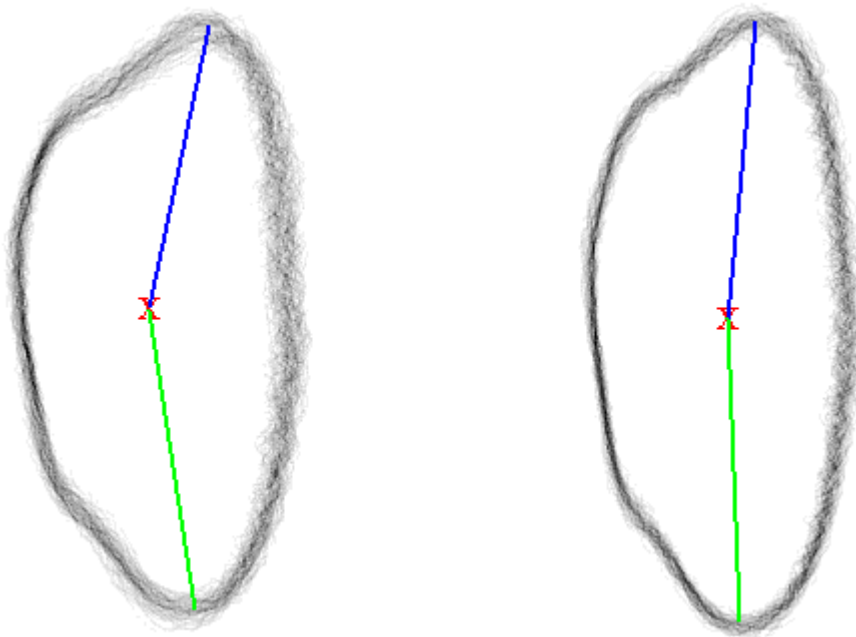


**Figure 5.74:** Sketch for the apex vectors for a typical shape of an old cod otolith (left) and a young cod otolith (right). Note the different angle between apex vectors.

S-Plus offers an initial statistics summary, which gives e.g. summaries on correlations. The summarised results for the data ranges and standard deviations for variables are shown below:

- Weight shows the strongest correlation to Age (0.934), followed by Size (0.914). Parameters related to shape have weaker correlations, e.g. Shape Factor F2 (0.761) and Angle (0.645)
- Most of the other parameters are mutually strongly cross-correlated, especially to Weight. This ultimately means that it is sufficient to concentrate on Weight as the most specific descriptor.
- The correlation between Weight and Size is very high. However, the theoretical dependence is  $\text{Weight} \sim \text{Size}^3$ . In a separate test, it was established that the correlation of Weight with  $\text{Size}^3$  is 0.973. As expected, this is slightly better than the correlation of Weight with Size alone (0.966).
- It is interesting to note that the correlation of Size with Age (0.91404856) is better than for  $\text{Size}^3$  with Age (0.9069402). This might indicate a high internal variability in Size. Thus, a transformation of Size to  $\text{Size}^3$  will generate even greater internal variations and finally result in a smaller correlation coefficient. Therefore, Size was used rather than its transform.

Box plots of data are a simple way of visualising the data value ranges. The very details of the partial datasets is revealed in scatter plots or histograms. The box plot feature of S-Plus includes a plausibility check for data, i.e. outliers can easily be detected.

In the following the box plots for all parameters over age are shown.

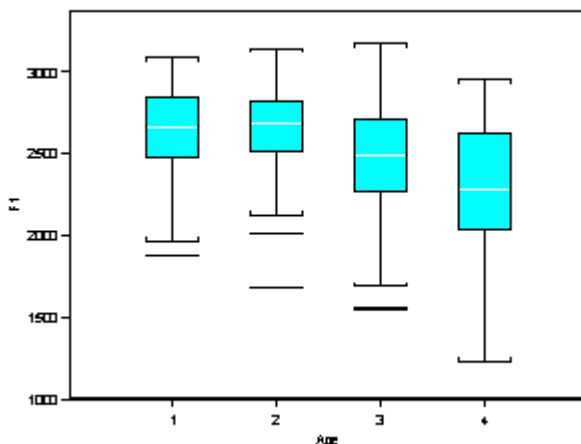


**Figure 5.75:** Shape factor (factorial coordinate) F1.

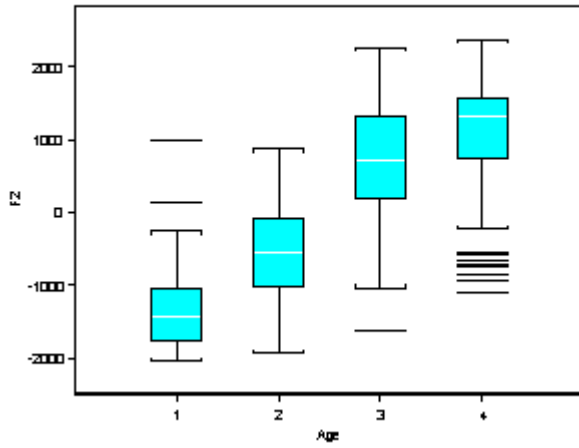


**Figure 5.76:** Shape factor (factorial coordinate) F2.

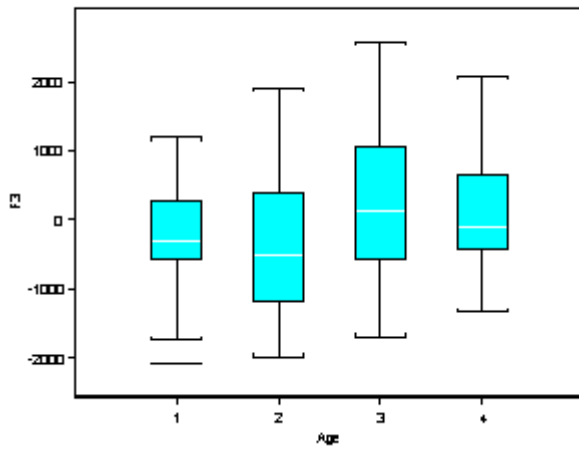


**Figure 5.77:** Shape factor (factorial coordinate) F3.

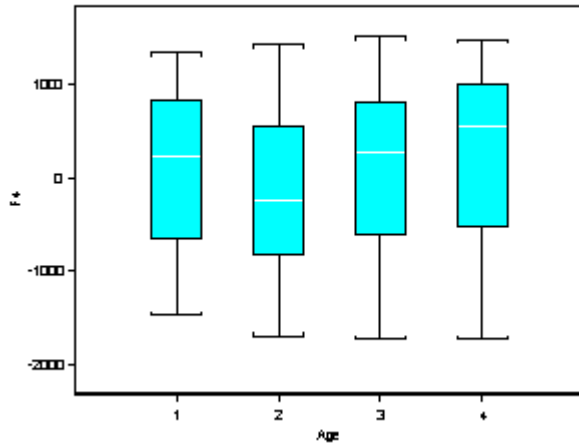


**Figure 5.78:** Shape factor (factorial coordinate) F4.

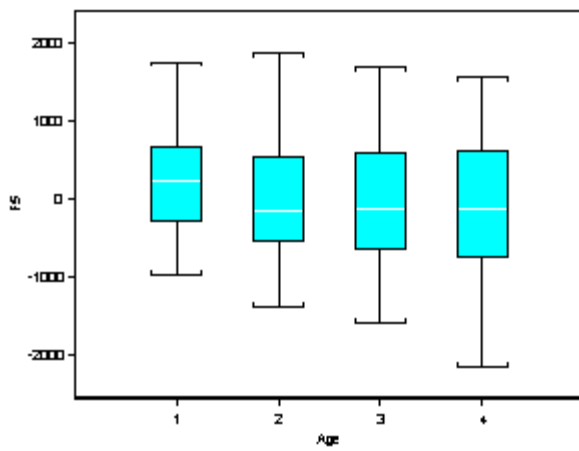


**Figure 5.79:** Shape factor (factorial coordinate) F5.

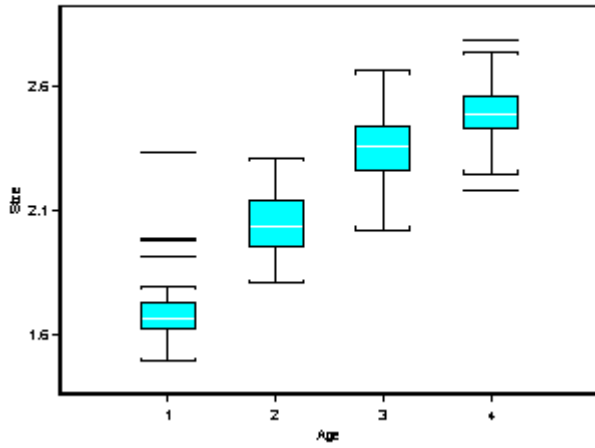


**Figure 5.80:** Size factor.

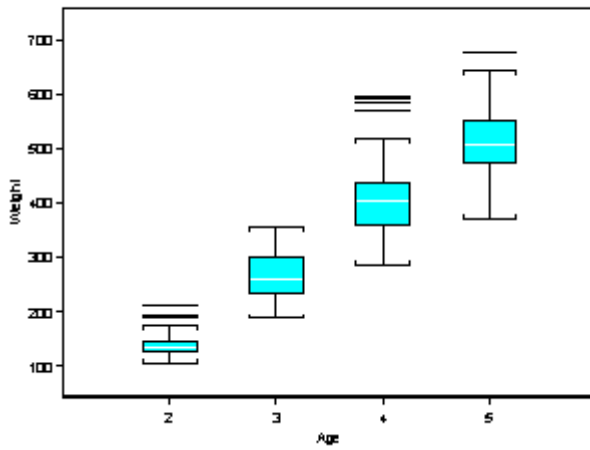


**Figure 5.81:** Otolith weight.

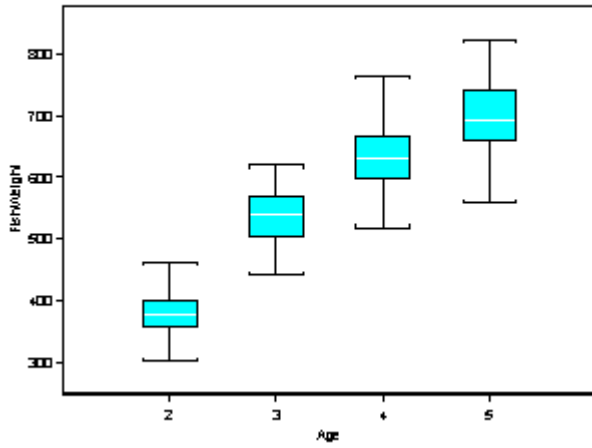


**Figure 5.82:** Fish weight.

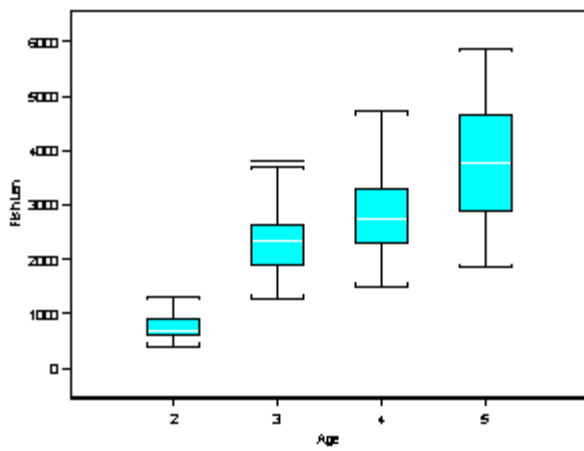


**Figure 5.83:** Fish length.

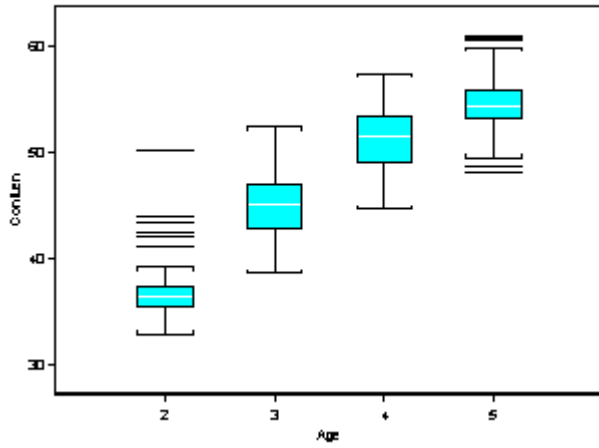


**Figure 5.64:** Contour length.

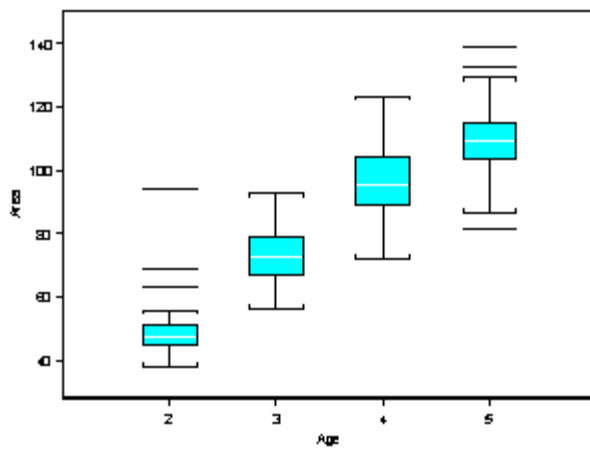


**Figure 5.85:** Otolith area.

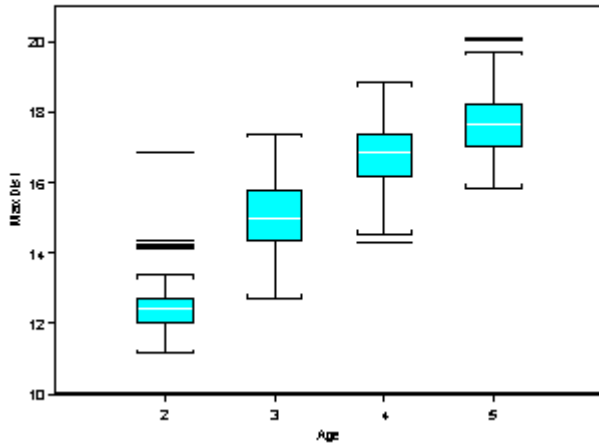


**Figure 5.86:** Maximum internal distance.

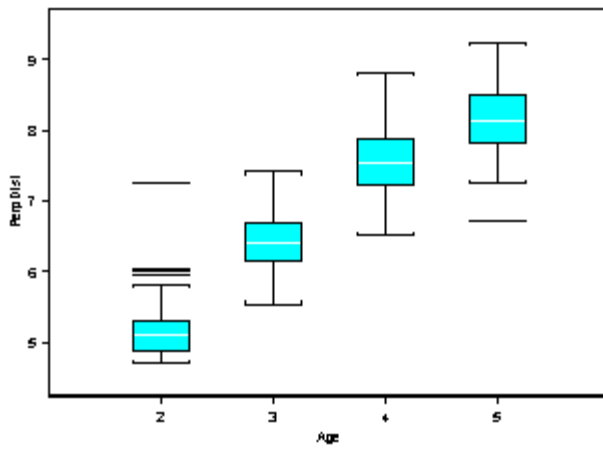


**Figure 5.87:** Maximum perpendicular distance.

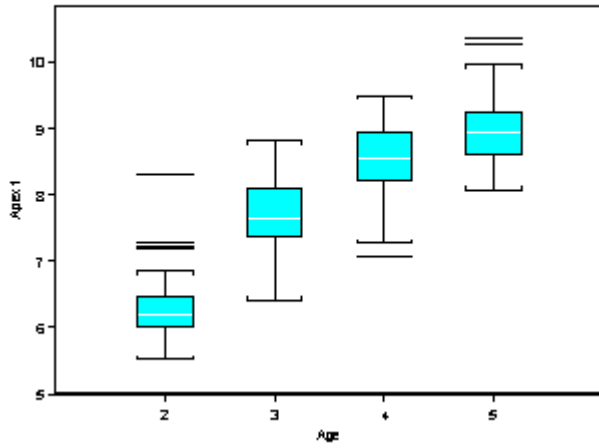


Figure 5.88: Apex 1.

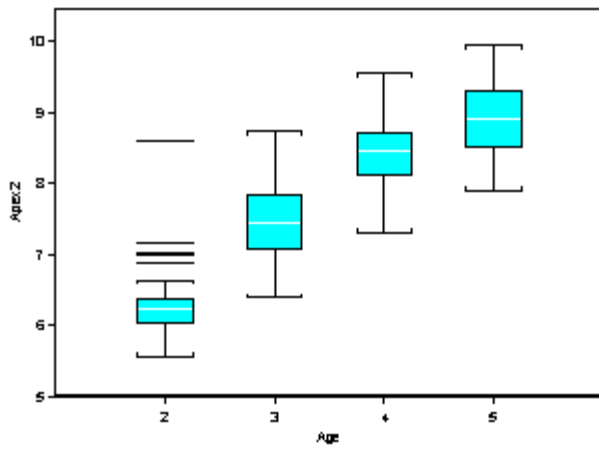
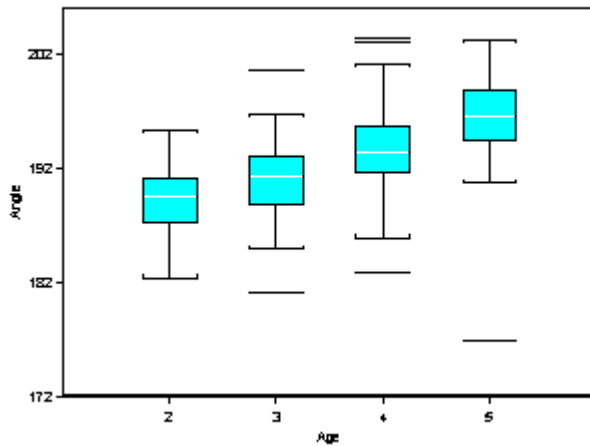


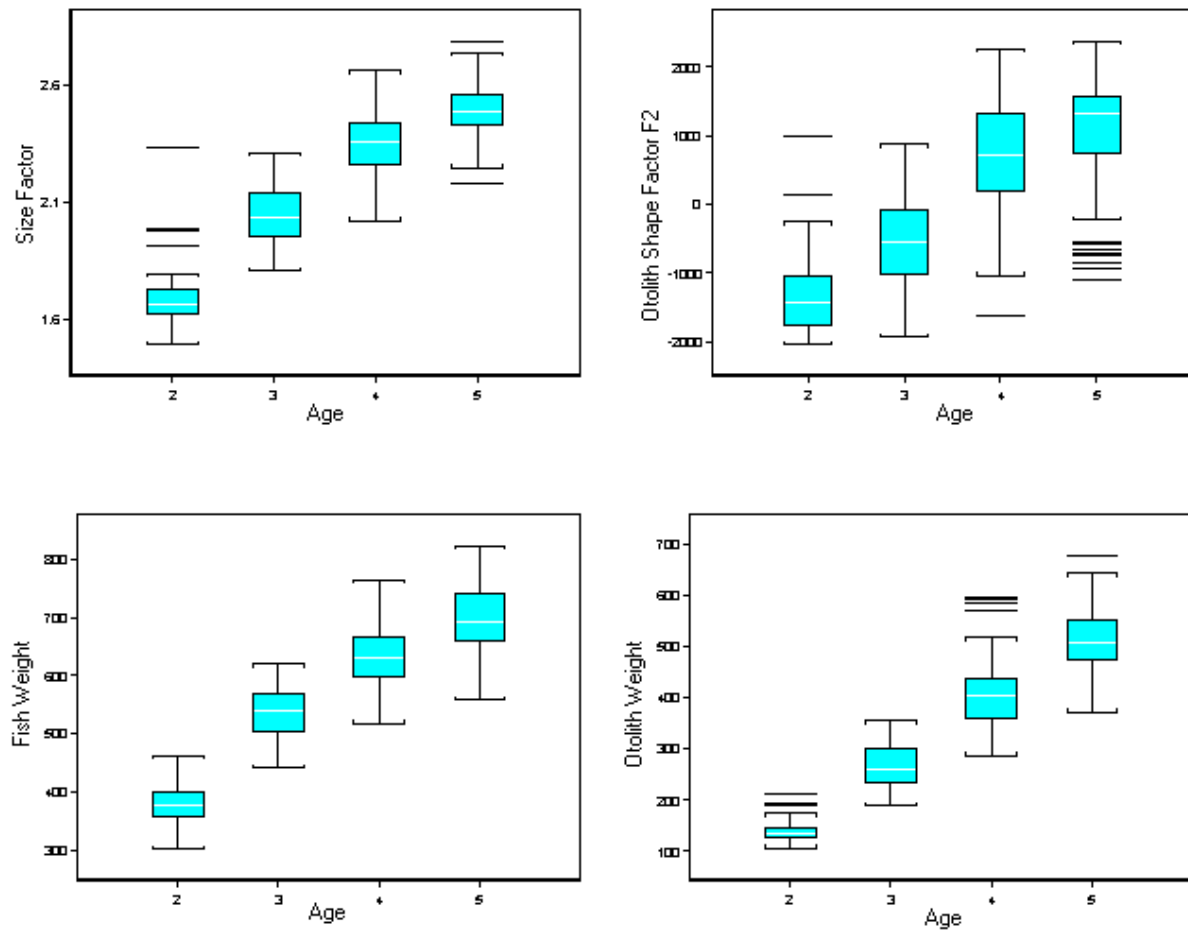
Figure 5.89: Apex 2.



**Figure 5.90:** Angle between Apex 1 and Apex 2.

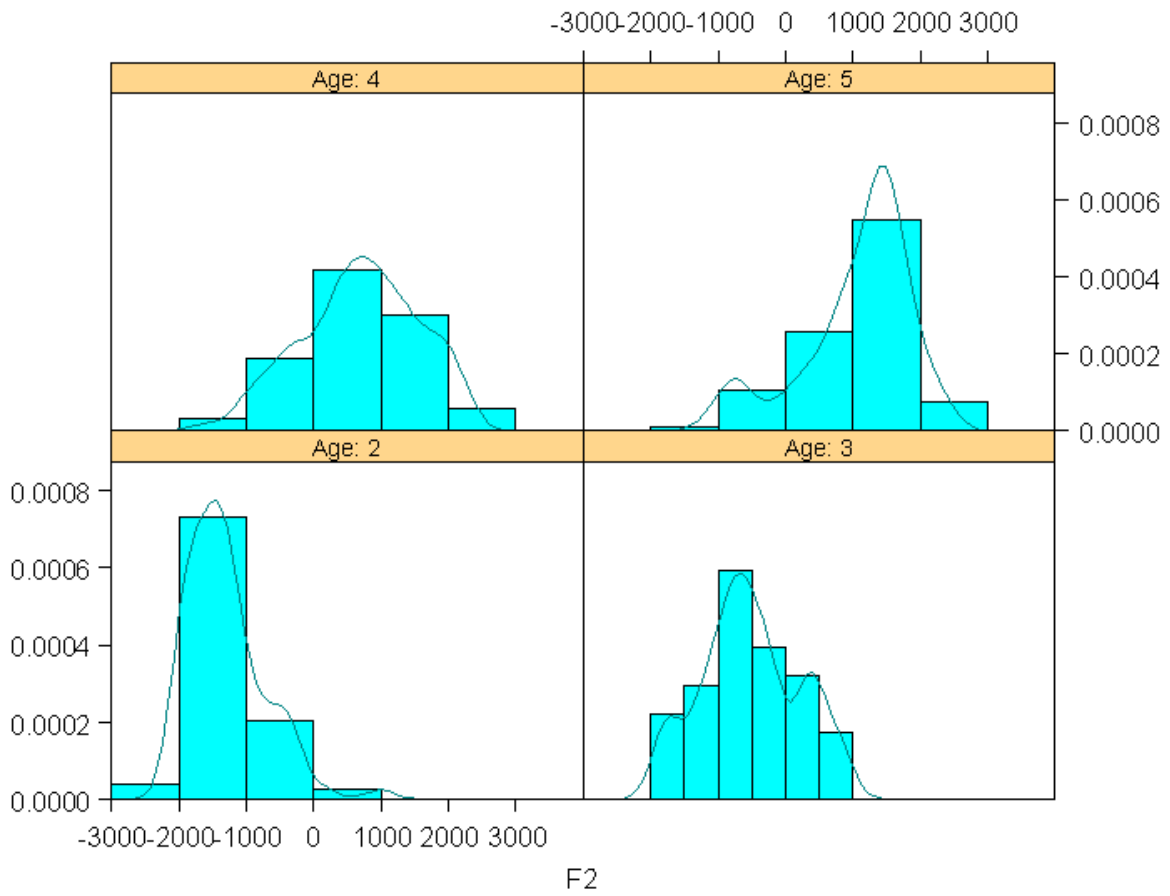
One can easily see that only for Otolith Weight all core-data boxes are separable. The next best situation is for Size Factor, where there is only a small overlap between boxes for Age 4 and Age 5. Box plots like for Factor F5 indicate that there is virtually no age-dependence in that parameter.

Fig. 5.91 shows a summary of the most effective predictors for Age.



**Figure 5.91:** Diagrams for the four best age predictors: Size Factor, Otolith Shape Factor F2, Fish Weight, and Otolith Weight.

In the following so-called Trellis-Plots of the feature distributions are shown. The datasets are split into the domains, i.e. age groups. Then the individual histograms of data are generated and shown in identical x/y frames. There are basically two aspects that can easily be derived from these types of plots: how the distribution of a parameter is presented and where it is centered around. One may take the following plots therefore as prove for single peaked distributions.



**Figure 5.92:** Trellis plot for Shape Factor F2.

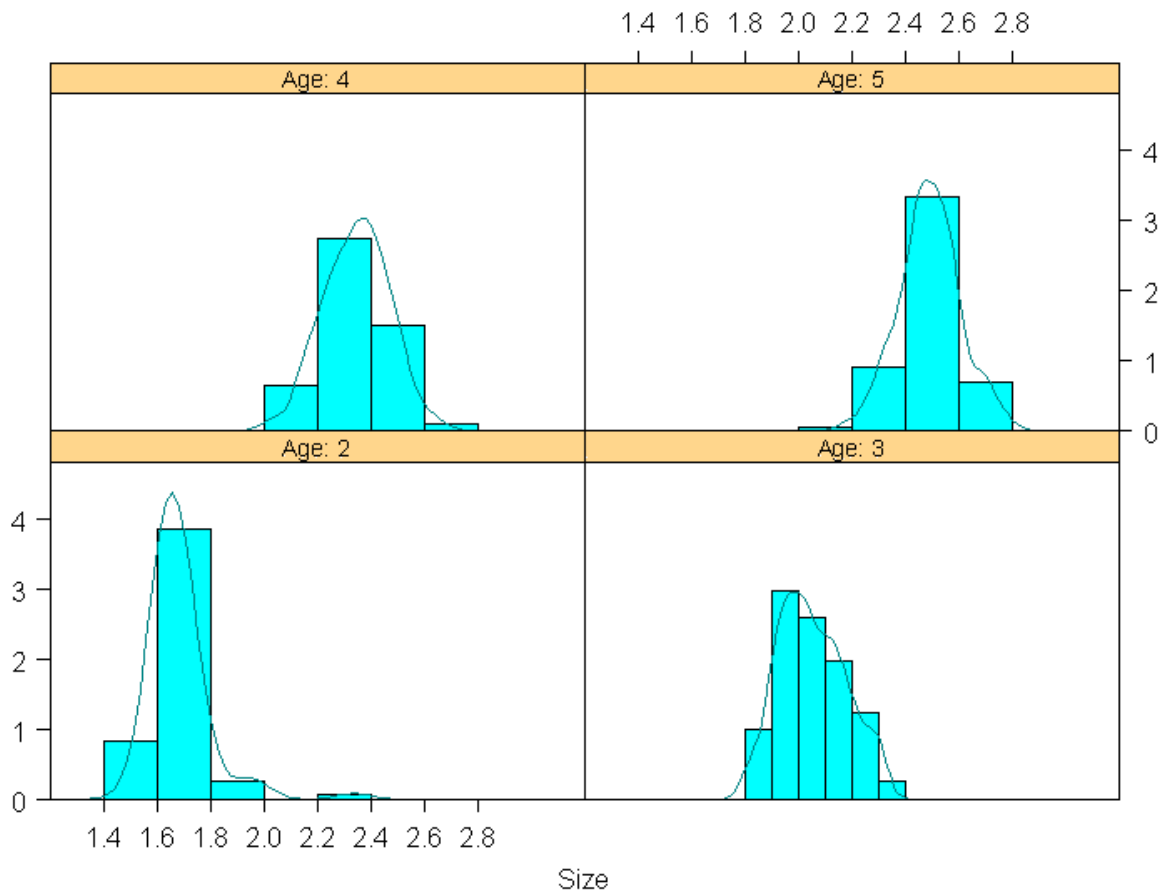


**Figure 5.93:** Trellis plot for Size Factor.

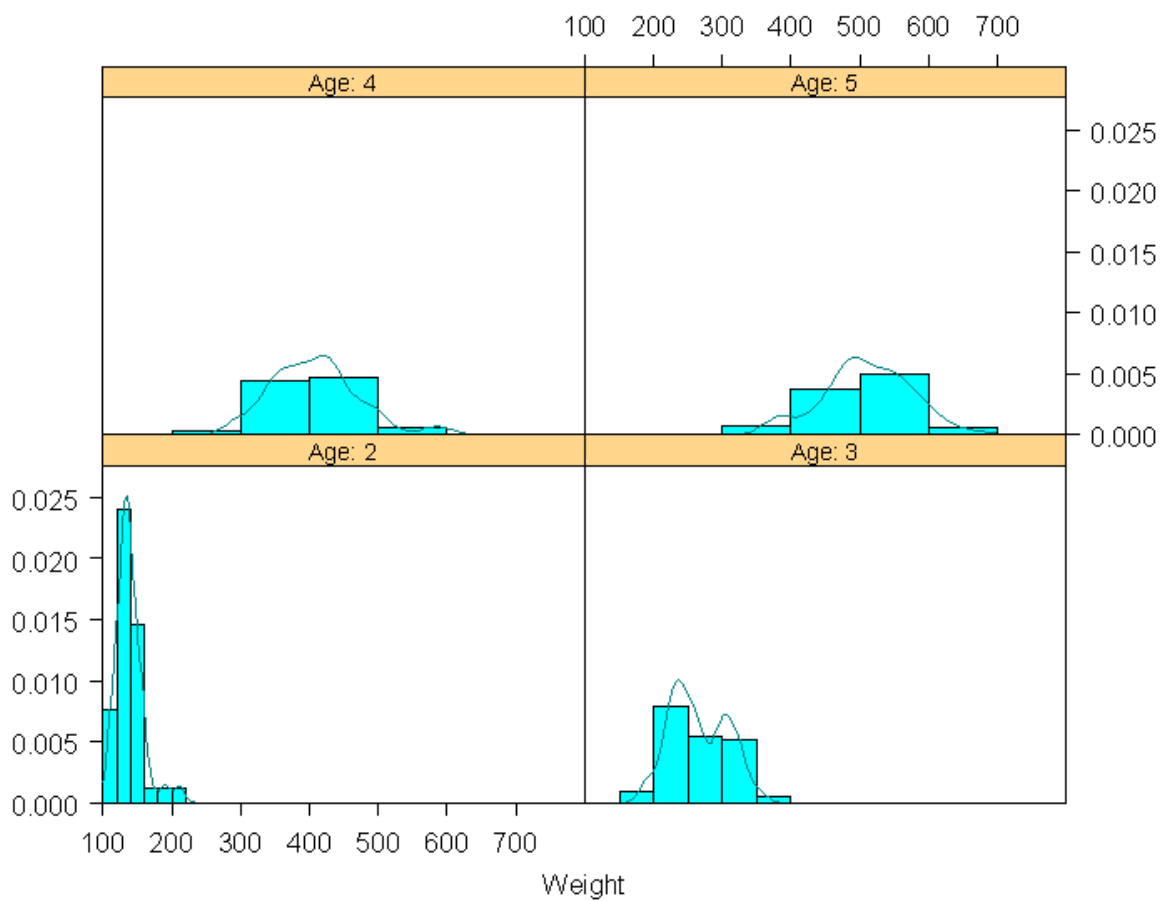


**Figure 5.94:** Trellis plot for Otolith Weight.

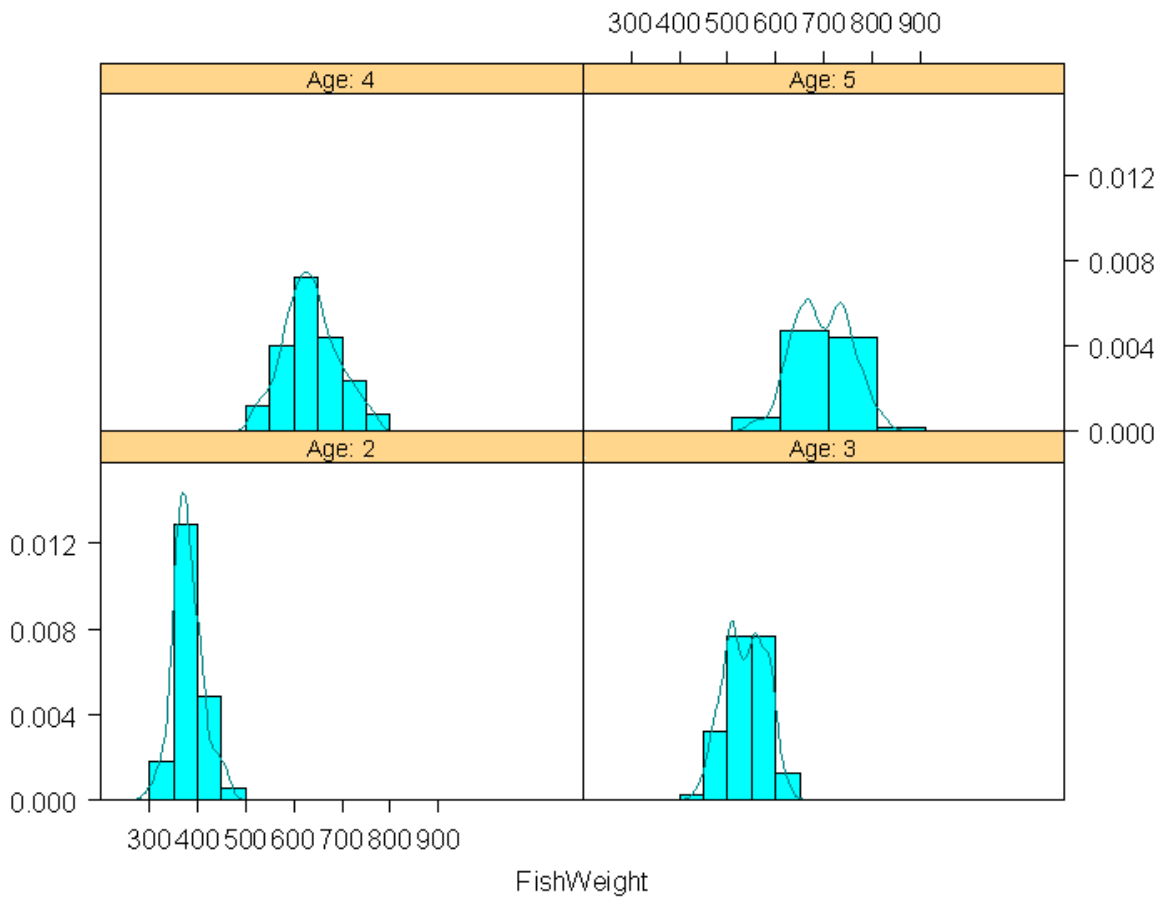


**Figure 5.95:** Trellis plot for Fish Weight.

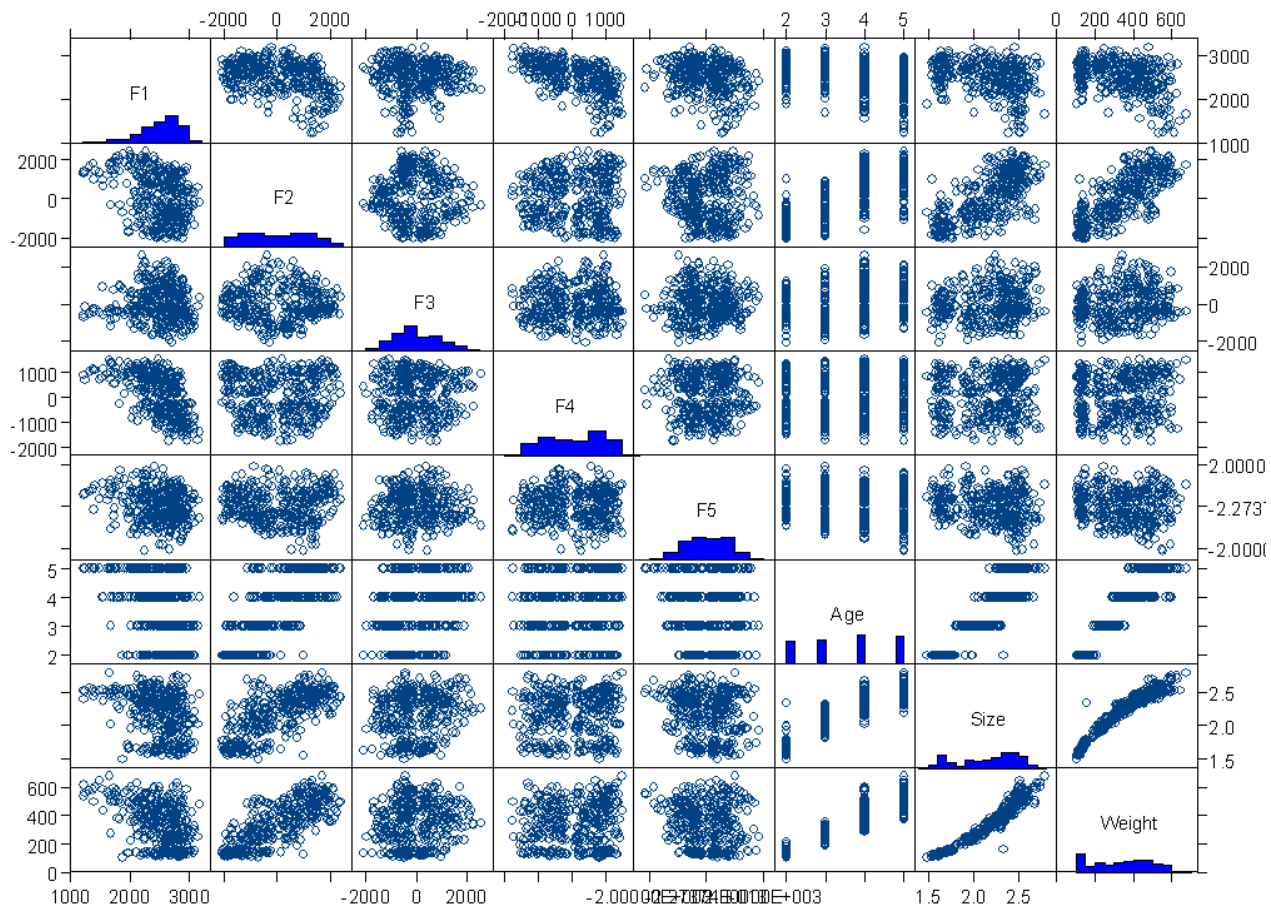


**Figure 5.96:** Matrix plot for all sample data.

The matrix plot summarises all data correlations in pictorial form. Otolith Size (Size) against Otolith Weight (Weight) suggests a close correlation. The diagram in Fig. 5.97 shows that the match of cubed size against weight is even better.

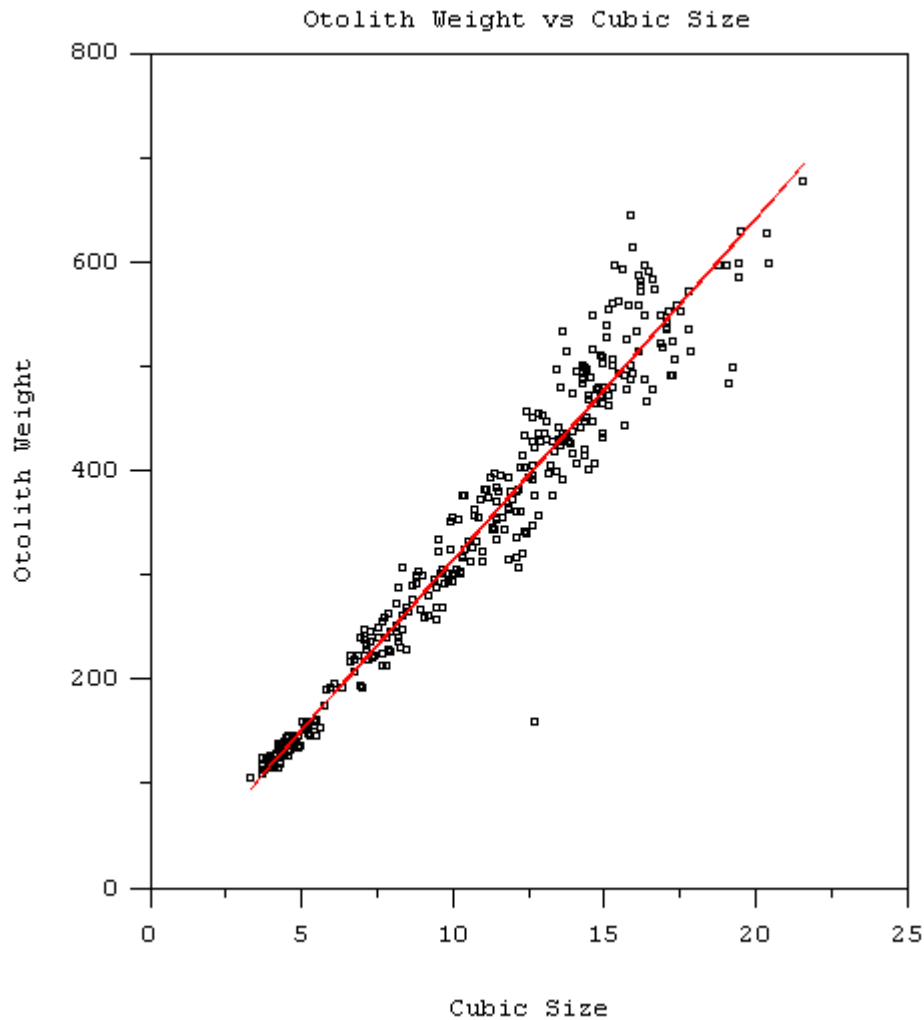


**Figure 5.97:** Well defined correlation between cubed otolith size factor and otolith weight. From this diagram one can conclude that the otolith growth (in 3D) is related to a constant accretion (in 1-D).

We wanted to inspect all sample data to find out hints to the most prospective statistical model for the fish age. We have indeed pin-pointed few highly significant sample features that have the highest propensity for use in an ageing model. One question was still to be answered. It concerns the nature of the statistical model. A quite general approach are Generalised Additive Models (GAM), which are a kind of extension of linear regression models. For specific reasons, which would take too long to be explained here, we did not use GAM modelling. Instead of this we applied Tree-Based Modelling, which is also featured by S-Plus.

In S-Plus the strategy to find optimal statistical models based on decision trees basically has two flavours. After the initial tree model has been build, one tree-pruning approach aims at optimising the number of correct predictions and another approach is based on optimising internal deviance. Furthermore pruning can be carried out guided by the cost-complexity criterion or simply by stating the wanted number of final classes. Instead of pruning a tree, the initial tree could be

shortened by using the tree-shrink tools of S-Plus. Summaries can be obtained for every model and thus it is possible to select the most favourable tree-model.

In the following, we will see that the factorial coordinates obtained from IMAGIC-5MSA do indeed represent the most significant factors. The initial model considered is of the form  $\text{Age} \sim F1 + F2 + F3 + F4 + F5$ , where F1 to F5 are the factorial coordinates.

A plot of the classification tree can be generated, however, the labelling is a little queer, so we leave the figure out here. The tree indicates that factor F2 is the most important, followed by factor F3, and so on, as expected.

The tree-based model is not very clear from the mature tree. The two techniques to streamline the model are pruning and shrinking. The results of pruning the tree into four target classes are shown below:

- Classification tree with 4 terminal nodes.
- Variables actually used in tree construction "F2".
- Residual mean deviance:  $1.855 = 647.2 / 349$ .
- Misclassification error rate:  $0.4278 = 151 / 353$ .

This result means that factor F2 is sufficient to split our ensemble into four age-groups. The misclassification error rate is about 42%. This value has to be compared to the error rate of the mature tree of  $0.2011 = 71 / 353$ , i.e. only 20%. We learn that we have to accept a trade off between low misclassification rate and complexity of the tree model.

Shrinking is another way of reducing the initial complexity of the classification tree. It is not so easily understood as pruning, since there is the somewhat obscure complexity fraction number k. Basically it was chosen so as to obtain an effective number of classes of 4. From the full text printout one finds a misclassification rate of  $0.4278 = 151 / 353$ , i.e. about the same reliability as obtained with tree-pruning. A plot of the labelled tree was generated and showed that again factor F2 is sufficient to split the dataset into the four age-groups.

The previous paragraph was mainly intended to make you familiar with tree-based modelling. The next chapter summarises results of the many explorations performed on the cod otolith dataset.

One remaining questions is of course: Which model has the highest reliability in age-prediction? In the starting model one might include all available factors. The formula for model "super" over the full data frame and its constructor are given below:

```
Super = tree(Age ~ F1 + F2 + F3 + F4 + F5 + Size + Weight +  
FishWeight + FishLen + ContLen + Area + MaxDist +  
PerpDist + Apex1 + Apex2 + Angle)
```

Variables actually used in tree construction:

```
[1] "Weight"      "FishLen"     "PerpDist"    "Angle"  
[5] "FishWeight" "F5"         "F4"         "MaxDist"  
[9] "F2"
```

Number of terminal nodes: 20  
 Residual mean deviance: 0.2217 = 73.83 / 333  
 Misclassification error rate: 0.05382 = 19 / 353

This is an extremely nice result, since it means that by selecting 9 of 16 factors we can build a model that gives roughly 95% correct age predictions!

But wait! Before drawing any final conclusions, we must compare this tree-model with other possible models. So let us have a look at the most powerful single-predictor model. Formula and summary are shown below:

Single = tree(Age ~ Weight)

Number of terminal nodes: 33  
 Residual mean deviance: 0.5151 = 164.8 / 320  
 Misclassification error rate: 0.1275 = 45 / 353

We calculate that the classification scores just dropped from 95 to 87%. In absolute numbers of misclassifications it means we had just 19 for the best model and 45 for the much more complex model! The question that comes up here is, if the difference of 26 cases justifies a much more complex model?

Tab. 5.37 summarises all results for pruning the simplest and other increasingly more complex tree-models.

Initial Model	Final Formula	Terminal Nodes	Misclassification Rate
Super	Age~Weight+FishLen+PerpDist+ Angle+FishWeight+F5+F4+ MaxDist+F2	20 (unrestricted)	0.05382 = 19 / 353
Super	Age~Weight+FishLen+PerpDist+ Angle+MaxDist+F4	12	0.05949 = 21 / 353
Super	Age~Weight+FishLen+PerpDist+A ngle+MaxDist	8	0.08499 = 30 / 353
Super	Age~Weight+FishLen	4	0.1275 = 45 / 353
Single	Age~Weight	33 (unrestricted)	0.1275 = 45 / 353
Single	Age~Weight	11	0.1275 = 45 / 353
Single	Age~Weight	4	0.136 = 48 / 353

**Table 5.37:** Comparison of several tree-based ageing models for the cod Faroe Plateau Pencege dataset. Note that the most complex model makes 95% correct predictions, while simple models based on the otolith weight can only give scores up to 87%.

At the level of dividing the dataset into four age-groups, the simplest as well as the most complex models yield about the same error rate. When we allow the number of terminal nodes to increase to 20, the "super" model is however the more effective. It appears as if basically four groups can be distinguished but for best results we need some more groups where we can put the "outliers". In the following, the simplest model, based on Otolith Weight, will be highlighted in more detail.

The simplest model with respect to structural complexity and effectivity is Age ~ Otolith Weight. The following plot shows the labelled tree-model and the predictor decisions.

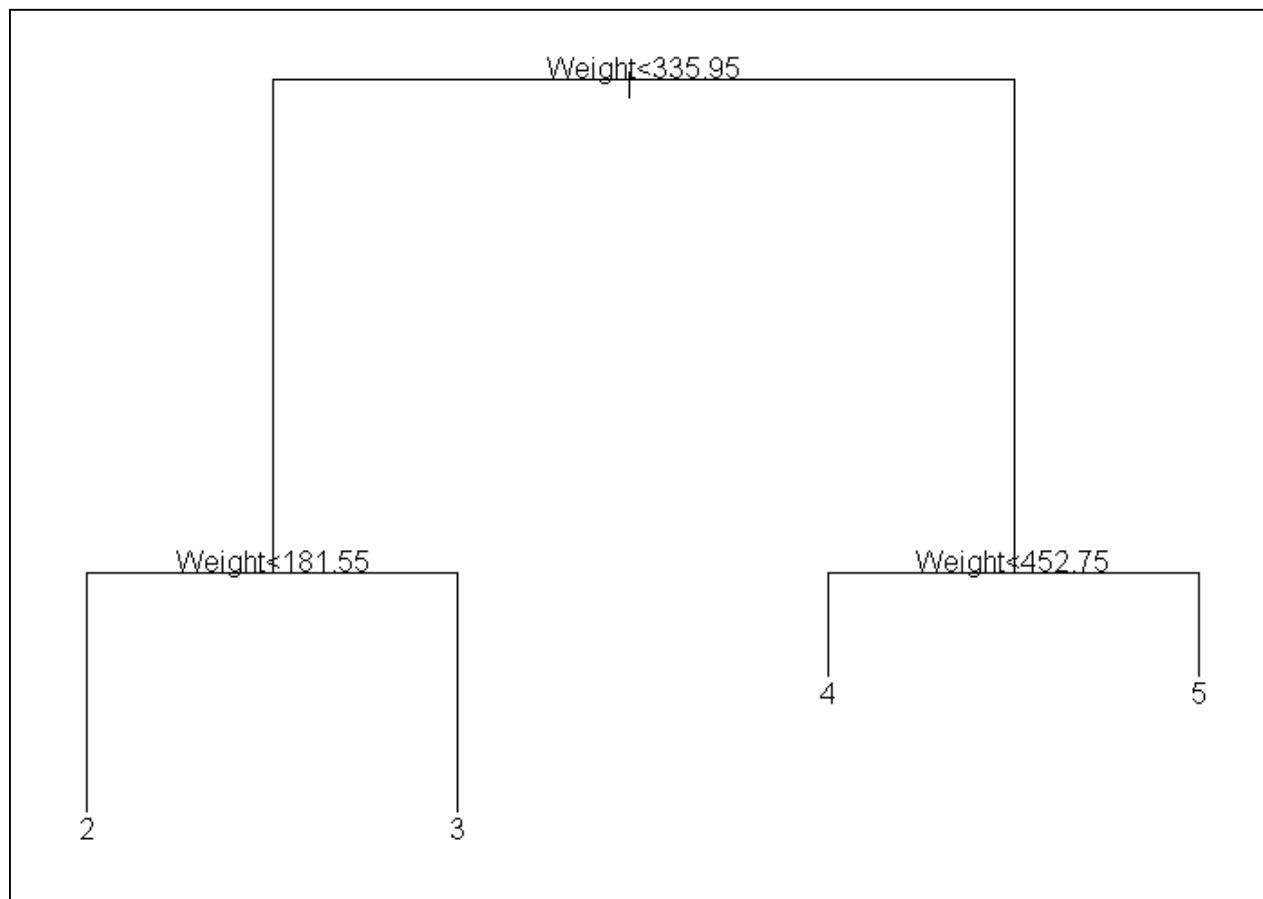


**Figure 5.98:** Graphical representation of the decision tree based on otolith weight alone. Numbers indicate the age group, while otolith weight is given in milligrams.

In Fig. 5.99, essentially the same decision tree is shown, however, the individual sample values are indicated.

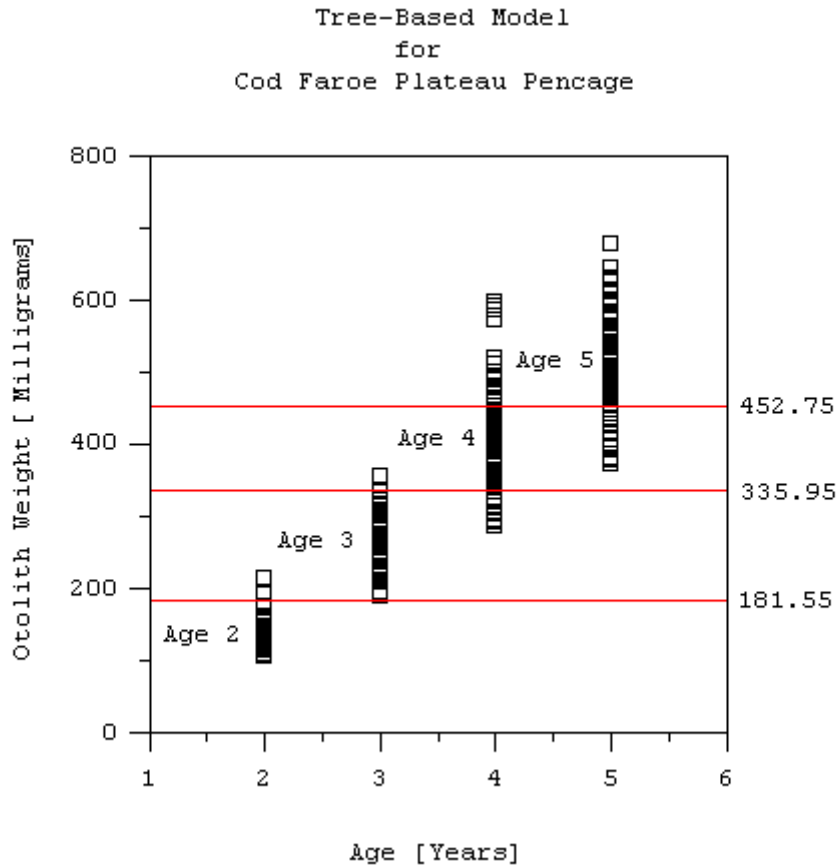


**Figure 5.99:** The decision levels for the otolith weight are marked by red lines. Individual sample data are indicated by black boxes.

One can compare the result presented here with the box plots shown in an earlier paragraph. It was already obvious from the box plot of Otolith Weight over Age that this variable has the highest propensity in Age prediction! Now we have verified this result using a tree-based classification approach.

We can summarise and give the following conclusions:

- S-PLUS proved to be an appropriate instrument for statistical evaluations.
- Simple box plots of parameters over age were extremely instructive.
- Single peaked parameter distributions can be assumed for all parameters.
- In our special case, GAM models cannot be used, however, tree-based models are adequate.
- Tree-based models suggest that, out of the five considered shape features, factorial coordinates F2 has the highest importance for age predictions.
- The most-complex tree-based ageing model is composed of nine variables and yields optimally about 95% correct classifications.
- The simplest statistical model is based on otolith weight only and gives scores of up to 87% correct classifications.

### 5.3. 3D Methodology and 3D Shape Analysis of Otoliths

By shape one usually refers to 2D shapes. However, for fish ageing it is clear that in connection with the otolith growth we have to consider the 3D shape because:

- both, the outer shape as well as the inner structure of an otolith change
- otoliths are often not flat and therefore show pronounced 3D curvatures
- otolith weight is related to the 3D volume
- 2D sections and the silhouette are related to the 3D bulk
- the 3D shape analysis of an intact otolith does not require any sample preparations

#### *X-ray tomography*

One of the methods to obtain 3D data for the relatively small otoliths under consideration is x-ray micro-tomography. Using this method we wanted to obtain the outer shape as well as a precise image of the inner structure, also called density (Hamrin et al., 1999). In the following we report about approaches to elucidate the inner structure within an intact otolith. Thereafter, we describe the database of 3D otolith shapes for anchovy, cod, eel, and turbot (Kastowsky et al., 2002d). Finally, we will present results showing how good the 2D shape can be obtained from the 3D shape.

The microtomograph uses a microscopically fine x-ray cone beam to shine through a massive body, while a detector registers the intensity. Of course one intensity value describes partial volume features only. Therefore, the body under investigation is probed systematically in many different directions and, hence, the name micro-tomography.

The actual measurements were all made with a standard desktop X-ray microtomograph (Skyscan 1072, Belgium). A full description of this instrument was reported previously (Sasov and van Dyck, 1998). Polychromatic X-rays with peak energy of 80 kV were generated by a microfocus X-ray air-cooled tube (Tungsten anode) with a focal spot size of 8-10 microns. As a detector a (1024\*1024) 12 bit low-noise CCD camera was used. Detector noise was several orders less than statistical photon noise. The camera had 25 micron pixel size on the silicon matrix that was reduced two times by fibre-optic coupling, covered with a 30 micron thick scintillator. For the device described average resolution is 10 microns. Scanning conditions were optimised in order to reduce the noise on the virtual slices. When necessary an aluminium filter was used for small otoliths; scanning time was adapted correspondingly, rotation step was 0.90°, magnification was adapted to the size of the object. The resolution obtained depends on the size of the otolith to be scanned. For scanning, otoliths were mounted vertically on the rotating stage in the microtomograph. For reconstruction of the cross-sections the software of the microtomograph was used.

X-ray micro-tomography is a non-destructive technique, resulting in virtual slices through an otolith without having to cut the sample. From consecutive cross-sections, 3D models can easily be reconstructed.

It should be pointed out that the reconstruction of the otolith internal density is very sensitive and therefore it was hoped to resolve the internal structures known as annual rings. In this respect it is

important to understand that with x-ray beams one probes the local electron density within the material. Since, however, an otolith is composed of the same material, i.e. biomineralised calcium carbonate, the resolution was expected to be low. In Fig. 5.100 a typical otolith x-ray micro-tomographical cross-section is shown.



**Figure 5.100:** A typical example of an x-ray micro-tomographical cross-section through a cod otolith (565tur0050424). There are no clear indications on an internal density variation within the otolith.

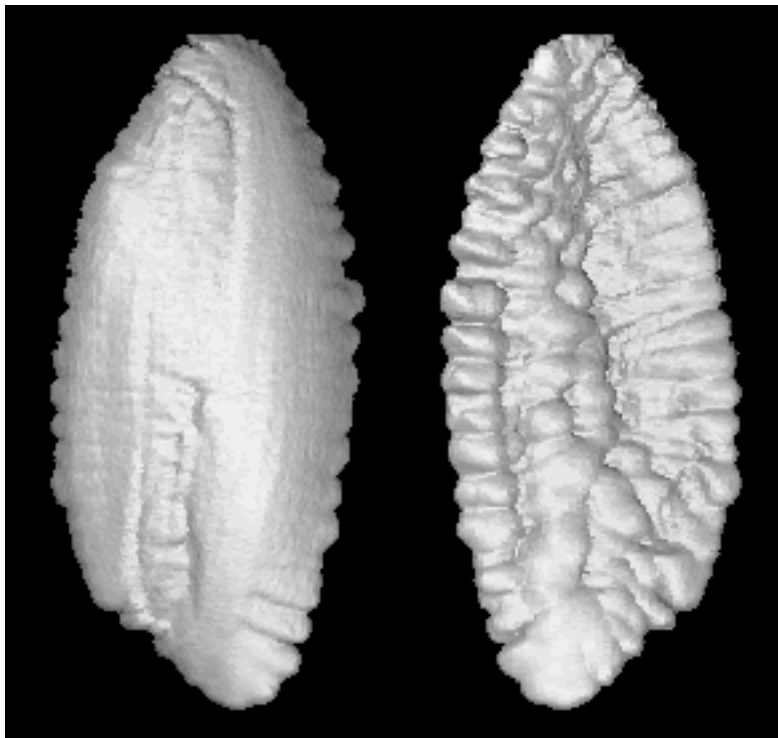


**Figure 5.101:** Surface representations from the x-ray density model data.

The complete absence of any internal structure within the otolith prompted us to try a variety of enhancements:

- investigations of otolith from different species with pronounced annual rings
- prolonged exposure to the x-ray beam in order to diminish noise
- analysis of thin sections for better contrasting
- treatment of otoliths in ionic solution for introduction of atomic labels
- contrast variations using different organic solvents

Neither of these trials was successful.

Even though X-ray tomography couldn't reveal the otolith internal structure, the method worked well for the probing of the outer structure, even for the smallest otoliths from anchovy. Since the tomographic scans are performed in an automated fashion, there is no alignment problem. This offers one great opportunity: it is possible to first obtain the outer 3D otolith shape and then cut it or grind it down to unveil the internal structure with other more appropriate methods. When care is taken that the analysed cross-sections can be identified within the previously established outer shape, one may be able to reconstruct a model for the otolith interior. This will be discussed in the next paragraph.

#### *Combination of X-ray tomography and light microscopy*

Since all the different attempts did not reveal the otolith inner structure. Therefore, we decided to apply a combination of light-microscopy and x-ray microtomography to gain insight into the interior of an otolith. Basically, a specimen is embedded into an x-ray transparent plastic material. The otolith is then subjected to x-ray scanning, which gives the outer shape of the object with high precision. Then, the plastic block with the otolith is milled down in small steps. At every step, a light-microscopic image is taken. The outer shape of the otolith defines a frame into which the light-microscopic densities are modeled, thus giving the complete inner otolith 3D structure.

The name of the selected cod specimen is '565tur005'. This name was assigned by the fishery department from which the sample originates and was for sake of back referencing taken over only slightly changed. It is an otolith from a 2 year old fish as established by conventional estimation.

This Western-Baltic cod sagitta otolith was casted in a two component epoxy resin. The sample was then first sent for a non-destructive X-ray scanning of the otolith embedded within the mold. The right sagitta otolith of the cod sample was identified as a well conducted X-ray scanning sample. The otolith preparation was therefore mounted in a Buhler diamond wafer sawing machine and cut and further polished at 73 successive planes transverse to the longitudinal axis from the post rostrum end towards the rostrum end as shown in Fig. 5.102 below.

**Cod Otolith Tur 565 #005 MZ6 0.5x1.0x1.0**

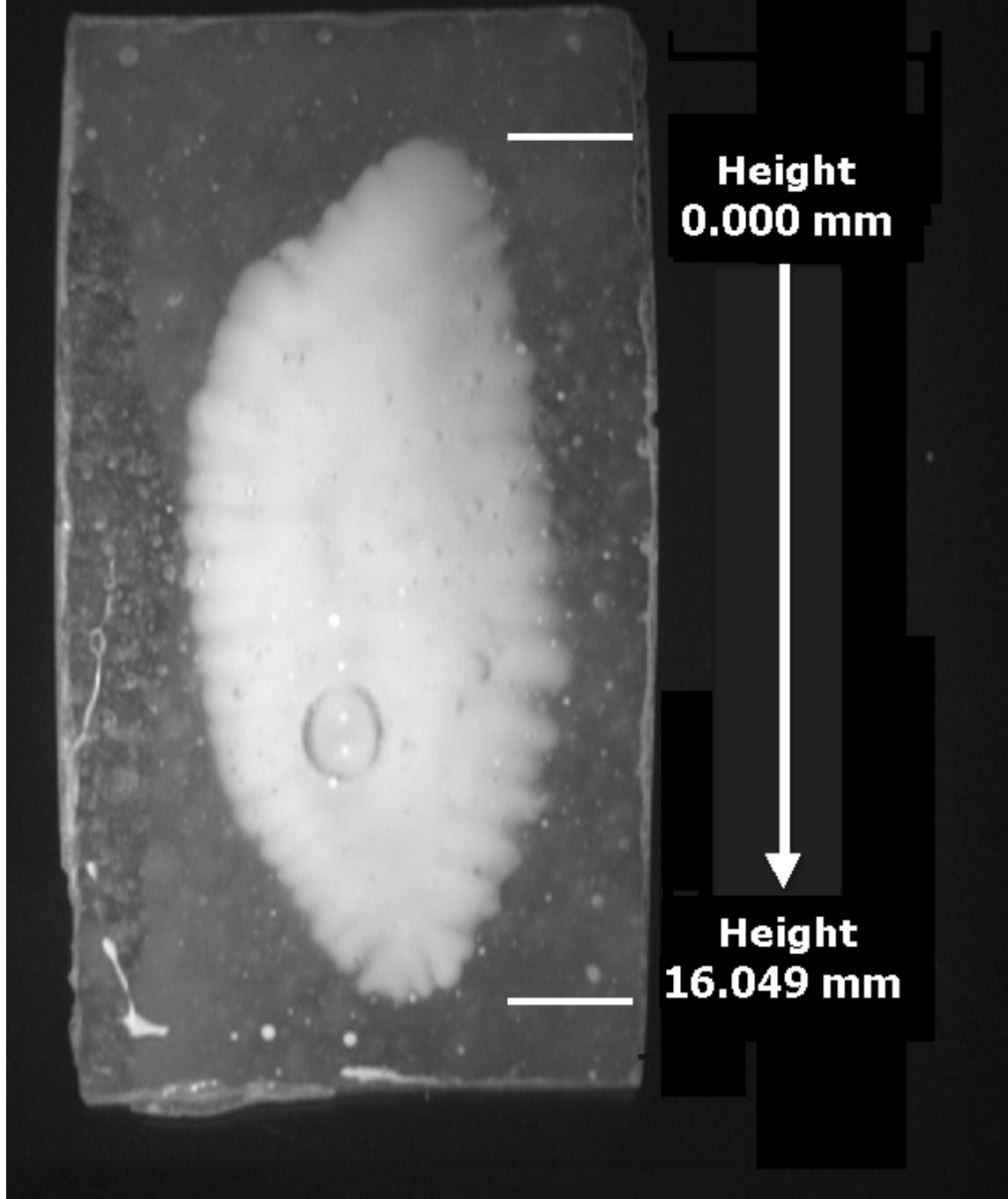


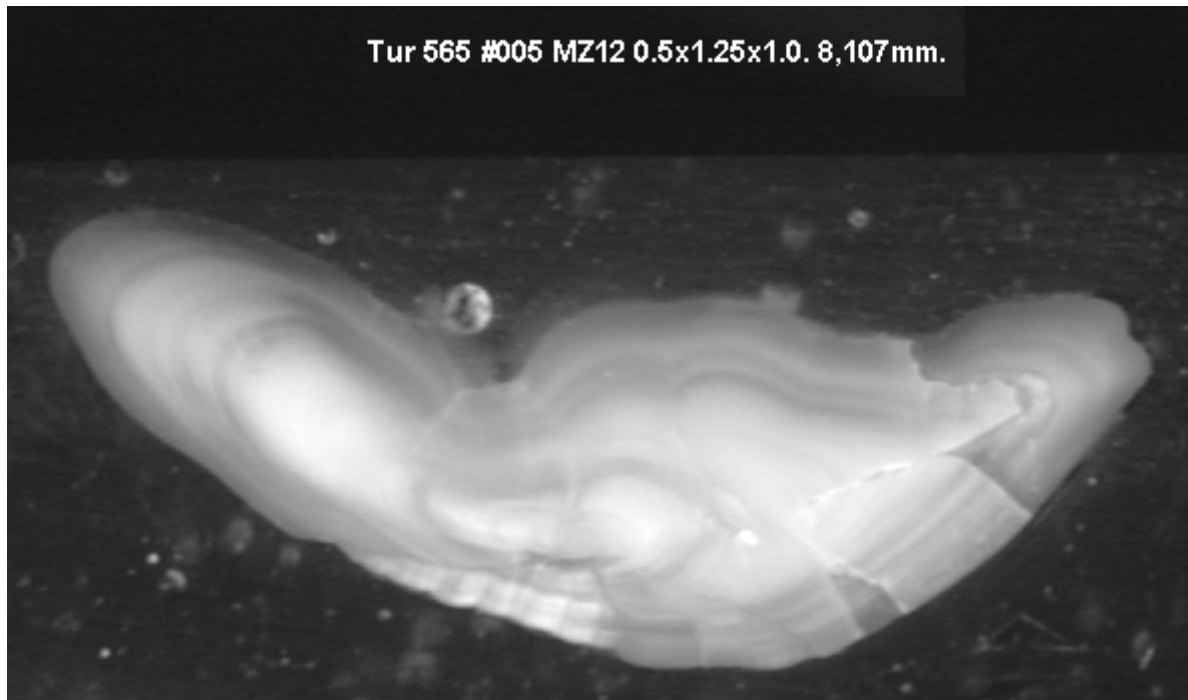
**Figure 5.102:** A cod otolith embedded in epoxy resin. Milling through the otolith started at zero height. A total of 73 light-microscopical cross-sections were imaged in reflected light. Note that we look at the concave otolith and side the sulcus side is the hidden backside.

At each sectioning plane the otolith was transferred to a high resolution dissection microscope where a black and white image of the sectioned surface was produced using reflected light, combined with a watering of the surface to increase visibility of the internal otolith structures. The preparation was manually aligned using the right-angled section of the mold.

Each section image is named with the distance in microns from the 0 level. Each image is furthermore annotated with a specimen identification, the depth in millimeters, as well as the magnification setting of the microscope, although all images were produced with the same magnification (0,5x1,25x1,0).

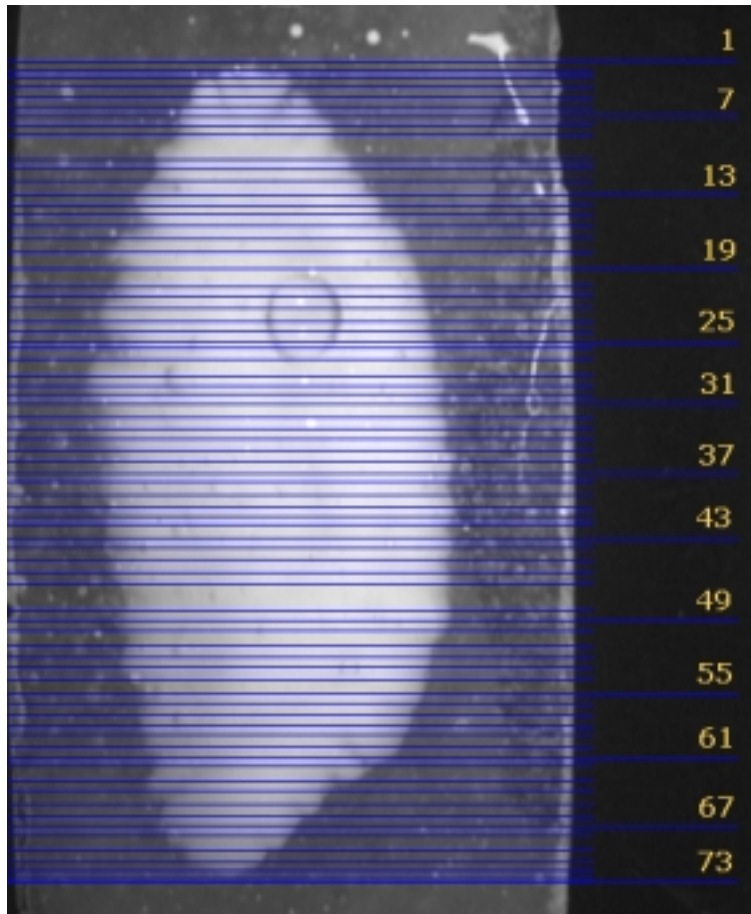
The first section surface #0 shows a tiny white spot only a few microns down into the otolith, the rest of the white otolith shadow lies below the surface. For many of the sections in the first half of the otolith, shadows of deeper positioned otolith lobes may be seen through the semi-transparent epoxy mold.

In the light-microscopic images, annual rings are clearly visible. However, there are also a number of artefacts, like cracks and halos shining through from deeper otolith layers. An example cross-section image is shown below.



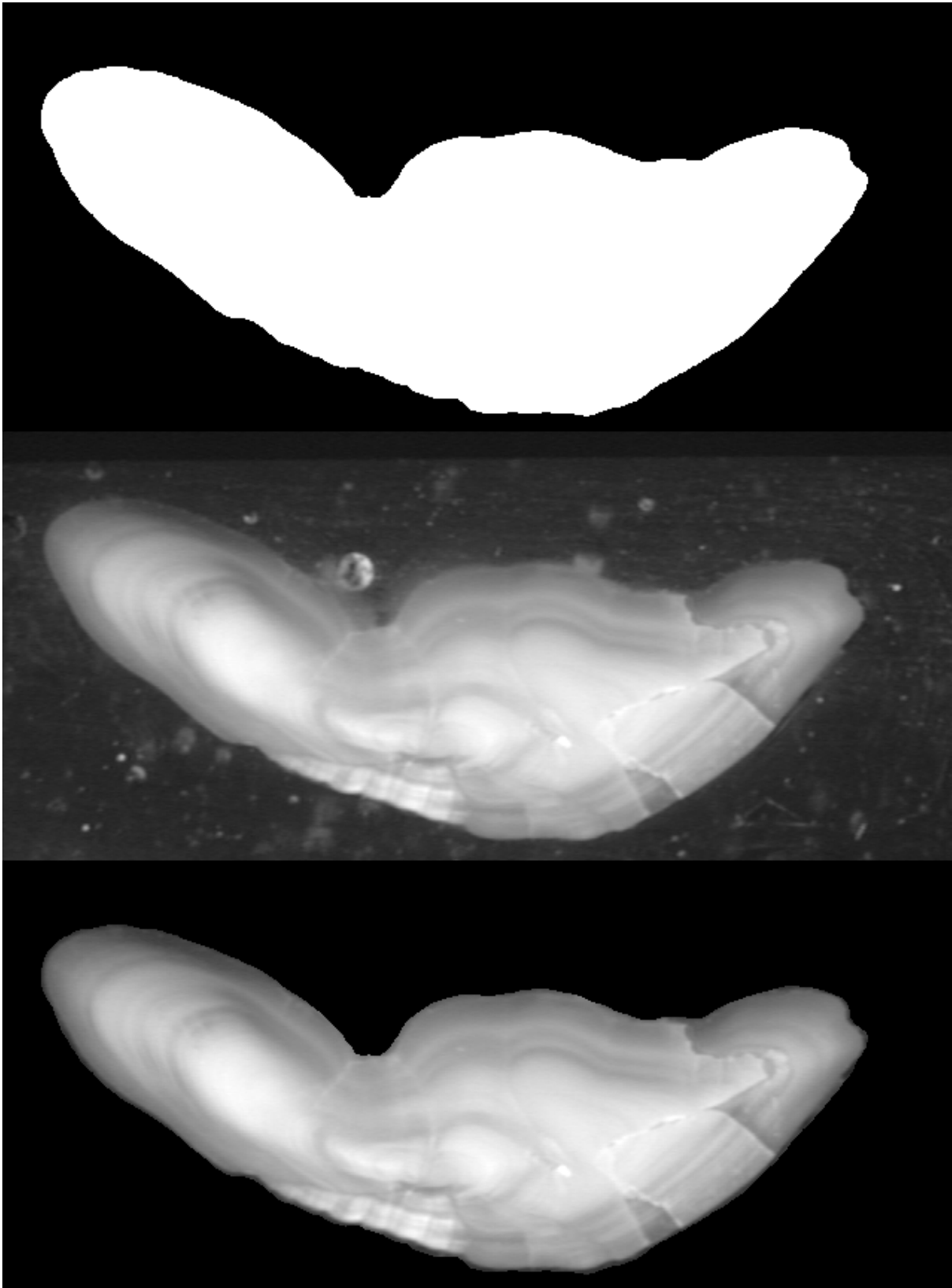
**Figure 5.103:** The light-microscopic cross-section through a cod otolith at height 8.107mm. Note the bubbles enclosed in the resin as well as some cracked zones at the right side. Besides this, inner ring structures are clearly visible. The otolith named 'oto565tur005' comes from a 2 year old cod.

Fig. 5.104 shows where the light-microscopic cross-sections are located within the 3D volume obtained from the x-ray scans.



**Figure 5.104:** Locations of the light-microscopic cross-sections.

The x-ray density model can be used to mask the light-microscopic cross-sections, which often contain quite annoying artefacts. Fig. 5.105 demonstrates how effective the masking can be.



**Figure 5.105:** A mask can be derived from the x-ray model and be used to eliminate artefacts in the epoxy resin outside the otolith cross-section.

While the image processing can all be done using established procedures, the alignment of the two models was found to be relatively difficult because it is hard to find a suitable way of defining a reference frame for the x-ray scans with respect to the light-microscopic images. In fact, we have tried some unsuccessful approaches, which are not reported here. The following list summarizes critical aspects:

- there are different number of cross-sections from x-ray scanning and light-microscopy
- cross-sections are at different height
- successive light-microscopic images have small but unacceptable random shifts
- the apparent illumination is different for different cross-sections
- deeper layers shine through the clear epoxy resin

In conclusion we can say that in reflected light, the otolith interior can be elucidated by successively grinding down thin layers. When these layers are arranged into a surface model from the x-ray tomography, a number of attractive possibilities become feasible. For example, an experienced otolith reader may mark corresponding zones within the otolith. One can then manually eliminate the respective otolith parts in the cross-section images and thereby create a model for the otolith at an earlier time. Thus, it would eventually be possible to construct a series of models for a number of states of growth.

### *Rapid Prototyping*

While the elucidation of the otolith inner structure is an important task in the project, it was thought to be important as well to have large-scale plastic models for selected otolith from each species. Of course we limited ourselves to the species that were also dealt with in the 2D methodology.

Initial attempts to create plastic models using a 3D plotter equipment were unexpectedly cumbersome, since own software had to be developed. Before 3D model surfaces could be built, a support structure had to be constructed onto which the surface layers could be deposited. One very large plastic model of a cod otolith was made and presented at a project planning meeting.



**Figure 5.106:** An image of the large-scale plastic model as fabricated by use of a 3D plotter.

However, later, when it became clear, how many different models were requested, a simpler approach needed to be established and we decided to have the prototypes made by a company specialised in that field. The costs were estimated to be lower than using the 3D plotter approach

but clearly higher than moulding and casting. However, it seemed inappropriate to go for the small series strategy with only a maximum of two copies for a given otolith.

### *Plastic replicas*

When the 3D model construction technique was established for production, one further step was tested, i.e. the small series production of plastic models. This strategy is based on casting and molding of large-scale otolith models. One could thus drastically lower by an order of magnitude the high cost of building each model individually. In the following we demonstrate that by using silicone rubber to cast the rapid prototyping model and then using Alumilite plastic (Alumilite Corp, MI, USA) to create molds, we are able to create replicas that are virtually identical to the rapid prototyping model.

The cast is made from cold curing silicone rubber and consists of two halves. It is helpful to embed the model in modeling clay (note that non-synthetic clays containing sulfur may inhibit the curing of the rubber! ) so that approximately half of it is clear off the clay. Next, a box is built around the modeling clay. Use a small ball, e.g. a mouse ball, to make impressions in the four corners of the modeling clay surrounding the model. These impressions will help fit the two halves of the cast together when molding. Add silicone and catalyst to the box so that the highest point of the model is covered by at least 1cm mixture, and let the rubber cure for 24 hours. Remove the modeling clay from the model, but make sure that the model stays in the rubber cast. Apply rubber-to-rubber release on the exposed parts of the rubber cast that will be covered by the other half of the cast and build the other half as described above. Use a knife to carve a hole in the cast for pouring in the Alumilite.



**Figure 5.107:** This image shows the two halves of the latex cast. An opening has been carved at the top sides of the two halves for pouring in the Alumilite. Half-spherical protrusions are visible at the four corners of the left cast, with corresponding impressions on the right cast - these are used for aligning the halves to one another and locking them into position.

Mix the two components of Alumilite in equal

proportions and pour quickly into the cast. As the mix begins to set, the color changes from brown to cream. Wait at least 15 minutes before opening the cast and extracting the replica. Results are shown in Fig. 5.108.



**Figure 5.108:** The original prototype (left) and the replica (right) are shown. The colors are due to the colored synthetic clay and other effects. After removal of the cast-hole parts, finishing the final model is advised.

We have proven that silicone rubber can be used for making very accurate casts of rapid prototyping otolith models. In fact, the replica is so accurate that some digitization artefacts of the electronic 3D model (quarter mil steps) are reproduced in the cast! According to the manufacturer, the cast can be used for creating at least 30 molds and although we did not try molding this quantity of otolith models, there was no visible wear of the cast after the three otolith molds that were produced. We found working with Alumilite rather tricky at first due to the short setting time. Careful preparation and a few tries were required to work out how to mix and pour the Alumilite. Once these details had been worked out, replicas could be produced in a standard and reproducible manner. No loss of visible detail was observable between the rapid prototyping model and the replica.

We estimate that the cost of casting and molding replicas is of an order of magnitude lower than building rapid prototyping models from scratch. Casting on the other hand is easy since, no special tools are required. Another advantage is that it is possible to add dyes to the Alumilite

component solutions in order to produce colored replicas. Further savings in material costs and model weight can be obtained by mixing the Alumilite solutions with micro-balloons. In summary, we have demonstrated that casting and molding can be used for overcoming the problem of high-costs associated with the use of the rapid prototyping model to build multiple copies of large otolith models.

### *3D Database*

The next steps involved the selection of appropriate samples from the so far established 3D shape database (Kastowsky et al., 2002d). For this purpose, a quality check was made and several problems were encountered.

The raw data files are cross-sections evaluated from x-ray cone-beam microtomographic scans. Due to the specific method of back-calculation of the density distribution from intensity data, there are very typical zonal artefacts. Some small concentric density modulations are present in all cross-section images but are mostly of no concern. Other, more detrimental artefacts are shown in Fig. 5.109.

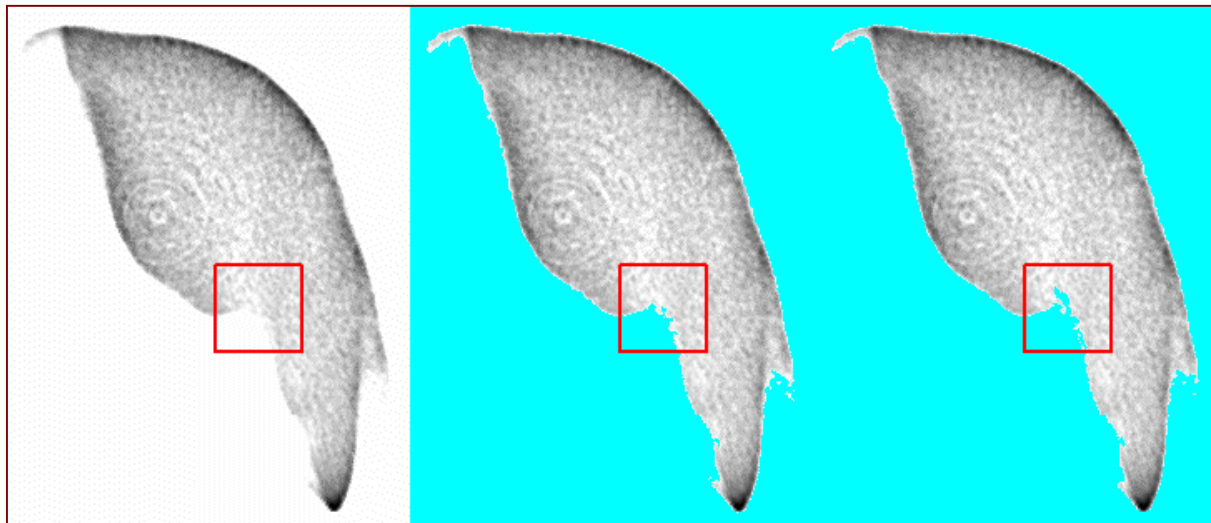


**Figure 5.109:** Due to the low contrast, a surface view for such an otolith would either show a rough surface or even have holes.

The contrast in the marked region is poor. When the background color is changed to light-blue with different tolerances, this becomes obvious. Note that the above example is not the worst case. For proper 3D-density processings, limitations by the low contrast must be kept in mind. One way to cope with the problems is coarsening and blurring, followed by masking and imposing of the initial densities into the masked regions.

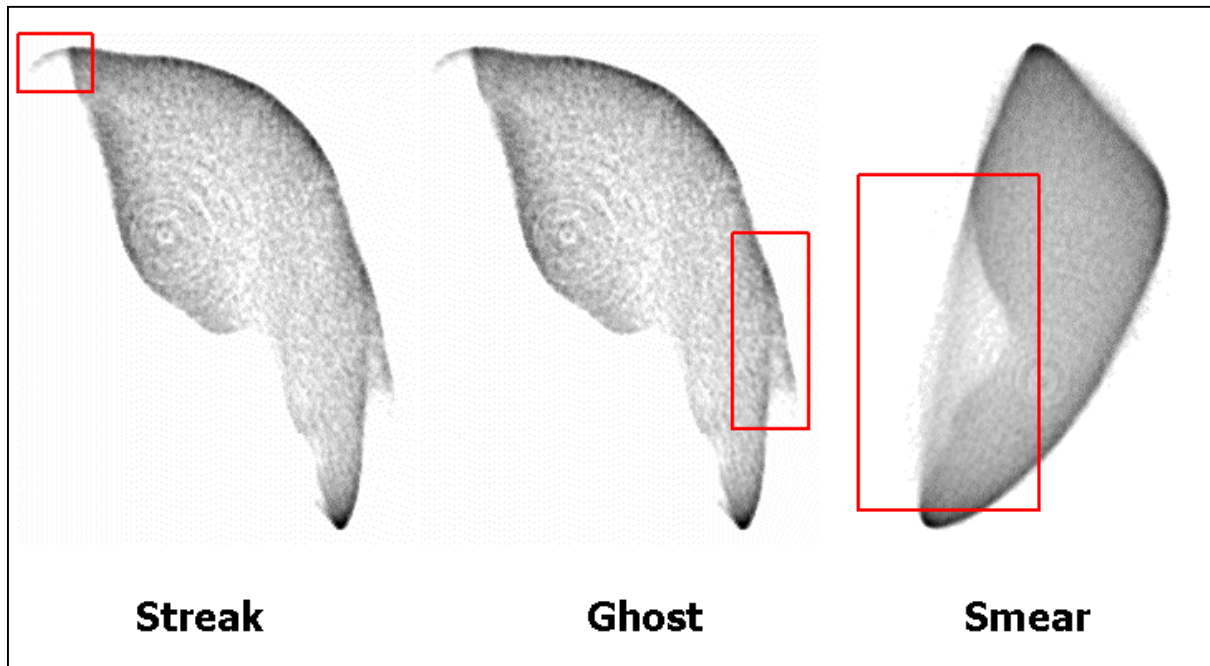


**Figure 5.109:** The indicated density artefacts are sometimes so heavy (middle) that the otolith shape cannot even be recognised by a human observer. The streaks shown to the left can usually be eliminated by choosing a proper grey-value threshold, however, the smear seen in the right image may pose severe problems, even if a human observer cannot be fooled about where the surface borderline runs.

The densities obtained from the x-ray tomographic scans are not the original raw data but are constructed from the cone-beam intensity data. The so-called Radon transform is used to reconstruct the densities from Radon space into the 2D or 3D space. Thus, the observed artefacts could originate from flaws in these procedures. Anyway, the density reconstruction artefacts are severe and are always present to different degrees in all cross-section images. Streaks can easily be identified, whereas ghosts are somewhat harder to recognize. Ghosts seem to suggest an alternative borderline farther outside the object. Such artefacts cannot be repaired automatically, since local density variations are too small. A human observer might be able to apply manual corrections. However, this is no real practical option, since there are usually several hundreds of cross-sections per 3D volume so that the manual work requirement is unacceptably high. The third kind of artefact is a density smear filling concave indentations of an object. In the above example, this smear lowers the contrast. It is mostly possible to define a proper threshold for the object-to-background discrimination so that the smear artefact is not too critical.

Name	Contrast	Smear	Streaks	Ghosts	QC
Age 2 oto 916 left	Low	Low	Many	Many	Reject
Age 2 oto 916 right	High	High	Many	Many	
Age 3 oto 1401 left	High	High	No	No	
Age 3 oto 1401 right	High	High	No	No	
Age 4 oto 32843 left	High	High	No	No	
Age 4 oto 32843 right	Medium	High	No	No	Reject
Age 5 oto 32365 left	Medium	High	No	No	Reject

Age 5 oto 32365 right	High	High	Few	No	
F-LAB74201	Medium	Low	Few	No	Reject
Oto 565 tur 003	High	Medium	Few	No	Reject
Oto 565 tur 005	High	Low	No	No	Pass
Oto 565 tur 006	High	Low	No	No	Pass
Oto 607 tur 003	High	Low	No	No	Pass
Oto 607 tur 006	High	Medium	No	No	
Oto 607 tur 010	High	Low	No	No	Reject
Oto 636 tur 003	High	Low	No	No	Pass
Oto 636 tur 004	High	Low	No	No	Reject
Oto 636 tur 005	High	Medium	No	Few	
Oto 688 tur 001	Low	Medium	No	No	Reject
Oto 688 tur 002	Medium	Medium	No	No	Reject
Oto 688 tur 005	High	Low	No	No	Pass
Spag23976-1	Low	Medium	No	No	Reject
TO-LG73951	Medium	Low	No	No	Reject
TO-LG74196	Low	Low	No	No	Reject
TO-LG75705	Medium	Low	No	No	Reject
21473	High	Low	No	No	
27013	Medium	Medium	No	Many	Reject

**Table 5.38:** Summary of the quality of cross-section raw-data obtained from x-ray microtomography. Evaluations are based on visual inspection. The final quality check (QC) was passed when calculated surface models looked acceptable.

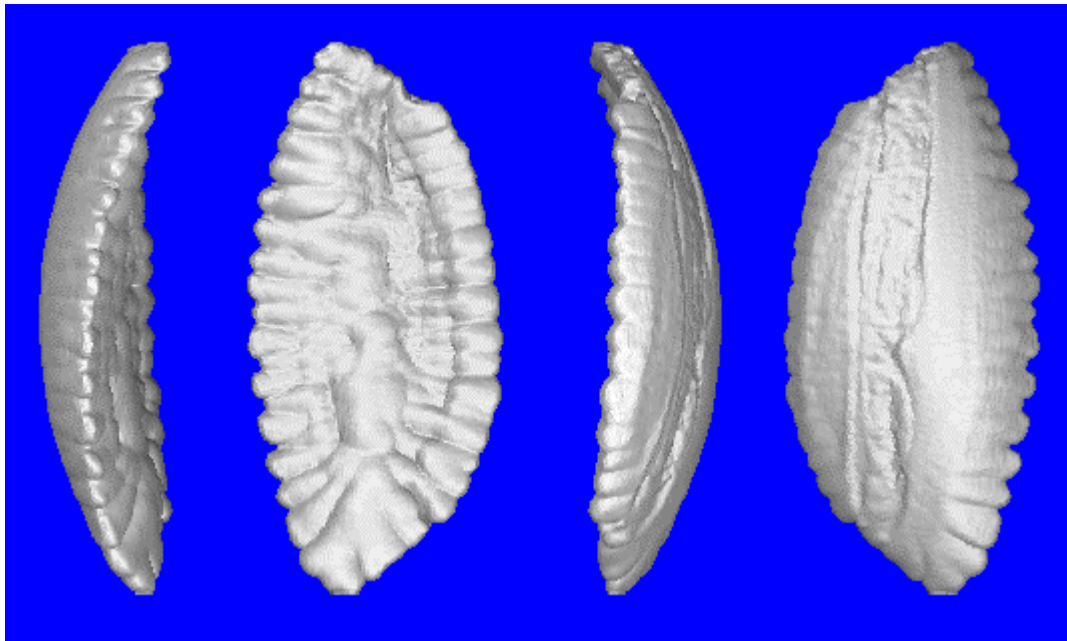


**Figure 5.110:** Optimal surface model of a cod otolith named 'Oto 607 tur 003' calculated for a greyvalue threshold of 60.

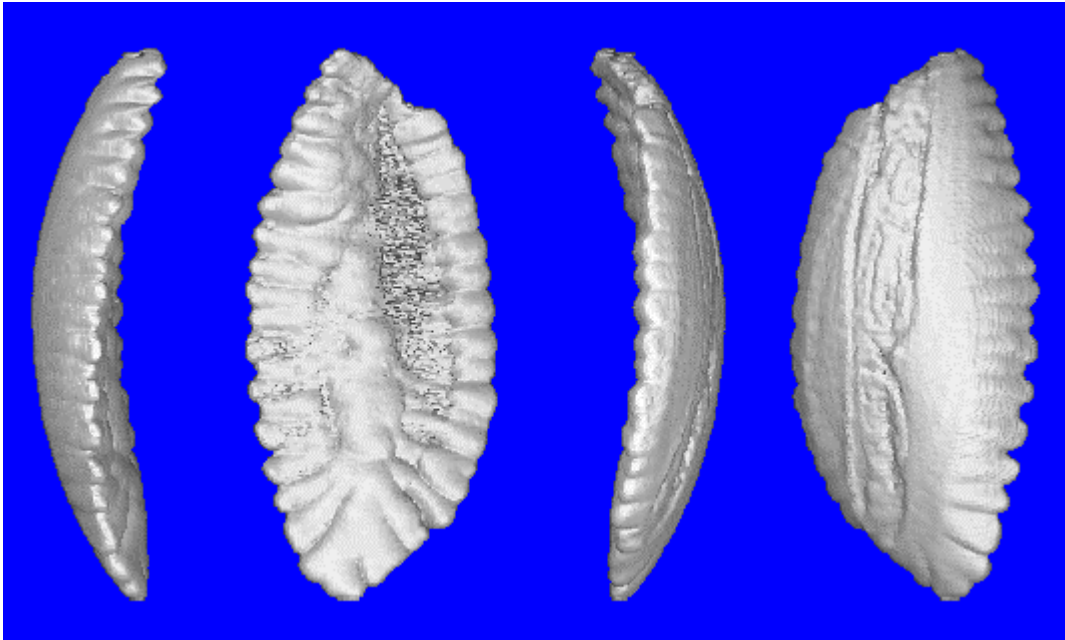


**Figure 5.111:** Surface model of a cod otolith named 'Oto 607 tur 003' calculated for a too high greyvalue threshold of 100. Note the appearance of artefacts (rough surface) clearly visible in the second image from the left.

As shown in the previous table, most of the cross-sections images contain some kind of density reconstruction problem. The critical evaluation left five specimen for which high-quality surface reconstructions were achieved. As can be seen in the previous figures, it is possible to determine an optimal thresholding value so that contrast problems can be minimised. The following table summarizes the best x-ray scanning datasets.

Name	Species	Age	Body Side
oto 565 tur 005	cod	2	right
oto 565 tur 006	cod	2	right
oto 607 tur 003	cod	3	right
oto 636 tur 003	cod	2	left
oto 688 tur 005	cod	2	left

**Table 5.39:** Summary for the five best x-ray microtomographic scans

Based on these results, it was suggested to build plastic models for the five best specimens only. However, several objections were made so that finally a decision was made to repeat some of the x-ray micro-tomographical scans. The repeated x-ray scans were performed such that to our best knowledge optimum conditions were chosen. In fact, the results indicate that we improved the raw data quality significantly. All samples were suitable for subsequent large-scale model building. The following table lists all final model datasets that were used for rapid prototyping.

Species	Age (young)	Age (middle)	Age (old)	Total	Comments
Cod	2 years	3 & 4 years	5 years	4	Faroe Plateau Pencage
Eel	8 years	13 years (pair)	19 years	4	Lake Frisksjön
Turbot	400 days	538 days	739 days	3	Ventral otoliths
Anchovy	0 years	1 year	4 years	3	Ancona

**Table 5.40:** Summary of all model datasets used for rapid prototyping.

Fig. 5.112 shows all large-scale otolith plastic models fabricated.



**Figure 5.112:** Large-scale plastic models of turbot, anchovy, cod and eel otoliths (from left to right). Note that the ruler shown in the upper left is 40cm long.

In conclusion, we were able to produce extremely large plastic models. The biggest was one eel otolith with a length of roughly 25cm. These plastic models can be used to inspect the growth pattern evolving during the life of a fish. Moreover, the models are also of interest for the participating institutes with respect to instructing new otolith readers.

## 2D / 3D

The 2D/3D cross-validation is a task that uses input from the 3D database. What we wanted to know is how reliable is the 2D shape as obtained by simply placing an otolith onto a glass plate for imaging? *Anchovy* and *turbot* otoliths are oblate and therefore the expected deviations are small. In general this is also true for *eel*, even if some specimen show a high curvature. However, for *cod* the 3D shape is a generally pronounced feature. *Cod* otoliths are bend similarly to a curved hand. There is even a typical twist along the longest axis. All these features influence the 2D appearance of a *cod* otolith. Therefore, it was decided to use a *cod* specimen for the 2D/3D shape variation investigations.

Within this project, the main application of the established 3D otolith data is

- for estimating the accuracy of the 2D shape measurements
- for testing the validity of the 2D shape approach.

These two objectives both include steps to derive 2D shapes from a 3D object. This goal can be achieved by projecting the 3D density onto a 2D plane. In our case we have about constant material density inside the otolith and thus the details seen in a projection image reflect the thickness of the object along the projection line. We do not need these information but can simply use a binarised image which essentially compares to the silhouette images usually taken with our otolith workstation equipment. An example of a projection image and the corresponding 2D shape is shown in Fig. 5.113.

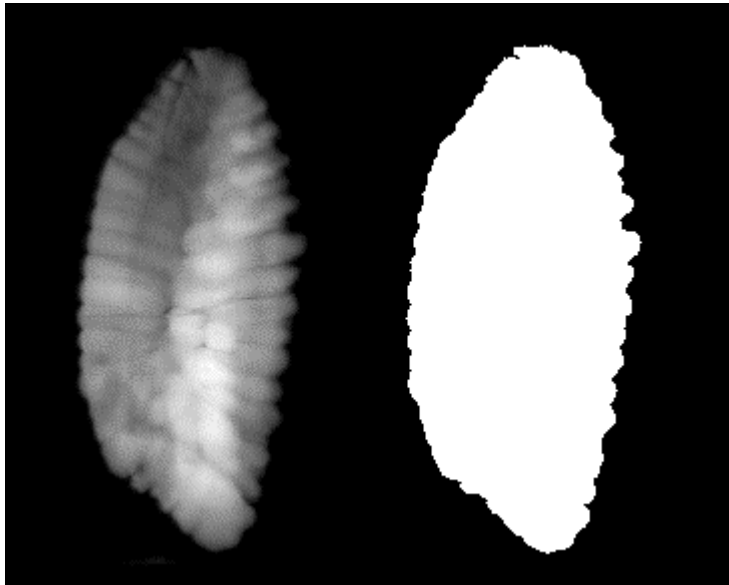


**Figure 5.113:** An example for a projection image (cod specimen named '565tur005') is shown to the left. The density variations reflect the thickness of the otolith along the projection line. The 2D silhouette shape information is obtained by thresholding the projection image against the background.

The projection of the 3D cod otolith density shown above corresponds to a typical silhouette image. We considered finding the mathematically exact projection direction, i.e. the same direction as in a practical experiment. For imaging, the placement of the otolith on a planar support is such that the otolith touches the support at three points, which gives a stable situation. It is in principle possible to find these three special support points on the 3D model surface but the computational effort is considerable. Therefore we decided not to use an exact simulation but accept arrangements that are sufficiently close to the exact placement.

The high-contrast 3D model density for cod specimen named '565tur005' was selected and used to calculate a number of 2D projections. A main projection direction was chosen such that the obtained 2D projection compares roughly to what is to be expected from imaging a real otolith, i.e. projections correspond to the broad-side of the cod otolith. The individual projection directions were randomly chosen using the following formula for Euler angles:  $\alpha = \alpha_0$ ,  $\beta = \beta_0 + \chi_\beta$ , and  $\gamma = \gamma_0 + \chi_\gamma$ , where  $\alpha_0 = 0^\circ$ ,  $\beta_0 = 90^\circ$ ,  $\gamma_0 = 160.5^\circ$  and  $\chi_\beta$  and  $\chi_\gamma$  are random angles from the interval  $[-5^\circ, +5^\circ]$ . The total number of random projections was 100. The 2D projection images were binarised and subjected to the usual input procedures as used for normal silhouette input images. The resulting Normalised Fourier Descriptors (NFDs) were used in all subsequent calculations.

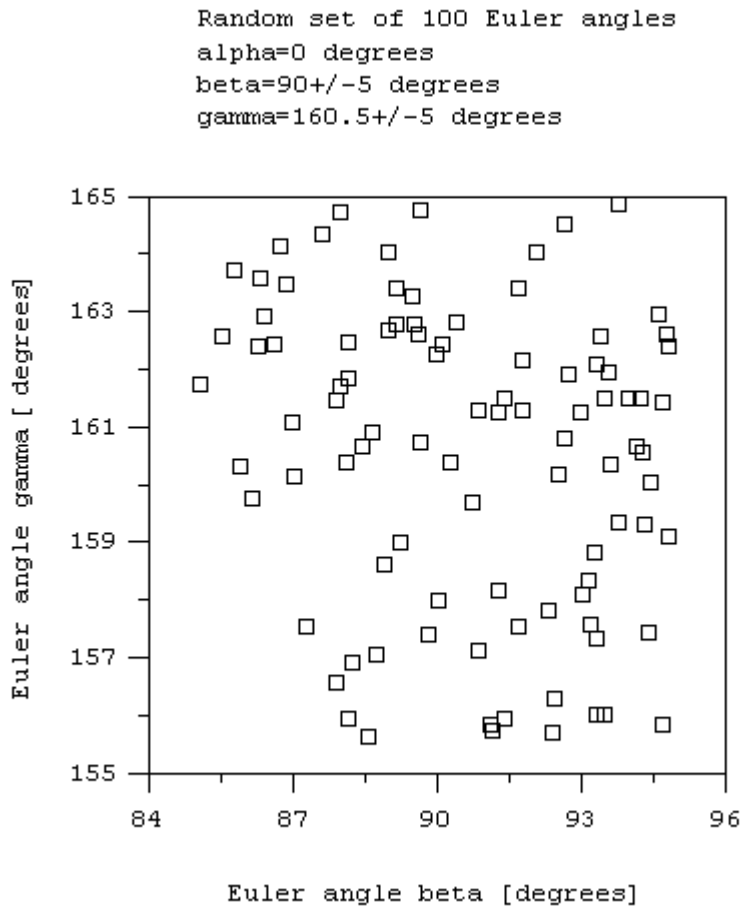


**Figure 5.114:** The Euler angles are randomly distributed. Thus, the corresponding projection images represent a random tilt series.

All mutual shape distances within the random projections set were determined. The most frequent shape distance was close to 175. This should be compared to the most frequent shape distance for a set of 785 different cod shapes, which is 638. These two values suggest that the shape variations from the differently tilted 3D object are relatively small as compared to the shape variations between different otoliths. Standard deviations are listed in Tab. 5.41.

Distribution	Number of shape distances	Average shape distance	Most frequent shape distance
All 785 cod	307720	807 ± 263	638
Nearest neighbours	785	407 ± 85	350

2D/3D variations	4950	$219 \pm 74$	175
------------------	------	--------------	-----

**Table 5.41:** Features of NFD shape distance distributions. A dataset of 785 different cod otolith shapes was arbitrarily chosen to obtain reference values for comparison. Each of the 785 members in the dataset has a nearest neighbour, i.e. a most similar shape. Nearest neighbour distances are a pessimistic (worst-case) measure for a shape distance between different shapes, while the average gives an optimistic estimate.

The comparison of the averages may give a too optimistic estimates because of the long tails of the shape distance distributions. A much more realistic comparison may be based on the most frequent shape distances, i.e. the distance where the distributions reaches its maximum. This situation is more clearly shown in Fig. 5.115.

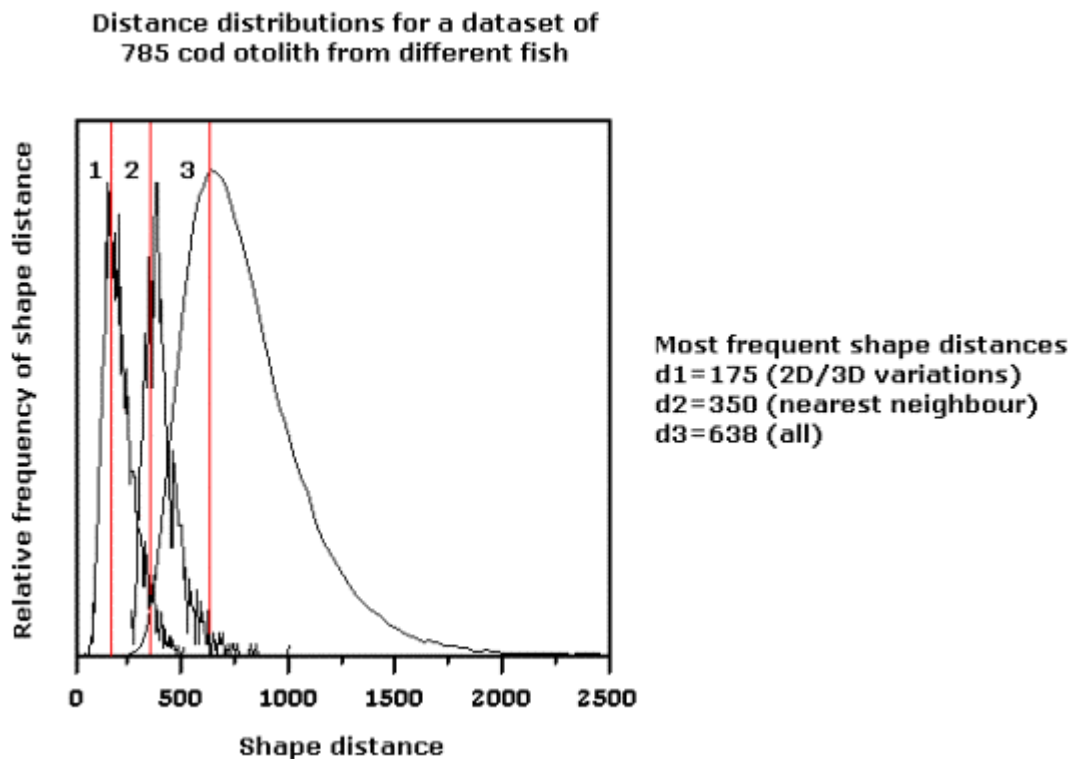


**Figure 5.115:** Comparison of shape distance distributions. Note that the most frequent distance values are indicated by red lines. Random projections have very small mutual shape distances. These are much smaller than shape distances to the most-similar (nearest-neighbour) but different shape within the set of 785 cod shapes. On average, arbitrary shape distances out of the 785 cod otolith dataset are four times larger than shape distance variations within the random projections set.

Within the dataset of 785 different cod otolith shapes, each single otolith has a nearest neighbour. The shape distance to the nearest neighbour is a fair measure for a practical accuracy limit. It

gives an estimate for the expected shape distance that we must clearly attribute to different shapes. This limit is much tougher than the average over all mutual shape distances would suggest. From the above table we can see that the most frequent nearest neighbour distance in the 785 cod dataset is about 350, while the most frequent shape distance from the random projections is only 175. Thus, we are clearly well below the accuracy limit.

Even if we haven't based our evaluations on more detailed numerical statistical evaluations, we can draw the following conclusions:

- Shapes derived from random projection images are similar to each other.
- Mutual shape distances within the set of random variations are smaller than expected.
- It is unlikely that two different otolith shapes are confused, even if small orientational variations are allowed.

Some final comments may be given here. More thorough statistical evaluations had been considered but were finally not performed because of the high complexity of the situation. The set of shape descriptors denote a point in a 256-dimensional space. Proper statistical treatment of random projections therefore requires application of multivariate statistics for repeated measurements. Basically, this means that one does not only account for relations between pairs of points (shape distance) but for all components of the difference vector. This may have important consequences. While a small shape distance may suggest that a critical situation can occur, it may not be so because the distance vector may be in a direction, where shapes cannot be confused with each other. A statistical estimate based on shape distances that ignored the directions must therefore give much too pessimistic limits.

Nevertheless, we have performed calculations - details are given in another chapter in this report - on the distance population overlaps to learn that the probability of confusing different shapes is in the order of  $P \approx 0.00238$ . As we have shown before, in the case of random projections the distribution overlaps are significantly smaller than for complete re-measurements. Therefore, we have  $P \ll 0.00238$ .

In summary we can say that the analysis of the relations between the 3D otolith shape and the apparent 2D shape registered during imaging under the microscope suggest for the critical case of highly 3D bend cod otoliths a superb degree of reproducibility. Random orientational variations than span up to  $10^\circ$  in two Euler angles were found to cause only small variations in shape descriptors that are much smaller than other experimentally unavoidable variations in illumination, magnification, focusing and positioning of the otolith.

## **6. DISCUSSION**

### **6.1 General background**

#### **6.1.1 Application of otolith analysis**

Processing information on population age-structure is an essential part of how fisheries stock assessment is performed for the majority of important exploited fish stocks. High fishing mortalities and thus low expectancy of life time duration in many fish stocks world wide makes the precise determination of age compositions even more important for the estimation of the state of the stocks and thus for a sustainable exploitation (Tyler et al., 1989, Richards et al., 1992).

One way to obtain information on the age of a fish is measuring body length, and relate it to an age/body-length key. Fish growth rate, and thereby the age/body-length relation is, however, subject to a high degree of variation being dependent on temperature, food availability, salinity, genetic factors etc. This limits the use of body length alone to estimate age, and age-body length keys have to be revised frequently. Age is usually obtained from analysis of increment formations in body hard parts such as otoliths and scales. Such age determinations may both be difficult and time consuming. They also involve a subjective element. Continued training of otolith readers and intercalibration exercises are therefore necessary.

Although it is generally realised that precise age estimation is a prerequisite for reliable stock assessment (e.g. Tyler et al., 1989) large variations in traditional ageing by annual zone counting is often found within and between laboratories; as shown in a number of studies (Boehlert and Yoklavic, 1984; Kimura and Lyons, 1991; Richards et al., 1992; Cardinale et al., 2000; Eklund et al., 2000). Errors caused by subjectivity in age determination are a common source of bias in otolith reading.

Because of these difficulties, there is a considerable interest in improved ageing methods by both validating and formalising the interpretation of traditionally identified growth structures or developing new methods for objective and robust age estimation. The initiative to start up the FAbOSA project adheres to the second approach.

#### **6.1.2 Otolith formation processes and development of shape**

It has long been known that otolith growth is more conservative, i.e. steady, than body growth, with the effect of slow growing fish having larger otoliths than faster growing fish of the same size (Templeman and Squires, 1956). Although much information is accumulating concerning the chemical mechanisms controlling the biomineralisation processes of otoliths, little is known about the actual control of shape development. The accretion of calcium carbonate onto the otolith surface starting in most species from a single growth centre with concentric layering gradually develops into a species-specific structure that indicates a high degree of genetic control.

Otoliths grow continuously through out the life span of the fish. Since the shape of the otoliths found in adult fish is species specific and since the shape also typically changes from simple

rounded (ellipsoidal) to more complicated patterns including, development of lobes, 3D curvatures or even concavities, the total change in shape must contain some information on age.

These were the basic considerations initiating the present study.

## **6.2 Methodology for 2D otolith shape analysis**

### **6.2.1 Otolith workstation**

The otolith workstation is intended to be used for very specific tasks and thus we could tailor a suitable and convenient solution. Since the 2D otolith shape imaging was the central feature, we have established an "otolith workstation" that is able to cope with the wide range of sample sizes while guaranteeing the highest possible optical accuracy. This was achieved by use of an aperture, two optics in a revolver and two different working distances. We thus obtain extraordinary huge depth-fields, which is important for precisely determining borders of the otolith silhouette. The otolith workstation is equipped for use in transmitted and also reflected light modes. The camera system was found to be simple to use and at the same time gave acceptable resolution. Nowadays, better cameras that are even cheaper are available. It is therefore clear that future otolith workstations will be equipped with such improved systems.

The otolith workstation imaging software was primarily meant to allow simple control of the camera. However, early in the beginning of the project it became clear that we had to make sure that the data collected by the different partners is compatible for subsequent processing into the databases. Therefore the otolith workstation imaging software was extended in such a way that operators could easily enter all required sample information in connection with the otolith scanning. We have thus avoided any difficulty with incompatible raw data. However, some minor aspects could still be improved. For example, we decided to give the otolith weight in milligrams. However, for some anchovy otolith sample the weight was given in grams. We have currently no provisions to let the user specify the dimension of a sample descriptor. This would be a point to be considered for an improved workstation software. Also, some people practically involved in the imaging pointed out that they would like to read the sample data from an already existing spreadsheet. The imaging software currently has no such provisions. This could also be considered for future updates.

Besides the tools needed for the otolith shape imaging, we supplied additional applications that help users to check the established databases. These tools help to prepare standard inputs to the IMAGIC-5 image analysis program (van Heel et al., 1996), thus allowing a huge range of image processing. These tools also allow for some database operations, such as separating database objects according to "Known Age" or other criteria. In summary, all these tools were successfully used for the construction of the 2D shape databases.

It should finally be noted that the otolith workstation computer operating a Windows NT 4 system was routinely updated to SP6 level. The computers worked fine. A future improvement would be to implement higher capacity storage drives.

In summary, the otolith workstation hardware and software components were assembled and then most successfully used for the creation of the shape database raw data.

## **6.2.2 2D Otolith Shape Databases for Eel, Cod, Anchovy and Turbot**

Databases were created from anchovy, cod, eel and turbot otoliths. Consistency checks and quality controls were performed for all images and all additional otolith and fish information. Most changes to the databases were necessary because of erroneous sample descriptions and only few cases were encountered where the otolith shape imaging as such failed. After all checks, the eel, anchovy, turbot and cod otolith shape images together amount to about 7000 images. All image processing in connection with the databases worked perfectly, except for one anchovy otolith shape image. This image had a contrast problem and was manually modified, after which it was processed without further problems. In other words, the imaging and image processing solution worked very reliably.

In the case of turbot, we had problems that were initially not fully understood. The turbot images were not made on an otolith workstation but they were taken with a different imaging hardware. It turned out that the camera had non-quadratic pixels. While we assumed quadratic pixels, the apparent effect was a linear distortion of the images in one direction. After we determined the nature of the distortions, the images were corrected with IMAGIC-5, after which they could be processed as usual.

The otolith weight was introduced into the database concept at a time where other sample data had already been compiled. Therefore, we needed to change the database format, which again caused some delay.

The final versions of the databases were established in close collaboration with the respective operators that had done the raw data collection. They contributed additional information such as imaging protocols and otolith glossaries. Therefore the final versions are useful and made available to people outside the project (Kastowsky et al., 2002a).

## **6.2.3 Reproducibility of otolith weight and 2D shapes**

Three major groups of variables were analysed to approach age determination using objective measurement criteria. Otolith weight was determined on an ordinary laboratory scale. Shape described by the silhouette contour line determined from light microscope images with low magnification and long working distance. Finally different morphometric variables were measured from grey tone images with a resolution of the surface structure of the otoliths, besides objectively identified measurements like area, maximum and minimum radius etc. For a small subset of otoliths, the more subjective variables, the so called landmarks were defined to measure distances between marks of otolith development that could not easily be found by automatic procedures.

Repeated measurements of the same otolith using the scanning and image software, with repositioning the otolith and resetting the light and focus conditions every time, showed a high degree of reproducibility. Differences in shape from repeated measurements, defined as the Euclidean distance between the 256 first Fourier Descriptors (FD's), were so small that the chance of mistaking a single repeated measurement with an otolith from another individual from the same stock was less than 2‰ (Kastowsky et al., 2002a).

From a methodological perspective, we have developed shape analysis tools, which can be directly applied for various tasks in fish biology. Our unbiased automatic classification of contours represents a robust method for the 2D otolith shape analysis, which exploits virtually all information present in the contours. 68 normalised Fourier descriptors proved to be sufficient for shape classifications (Kastowsky et al., 2002b; 2002c).

#### **6.2.4 Methodology for 2D shape analysis**

##### ***2D Shape Analysis***

It should be pointed out that we did not invent totally new approaches with respect to the applied 2D methods. The basic concepts are all described in the literature so that we could concentrate on the creation of a versatile set of IMAGIC-5 commands. The suite of programs that finally constitute the specific 2D shape tools is enormous. What makes this selection of tools probably unique within the realm of currently available 2D shape software is the ease by which any combination of tools can be achieved. We will give one example here.

While shape and size are separable by using Normalised Fourier Descriptors (NFDs) (Wallace and Wintz, 1980), we all live in a world of objects with given shape and size. That means we like to work with NFDs but not forget about size totally. Now consider a shape classification based on NFDs. Usually, results will be visualised in the form of class averages. However, in this case we average over normalised objects. IMAGIC-5 allows to produce sized shape reconstructions and these can now be used in the calculation of class averages. The result is then a visualisation of all the individual shapes in a shape class. Since all the shapes are to scale with respect to their absolute or real-world size, such a visualisation allows a direct inspection of the size-homogeneity of a shape class. In other words, we will easily find out if a shape class consists of shapes of specific sizes only, or not.

This is just one example for the huge number of possible combinations of IMAGIC-5 commands for 2D shape analysis. One very important fact should not be left out here. It concerns the standard eigenimage analysis tools of IMAGIC-5. We made use of these tools when we tried to understand the most important shape changes inherent in a set of otolith contours. There are only few other software packages in the world that allow eigenimage analysis. To the best of our knowledge, these software packages have limited other 2D tools and thus we feel correct in saying that the current system of 2D specific and the many further standard IMAGIC-5 features constitutes one of the most advanced 2D shape analysis tools on the world market.

##### ***2D Shape Classes***

The performance of the IMAGIC-5 software with respect to revealing shape classes within a given dataset is unquestioned. However, since, for example, the shape classes derived for anchovy otolith contours are so similar to each other, a human observer is unable to appreciate that kind of information. We have therefore employed the eigenimage analysis (van Heel, 1984; 1989) to better understand the main shape changes within a dataset. Results from these studies yield the most important shape changes in form of the extreme shapes (Kastowsky et al., 2002b).

If one assigns 100% to the maximum shape change, then in a first approximation, the shape difference between N shape classes is on average  $100\%/N$ . We have shown 25 shape class averages in the results chapter. According to the above approximation, the shapes differ by only 4% of the maximum shape change. This makes understandable, why human observers have tremendous problems in appreciating the differences between the individual shape classes.

While this is a problem when conclusions have to be drawn from a visual inspection of shape classes, there are absolutely no problems for statistical evaluations based on the computer-generated classification schemes. We could therefore successfully apply simple statistics to shape classes. In most cases we obtained rather inconsistent class compositions, i.e. there were a number of otolith shapes clearly belonging to the same shape class but the corresponding fish were of quite arbitrary age. According to our scheme for logical implications, we cannot imply anything for such a shape class. What we need instead is a shape class that has a very clear age relation. Taking all shape classifications for the different species into account, there were mostly about one third of all samples in shape classes with consistent age-composition. In the best scenario this means that only one third of all samples can be aged.

In conclusion, we find that the shape classification as such worked satisfactorily but the statistical results based on the shape classes suggest a high degree of age-inconsistency in these shape classes. Shape classifications suggest that only one third of all samples falls into age-consistent shape classes.

### ***Eigenimage Decomposition***

The Multivariate Statistical Analysis (MSA) package within the IMAGIC-5 environment (van Heel, 1984; 1989, van Heel et al., 1996) is one of the most powerful tools applicable to a range of tasks. In the context of 2D shape analysis, we found that MSA was extremely helpful in what we like to call shape understanding, rather than only calling it shape analysis. The high qualification of this tool comes from the fact that the analysis of shapes in the form of contour lines gives eigenimages of a special type as result. Some of the most important eigenimages are composed of two components that represent the extreme shapes within the dataset. One can decompose the combination into the constituents and then e.g. compare them to each other.

We applied this strategy to establish the most significant otolith shape changes within the datasets for each of the species (Kastowsky et al., 2002c). As a result, we could show that for eel there was a very clear shape variation, which was found to be uncorrelated to age. For other species, there were clear shape features evolving in a specific way with age.

The eigenimage analysis followed by shape understanding through decomposition of eigenimages is again a demonstration of the high performance possible by using combinations of different tools in IMAGIC-5. Here we combined the image reconstruction features based on the Normalised Fourier Descriptors together with the standard MSA capabilities.

## ***2D Shape and Size***

There is no general applicable way to combine pure shape and size. We have focused on pure shape because if one wants to deal with the size information only, most of the developed 2D image analysis methods are not strictly required for a simple analysis. For example, weighing an otolith would probably provide an easier access to a size-related parameter. However, our results demonstrate that pure shape alone is a poor predictor for age. Therefore we have tried one approach to combine shape and size information into a single ageing model. Our approach was based on shape classes. We performed classifications based on weighted shape and size information. The weights were determined such that the optimum classification scores regarding age were obtained. The final result showed that the classification score basically increased with increasing weight of the size information. In other words, in a mixed-influence model of shape and size, the shape information was obsolete.

This finding may be considered in the light of three theoretically possible situations. In the most favourable situation, the combination of two features gives a better prediction, i.e. the predictors conform. In the worst case, one predictor disagrees with the other and weakens any combined model. In the third case, one of the features has no influence on the predictions from a combined model. The situation described in the previous paragraph falls into the first or last category. For eel, we have some indications for the second case, i.e. we might have disagreeing predictors. For anchovy and turbot we probably have no useful improvement of age predictions for combined models. Only for cod we have demonstrated that more complex models including some shape information along with size give better age predictions.

It should be mentioned that we could not test all possible ageing strategies. For example we discussed stratification procedures based on otolith shape classes as well as on size classes. In other words, we first classify an otolith shape into some shape class. Then we look at the size and predict the individual age. Of course, the statistical models for the size-age relation would have to be defined individually for each otolith shape class. Similarly, one could have assigned the otolith to a size class first and then base the age on the actual shape within this size class. Both such approaches have not been tested because of time limitations.

## ***Tree-Based Ageing Model***

A number of different statistical approaches are feasible to develop models for fish ageing based on otolith shape and other samples features. We have chosen tree-based modelling to explore one specific dataset for cod, for which a relatively strong otolith shape-age relation was found. What we wanted to know is if the individual age predictions can substantially be improved by finding an optimal ageing model. In other words, we had obtained the notion from other investigations that shape is ultimately not very useful to individually age fish. However, was this just because we did not apply the full power of statistics?

The results from our tree-based modelling on the first sight indeed suggest that we could improve our age prediction score from 87% to 95%. But here we have to critically look again at the results. Simple ageing models that are based on otolith weight or on otolith weight and fish length give 45 misclassifications out of 353, which corresponds to a score of 87% correct predictions, whereas the best tree-based ageing model gave 19 misclassifications out of 353. This latter model

therefore seems to be the preferred choice. However, this model is extremely complex and includes nine different sample features. The question is, does this extremely complex model appear just better because it has more degrees of freedom. Consider that the difference of 45-19=26 misclassified samples is in the order of the number of outliers. For example, take the otolith weight. While most otoliths within an age class fall within a certain weight range, some are clearly outliers. Any ageing model must have difficulties dealing with such outliers, because the weight is obviously dubious. We have not checked in great detail but it seems likely that the different scores of the tree-based models merely reflects the fact that the more complex model can deal better with such kind of outliers.

There are other ways of testing this hypothesis. One would be to randomly divide the dataset into two or more subsets. The ageing model would then be established using data from one subset and the consistency of the model is then tested against another subset. We have not performed such an analysis, since our knowledge that other sample descriptors such as otolith weight alone are extremely powerful age descriptors made further efforts towards employing otolith shape appear useless.

### **6.3 Age determination based on 2D shape**

#### **6.3.1 General aspects to age determination**

Age determination of an individual fish is based on two processes. First the number of annual growth increments in the otolith is enumerated and then a specific age is assigned taking into account the conventional birthday and the date of capture of the fish. That is to say that all fish are considered as born on the same day of the year. This simplification is necessary for stock assessment purposes and is based on the fact that annual growth increments are counted on the otolith, thus discrete units. In reality fish growth is a rather continuous process, and otolith growth too, moreover fish can be born in different period of the year according to the extension of the spawning season. Also the occurrence of a specific annual increment can vary during the year (Beckmann and Wilson, 1995). Therefore ageing protocols are necessary to establish a series of rules in order to reduce all the above mentioned source of variability and assign each individual to a specific year class.

#### **6.3.2 Ageing of cod otoliths by 2D shape analysis**

The growth of cod sagitta otoliths starts in the pre hatch stage with a single growth centre around which concentric daily increments are formed. At the late larval stage about 25-60 days old the 12-15 mm long cod starts to form secondary otolith growth centres that changes the shape from a disc to a elongated ellipsoidal form, additionally differential growth along different radii gradually develop lobes around the periphery of the otolith. At a size of 10cm and an age of less than half a year the juvenile cod has attained the general sagitta otolith shape that it will to a high degree retain for the rest of its life. Our investigations showed that new lobes will form and old ones will disappear by overgrowth with an annual rate of about 10% however not systematically change the absolute numbers significantly.

Our findings that most of the age related shape changes in cod otoliths occur among the NFDs with the very lowest frequencies are therefore not surprising. Since, overall shape features are captured in the low-frequency NFDs, the fine details of lobes require more high-frequency NFDs. However, even among individuals with same age lobes, especially the positions where lobes occur along the otolith contour, are not consistent features and therefore a relatively small number of NFDs suffices. But since introducing more than required otolith contour details into the shape classification or eigenimage analysis does not give any problems, we decided to give the user a chance to decide for either 68 or 256 NFDs, with the suggested default being 256.

There are characteristic otolith shapes for young and old cod. The otolith size alone is an accurate predictor for the age of the fish. Cod is one species for which the otolith shape analysis gives some additional information that makes an age prediction more reliable.

Tree-based models suggest that, out of the five considered shape features, factorial coordinates F2 has the highest importance for age predictions. The most-complex tree-based ageing model is composed of nine variables and yields optimally about 95% correct classifications. The simplest statistical model is based on otolith weight only and gives scores of up to 87% correct classifications. We used relatively young cod in their fast growth period. The classification success for cod with an age above ten years will probably be lower.

### **6.3.3 Ageing of eel otoliths by 2D shape analysis**

There is no theoretical approach to determine the most appropriate number of classes into which a set should be divided. From the standpoint of the classification algorithm, 40 shape classes are well defined. The variability in otolith shapes is usually the limiting factor and not the level of detail in shape description. From otolith shape alone age could be predicted only for less than 1/3 of all eel samples, whereas using otolith size the predictive power is much better. Eigenimage decomposition showed that the shapes of eel otolith are highly variable and that they are not age-related.

- The age composition of pure shape classes does not suggest any exploitable shape-age relation.
- Otolith size alone is almost as good a predictor for age as a combination of otolith shape size.
- The most significant shape change within the Lake Frisksjön dataset is not age-related.

The European eel is a slow-growing species with a strong phenotypic plasticity, i.e. individuals could differ a lot, both within a locality (e.g. a lake) and between sites without being genetically different. For a long time, the Atlantic eels were looked upon as perfect panmictic species, i.e. they have single breeding populations with a common gene pool resulting from completely random mating. Any genetical differences result from differential mortalities and not an evidence of a genetical substructure in the population. However, this has been questioned recently (Wirth and Bernatchez, 2001). A variation of otolith shapes irrespective of age is perhaps not that surprising in such a varying species, especially if the genetical factors cannot be ruled out. This can explain our results that the shape of eel otoliths is not related to the age of the fish.

#### **6.3.4 Ageing of turbot otoliths by 2D shape analysis**

Turbot otolith shape appears to gradually change from a round shape in juvenile turbot to a more elongated shape in older turbot. The differences are, however, small compared to the individual variability in shape. In the dataset for reared turbot, samples of fish of same body length were taken every second week for approximately one year. It was not possible to see a gradual change in shapes during this period. Therefore, in order to maximise the age signal, the shape analysis concentrated on the youngest and the oldest fish. Otolith shapes could be aggregated into classes. Five out of twelve classes contained primarily “young” or “old” turbot. The five classes contained 33% of the otoliths. In these classes on average 84% of the fish belonged to the dominating age group. An age signal is therefore observed, but it is weak compared to the general variability in otolith shape. It remains to be investigated whether the five age related shape classes could be identified in future datasets.

Variability in otolith size is compared to variability in body size in a group of field-caught and traditionally aged Baltic turbot. The results showed that otolith size generally is related directly to body size and otolith size may therefore be used instead of ageing based on age-body lengths keys. Otolith weight was less variable than could be expected from the variation in otolith length. Otolith weight is therefore a better predictor of age in individual fish.

A clear age effect on otolith size was observed with older fish having relatively larger otoliths than young fish of same body size. This effect was observed measuring otolith length, otolith area and otoliths weight. Measurements of otolith size may therefore improve ageing based on age-length keys.

In summary we can say for turbot, that the age-shape relation is so weak that shape analysis is not directly suited for ageing. Shape analysis or calculation of otolith size in relation to body size may, however, be able to increase precision of ageing based on age-length keys. In most cases, traditional ageing based on otolith annuli readings will probably provide better results with less effort.

#### **6.3.5 Ageing of anchovy otoliths by 2D shape analysis**

The main result is that there is a shape-age relation but it cannot practically be used for reliable ageing.

Since the main result for anchovy suggests that the age-discriminative power of otolith shape is not sufficient for practical use, we considered if by looking at smaller subparts of the contour we could improve the importance of shape. The partial contour segment does not give better results concerning an age prediction.

There are only small shape variations between average shapes of age class 1 to 4.

There is a simple round-to-elongated transition from age class 1 to 4. The reliability for the ration of length-to-width measures does not at all suffice the requirements for an acceptable ageing procedure. The overall size of an otolith is more powerful for ageing than this simple otolith shape feature.

Classification results are very consistent with the findings from the eigenimage analysis, where the dataset was easily separable into age 0 and age 4 samples; however, all age groups together are heavily overlapping with respect to shape features.

For anchovy, we have to acknowledge that many shape analysis tools yield consistent insight into the otolith shape features unambiguously revealing small trends but failing to provide a practically useful strategy to use otolith shape for ageing.

Even considering them as non-random events, the prediction score is low and cannot probably be used at the level of assigning individuals reliably to one of the two catch sites.

### **6.3.6 Ageing of otoliths by 2D shape analysis: Eel, turbot, anchovy, cod**

There are basically two different features involved in what usually is meant by shape. These are the pure shape or form of an object and the overall size. The calculation of NFDs for shape includes a size-normalisation step. However, this information is not lost but available in the form of the so-called size-factor.

For all four targeted species we found that the size-factor was more powerful for age prediction than the pure shape. The significance of shape for age prediction increased from eel over anchovy to cod. For turbot, the shape-age relation was inconsistent and a high variability in shapes was observed even in individuals of same size and life history, only differing in age. Selecting the oldest and youngest individuals of same size made it possible to identify some shape classes primarily containing young or old individuals. In conclusion, the assumption that the otolith shape information is sufficient for an individual age prediction is wrong. However, shape contains a limited amount of information on age, which may be used together with information on fish body size, otolith size, otolith relative size and otolith annuli to estimate age.

Our results concerning the importance of the otolith size-factor are absolutely consistent with the well-established knowledge that otoliths tend to grow at a relatively constant accretion rate. While a fish might shrink in body size due to poor feeding, the otoliths keep growing. This means that otolith-growth related features are more reliable age-descriptors than for example fish length or fish weight.

For turbot, anchovy and cod we found allometric 2D shape changes for all species, i.e. there are changes in proportions of shape features as the overall size increases. For eel we could clearly establish prominent shape changes, however, these were not age related and therefore it was not clarified if the shape changes were allometric at all. However, even for the other three species with allometric 2D otolith shape changes, the trends were so poor that they could hardly be employed for the construction of consistent ageing procedures. For example, in one evaluation, we obtained an error rate of 42% for the age-predictions based on pure shape, while the single-predictor model based on otolith weight only, gave 87% correct predictions. However, a small amount of shape information can help to improve the age predictions, as was demonstrated by the best tree-based ageing-model giving 95% correct predictions.

We must therefore conclude that the established age-related pure shape features are not sufficient for individual age prediction. Not unexpectedly, the overall size-factor gives much better ageing-models. Combinations of pure shape features with other sample descriptors might be more powerful in age prediction than single parameter models.

## **6.4 Methodology for 3D otolith shape analysis**

The function of the otoliths both as part of the auditory and as part of the balance/acceleratory sensory systems is dependent on the entire 3D structure and density. However a large part of this information may be retained in the projected 2D silhouette shape in combination with weight and volume.

### **6.4.1 3D Methodology**

Most of the standard IMAGIC-5 software tools could directly be applied to the 3D otolith datasets. For some special cases, however, modified commands have been programmed. One of these extra tools concerned a tool that allows one to read in arbitrary cross-section data and convert internally to constant-Z-increment, i.e. interpolation is performed where needed. This command was employed for input of the light-microscopic images.

For the construction of the 3D basic framework required with the 3D plotter equipment, some special programs were developed and used. Later on we decided to have the other models build by a commercial company, so that the 3D plotter approach was dismissed.

The other standard IMAGIC-5 features worked well. For instance, the standard surface rendering was used to create surface views that were then used to create animated GIF files. The latter are very useful for quickly identifying samples and such animated GIF files were added to the 3D databases (Kastowsky et al., 2002d).

We used procedures outside IMAGIC-5 to convert surface models to the STL format, which is an accepted general standard within the 3D community. Since IMAGIC-5 can produce MRC files, which are subsequently converted to STL, the whole procedure is not complicated. However, it is worth to think about an additional IMAGIC-5 command to directly create STL files.

### **6.4.2 3-D Otolith Shape Databases for Eel, Cod, Anchovy and Turbot**

The description of the outer 3D shape, e.g. as surface models, was achieved by use of X-ray micro-tomography (Sasov and van Dyck, 1998). The quality of scanning was sometimes critical but there were no general problems encountered. Thus, for all species we could produce large-scale plastic models of selected otoliths. However, initially it was intended to elucidate the otolith inner structure, e.g. to detect the variations in the bulk material properties (Hamrin et al., 1999). While it is clear that such material property variations exist, the question is if these are large enough to be detected with the X-ray scanning device. In fact, we failed in several approaches, which included increased time of measurement, thin plate analysis, external contrast variation, and soaking otoliths in ionic solutions. Neither attempt indicated any inner structure. Therefore

we combined the outer shape information with light-microscopical one. Thus, we obtained two reference sets with complementary information and therefore a way to the otolith inner structure is demonstrated.

We were much more successful using the outer shape for a series of 3D / 2D correlations. We found that the 2D shape is a very appropriate descriptor of shape. The extremely stable mapping between 3D volume and 2D shape means that any errors, due to slight variations in the way the otoliths sits on the glass support, are negligible. In a more general sense it means that the 2D shape extracts a consistent feature from the 3D shape.

### 6.4.3 Surface Models

The 3D otolith outer shape has different importance for the otoliths from different species. The 2D surface of eel otoliths reveals a groove forming the *sulcus acusticus*. A similar groove is found in turbot otoliths. However, turbot otoliths are generally rather flat, while eel otoliths are sometimes curved. For eel and turbot rather few suggestions exist about the meaning or use of such surface structures for fish ageing.

For anchovy the 3D shape follows somehow a simple pattern. Basically, the initial form can be considered as an oblate and relatively thin object. Accretion to this body leads to more or less proportional growth in all directions. Therefore, the 3D shape of an anchovy otolith is not essentially different for young and old fish. Also, remember that we found relatively small changes in the 2D otolith shape during growth of the fish.

A quite different situation is given for cod. Cod otoliths are curved in a direction perpendicular to the long axis, which runs from the posterior to the anterior end. Along this very same axis, the otolith is further twisted. Moreover, the 3D shape of a cod otolith is extremely complex due to the lobes. Since the lobes and the gaps between them are locations where the accretion to the body produces the most obvious effects, seasonal growth effects have been identified in some cases. Up to now, the growth process is not fully understood so that we cannot refer to an established model. For example it is hard to evaluate the importance of surface structures such as the gaps and grooves on the surface of cod otoliths. However, we would like to stress here that the 3D data obtained from by X-ray micro-tomography constitute a means of registering the surface structure. The surface representations calculated with IMAGIC-5 tools were able to reproduce even the finest surface details.

### 6.4.4 Inner Structure

We should first discuss why X-ray micro-tomography could not reveal electron density variations in the interior of an otolith. Consider the following example. Onto a clean mirror we put a fingerprint clearly visible. The same mirror, when scanned in an X-ray micro-tomograph, will probable not reveal any recognisable structures for the fingerprint. This example might help to understand that different physical methods probe matter in quite different way and one and the same thing might well be detectable by one method (probing reflectivity of the mirror), while largely undetectable by others (probing electron density). An otolith is made of bio-mineralised calcium carbonate. This material has an average electron density, which depends on the

crystalline framework within an otolith. While there are zones of micro-crystallites with different orientation, the crystal structures are not much different and therefore, the average electron density is probably not different at all. Since X-ray probes the electron density, they cannot reveal differences. At least this appears to be the case with otoliths. In contrast to this, X-ray micro-tomography has been successfully employed to reveal the inner structure of diamonds. While the diamond material density and physical state is more or less same within the diamond, some cracks or crystal plane deviations may stand out. Unfortunately, such a result could not be obtained for otoliths. So we can only speculate that the interior of an otolith is on the one hand "constant" enough and on the other hand "distorted" enough to disallow revealing of any inner structures. The mentioned distortions within an otolith may come from different kinds of micro-crystallites and inclusion of different amounts of protein material.

While we can only speculate here, we did try to improve the contrast within an otolith. One series of experiments aimed at reducing the X-ray scanning noise-level. Noise can be reduced by longer exposure times. Also, thin sections instead of full otoliths were scanned. Otoliths were immersed into alcohol and other solvents to change the otolith-to-environment electron-density contrast. Another set of experiments concerned dipping an otolith into an ionic solution in order to obtain differential elemental marking after diffusion of ions into the bulk. Neither of these approaches was successful.

At this point, we decided to employ the well-established reflected-light microscopy to obtain otolith internal structure information. In reflected-light the otolith internal zones according to seasonal effects become visible. Of course, to reveal these inner structures it is necessary to cut the otolith into thin slices or grind down plane by plane.

The cross-section information obtained from such approaches can be combined into a 3D model when it is possible to fulfil two requirements. First, the 3D spatial alignment of any given cross-section with respect to other cross-sections must be known and the probed qualities of different cross-sections must be scalable. The first, issue means that we must know where any given cross-section sits, e.g. with respect to a given 3D surface or outer shape model. Since we can obtain the outer shape from X-ray scans, the first requirement is principally achievable. The scalability of cross-sections, however, is a real problem. In our case of reflected-light images, it means that we have to find a way to calibrate the grey-tones from different images into one consistent system. However, since each cross-section was imaged independently from another cross-section, there is no way as to exactly calibrate all images. One practical approach would be no calibration at all. In one of the cases this was a fair approximation for most cross-sections. However, there were some images where the incident light may have been slightly different, giving rise to much brighter images than usual. In other cases, there were cracks in the surface, which produced a lot of bright artefact, which in turn had an influence on the overall brightness in the image. In our approach, we have completely ignored such difficulties and taken the original cross-section images. It means that we have to leave it to the user of our databases to make sure that the inner structure data is interpreted with some care. Also, any automatic processing should be checked carefully before conclusions are drawn. At this point we cannot improve the current situation.

### **6.4.5 Model Replication by Moulding**

The replication of large-scale otolith models was of some interest in the beginning of the project, since some project partners stated their interest to have multiple copies of large-scale plastic models. At that time, the use of a 3D plotting device was extremely costly and time consuming. Therefore, replication by moulding was anticipated. The practical solution involved production of the two halves for the mould starting from one large-scale master copy.

Our practical findings showed that replicas could be produced in a standard and reproducible manner with virtually no loss of visible detail between the rapid prototyping model and the replica. We estimated that the cost of casting and moulding replicas is of an order of magnitude lower than building rapid prototyping models from scratch.

At a later stage of the project it was deduced that smaller numbers of copies from one specific otolith were wanted but the total number of different models was high. It was therefore not advised to replicate these few models by moulding but we rather decided to have the two copies each build individually.

### **6.4.6 Large Scale Plastic Models**

In order to finally produce large-scale plastic models of otoliths from anchovy, cod, turbot and eel we selected three to four otolith per species that somehow represented an old, a middle-aged and a young specimen. Even for the smallest otolith from anchovy, which are in reality only 1-2 millimetres long, nice 10-20 centimetre long models were produced. Surface details were fairly well reproduced in all cases. In order to avoid a nasty artificial surface roughening, we had used 3D density data with a relatively high coarsening parameter, which may be envisioned as surface smoothing. For the cod large-scale models this smoothing may have been a little bit too much, since the original 3D raw data suggested sufficient contrast so that less coarsening would have sufficed. In all other cases the chosen smoothing was adequate.

## **6.5 2D / 3D considerations**

### **6.5.1 Combining 3D shape and 2D inner structure information**

The description of the outer 3D shape, e.g. as surface models, was achieved by use of X-ray micro-tomography. The quality of scanning was sometimes critical but there were no general problems encountered. Thus, for all species we could produce large-scale plastic models of selected otoliths. However, initially it was intended to elucidate the otolith inner structure, e.g. to detect the variations in properties of the bulk material. While it is clear that such material property variations exist, the question is if these are large enough to be detected with the X-ray scanning device. In fact, we failed in several approaches, which included increased time of measurement, thin plate analysis, external contrast variation, and soaking otoliths in ionic solutions. Neither attempt indicated any inner structure. Therefore we combined the outer shape information with light-microscopical one. Thus, we obtained two reference sets with complementary information and therefore a way to the otolith inner structure is demonstrated.

### **6.5.2 Applicability of standard 2D / 3D IMAGIC-5 tools**

The software tools for creation of 2D projections are standard procedures in IMAGIC-5. The plane onto which the 3D density is projected is specified by the Euler angles. We created a set of random Euler angles centred around one reference situation. The reference was chosen to be close to the situation encountered in 2D silhouette imaging. Initially, we tried to precisely define the Euler angles by finding the three points on the otolith surface that touch the glass plate during imaging. We discarded the approach because the results obtained by defining a reference and looking at differences with respect to this arbitrary reference seemed to be acceptable.

### **6.5.3 Transformation between 3D and 2D shape information**

We were much more successful using the outer shape for a series of 3-D/2-D correlations. We found that the 2D shape is a very appropriate descriptor of shape. The extremely stable mapping between 3D volume and 2D shape means that any errors, due to slight variations in the way the otoliths sits on the glass support, are negligible. In a more general sense it means that the 2D shape extracts a consistent feature from the 3D shape.

Cod otolith 3D-contours were reconstructed from X-ray micro-tomography and translated into 2D maximum projected contour using specially developed algorithms. The close resemblance between light microscope 2D contours and the tomographically reconstructed maximum 2D contour shows the general reproducibility of the applied methods.

### **6.5.4 2D/3D Reproducibility**

When we analysed the silhouette shapes for one hundred different projections, an extremely small variation in shape was found. Each of the three Euler angles had been randomly chosen from a 20° angle segment, so that the outcome of the analysis was unexpected. There are however some considerations that explain why the apparent shapes were not so different as expected. One has to consider that each silhouette shape is normalised in size before it is then compared to other shapes. This comes from the used concept of NFDs for shape. Therefore, when a cod otolith is tilted along an axis perpendicular to its long axis, the maximum shape change is produced. Apparently, however, the cod looks smaller in the direction of the long axis. Now, the size normalisation takes place and neutralises part of this effect. As a result, the large variation along the otolith long axis is counteracted and instead of this, a much smaller apparent variation along the otolith minor axis is left over. Thus, the initial effect is large but is cancelled out in part by the size normalisation step inherent in our procedures.

The results of the 2D / 3D cross-validations suggest that the shape of an otolith placed on a glass plate for imaging is not much affected if we consider small tilts of the otolith. In practise, we learned from imaging of several thousand otoliths that such tilts do virtually never occur. However, in a more general way we may consider differently tilted otoliths producing a point cloud in shape descriptor space. The fact that these point lie dense in the shape space means that we do indeed select rather characteristic fingerprints for a given otolith. If that would not be the case, shape classifications would be rather arbitrary with respect to the specific 2D projection we

selected. So we have a nice indication that even though an otolith is placed on a glass plate for imaging without thinking too much about the specifics, we do capture the characteristic 2D features encoded in the more complex 3D volume.

We tried to estimate some statistical figure of merit for this fortunate situation but a mathematically exact treatment is extremely complicated. We have to consider mappings between the three-dimensional Euler-angle space and the 256-dimensional NFD shape-space. From these mappings suitable variational parameters have to be extracted so that finally the overlap between shape states could be calculated. We have not followed that line but employed the much easier approach based on the complete matrix of all mutual shape distances. Our simplified way of reasoning is that the set of projections gives us an idea of how the internal shape distances are distributed. Also, by looking at a sufficiently large set of other distinct otolith shapes we obtain an idea of the distribution of such shape distances. Now we evaluate the overlap of these two distributions and obtain a statistical estimation for how characteristic our set of 2D / 3D variations is. We found the probability of confusing different shapes is in the order of  $P \approx 0.00238$ . In other words, two out of a thousand shapes are confused with another one, even if they are in fact different. This is not too bad but the estimate is probably much too pessimistic since in this simple approach we did not account for directions between two points in shape space but did only consider distances between points in shape space.

## 7. CONCLUSIONS

Overfishing of fish stocks is a fact of life and their management is thus a matter of utmost importance that affects much more than the economic existence of fishermen. Fish ageing is a primary tool for the assessment and management of exploited fish stocks. Thus, any improvement of the quality of such measurement tools can lead to better decisions in fish stock management and thus can represent some real improvement to the fisheries industry on a global scale.

In the FAbOSA project the primary goal was to evaluate the contribution that simple and easily-accessible otolith two-dimensional (2D) shape information can make towards a precise age determination of individual fish. Such 2D contour information is directly obtainable from just looking at an otolith through a CCD camera. We have investigated the basic data that determines the 2D contours of otoliths, that is, their three-dimensional (3D) shape. We have developed extensive tools to study the 2D contours, and have collected large otolith data sets of known age in order to test the new tools. We are happy to have achieved most of the results we had as our goals.

### WHAT HAS BEEN ACHIEVED IN THIS STUDY?

- We have undertaken what probably was the most extensive study of the otolith shape - age relationship to date.
- A complete set of analysis tools was created in the course of the project for studying contours using complex Fourier descriptors. We have created what is likely to be the most complete set of software tools available for this purpose.
- We have developed a novel approach to the contour analysis problem using the eigenimage approach.
- We have for the first time calculated 3D volumes of otoliths using the new tool of X-ray micro-tomography.
- Various 3D otolith volumes, for different species and ages have been measured and will be made available on CD-ROM to the scientific community.
- These 3D density distributions have been used to generate oversized 3D plastic models for use in demonstrations and teaching.
- A hardware/software otolith workstation was designed and assembled. This workstation was continuously updated, based on user feedback and has now been in routine use for several years.
- Otolith databases containing images and contours have been assembled for: cod, eel, turbot and anchovy. Otoliths of the first three species are of known age.
- These four shape databases are now available to the scientific community on CD-ROM.
- Using the new software, the relationship between otolith shape and otolith age has been investigated extensively. For certain species, like cod, including shape information in age determination procedures will significantly improve age assessment over a simple weighing of the otoliths.

- For most species, however, simple measurements of the otoliths like their weight and length have a much higher predictive power for age determination than shape analysis alone.

## BOTTOM LINE

Otolith Shape analysis by itself is not a definitive tool that will solve all age determination problems. The assumption that pure otolith shape information, disregarding other easily accessible information such as otolith length or weight, is sufficient for age measurement of individual fish is not correct. Indeed, simple direct measurements of otoliths like size and weight have been shown to be among the best measures of fish age. Detailed analysis of the otolith shapes can clearly add to the precision on the age measurement for many species. For species like eel, however, the internal shape variations within one age group are already much larger than a possible small shape differences with age. Adding such information may even be detrimental to age determination. Whereas a precise ( $\pm 0.5$  year) age determination based on otolith data alone may not always be possible, that determination may actually not always be relevant. We would thus very much welcome others to take on a follow-up study to investigate how precisely one can determine the age distribution of a fish population based on otolith data, without explicitly assigning a year class to each individual in the sample.

## 8. REFERENCES

- Araya, M., L. A. Cubillos, M. Guzmán, J. Penailillo and A. Sepúlveda, Evidence of a relationship between age and otolith weight in the Chilean jack mackerel, *Trachurus symmetricus murphyi* (Nichols), 2001. Fisheries Research 51: 17-26.
- Beckmann, D. W. and C. A. Wilson, 1995. Seasonal timing of opaque zone formation in fish otoliths. In: D. H. Secor, J. M. Dean and S. E. Campana (Editors), Recent developments in fish otolith research. University of South Carolina Press, pp. 27-43.
- Bedford, B. C., 1983. A method for preparing sections of large numbers of otoliths embedded in black polyester resin. J. Con. Int. Explor. Mer. 41: 4-12.
- Begg, G. and R. Brown, 2000. Stock identification of Haddock *Melanogrammus aeglefinus* on Georges Bank based on otolith shape analysis. Transactions of the American Fisheries Society, 129: 935-945.
- Berg, R., 1990. The growth of eels: A critical assessment of data from open waters. Int. Rev. Gesamt. Hydrobiol, 75: 755-62.
- Boehlert, G. W., 1985: Using objective criteria and multiple regression models for age determination in fishes. Fish. Bull. 83: 103-117.
- Boehlert, G. W. and M. M. Yoklavic, 1984: Variability in age estimates in *Sebastes* as a function of methodology, different readers, and different laboratories. Calif. Fish Game 70: 210-224.
- Campana, S. E., 1990. How reliable are growth back-calculations based on otoliths? Can. J. Fish. Aquat. Sci., 47: 2219-2227.
- Campana, S. E., 1999: Chemistry and composition of fish otoliths: pathways, mechanisms and applications. Mar. Eco. Prog. Ser. 188: 263-297.
- Campana, S. E., 2001. Accuracy, precision and quality control in age determination, including a review of the use and abuse of age validation methods. Journal of Fish Biology 59: 197-242.
- Campana, S. E. and J. M. Casselman, 1993. Stock discrimination using otolith shape analysis. Can. J. Fish. Aquat. Sci., 50: 1062-1083.
- Campana, S. E. and S. R. Thorrold, 2001. Otoliths, increments, and elements: keys to a comprehensive understanding of fish populations? Can. J. Aquat. Sci. 58: 30-38.
- Cardinale, M., F. Arrhenius, B. Johnsson, 2000. Potential use of otolith weight for the determination of age-structure of Baltic cod (*Gadus morhua*) and plaice (*Pleuronectes platessa*). Fisheries Research 45: 239-252.
- Cardinale, M. and F. Arrhenius, 2002. Application of the otolith weight-age relationship to estimate the age-structure of Haddock (*Melanogrammus aeglefinus*). *Journal of Applied Ichthyology*, in press.
- Casselman, J. M., J. J. Collins, E. J. Crossman, P. E. Ihssen and G. R. Spangler, 1981. Lake whitefish (*Coregonus clupeiformis*) stocks of the Ontario waters of Lake Huron. Can. J. Fish. Aquat. Sci. 38: 1772-1789.

- Castonguay, M., P. Simard and P. Gagnon, 1991. Usefulness of Fourier analysis of otolith shape for Atlantic mackerel (*Scomber scombrus*) stock discrimination. *Can. J. Fish Aquat. Sci.* 48: 296-302.
- Cingolani, N., E. Arneri, G. Giannetti, A. Santojanni and A. Belardinelli, 1998. Valutazione degli stocks di alici e sardine in Adriatico con metodi di dinamica di popolazione. *Biologia Marina Mediterranea*, 5 (3): 321-330.
- Crenshaw, M. A., 1982. Mechanisms of normal biological mineralization of calcium carbonates. In *Biological mineralization and demineralization* (Nancollas, G. H., eds), pp. 243-257. Berlin, Heidelberg, New York: Springer-Verlag.
- Degens, E. T., W. G. Deuser and R. L. Haedrich, 1969. Molecular structure and composition of fish otoliths. *Marine Biology* 2: 105-113.
- Doering, P. and J. Ludwig, 1990. Shape analysis of otoliths -- a tool for indirect ageing of eel, *Anguilla anguilla* (L.)?. *Internationale Revue der gesamten Hydrobiologie*. Berlin, vol. 75 (6): 737-743.
- Doering, P., Ludwig, J. and G. Gmel, 1992. Preliminary results of otolith shape analysis with eels of known age. *Irish Fish. Invest. Ser. A (Freshw.)* 36: 105 (Abstract only).
- Dunkelberger, D. G., J. M. Dean and N. Watabe, 1980. The ultrastructure of the otolithic membrane and otolith in the juvenile mummichog, *Fundulus heteroclitus*. *Journal of Morphology* 163: 367-377.
- Eklund, J., R. Parmanne and G. Aneer, 2000. Between-reader variation in herring otolith ages and effect on estimated population parameters. *Fish. Res.* 46: 147-154
- Fjallstein, I. and S. H. Jákupsstovu, 1999: Release, recapture and migration of reared Atlantic cod (*Gadus morhua* L.) on the Faroe Islands. In: B. R. Howel, E. Moksnes and T. Svåsand (eds.), *Stock Enhancement and Sea Ranching*. Fishing News Books, 231-242.
- Fletcher, W. J., 1991. A test of the relationship between otolith weight and age for the pilchard *Sardinops neopilchardus*. *Can. J. Fish. Aquat. Sci.* 48: 35-38.
- Fletcher, W.J., 1995. An application of the age-otolith weight relationship for the pilchard *Sardinops sagax neopilchardus*. *Can. J. Fish. Aquat. Sci.* 52: 657-664.
- Fletcher, W. J. and S. J. Blight, 1996. Validity of using translucent zones of otoliths to age the pilchard *Sardinops sagax neopilchardus* from Albany, Western Australia. *Mar. Freshwater Res.* 47: 617-624.
- Friedland, K. D. and D. G. Reddin, 1994. Use of otolith morphology in stock discriminations of Atlantic salmon (*Salmo salar*). *Can. J. Fish Aquat. Sci.* 51: 91-98.
- Gauldie, R. W., 1986. Vaterite otoliths from chinook salmon (*Oncorhynchus tshawytscha*). *New Zealand Journal of Marine and Freshwater Research* 20, 209-217.
- Gauldie, R. W., 1991. The morphology and periodic structures of the otolith of chinook salmon (*Oncorhynchus tshawytscha*), and temperature-dependent variation in otolith microscopic growth increment width. *Acta Zoologica* 72: 159-179.
- Gauldie, R. W., 1993. Continuous and discontinuous growth in the otolith of *Macruronus novaezelandiae* (Merluccidae: Teleostei). *Journal of Morphology* 216: 271-294.

- Giannetti, G., 1985. Age-reading of anchovy otoliths. A methodological note. *Quaderni dell'Istituto Ricerche Pesca Marittima*, 4(1): 47-50.
- Graynoth, E., 1999. Improved otolith preparation, ageing and back-calculation techniques for New Zealand freshwater eels. *Fisheries Research*, 42: 137-146.
- Hamrin, S. F., E. Arneri, P. Doering-Arjes, H. Mosegaard, A. Patwardhan, A. Sasov, M. Schatz, D. van Dyck, H. Wickstrom and M. van Heel M., 1999. A new method for three-dimensional otolith analysis. *J. Fish Biol.* 54: 223-225.
- Hecht, T. and A. Hecht, 1979. A descriptive systematic study of the otoliths of the neopterygean marine fishes of South Africa. Part 3. Elopiformes, Gonorhynchiformes, Clupeiformes and Salmoniformes. *Trans. R. Soc. S. Afr.*, 44(1): 73-95.
- Holmgren, K. and H. Wickström, 1988. Sättälens kvalitet 1987: en studie över kön, storlek, ålder och skador (English summary: The quality of Swedish yellow eels used for stocking in 1987 – a study of sex, size, age and wounds) *Information från Sötvattenslaboratoriet, Drottningholm* 8: 38p.
- Hu, L. C. and P. R. Todd, 1981. An improved technique for preparing eel otoliths for aging. *New Zealand Journal of Marine and Freshwater Research*, 15: 445-446.
- Jákupsstovu, S. H. and J. Reinert, 1994: Fluctuations in the Faroe Plateau cod stock. *ICES mar. Sci. Symp.*, 198: 194-211.
- Kalish, J. M., 1989. Otolith microchemistry: validation of the effects of physiology, age and environment on otolith composition. *Journal of Experimental Marine Biology and Ecology* 132: 151-178.
- Kalish, J. M., 1990. Use of otolith microchemistry to distinguish the progeny of sympatric anadromous and non-anadromous salmonids. *Fishery Bulletin* 88: 657-666.
- Kalish, J. M., 1991. Determinants of otolith chemistry: seasonal variation in the composition of blood plasma, endolymph, and otoliths of bearded rock cod, *Pseudophycis barbatus*. *Marine Ecology Progress Series* 74: 137-159.
- Kastowsky, M., E. Arneri, N. Bergström, P. Clevestam, G. Giannetti, P. Doering-Arjes, S. F. Hamrin, H. Mosegard, H. Paulsen, M. van Heel, H. Wickström and M. Schatz, 2002a. Otolith Shape Databases for Anchovy, Cod, Eel, and Turbot. *ICES J.*: submitted
- Kastowsky, M., M. van Heel and M. Schatz, 2002b. 2-D shape classification of fish otoliths. In preparation.
- Kastowsky, M., M. van Heel and M. Schatz, 2002c. Evaluation of Combined Strategies for Shape Analysis. In preparation.
- Kastowsky, M., A. Patwardhan, N. De Clerk, E. Claes, M. Schatz and M. van Heel, 2002d. Three-dimensional otolith shape data-base. In preparation.
- Kimura, D. K. and J. J. Lyons, 1991. Between reader bias and variability in the age-determination process. *Fish. Bull.* 89: 53-60.
- Lombarte, A. and J. Lleonart 1993. Otolith size changes related with body growth, habitat depth and temperature. *Environ. Biol. Fishes* 37: 297-306.
- Mann, S., S. B. Parker, M. D. Ross, A. J. Skarnulis and R. J. P. Williams, 1983. The ultrastructure of the calcium carbonate balance organs of the inner ear: an ultra-high

- resolution electron microscopy study. Proceedings of the Research Society of London (B. Biological Sciences) 218: 415-424.
- Messieh, S. N., C. MacDougall and R. Claytor, 1989. Separation of Atlantic herring (*Clupea harengus*) stocks in the Gulf of St. Lawrence using digitized otolith morphometrics and discriminant function analysis. Can. Tech. Rep. Fish. Aquat. Sci. 1647, 22p.
- Morales-Nin, B., 1985. Características de los otolitos cristalinos de *Genypterus capensis*. Investigacion Pesquera 49, 379-386.
- Morales-Nin, B., 1986a. Chemical composition of the otoliths of the sea bass (*Dicentrarchus labrax* Linnaeus, 1758) (Pisces, Serranidae). Cybium 10, 115-120.
- Morales-Nin, B., 1986b. Structure and composition of *Merluccius capensis* otoliths. South African Journal of Marine Sciences 4, 3-10.
- Moriarty, C., 1972. Studies of the eel *Anguilla anguilla* in Ireland. I. In the lakes of the Corrib system. Irish Fish. Invest. Ser. A 10. 39p.
- Moriarty, C., 1973. A technique for examining eel otoliths. Journal of Fish Biology, 5: 183-184.
- Mugiya, Y., 1987. Phase difference between calcification and organic matrix formation in the diurnal growth of otoliths in the rainbow trout, *Salmo gairdneri*. Fishery Bulletin 85: 395-401.
- Panfili, J. and M. C. Ximenes, 1992. Measurements on ground or sectioned otoliths: Possibilities of bias. Journal of Fish Biology (41) 2: 201-207.
- Panfili, J. and M. C. Ximenes, 1994. Age and growth estimation of the European eel (*Anguilla anguilla* L.) in continental waters: Methodology, validation, application in mediterranean area and comparisons in Europe. Bulletin Francais de la Peche et de la Pisciculture: 44-66.
- Panfili, J., M. C. Ximenes and A. J. Crivelli, 1994. Sources of variation in growth of the European eel (*Anguilla anguilla*) estimated from otoliths. Canadian Journal of Fisheries and Aquatic Sciences, 51: 506-515.
- Pawson, M. G., 1990: Using otolith weight to age fish. J. Fish Biol. 36: 521-531.
- Payan, P., A. Edeyer, H. De Pontual, G. Borelli, G. Boeuf, and N. Mayer Gostan, 1999. Chemical composition of saccular endolymph and otolith in fish inner ear: lack of spatial uniformity. American Journal of Physiology Regulatory Integrative and Comparative Physiology 46: R123-R131.
- Poole, W. R. J. D. and Reynolds, 1996. Age and growth of yellow eel, *Anguilla anguilla* (L.), determined by two different methods. Ecology of Freshwater Fish, 5: 86-95.
- Radtke, R. L., and T. F. Hourigan, 1990. Age and growth of the Antarctic fish *Notototheniops nudifrons*. Fish. Bull. 88: 557-571.
- Reeves S. A., 2001. Age-reading problems and the assessment of Eastern Baltic Cod. ICES CM 2001/ACFM:18.
- Richards, L. J., J. T. Schnute, A. R. Kronlund and R. J. Beamish, 1992. Statistical models for the analysis of ageing error. Can. J. Fish. Aquat. Sci. 46: 108-112.

- Saitoh, S. and J. Yamada, 1989. Ultrastructure of the saccular epithelium in the otolithic membrane in relation to otolith growth in tilapia, *Oreochromis niloticus* (Teleostei: Cichlidae). Transactions of the American Microscopy Society 108: 223-238.
- Sasov, A. and D. Van Dyck, 1998. Desk-top microtomography: Gateway to the 3D-world. Microscopy and Analysis (European edition) March 1998, 21-23.
- S-PLUS 2000, 1999. Professional Release 3. MathSoft Inc, 1988-2000.
- Svedäng, H., Wickström, H., Reizenstein, M., Holmgren, K. and Florenius, P., 1998. Accuracy and precision in eel age estimation, using otoliths of known and unknown age. Journal of Fish Biology, 53: 456-464.
- Templeman, W., H.J. Squires, 1956. Relationship of otolith lengths and weights in the haddock *Melanogrammus aeglefinus* (L) to the rate of growth of the fish. Journal of the Fisheries Research, Board of Canada. 13 (4): 467-487
- Tyler, A. V., R. J. Beamish and G. A. McFarlane, 1989. Implications of age determination errors to yield estimates. In: Effects of Ocean Variability on Recruitment and an Evaluation of Parameters used in Stock Assessment Models (R. J. Beamish and G. A. McFarlane, eds.), Canadian Special Publication of Fisheries and Aquatic Sciences 108: 27-35.
- Tzeng, W. N., K. P. Severin and H. Wickström, 1997. Use of otolith microchemistry to investigate the environmental history of European eel *Anguilla anguilla*. Mar. Ecol. Prog. Ser. 149: 73-81.
- Van Heel, M., 1984. Multivariate statistical classification of noisy images (randomly oriented biological macromolecules). Ultramicroscopy 13: 165-184.
- Van Heel, M., 1989. Classification of very large electron microscopical image data sets. Optik 82: 114-126.
- Van Heel, M., G. Harauz, E. V. Orlova, R. Schmidt and M. Schatz, 1996. A new generation of the IMAGIC image processing system. J. Struct. Biol. 116: 17-24.
- Van Heel, M., B. Goven, R. Matadeen, E. V. Orlova, R. Finn, T. Pape, D. Cohen, H. Stark, R. Schmidt, M. Schatz and A. Patwardhan, 2000. Single-particle electron cryo-microscopy: towards atomic resolution. Quart. Rev. Biophys. 33: 307-369.
- Wallace, T. P. and P. A. Wintz, 1980. An efficient three-dimensional aircraft recognition algorithm using normalised Fourier descriptors. Computer Graphics and Image Processing, 13: 99-126.
- Ward, J. H., 1982. Hierarchical grouping to optimize an objective function. J. Am. Statist. Assoc. 58: 236-244.
- Wickström, H., 1984. The Swedish Eel Stocking Programme. EIFAC Tech. Pap. (42) Suppl. Vol. 1: 68-83.
- Wickström, H., L. Westin and P. Clevestam, 1996. The biological and economic yield from a long-term eel-stocking experiment. Ecology of Freshwater Fish, 5: 140-147.
- Wilson, C.A., J. M. Dean, E. D. Prince and D. W. Lee, 1991. An examination of sexual dimorphism in Atlantic and Pacific blue marlin using body weight, sagittae weight, and age estimates. J. Exp. Mar. Biol. Ecol. 151: 209-225.

- Wirth, T. and L. Bernatchez 2001. Genetic evidence against panmixia in the European eel. *Nature* (409): 1037-1040.
- Worthington, D. G., A. J. Fowler and P. J. Doherty, 1995a. Variation in the relationship between otolith weight and age: implications for the estimation of age of two tropical damselfish (*Pomacentrus moluccensis* and *P. wardi*). *Can. J. Fish. Aquat. Sci.* 52: 233-242.
- Wright, P. J., N. B. Metcalfe, and J. E. Thorpe, 1990. Otolith and somatic growth rates in Atlantic salmon parr, *Salmo salar* L.: evidence against coupling. *Journal of Fish Biology* 36: 241-249.
- Wright, P. J., D. Rowe, and J. E. Thorpe, 1991. Daily growth increments in the otoliths of Atlantic salmon parr, *Salmo salar* L., and the influence of environmental factors on their periodicity. *Journal of Fish Biology* 39: 103-113.
- Wright, P. J., C. Thalbot and J. E. Thorpe, 1992. Otolith calcification in Atlantic salmon parr, *Salmo salar* L., and its relation to photoperiod and calcium metabolism. *Journal of Fish Biology* 40: 779-790.
- Zhang, Z. and N. W. Runham, 1992. Otolith microstructure pattern in *Oreochromis niloticus* (L.). *Journal of Fish Biology* 40: 325-332.

## 9. Dissemination List

### Publications

- CARDINALE, M., P. DOERING-ARJES, M. KASTOWSKY, H. MOSEGAARD: Effects of sex, stock and environment on the shape of Atlantic cod (*Gadus morhua*) otoliths. Submitted to the Canadian Journal of Fisheries and Aquatic Sciences.
- FAIR-CT97-3402 (SC): Fish Ageing by Otolith Shape Analysis – FAbOSA. Project Synopses, Vol. VI: Fisheries and Aquaculture (FAIR 1994-98), 3<sup>rd</sup> Europ. MAST, Lisbon 23-27 May 1998, European Commission, 259-261.
- HAMRIN, S. F., E. ARNERI, P. DOERING-ARJES, H. MOSEGAARD, A. PATWARDHAN, A. SASOV, M. SCHATZ, D. VAN DYCK, H. WICKSTRÖM & M. VAN HEEL: A new method for three dimensional otolith analysis. Brief Communication in the Journal of Fish Biology (1999) 54, 223-225.
- KASTOWSKY, M., E. ARNERI, N. BERGSTRÖM, P. CLEVESTAM, G. GIANNETTI, P. DOERING-ARJES, S. F. HAMRIN, H. MOOSEGARD, H. PAULSEN, M. VAN HEEL, H. WICKSTRÖM, AND M. SCHATZ: Otolith Shape Databases for Anchovy, Cod, Eel and Turbot. Submitted to ICES Journal of Marine Sciences.

### Lectures

- DOERING, P.: Presentation of the recently started EC research project FAbOSA. Inst. of Freshwater Research Seminar, Drottningholm, Sweden, 7 May 1998.
- DOERING-ARJES, P.: First Progress report of the FAIR project FAbOSA - Fish Ageing by Otolith Shape Analysis. EFAN 3<sup>rd</sup> Plenary Meeting, Porto, Portugal, 30 Sept.-3 Oct. 1998.
- DOERING-ARJES, P.: Relation between shape and age within otoliths. Invited speaker to CfÅ (Centre for Ageing of Fish) course, 27-29 April 1999, Drottningholm.
- DOERING-ARJES, P.: Report from the FAbOSA Workshop in May 2000. Invited speaker at the 5th EFAN Plenary Meeting, Palma di Mallorca, 2-7 October 2000.
- DOERING-ARJES, P., CARDINALE, M., AND HAMRIN, S. F: Ageing fish faster – a proof with known age cod (*Gadus morhua*). Inst. of Freshwater Research Seminar, Drottningholm, 17 January 2001.
- DOERING-ARJES, P., CARDINALE, M., AND HAMRIN, S. F: Ageing fish faster – a proof with known age specimen, SIL, 4-10 February 2001, Melbourne, Australia.
- KASTOWSKY, M.: IMAGIC - A software for image analysis and its application to otolith shape analysis. Invited speaker at the 3<sup>rd</sup> EFAN Plenary Meeting in Porto, Portugal, 30 Sept.-3 Oct. 1998.
- KASTOWSKY, M.: Importance of proper imaging conditions and pre-processings in otolith shape analysis. Invited speaker at the 4th EFAN Plenary Meeting in Heraklion, Crete, Greece, 4 Oct. 1999.
- KASTOWSKY, M.: 2-D Shape Analysis and classification using IMAGIC-5. Workshop in Altea, 2000.
- KASTOWSKY, M.: Shape Analysis with IMAGIC-5. Workshop in Älvkarleby, 25-27 May 2000.
- PAULSEN, H.: The FAbOSA EU project. Presentation at the Danish Institute for Fisheries Research, Hirtshals, Denmark, 10 December 1998.
- WICKSTRÖM, H.: Presentation of the FAbOSA project at a meeting with the CfÅ (Centre for Ageing of Fish) at the Institute of Marine Research in Lysekil, Sweden, 12–14 May 1998.
- WICKSTRÖM, H.: Shape analysis. Workshop “Analysis, Interpretation, and Application of Fish Otoliths and Other Hard parts: The State-of-the-Art”, June 1-2, 2001, SUNY ESF, Syracuse, New York, USA.

## Posters

- ARNERI, E., F. DONATO & G. GIANNETTI: Growth of juvenile anchovy, *Engraulis encrasicolus*, in central Adriatic Sea. 2<sup>nd</sup> International Symposium on Fish Otolith Research and Application, Bergen (Norway) 20-25 June 1998.
- DOERING, P., S. F. HAMRIN, A. SASOV, R. SAYLES, M. SCHATZ, D. VAN DYCK, M. VAN HEEL, H. WICKSTRÖM, E. ARNERI: A non destructive technique for three dimensional reconstruction of fish otoliths. 3<sup>rd</sup> European Marine Science and Technology Conference, 23-27 May 1998 in Lisbon, Portugal. *Award for one of the 7 best posters.*
- DOERING, P., S. F. HAMRIN, A. SASOV, R. SAYLES, M. SCHATZ, D. VAN DYCK, M. VAN HEEL, H. WICKSTRÖM, E. ARNERI: A non destructive technique for the three dimensional reconstruction of fish otoliths. 2<sup>nd</sup> International Symposium on Fish Otolith Research and Application, Bergen, Norway, 20-25 June 1998.

## Exploitable Results

- 2D Shape Analysis of Otoliths: Within the image processing and image analysis software package IMAGIC-5 a new module "OTOLITH" was created containing tools (commands) for 2D otolith shape analysis.
- Otolith workstation: CCD camera, high-frequency illumination system, state-of-the-art PC, scanning and 2D shape analysis software implemented.
- Otolith Database CD-ROMs: databases of fish otolith shapes for anchovy, cod, eel and turbot. These databases contain a large number of otolith images as well as a characterisation of their appearance in terms of Fourier shape descriptors. Various other attributes such as otolith weight, fish length and fish weight are linked to each of the otolith database entries.

## Miscellaneous

- Workshop on Fish Ageing by Otolith Shape Analysis: Conducted with participants from all partners and subcontractors and with invited external experts on landmarking, statistics and otoliths. 25 – 27 May 2000, Älvkarleby, Sweden.

### IMAGE SCIENCE:

[www.ImageScience.de/fabosa](http://www.ImageScience.de/fabosa)  
[www.ImageScience.de/otolith](http://www.ImageScience.de/otolith)  
[www.ImageScience.de/otolith/hardware.htm](http://www.ImageScience.de/otolith/hardware.htm)  
[www.ImageScience.de/otolith/software.htm](http://www.ImageScience.de/otolith/software.htm)

### INSTITUTE OF FRESHWATER RESEARCH:

[www.Fiskeriverket.se](http://www.Fiskeriverket.se) – laboratorier – Sötvattenslaboratoriet – projekt – internationellt samarbete - Åldersbestämning av fisk genom bildanalys av otoliter – FAbOSA.